Power management and sizing optimisation of renewable energy hydrogen systems

G Human

20828179

Thesis submitted in fulfilment of the requirements for the degree *Philosophiae Doctor* in Electrical and Electronic Engineering at the Potchefstroom Campus of the North-West University

Promoter: Prof G van Schoor

Co-promoter: Prof KR Uren

May 2015

Acknowledgements

I would like to use this opportunity to thank and acknowledge the following individuals and institutions:

- Most importantly my Father in heaven for providing me with the ability, opportunity, perseverance and the best support group to push forward and complete this work,
- my study leaders Professor George van Schoor and Professor Kenny Uren for excellent guidance and support,
- my wife Elma for her support and standing by me through all the late nights,
- my father, mother and brother Barend for their support and encouragement,
- Dr Dmitri Bessarabov and HySA Infrastructure for financial support and resources, and
- the National Research Foundation (NRF) for financial assistance.

"Whatever you do, work at it with all your heart, as working for the Lord, not for men, since you know that you will receive an inheritance from the Lord as a reward. It is the Lord Christ you are serving." Colossians 3:23 - 24 [NIV]

Abstract

Solar and wind renewable energy (RE) sources are widely available and a viable alternative for generating cleaner energy. These RE sources are however intermittent and dependent on location, time of day and season. Adding to this, non-linear components make determining sizes for the components of these systems a complicated and difficult task. Optimisation techniques are currently being used to perform the sizing of these systems, with system sizing and control optimisation performed separately. Objectives other than cost such as efficiency and reliability are not currently considered.

The first objective of this study is to develop an integrated sizing and control optimisation strategy for a small-scale stand-alone RE system using multiple objectives while considering sizing and control simultaneously. A sizing and control optimisation algorithm is developed consisting of two optimisation algorithms simultaneously optimising sizing and control variables. A single objective genetic algorithm (GA) is implemented for control optimisation and a strength Pareto evolutionary algorithm (SPEA) is implemented for the sizing optimisation. The developed strategy is referred to as SPEAGA in the rest of the document. Multiple objective functions fo cost, efficiency and reliability are used. An optimal control configuration is determined from the single objective GA which then determines an optimal sizing configuration for all three objective functions using the SPEA. Design, analysis and optimisation require a mathematical model of the system which is developed and validated. The SPEAGA is implemented on the system model. Results obtained from the optimisation process consist of non-dominated solution vectors known as Pareto optimal solutions. Each solution vector consist of six control variables, nine sizing variables and three objective function values. A second objective of this work is a genetic fuzzy system (GFS) developed to analyse the results and provide a reduced set of rules. A GA is implemented to train the fuzzy system which results in a rule-base for each objective of each site. Further a membership function reduction approach is followed to reduce the complexity of each rule-base by eliminating membership functions. A third objective is the insights derived from the fuzzy rule bases.

Contributions made by this study include the multi-objective optimisation of sizing and control variables simultaneously through the development of the novel optimisation architecture, SPEAGA. Optimising sizing and control for multiple objectives presents an additional contribution in the sense that it analyses the information in a new way giving new insight. The developed GFS is successfully used to generate rules relating system inputs to outputs and is useful for system design. The SPEAGA successfully optimises a small-scale rural RE hydrogen (H_2) system for three sites. Further results include a comparison between the standard SPEA

and the developed SPEAGA. The SPEAGA provided improved values for both efficiency and reliability. These results provide new insight into system design in terms of sizing and power management when considering multiple conflicting objectives. Efficiency and reliability are shown to be dependent on control parameters and are therefore improved using the SPEAGA through the additional control optimisation which is highlighted by the results. Insights are obtained from the GFS which are considered useful for future system developments.

keywords: Multi-objective optimisation, Strength Pareto evolutionary algorithm, Genetic algorithm, renewable energy, hydrogen, fuzzy logic, power management, optimal sizing.

Contents

List of Figures

List of Tables

LIST OF ABBREVIATIONS

3D	Three dimensional
AC	Alternating current
Ah	Ampere-hour
ANN	Artificial neural networks
BB	Battery bank
BB1	Battery bank 1
BB2	Battery bank 2
BCM	Battery charge mode
BDM	Battery discharge mode
CC	Charge controller
CO_2	Carbon dioxide
CMPPT	Current based maximum power point tracking
CSP	Concentrated solar power
DC	Direct current
DC/DC	DC to DC converter
DIRECT	Dividing rectangles
DOD	Depth of discharge
EA	Evolutionary algorithm
EMOO	Evolutionary multi-objective optimisation
FL	Fuzzy logic
GA	Genetic algorithm
GFS	Genetic fuzzy system
GenOpt	Generic optimisation program
H_2	Hydrogen
HRR	Highest ranking rule
HOGA	Hybrid optimisation by genetic algorithm
HOMER	Hybrid optimisation model for electric renewables
IRENA	International renewable energy agency
ILP	Interval linear programming
LAB	Lead-acid battery
LOLP	Loss of load probability[1]
LP	Linear programming
LPSP	Loss of power supply probability[2]
MF	Membership function
MOEA	Multi-objective evolutionary algorithm
MOLP	Multi-objective linear programming
MOO	Multi-objective optimisation
MPPT	Maximum power point tracking
NSGA	Non-sorting genetic algorithm
NWU	North-West University
O_2	Oxygen

[1] Power failure time period divided by a specified time period, normally one year.
[2] Probability of an insufficient power supply resulting due to the REHS being unable to satisfy the load demand.

O&M	Operation and maintenance
OM	Operating mode
PCD	Power conversion devices
pdf	Probability density function
PEM	Proton exchange membrane
PSO	Particle swarm optimisation
PV	Photovoltaic
RAPSIM	Remote area power supply simulator
RE	Renewable energy
REHS	Renewable energy hydrogen system
RES	Renewable energy system
RMSE	Root mean squared error
SI-FSP	Superiority-inferiority fuzzy-stochastic programming
SOC	State of charge
SOGA	Single objective genetic algorithm
SPEA	Strength Pareto evolutionary algorithm
SPEAGA	Strength Pareto evolutionary algorithm-genetic algorithm
STP	Standard temperature and pressure
TLCC	Total life-cycle cost
TRNSYS	Transient energy system simulation program
TSP	Two-stage programming
UL	Unmet load[3]
WT	Wind turbine
ZAR	South African Rand

LIST OF SYMBOLS

Symbols are listed alphabetically per section.

Weather input data - Section 4.3.1

Solar radiation

A_i	Anisotropy index	
β	PV slope angle	[$\angle degree$]
δ	Declination	[$\angle degree$]
E	Mean and true solar time correction	[Minute]
γ	Surface azimuth angle	[$\angle degree$]
G_b	Beam radiation	[W/m^2]
G_d	Diffuse radiation	[W/m^2]
G_o	Solar radiation incident on a horizontal surface outside the atmosphere	[W/m^2]
G_{on}	Extraterrestrial radiation	[W/m^2]
G_{sc}	Solar radiation constant (1367 W/m^2	[W/m^2]
G_T, S	Total radiation on a tilted surface	[W/m^2]
k_T	Clearness index	

[3]Non-served load divided by the total load over a specified time period, normally one year

$\bar{K}_T$	Average monthly clearness index	
L_{loc}	Longitude	[$\angle degree$ west]
L_{stdm}	Local time zone standard meridian	[$\angle degree$ west]
n	Day of the year	
ω	Hour angle	[$\angle degree$]
ϕ	Latitude	[$\angle degree$]
R_b	Ratio of beam radiation on a tilted surface to that on a horizontal surface	
ρ_g	Ground reflectance coefficient	
t_{sol}	solar time	[Minute]
t_{std}	Local time zone standard time	[Minute]
θ	Angle of incidence	[$\angle degree$]
θ	Angle of incidence	[$\angle degree$]
Wind speed		
c	Scale factor	[m/s]
k	Shape factor	
σ	Standard deviation	
v_w	wind speeds	[m/s]
$\bar{v}_w$	Mean of wind velocity	[m/s]
Photovoltaic module model - Section 4.3.2		
A_{PV}	PV module effective area	[m^2]
α	Thermal voltage timing compilation factor	[V]
α_{std}	Thermal voltage timing compilation factor at standard conditions	[V]
C_{PV}	PV module heat capacity per unit area	[J/^{o}C$\cdot$ m^2]
ϵ	Band gap energy of the material (1.12 eV for silicon)	[eV]
I_L	Light current	[A]
$I_{L,std}$	Light current at standard conditions	[A]
$I_{mp,std}$	Maximum power point current	[A]
I_o	Diode reverse saturation current	[A]
$I_{o,std}$	Diode reverse saturation current at standard conditions	[A]
I_{PV}	PV operating current	[A]
$I_{sc,std}$	Short-circuit current	[A]
$k_{in,PV}$	PV cell transmittance-adsorption product	[W/^{o}C$\cdot$ m^2]
k_{loss}	Heat loss coefficient	[W/^{o}C$\cdot$ m^2]
μ_{Isc}	Short-circuit current temperature coefficient	[A/^{o}C]
μ_{Voc}	Open-circuit voltage temperature coefficient	[V/^{o}C]
N_s	Number of cells in series of a PV module	
P_{PV}	PV module power output	[W]
R_s	Series resistance	[Ω]
S_{std}	Solar irradiance at standard conditions (1000 W/m^2)	[W/m^2]
T_a	Ambient temperature	[^{o}C]
T_c	PV cell temperature	[^{o}C]
$T_{c,std}$	Temperature at standard conditions (25 ^{o}C)	^{o}C
$V_{oc,std}$	Open-circuit voltage	[V]
$V_{mp,std}$	Maximum power point Voltage	[V]

V_{PV}	PV operating voltage	[V]
Wind turbine generator model - Section 4.3.3		
$A_{turbine}$	Turbine blade swept area	[m^2]
C_p	Betz limit ($C_p = 0.593$)	
E_w	Kinetic energy of the moving air masses	[J]
m_w	Air mass	[kg]
P_w	Power available in the wind	[W]
P_{WT}	Power extracted from the wind by the rotor blades	[W]
ρ_w	Air density	[kg/m^3]
v_d	Downstream wind velocity	[m/s]
v_u	Upstream wind velocity	[m/s]
v_w	Wind velocity	[m/s]
Proton exchange membrane electrolyser model - Section 4.3.4		
a_{H_2O}	Water activity	
α	Charge transfer coefficient	
C_p	Electrolyser overall thermal capacity	[J/K]
E_0	Standard reversible potential	[V]
$E_{A,a}$	Anode activation energy	[J]
$E_{A,c}$	Cathode activation energy	[J]
η_a	Activation over-potential at the anode	[V]
η_c	Activation over-potential at the cathode	[V]
η_{ion}	Ionic over-potential	[V]
η_{ohm}	Ohmic losses	[V]
F	Faraday's constant (96487 C/mol)	[C/mol]
γ_M	Roughness factor	
h	Electrolyser overall thermal admittance	[W/K]
I_{el}	Electrolyser operating current	[A]
J	Electrolyser current density	[A/m^2]
$J_{0,a,ref}$	Reference anode exchange current density	[A/m^2]
$J_{0,c,ref}$	Reference cathode exchange current density	[A/m^2]
$J_{0,i}$	Exchange current density	[A/m^2]
L_{mem}	Membrane thickness	[m]
λ_a	Water content at the anode-membrane interface	
λ_c	Water content at the cathode-membrane interface	
λ_{mem}	Membrane water content	
p_{H_2}	H_2 partial pressures	[atm]
p_{O_2}	O_2 partial pressures	[atm]
R	Universal gas constant (8.3144 J/mol·K)	[J/mol·K]
σ_{mem}	Ionic conductivity	[S/m]
$\sigma_{mem,ref}$	Ionic conductivity at the reference temperature	[s/m]
T_a	Ambient temperature	[K]
T_c, T_{el}	Electrolyser cell temperature	[K]
$T_{el,ref}$	Reference temperature	[K]
v_e	Stoichiometric coefficient of electrons	
V_{ely}, V_{el}	Applied electrolyser voltage	[V]
V_{rev}	Reversible potential or open circuit voltage	[V]

V_{th}	Thermo-neutral cell voltage	[V]
x	Location in the membrane measured from the anode	[m]
Lead-acid battery model - Section 4.3.5		
C	Battery capacity normalized with respect to C_{10}	[Ah]
C_{10}	10 hour rated battery capacity	[Ah]
C_F	Fractional discharge	[Ah]
$C_{F,i}$	Fractional depth of the i^{th} cycle	
D	Fractional damage	
ΔT	Differential between the cell reference temperature	[^{o}C]
η_B	Battery conversion efficiency	[%]
I	Battery current	[A]
I_{10}	C_{10} rating discharge current	[A]
N_i	Battery i^{th} cycle	
SOC	Battery state-of-charge	[%]
SOC_0	SOC at the time t_0	[%]
T_{ref}	Reference temperature (25 ^{o}C)	[^{o}C]
V_c	Charging voltage	[V]
V_d	Discharging voltage	[v]
V_{ec}	End of charge voltage	[V]
V_g	Beginning of gassing voltage	[V]
q_{new}	New battery capacity	[Ah]
q_{nom}	Manufacturer rated battery capacity	[Ah]
q_{prev}	Previous battery capacity	[Ah]
Power conversion device model - Section 4.3.6		
P_0	Idling power	[W]
P_{in}	Input power	[W]
P_{out}	Output power	[W]
R_i	Internal resistance	ω
V_s	Voltage set point voltage	[V]
V_{out}	Output voltage	[V]
Power controller models - Section 4.4		
I_{bat}	Total current from the battery	[A]
I_{BB1}	Battery bank 1 charging and discharging current	[A]
I_{BB2}	Battery bank 2 charging and discharging current	[A]
k_3	Battery discharge constant for **OM3**	[%]
k_{12}	Battery/electrolyser constant for **OM12**	[%]
$P_{bat,c}$	Battery charging power	[W]
$P_{bat,d}$	Battery discharging power	[W]
P_{dump}	Power dumped	[W]
P_{ely}	Power to the electrolyser	[W]
$P_{ely,max}$	Maximum allowable electrolyser current density	[A/m^2]
$P_{ely,min}$	Minimum allowable electrolyser current density	[A/m^2]
P_{RE}	Power from the RE sources	[W]
SOC	Batteries SOC	[%]
SOC_{max}	Maximum allowable SOC level	[%]

SOC_{min}	Minimum allowable SOC level	[%]
SOC_1	SOC of battery bank 1	[%]
SOC_2	SOC of battery banks 2	[%]
Optimisation - Section 6.3		
A_{ely}	Electrolyser cell area	$[cm^2]$
β	PV module slope	$[\angle degree]$
c foot-script	Subscript indicating control parameters	
C_{10}	Battery rating	[Ah]
E_{in}	Energy in	[J]
E_{out}	Energy out	[J]
η_{Ely}	Electrolyser efficiency	[%]
f_k	Objective function	
g foot-script	Generation identifier	
$I_{ely,max}$	Electrolyser maximum current density	[A/cm^2]
$I_{ely,min}$	Electrolyser minimum current density	[A/cm^2]
k foot-script	Objective function identified $k = 1 : K$ $(K = 3)$	
k_3	Operating mode OM3 variable	[%]
k_{12}	Operating mode OM12 variable	[%]
n foot-script	Iteration identifier	
N	Maximum number iterations	
$N_{B,p}$	LAB in parallel	
$N_{B,s}$	LAB in series	
N_{ely}	Number of electrolyser cells	
$N_{PV,p}$	PV panels in parallel	
$N_{PV,s}$	PV panels in series	
P_{BB1_c}	Battery bank 1 charging power	[W]
P_{BB1_d}	Battery bank 1 discharge power	[W]
P_{BB2_c}	Battery bank 2 charging power	[W]
P_{BB2_d}	Battery bank 2 discharge power	[W]
P_{Ely}	Electrolyser power	[W]
P_{PV}	PV power	[W]
P_{WT}	WT generator power	[W]
s foot-script	Subscript indicating sizing parameters	
SOC_{max}	Battery maximum SOC	[%]
SOC_{min}	Battery minimum SOC	[%]
$\bar{x}$	Solution vector	
Objectives - Section 6.6		
C_{comp}	Components investment cost	[ZAR/kW /unit]
C_I	System investment cost	[ZAR]
$C_{O\&M}$	Operation and maintenenace cost	[ZAR]
$C_{O\&M_0}$	O&M cost as a percentage of the investment cost	[%]
C_R	Replacement cost	[ZAR]
d	Discount rate	[%]
m_{H_2}	Mass of H_2 produced annually	[kg]
N_{comp}	Number of modules of a component	
p foot-script	Number of components	

P_{comp}	Component power rating	[W]
$q_{BB1_{lost}}$	Battery bank 1 annual capacity lost	[%]
$q_{BB2_{lost}}$	Battery bank 2 annual capacity lost	[%]
R_{BB}	Battery reliability	[%]
R_{ely}	Electrolyser reliability	[%]
$T_{ely,avg}$	Actual average time per electrolyser ON cycle	[h]
$T_{ely,avg_{max}}$	Calculated average time per electrolyser ON cycle	[h]
Y	Life of system	[y]
Y_r	Component replacement time	[y]
Pareto density function - Section 7.2		
b	Solution vector identifier	
d	Distance $d(\mathrm{F}_b,\mathrm{F}_{b_0})=\lvert\mathrm{F}_b - \mathrm{F}_{b_0}\rvert$	
F_b	Location of solution vector	
F_{b_0}	Location of the centre of a closed ball	
Fuzzy logic system - Section 7.4		
F_i^ℓ	Fuzzy sets in $U_i \subset \mathbb{R}$	
G^ℓ	Fuzzy sets in $V \subset \mathbb{R}$	
i foot-script	Input vector number identifier	
j	Input output pair identifier	
ℓ	Fuzzy rule identifier	
M	Number of rules (clusters)	
n foot-script	number of input vectors	
N	Number of input output pairs	
R	Fuzzy rule	
$U \subset \mathbb{R}^n$	Fuzzy sets in the input universe of discourse	
$V \subset \mathbb{R}$	Fuzzy sets in the output universe of discourse	
$\bar{x}$	Input vector set	
$\underline{x}$	Input linguistic variable vector	
$\tilde{x_i^\ell}$	Input variable centre value	
y	Output linguistic variable	
$\tilde{y^\ell}$	Output variable centre value	
Root mean squared error - Section 7.4.1		
$f\left(\bar{x_j}\right)$	Predicted output	
$RMSE$	Root mean squared error	
$\bar{x_j}$	Input variable	
$\hat{y}_j$	Output variable	

Chapter 1

Introduction

1.1 Background

Primary energy sources are divided into two main groups: renewable and non-renewable. RE refers to energy sources that are replenished by natural processes at a rate faster than it is being used. By this definition both fossil fuels (coal, oil and natural gas) and mineral fuels (natural uranium) are non-renewable. The answer lies in the energy available in RE sources providing energy service in a sustainable manner and is expected to play a major role in rural electrification with the implementation of small-scale stand-alone RE systems.

Generally the problem of implementing RE is that it is not always available when needed and not always needed when available. For intermittent RE sources to be more reliable, energy storage is a requirement. A further additional requirement for the need for storage arises from the need for energy to be transported, either to a remote location from the source or as fuel for transportation. Energy storage is available in various forms: mechanical energy, thermal and electrical energy from chemical bonds and electrical energy directly from terminals [1]. One storage technology receiving much attention from research and industry is hydrogen (H_2) energy storage. Hydrogen is produced with excess energy and then converted to usable energy when required.

Renewable energy system (RES) design and performance are dependent on location, time of day and climate conditions, while some components have non-linear performance characteristics. Additionally, certain component's performance and reliability are dependent on the power profile that they are subjected to [2]. A system designed for one site will most probably be inadequate or over designed for a different site having identical load profiles. These systems have been installed for decades, although their performance and cost would be substantially improved by applying optimization techniques in their design [3]. An evaluation by Banõs et al. [4] concludes that optimization algorithms deem a suitable tool for solving complex problems in the field of RE. Also since there is a steady increase in hybrid RES optimisation, ongoing research and development of these systems is a necessity.

1.2 Areas where contribution can be made

A survey on the simulation and optimization of hybrid systems by Bernal-Augustí and Dufo-Ló pez [3] listed two aspects of hybrid systems which warrant further research. The first is the paucity of research about multi-objective optimum design in hybrid systems. The second is the requirement to consider other objectives besides cost. Examples include CO_2 emissions, reliability and efficiency. Another survey on optimisation methods applied in the field of renewable and sustainable energy by Banõs et al. [4] concluded further research is required on the use of heuristic Pareto-based multi-objective optimization (MOO) in the field of RE. A survey on multi-objective evolutionary algorithm (MOEA) optimisation of a stand-alone hybrid RE system by Fadaee and Radzi [5], stated that future research should focus on the application of MOEA optimisation of a hybrid RES. RE sources are very sensitive to local conditions creating a promising research area for finding solutions to multiple objectives by implementing MOEA.

Seeling-Hochmuth [6] reports that studies of RESs frequently experience unanticipated problems such as premature battery degradation. Two causes identified are component sizing and control. In another study by Seeling-Hochmuth [7] the interdependency of control and sizing of a RES is emphasised. This is also supported by Bernal-Augustí and Dufo-Ló pez in [8] and [9]. In [7] a single objective (cost) is evaluated for both sizing and control while, [8] and [9] evaluate multiple objectives for sizing (cost, CO_2 emissions, unmet load) but only a single objective for the control which is cost. It is evident that there is much opportunity to develop and evaluate new methods for interdependent sizing and control optimisation of small-scale hybrid RESs. An additional area of contribution identified is to evaluate the relationship between sizing and control with respect to multiple objectives and more importantly to evaluate the influence of control optimisation on the sizing of the system with regard to each of the multiple objectives.

1.3 Problem statement

The focus of this thesis is on the development of a sizing and control optimisation strategy for a small-scale, stand-alone hybrid RE H_2 system optimising multiple objectives for sizing and control simultaneously. The results obtained from the multi-objective combined sizing and control optimisation strategy are provided in the form of Pareto optimal sets due to the conflicting nature for the objectives. These Pareto optimal sets will be analysed using a rule-based technique to gain insight into the influence of sizing and control variables on the objectives. This will provide insight into the design and operation of such systems.

1.4 Research aims and objectives

The following research aims and objectives are identified:

- Develop a RE H_2 production system model

- Develop an integrated multi-objective sizing and control optimisation strategy
- Implement optimisation strategy to generate Pareto optimal sets
- Analysis of Pareto optimal sets for three different geographic sites
- Interpret rules and derive insights from analysis

1.5 Research methodology

The methodology used to address the research aims and objectives as discussed in the previous section is as follows:

Model development: Individual validated component models are developed and combined into a single platform as a complete system model. These models are identified from literature and implemented in Simulink™. A power controller is also developed and implemented in the complete system model. Required characteristics are considered for model selection on the basis of generalised implementability, performance characteristics and for some components, degradation.

Multi-objective combined sizing and control optimisation: An optimisation strategy implemented in Matlab® is developed, using existing and new methods, and is capable of simultaneously optimising sizing and control variables for multiple objectives. Three objectives: efficiency, cost and reliability are optimised. Additional to the new strategy developed, an existing multi-objective strategy is implemented on the same input data for comparison.

Implementation of optimisation strategy: The developed optimisation strategy is implemented on three different geographic sites selected to cover a diverse mix of RE resources. The multiple conflicting objectives necessitates the implementation of a Pareto optimal set. Pareto optimal sets are obtained for the three sites using the new optimisation strategy developed and an existing multi-objective strategy.

Pareto optimal set analysis: Firstly the Pareto data is analysed to obtain insights and compared between the different sites. Next, the new optimisation strategy is compared to the existing one. The Pareto optimal sets are then analysed using a novel genetic fuzzy rule-based technique that implements a membership function reduction approach.

Generate insights and generalisations from analysis : Insights that are derived from the different analysis techniques are provided. Specific attention is given to the genetic fuzzy system with membership function reduction. Useful information derived from the analysis is provided and highlighted.

1.6 Contribution of research

In this thesis three novel contributions are made. The first contribution is the development and successful implementation of a multi-objective combined sizing and control optimisation strategy. The three objectives evaluated are efficiency, cost and reliability, where previous work have not yet considered these three multiple objectives for sizing and control combined. The results of the optimisation exercise are values for the three objectives given as Pareto optimal sets. As a result, the second contribution from this thesis is the implementation of an analysis technique using genetic fuzzy systems and a membership function reduction approach. A genetic algorithm is used to train the parameters of a fuzzy-logic system. The result of the GFS is a rule-base consisting of several rules and membership functions. The complexity of the rules are reduced by eliminating low contributing membership functions. The third contribution of this thesis is the new insights obtained from the optimisation and also the analysis procedures implemented.

1.7 Thesis overview

The thesis presents the development and analysis of a multi-objective combined sizing and control optimisation strategy for RE hydrogen production systems. A unique genetic fuzzy system with membership function reduction is implemented to analyse the data and provide insights.

Chapter 2 presents relevant literature on the use and possibilities of RE sources. Several RE sources are evaluated and discussed based on resource potential and scale with a focus on H_2 energy storage. The concept of hybrid RE sources is also provided followed by a discussion on energy storage technologies. The chapter concludes with a summary of the appropriate technologies for small-scale, stand-alone hybrid RE H_2 systems.

Chapter 3 presents a detailed literature study on RE system sizing. Conventional sizing methods are discussed followed by a more detailed discussion on mathematical optimisation methods. Next an overview of existing software based optimisation tools is given. This is followed by a literature review where optimisation algorithms are implemented on RESs with several different purposes for the optimisation. Next a discussion is given on intermittent sizing and control optimisation with the chapter concluding with a summary.

Chapter 4 describes in detail the component models of the small-scale stand-alone hybrid RE H_2 production system. The chapter provides a discussion on the models' requirements which is followed by detail descriptions of the individual component models. Individual component models are developed for the weather input data for profiles of the solar irradiance and wind speed, a photovoltaic (PV) module, a wind turbine (WT) generator, a proton exchange membrane (PEM) electrolyser cell, a lead-acid battery (LAB) cell and power conversion devices. Next, a description of the system power management controller is provided which is followed by a discussion on the battery power management controller.

Chapter 5 presents the testing and verification of the key system component models developed in Chapter 4. These models are to be used in the simulation and optimisation in Chapter 6 of a stand-alone RE hydrogen production energy system. The following models are evaluated: PV module, WT generator, PEM electrolyser, LAB, power conditioning equipment and power controllers. The models are validated through comparison with experimental data. The complete system model and power controllers are validated by ensuring that there is no resultant energy and power flows between components.

Chapter 6 presents the detailed optimisation strategy developed and implemented in this work. The chapter first provides a quick introduction to optimisation and fitness assignment using the Pareto optimality. Next a high level overview of the optimisation strategy is provided which is followed by a detailed discussion of the optimisation strategy developed. This is followed by a detailed presentation of the decision variables implemented. Finally detail is presented on the calculations used for the objective functions.

Chapter 7 presents the results obtained, analyses of the results and a summary of findings. The optimisation structure described in Chapter 6 determines values for the independent variables and eliminates all dominated solutions resulting in solution sets that lie on the Pareto front. The first section gives information of the three different geographic sites and further gives an explanation of the analysis procedure implemented. Next results from the optimisation exercise is provided. The process followed to perform the analysis is also described in detail. Next a comparison is provided between the new optimisation strategy developed for this work and a standard MOO strategy. This is followed by the implementation of the genetic fuzzy system and membership function reduction used in the analysis to gain information from the Pareto sets. The chapter concludes with a summary of the findings.

Chapter 8 starts with a short overview of the work presented which is followed by a section that highlights the contributions of the present work. Future work is also suggested and the thesis is concluded with a closure paragraph.

Chapter 2

Renewable energy and energy storage

This chapter provides relevant literature on the use and possibilities of RE sources. Several RE sources are evaluated and discussed based on resource potential and scale with a focus on H_2 energy storage. The concept of hybrid RE sources is also provided followed by a discussion on energy storage technologies. The chapter concludes with a summary of the appropriate technologies for small-scale stand-alone hybrid RE H_2 systems.

2.1 Introduction

RE is available from solar, geophysical or biological energy sources that replenish themselves through natural processes faster or equal to the rate that they are being used [10]. Heat from the sun and the varying surface temperature of the earth cause air masses to heat up and cool down resulting in powerful winds. The wind along with tidal forces and additional heat from the sun result in deep ocean currents and surface waves. Evaporation and precipitation caused by the wind and sun's heat result in streams, rivers and lakes. Energy from the sun has a share of more than 99.9% of all converted energy on earth [11]. Sunlight and water result in food for vegetation. There is therefore an abundance of energy from the sun that can be harnessed as RE. RE can be converted to sources of electricity, heat and fuel for transportation. The environmental benefits of RE is significant in that it does not consume any fuel and produce no air, water or thermal pollution during the conversion process. RE systems utilise energy from the atmosphere and transform it into a usable form of energy. The energy utilised is a negligible portion of that which is available in the atmosphere, and as a result there are virtually no negative effects on the environment [12]. RE sources include, direct solar energy, wind energy, hydroelectric power, wave energy, tidal energy, ocean currents, ocean thermal energy, geothermal heat and biomass [10]. The next couple of sections discuss each of these in terms of their advantages, disadvantages and possibility for stand-alone rural applications.

2.2 Direct solar energy

There are a variety of solar energy conversion methods available each suitable for different applications. Two main groups exist: PV cells and thermal conversion systems or concentrated solar power (CSP) systems. PV cells have reported efficiencies as high as 20% [13] with experimental cells reaching efficiencies up to 40% [14]. CSP include parabolic trough, central receiver and parabolic dish. Thermal systems have shown efficiencies between 40 and 60% [13]. CSP is mostly utilised for large-scale applications exploiting many MWs requiring large flat open spaces and extensive infrastructure. PV cells are easily applied in small-scale applications from a few hundred watt up to a few MW and can be implemented on existing structures such as rooftops. Approximately 1.75×10^5 TW of sunlight reaches the earth's atmosphere continuously. Roughly 40% is lost through the atmosphere and converted into other forms of energy (e.g. wind, hydro, geothermal) resulting in 1.05×10^5 TW irradiating the earth's surface. This is equal to 9.2×10^8 TWh per year [13]. In 2008 the world total primary energy production was 144 487 TWh and is projected at 225 606 TWh by 2035 [15]. Converting only 0.3% of the 9.2×10^8 TWh with an efficiency of 10% would result in 276 000 TWh annually, sufficient to satisfy the entire world's primary energy need projected for 2035. A detailed study by Fluri [16] on solar energy determined the potential nominal capacity for CSP in Southern Africa to be 547.6 GW subject to a set of essential criteria to eliminate sites not suitable for large-scale CSP plants. Criteria include solar resources, proximity to transmission lines, land use profile, slope and threatened vegetation. Small-scale stand-alone applications only have solar resource as criteria since stand-alone systems do not require grid connection and due to it's small footprint and flexible installation possibilities is also not subject to land use profile, slope or threatened vegetation. Human et al. [17] used the information from Fluri [16] and determine the potential for rural small-scale applications to be 245.5 GW subject to the same criteria mentioned above. The 245.5 GW will be even higher for small-scale stand-alone systems. A major drawback is that no direct sunlight is available on cloudy days or at night. Solar energy is intermittent with it's intensity varying for each geographic site, time of day, season and local weather conditions. For solar energy to be utilised energy needs to be stored when it is available so that it can be used at night and during low sunshine days.

2.3 Wind energy

A never-ending cycle of atmospheric wind can be harnessed to produce enormous amounts of electricity using WTs which absorb the kinetic energy in the wind through aerodynamic blades mounted on a rotor. The rotor is connected to a drive-shaft turning a generator, converting mechanical energy into distributable electrical energy. Currently wind energy supplies approximately 1.1% [15] of global energy. It is the fastest growing of all RE sources. Wind energy is however dependent on unpredictable weather conditions and as a result has an average capacity factor of only 20% in some areas [11]. Energy that can be extracted from the wind is dependent on the tower hight, blade swept area, available wind resource and type of ground cover. Hagemann [18] determined the optimistic available wind power generation potential for large-scale wind farms in Southern Africa to be 157.18 TWh annually. Criteria used to de-

termine appropriate sites are wind resources, proximity to roads and proximity to transmission lines. Wind turbines with 100 m hub-height and 80 m turbine rotor blades are considered. Human et al. [17] used the results from Hagemann [18] to calculate the available wind energy for small-scale stand-alone systems by downsizing the tower hub height to 10 m and turbine rotor to 4 m which is realistic values for small-scale WTs. This resulted in a value of 146.5 GWh annually from small-scale WTs. This value will be considerably higher if the limitations placed on the large-scale systems, which are not applicable to small-scale systems are not considered. Small-scale stand-alone systems do not need to be close to power lines or roads. It is not currently economically possible to rely on intermittent wind energy to supply the majority of future energy needs. It can however supply a small and clean portion for specific load requirements [12]. Moriarty and Honnery [19] considers wind power along with PV modules to be the only viable solution for small-scale stand-alone applications for rural energy supply. Wind energy like PV requires energy to be stored when wind is available in order to use the energy when wind is not available for a secure supply.

2.4 Hydroelectric power

Hydroelectric power world wide is the most widely implemented RE source for electric power generation. Pumped storage schemes are however not sustainable forms of power generation and is therefore not a form of RE but a form of energy storage discussed later in Sec. 2.9. Very little hydroelectric power potential can be further exploited. Small (500-10 000 kW), mini (101-500 kW) and micro (<100 kW) plants have some potential however there are a number of barriers hindering it's exploitation. Barriers include a lack of information about potential sites, scarceness of local skills, unawareness, and lack of private and public sector participation [11, 20].

2.5 Ocean energy

The ocean is an abundant source of energy that can be harnessed from surface waves, deep-ocean currents, tides and through ocean thermal gradients. The potential and kinetic energy in the ocean surface waves are caused by strong offshore winds and can be captured and used to generate electricity. According to Banks and Schäffler [21] the energy intensity along Southern Africa's coastline is approximately 25 MW/km. Both surface and deep ocean currents are directed, constant flows of water between continents and is harnessed with turbines similar to WTs [22]. The sun and moon's gravitational pull on the earth's rotational pull cause ocean tides resulting in periodical high and low ocean water levels and is harnessed by tidal energy systems consisting of a dam or tidal barrage filling a tidal basin with sea water during incoming high tides and emptying through a turbine during the outgoing tides. Tidal power is however only available for relatively short periods of time [11]. Ocean thermal gradients between deep water (4 to 7 ^{o}C) and surface water (22 to 28 ^{o}C) can be used to generate energy using an open or closed Rankine cycle. The small temperature difference only allows efficiencies of 1 to 3% resulting in high energy costs [11]. Ocean energy is difficult to harness and although plenty

of deep oceans exist to exploited, these technologies are costly as they require large infrastructures, have low efficiencies, problematic maintenance due to their location, limited sites and require expensive power lines to transport power inland [14].

2.6 Geothermal energy

Geothermal energy is generated and stored in the Earth's crust, or lithosphere, in tectonically active regions [11]. There are four types of geothermal resource categories. These are hydrothermal systems, geo-pressurised zones, hot and dry rocks and magma from the earth's core. Hydrothermal systems are found where deep ground water reservoirs are heated by hot rock. The water rises back to the surface through natural convection and is the source of hot springs. The steam and hot water are both utilised to generate electricity either directly in a steam turbine or through a secondary cycle. Geo-pressurised zones are underground zones where salt-water is trapped between layers of hot rock which can be tapped to generate electricity. Hot and dry rocks are found everywhere among he earth's crust and upper mantle. This type of hot rock is at depths greater than 3 km below the earth's crust and the dry refers to the absence of a liquid to carry the heat to the surface. To harness this heat wells are drilled into the rock at high pressure creating fracture networks, essentially forming hydrothermal reservoirs. Most magma originates at 30 km or more below the earth's surface, however, significant amounts can also be found closer to the surface near volcanoes and mid-ocean ridges. Heat from these magma reservoirs is extracted similar to the hot and dry rocks although the technology required is still under development due to the great depths that need to be drilled and high temperatures involved. All these technologies are very site specific, still require many years of testing, need considerable infrastructure and know how to develop, maintain and operate and is only economically viable for large scale (MW) systems. Small-scale geothermal heat pumps are implemented and utilise the temperature in the shallow grounds for direct applications in generating heat for air-conditioning and hot water [11]. Limitations of the technology are found on the temperature gradients at the site of installation, determining the depth required to have these systems operate efficiently and economically. Temperature gradients available at locations in countries such as South Africa are amongst the lowest in the world at approximately 10 degree C/km whereas much higher temperature gradients are measured in tectonically active areas such as Iceland where up to 200 degree C/km can be measured [22].

2.7 Biomass energy

Biomass is defined as any organic material made from plants or animals. Sources of biomass energy include wood, food crops, grasses, agricultural by-products, manure and other solid organic municipal waste. Biomass energy applications include bio-power, bio-fuels and bio-products. Bio-power includes the heat and electricity produced by directly burning the biomass or converting it into burnable bio-gasses or liquids. Bio-fuels are liquid fuels used for transportation that burn cleaner than conventional fuels. Efficiencies of bio-fuels are less than 1% due to the energy required for growing, maintaining and harvesting vegetation. Bio-products

refer to consumer and industrial products made from biomass material and include building materials, pulp and paper, forest products, etc. Biomass energy is carbon neutral since the amount of CO_2 released is exactly equal to the amount of CO_2 absorbed during photosynthesis. Biomass is not strictly renewable since it is possible to use up the biomass material faster than it can be produced [10]. According to Banks and Schäffler [21] biomass energy is the largest contributor of RE in South Africa adding around 9% of South Africa's energy needs as most rural households rely on wood for cooking and heating of space. Biomass energy is also used to generate electricity by the sugar and paper industries. Biomass waste would not be sufficient to produce the energy requiring vast areas of land to be converted for crops. There is already a worldwide shortage of food arising from a shortage of crops and farming skills. These systems also require special skills and knowledge to develop, maintain and operate safely [11, 14, 21].

2.8 Hybrid renewable energy systems

A hybrid RES consist of two or more renewable sources. The variable nature of intermittent RE sources can be somewhat overcome with the combination of different RE sources. Using multiple different RE sources increases system efficiency and reliability, reduces cost and also reduces the storage requirement used as an energy buffer [5]. Ould Bilal et al. [23] shows that the intermittent nature of specifically wind and solar energy sources can be partially improved by combining the two sources with proper calculation of the optimal combination. Furthermore a hybrid RES consisting of wind and solar generating units can reduce energy storage requirements considerably. Koutroulis et al. [24] verify that a hybrid wind and solar generation system results in lower cost when compared to single wind or solar generation systems. Hybrid systems are however not always the optimal solution as is shown by Human et al. [17] where the wind resources in the location evaluated is very poor and a PV only system is the most economical. Results from simulations did however indicate that an increase in the wind contribution to the system reduces energy storage requirements. Careful sizing of the components are required for every site since every site has a different optimal combination of RE source and storage requirements.

2.9 Energy storage

Various studies on energy storage technologies have highlighting advantages and disadvantages of different technologies for different applications [1, 11, 25, 26]. Fig. 2.1 illustrates a comparison between the specific power and energy storage potential of some energy storage technologies [1, 25].

For stand-alone RESs, storage technologies capable of storing energy in the order of hours to days are considered [27]. This requirement eliminates superconducting magnetic energy storage, super-capacitors and flywheels which are all short-term energy storage technologies capable of supplying energy in the orders of seconds to minutes. Further, only technologies that

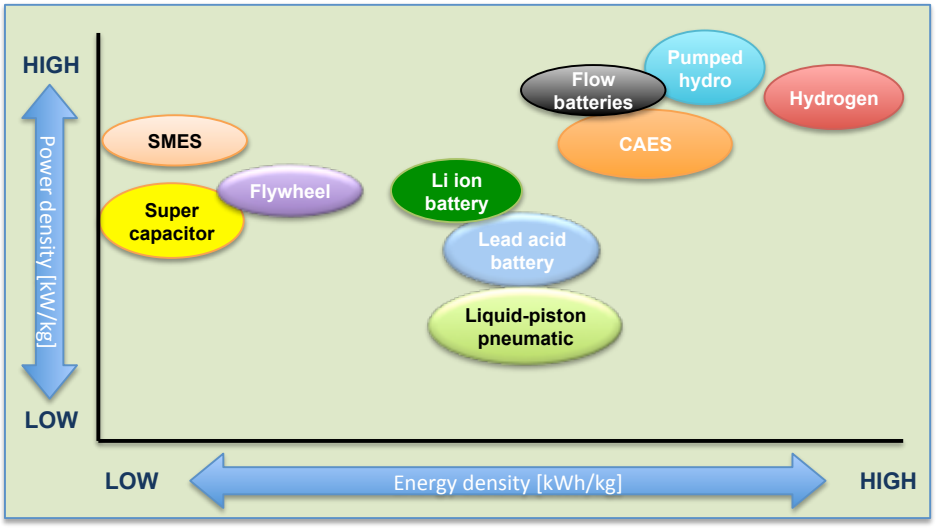

Figure 2.1: Specific power vs. energy storage potential.

are suitable for distributed grid applications is considered [13]. These include LAB, lithium-ion battery and H_2 storage. The conventional LAB is still the most utilised energy storage device [28]. Although the energy density from lithium-ion is five times more than that of lead-acid the price is ten times more. Where space and weight is limited in portable devices, lithium-ion is preferred whereas lead-acid is the preferred for stationary applications where light weight and compact size is not a requirement. LABs are robust whereas lithium-ion batteries are fragile and require protection circuits for safe operation [25].

Bernal-Augustí and Dufo-Ló pez [3] report that the current cost of H_2 storage and it's low round trip efficiency (25-35%), compared to that of LABs (80 %), make H_2 storage economically impractical. Kaldellis et al. [1] state 35-45% for H_2. Experimental results by Stevens and Corey [29] on the other hand show LAB efficiencies to be as low as 50% when subjected to incremental operation which is what it would experience from an intermittent RE source. The report also indicates that the efficiencies of LABs decreased as the battery nears full charge. Non-varying efficiencies often implemented in models from literature vary from 70 % to 80% [26]. Li et al. [28] studied three stand-alone, small-scale PV systems using LAB storage, H_2 storage and a combination of LAB and H_2 storage. Maximum efficiency is achieved with battery storage only, but at the highest system cost. H_2 storage only resulted in the lowest efficiencies with the hybrid storage configuration giving a low cost, high efficiency solution. These results are consistent with Vosen and Keller [30] showing that a combination of high cost, high efficiency, short-term storage (LAB) with less efficient long term storage, capable of storing large amounts of energy inexpensively (H_2) is the optimal design.

2.9.1 Hydrogen production

Various technologies are available for H_2 production, however not all are compatible with intermittent RE sources. Industrial methods include production from fossil raw materials, ammonia dissociation and water electrolysis. It is already stated in Section 2 that wind and PV are the

only possibility for small-scale stand-alone electricity production and are also the only possibilities for small-scale, stand-alone H_2 production systems. The only H_2 production technology compatible with intermittent RE sources, and suitable for distributed on-site production of H_2, is water electrolysis. There are three main water electrolyser technologies: alkaline electrolysers; PEM electrolysers; and high temperature electrolysers [31]. Although PEM based H_2 production is the more expensive technology, it offers several attributes that make PEM technology ideal for integration with intermittent RE sources. A comparison between electrolysis H_2 production technologies is available in [32] concluding that PEM technology is preferred to be used for small-scale stand-alone H_2 generation [33]. PEM water electrolysis is shown to have some drawbacks with regard to power supplied directly from an intermittent power source. Barbir [34] addresses specific issues with regard to the use of PEM electrolysers with RE sources. Battery storage is necessary to act as a buffer to smooth the energy supply

2.10 Conclusion

In this chapter a number of RE sources have been reviewed for their potential to supply energy to rural communities in a stand-alone manner. Several RE sources have been shown to be infeasible. Hydroelectric power is limited to location and still have to undergo development to be viable for small-scale systems. Ocean energy is difficult to harness and is limited to coastal areas. Geothermal energy is not viable due to its complexity to harness. Biomass energy is reliant on energy sources which are often based on sources required for food. Shortage of crops and a lack of special skills for maintenance and operation will need to be overcome before this technology becomes a viable solution. Hybrid systems is shown to have several advantages over single source systems. Wind and solar energy both have low maintenance requirements, is available in abundance and are considered the only viable solutions for small-scale stand-alone rural applications. Due to their indeterminacy a form of energy storage is required. Long term storage in the form of H_2 is shown to be a viable solution. Hydrogen production via PEM electrolysis is possible with intermittent RE sources. Combining H_2 as long-term storage with short-term LAB storage is considered to be an optimal solution.

Chapter 3

Literature survey

This chapter will focus on literature available for RES sizing. Conventional sizing methods are discussed followed by a more detailed discussion on mathematical optimisation methods. Next, an overview of existing software based optimisation tools is given. This is followed by a literature review where optimisation algorithms are implemented on RESs with several different purposes for the optimisation. Finally a discussion is given on intermittent sizing and control optimisation.

3.1 Renewable energy system sizing

RESs consist of a number of components that are required to function in the system as efficiently as possible. RE sources vary with time of day, season and geographic site. As a result, the same RES will perform completely different for different geographic sites and each RES will have a different set of available resources, requirements in terms of hardware and strategy with which the power is managed, also referred to control. It is not realistic to design a single system with the expectation that it can supply the same load for two different geographic sites. Each system requires a unique design in terms of its sizing and power management which is dependent on the load required and site specific RE resources available. For this reason the sizing and power management of these systems are of highest importance to ensure that the optimum combination of components and power management are achieved for each system.

3.1.1 Conventional sizing methods

Some conventional approaches for sizing a hybrid RES are discussed by Seeling-Hochmuth [6]. These are the rule of thumb methods, paper-based methods and software-based methods implementing mathematical optimisation. The rule of thumb method for sizing hybrid systems was developed at a workshop on hybrid system design held at the National Renewable Energy Laboratory in 1996. A number of decisions were made that were based on experience gained from existing systems. The rule of thumb gives guidelines for the sizing and operation of the RE sources, diesel generator, battery bank, direct current bus voltage and power electronic

equipment based on the required load energy, peak demand and availability requirements. A table of the most common rules of thumb is provided by Seeling-Hochmuth [6]. However, on further reading, the rules of thumb are not as open-and-shut as it at first appears. For the renewable sources a value of 40-60% of the load is suggested. The sizing of the diesel generator is dependent on the availability required and the more importantly the availability that can be afforded. For sizing the battery bank numerous rules of thumb exist, each having its own reasoning, and is influenced not only by availability but also application and battery type. For example a system consisting of only renewable sources is recommended to have storage for three to five days while a very remote telecommunication repeater station requiring high reliability is recommended to have five to ten days of storage. Thus, after further investigation, even with the implementation of the rule of thumb method, there is still more detailed investigation required if the sizing is to be done accurately. At the end of the day the rule of thumb method only gives guidelines for design and does not provide the optimal solution to be implemented.

Another sizing method is known as the ampere-hour (Ah) design method. For the Ah method the daily energy usage of each load is determined. Efficiencies of power electronic equipment, battery banks and wire resistances are also considered. An Ah value for the load is calculated and used along with the required number of days autonomy, selected bus voltage, battery rating and series and parallel numbers. The renewable source requirement is determined from the daily energy needs of the load, peak sun hours per day and also the selected bus voltage. The decision to add a diesel generator is determined by the percentage of load required to be supplied by the PV panels. Rules for the decision to add a diesel generator is given in Seeling-Hochmuth [6]. The size of the diesel generator required is selected to have the ability to supply the peak load demand and charge the battery bank simultaneously. As with the rule-of-thumb method, the Ah method does not consider daily, monthly and seasonal weather patterns, and also does not consider any dynamic behaviour of some of the components that have non-linear characteristics. These two methods base their sizing on lumped component efficiencies and average energy input values from the RE sources. The rule-of-thumb method can not provide guidelines for choosing a mix of different renewable sources, while the Ah method only considers PV panels as a RE source. There are also no guidelines for operating such a system using the Ah method. The drawbacks of the rule-of-thumb and Ah sizing methods can be overcome with the implementation of mathematical optimisation algorithms.

3.1.2 Mathematical optimisation

The concept of optimisation was first introduced in the early 1940s with the introduction of linear programming [35]. Optimisation found its origin in a field of mathematics and more specifically calculus, called calculus of variations which deals with maximising and minimising a functional, which is the mapping from a set of functions to real numbers. Since its introduction optimisation has over the past 70 years found its way into almost every industrial sector but have intensively been utilised in the financial, manufacturing and engineering design disciplines with great success [35]. From the first introduction of linear programming, the field of optimisation has evolved to include many classes and forms of optimisation algorithms that find its origin in nature by imitating nature through the implementation of algorithms based

on natural selection, natural genetics and the social behaviour of nature to solve optimisation problems [36]. Optimisation is the process of finding inputs to a function that produces the optimal value for some value of the function. The purpose of optimisation is to find a solution that makes the most effective use of the system resources. An optimal value can either be maximised or minimised depending on the objective. For example, a system's life cycle cost would be minimised while annual profit would be maximised. The value of the function to be maximised or minimised is the objective value. The objective value is the measure used to determine the performance of the function to be optimised. The objective depends on certain system characteristics which are known as decision variables. The task of optimisation is to find values for these decision variables that optimise the objective. In almost all optimisation problems the decision variables are constrained. Constraints are either physical limits of components and values or boundary limits selected by the user. Part of the optimisation problem is defining the decision variables, constraints and optimisation algorithm operating parameters [35]. Optimisation is divided into three categories; enumerative, deterministic and probabilistic given in Fig. 3.1 [37]. A number of these optimisation techniques have been implemented in

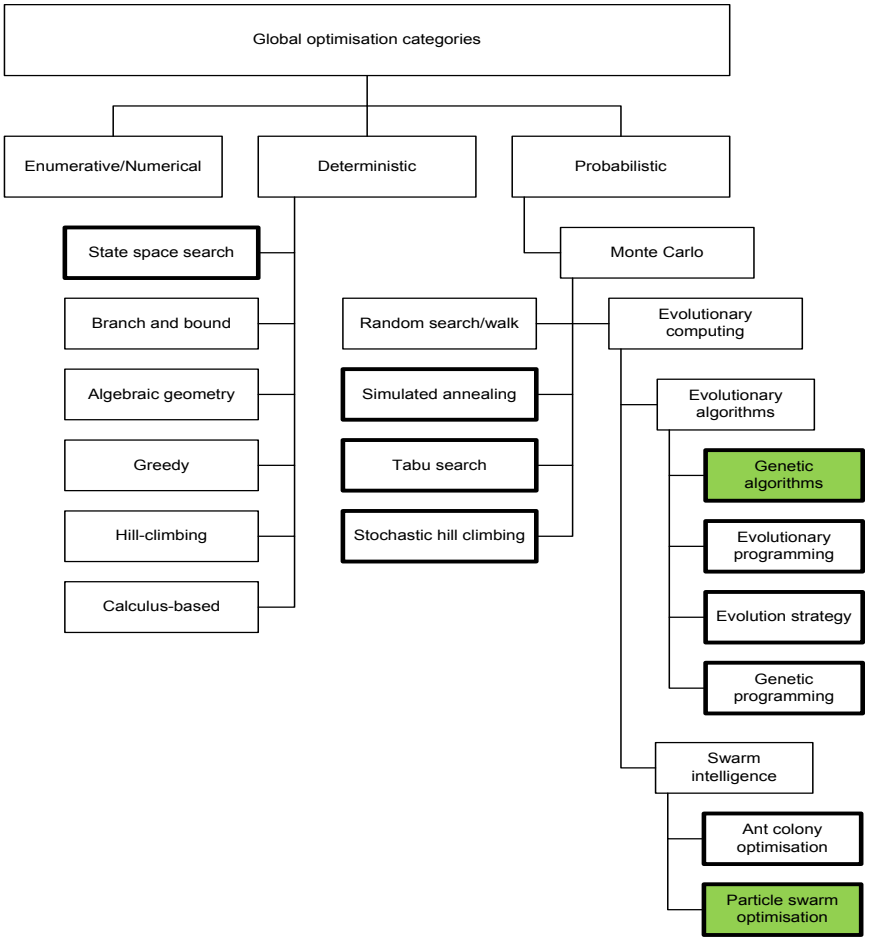

Figure 3.1: Global optimisation algorithms.

literature on RESs. These are emphasised with a thicker border [38]. The two most popular optimisation techniques implemented in the field of RES optimisation are two population based

search methods, GA and particle swarm optimisation (PSO) [5]. A comparison study by Angeline [39] showed that the GA achieved better fitness values than PSO in several comparison scenarios. According to Angeline [39] the GA is in terms of accuracy preferred over PSO. GAs are used in optimisation because of there flexibility, ease of implementing on non-differentiable functions, ability to work with discrete search spaces and ability to solve global optimization problems [40].

In real-life engineering problems it is quite common to encounter the need to for MOO. In MOO the objectives are mostly conflicting, implying that straight forward simultaneous optimisation of both criteria is not possible. Improving the first objective will cause the second to weaken and vice versa. A frequently encountered example is the need to minimise cost while simultaneously maximising performance. Cost and performance in probably all systems are two conflicting objectives. With each addition of an objective the implementation and execution becomes more complex and time consuming [41]. Evolutionary algorithms (EAs) have several characteristics that make them suitable for solving MOO problems. EAs consist of a set of probabilistic optimisation techniques that simulate the progression of natural evolution and have been in use since the 1970s [42]. The general area of EAs that deal with multiple objectives is called evolutionary MOO (EMOO) and the algorithms are referred to as multi-objective evolutionary algorithms (MOEAs). In the works of both Konak et al. [41] and Coello et al. [38] several MOEAs are listed. Many researchers prefer to customize their own algorithm by adapting strategies from existing variations of MOEAs. This is why Konak et al. [41] introduces the different components of MOEA optimisation and not the many variations available. Works by Zitzler and Thiele [43, 44] on MOEA compares several MOEAs with SPEA. MOEAs evaluated include vector evaluated genetic algorithm (VEGA), weight-sum-based genetic algorithm (WBGA), niched Pareto genetic algorithm (NPGA), non-dominated sorting genetic algorithm (NSGA). SPEA outperformed the other MOEAs by a wide margin. SPEA even outperformed some single objective EAs and is therefore preferred for MOO.

3.1.3 Existing software based simulation and optimisation tools

Three independent research works by Bernal-Augustín and Dufo-López [3], Seeling-Hochmuth [6] and Klise and Stein [45] reviewed existing hybrid RES simulation and optimisation software tools. Table 3.1 lists all the software tools evaluated and indicates for each tool it's ability to perform simulations, capability to do optimisation, whether it includes a H_2 component and it's ability to perform MOO. From all the tools listed in Table 3.1 Dymola/Modelica, HOGA, HOMER, HYBRID2, IPSYS, RETScreen and HYDROGEMS include H_2 components. From these seven, HOGA and HOMER can perform both simulation and optimisation while HYDROGEMS requires the optimisation software tool GenOpt® for optimisation. Each software tool listed in Table 3.1 optimises for cost. Many of the ones that do not optimise can perform evaluation of cost and performance for a user specified system. HOGA is the only tool that allows for MOO. The first objective however is always cost with the second selected by the user to be either CO_2 emissions or unmet load where the program will offer more than one solution as the objectives are conflicting. Most of these software tools evaluate the systems' performance based on user pre-defined component configurations. These tools are designed to evaluate hybrid system designs and allow the user to evaluate the effect on certain system characteristics

Table 3.1: Hybrid system simulation and optimisation software tools.

	ARES-II [46]	Dymola/Modelica [47]	HOGA [48]	HOMER [49]	HYBRID2 [50]	HYBRIDS [3]	HySyS [51]	INSEL [52]	IPSYS [53]	PHOTO [6]	RAPSIM [3]	RAPSYS [6]	*RETScreen*[3] [54]	SIRENE [6]	SOMES [45]	SOLSIM [3]	*HYDROGEMS*[4] [55]
Simulate	✓	✓	✓	✓	✓	✓	✓	✓	✓	✓	✓	✓	✓	✓	✓	✓	✓
Optimise			✓	✓													✓
H_2 component		✓	✓	✓	✓				✓				✓				✓
Multi-objective			✓														

by changing component sizes and control set-points. Several research works have also successfully implemented Matlab®, Simulink™ and LabView™ for simulation and optimisation [56–61].

3.2 Literature review of renewable energy system optimisation

A great deal of literature is available on RES sizing and control that include various combinations of the RE sources discussed in Chapter 2. The main concern mentioned about RE however is it's intermittency and as a result requirement for some form of auxiliary supply or storage. Many research works implement diesel-generators or grid-tie connections for back-up power. Many forms of energy storage discussed in Section 2.9 are also evaluated and implemented in literature. Optimisation techniques evaluated include traditional approaches with a growing number of literature implementing heuristic techniques. Especially GA and PSO have received much attention [4]. Fadaee and Radzi [5] give five purposes for optimisation. Defining the purpose of optimisation is crucial for the selection of optimisation objectives, decision variables and constraints. These purposes include planning, placement, design, sizing and control. Literature focussing on these five and combinations are reviewed in the next few sections.

3.2.1 Planning

Chakraborty et al. [63] presented a methodology for generation planning for integrating thermal units with wind and solar plants. The optimisation is performed using a hybrid combination of GA and PSO. It is referred to as a GA operated PSO (PSO-GA). This method speeds

[3]The H_2 component included is as a combustible fuel.

[4]Hydrogems® is only a hybrid systems library developed for the TRNSYS® and EES® environments. Optimisation is possible using the GenOpt® optimisation software [62].

up convergence to a solution. Components of the system are sized with cost being the objective. Cai et al. [64] presented an optimisation method for small-scale RE management systems, combining interval linear programming (ILP), two-stage programming (TSP) and superiority-inferiority fuzzy-stochastic programming (SI-FSP) algorithms, allowing for the reflection of several uncertainties in planning of RE management systems. The optimisation objective is the cost associated with the generation, conversion and transmission of energy. Dicorato et al. [65] employed linear programming (LP) on an energy flow model in order to evaluate contribution of distributed generation and energy efficiency applications for energy planning purposes. The objective is cost, taking into consideration both technical constraints and the constraints of policies with regards to the energy sector. Alarcon-Rodriguez et a. [66] performed a review on optimisation with regards to the planning of distributed energy sources. Distributed RE sources. The parameters to be optimised vary from location, size and type of resource. Objectives specific to optimisation with regards to planning included: cost, power line losses, minimising requirements for network expansion, energy produced, minimising the quantity and rating of network connections, back-up energy requirement and CO_2 emissions. The most common optimisation method applied is GA optimisation. Soroudi et al. [67] presented a multi-objective model for the planning when expanding distributed networks. Objectives were cost and CO_2emissions. The method used determines the optimal sizing, placement and investment dynamics. A two-stage solution is proposed, where the first, an Immune-GA, finds the Pareto optimal front, consisting of several solutions, each being a vector containing the installation decisions, like component sizes, installation site, time, etc. A second fuzzy satisfying method is utilised to find the most preferred solution from those in the Pareto optimal front. Matevosyan et al. [68] presents a method for day-ahead planning of the coordination between WT and hydro power consisting of multiple reservoirs. The objective is cost. Similarly Castronuovo and Lopes [69] presents an method to optimise the utilisation of water storage ability for improving the economic gains of wind farms. The output of the optimisation is a daily operation schedule for the WT-hydro system. Lee and Chen [70] implements PSO for optimising the coordination between the hybrid RES and a time-of-use rate user. The objective is the cost-ratio for investors.

3.2.2 Placement

Especially for wind farms the placement of each individual tower is affected by many different factors. GA optimisation for optimal wind farm layout is implemented by Grady et al. [71], Rašuo and Bengin [72], Emami and Noghreh [73] and González et al. [74]. All have the same single objective of improving some form of cost. Mustakerov and Borissova [75] implement numerical optimisation to achieve the same objective. Kusiak and Song [76] also optimise wind farm layout by using the MOEA, SPEA. The first objective is the energy output and the second objective is to minimise constraint violations. Instead of optimising wind farm layout Zhao et al. [77] optimises the electrical system layout using GA optimisation with the objective again being cost.

3.2.3 Design

Benini and Toffolo [78] proposes the mechanical design for the rotor configuration of a horizontal-axis WT using a MOO method called the genetic diversity evolution method (GeDEM). The objectives are to maximise the annual energy produced per square meter of wind park and minimise cost. Maalawi and Negm [79] implemented numerical optimisation with the same purpose but the objective is to maximise the system natural frequencies, which are advantageous for reducing steady state and transient responses of the structure being excited. Li et al. [80] focussed on optimising the gear-box ratios of a permanent-magnet wind conversion system with the objective being cost. Varun [81] implemented GA optimisation to determine the parameters of a flat plate solar air heater with the objective to maximisation of the thermal performance while Zagrouba et al. [82] also used GA optimisation to identify the parameters of a PV solar cell to determine the maximum power point tracker (MPPT) from current-voltage characteristics. The objective is to minimise the difference between the theoretical and experimental current values. Kusiak et al. [83] implemented SPEA for WT mechanical design to improve the power output and reduce drive train an tower vibrations.

3.2.4 Sizing

Some of the earlier research topics reviewed for sizing optimisation of RESs implement numerical optimisation which was common for the time. Borowy and Salameh [84] determined the optimal component sizes by using 30 years of available wind speed and irradiation data to calculate the energy generated from WT and PV components. Kellogg et al. [85] determined the optimal generation capacity and storage requirements for three types of stand-alone systems: PV-alone, WT-alone and a hybrid PV/WT system. Battery storage size was calculated for each of the configurations with a diesel-generator included as back-up and optimisation objective being cost. Results showed that a WT-alone system is the most cost effective. This is however not true for all sites and is one of the reasons why every RES require optimisation to ensure the optimal combination and type of components are selected. Ghosh [86] optimised to comparing the cost of storage. Badejani et al. [87] presented an approach for sizing based on the estimated annual power consumption, average wind speed and sun radiation. The optimal combination of components was determined in order to satisfy a specified load profile with the objective being cost. Garcia and Weisser [88] provided a combination of capacities for a WT/PV/battery system. A second optimisation method, a fixed dispatch method, evaluated several capacities and selected the cheapest. Both methods applied, optimised for cost. Ashok [89] developed a general model to find the component combination to supply a rural community in India. The objective again was cost. Both Yang et al. [90] and Diaf et al. [91] optimised a PV/WT/battery system for minimum cost. Dalton et al. [92] used HOMER and HYBRIDS to compare various stand-alone system combinations. The objective was cost. Results showed that RE components alone can satisfy the required load, while the system consisting of WT, batteries and diesel-generator components provided the solution with the lowest cost for the site which was a large hotel in Queensland, Australia. Also mentioned is that the results would be considerably different for different geographic sites and weather conditions. HOMER was also used by Shaahid and Elhadidy [93], Kenfack et al. [94] and Balamurugan et al. [95] for

techno-economic evaluation of stand-alone systems. HOMER is not an optimisation tool and only evaluates several user defined solutions by comparing them.

In the last few years heuristic optimisation techniques have become more common. Dufo-López and Bernal-Augustín [96] compared a PV/diesel-generator system with a PV only system. In both configurations battery storage was utilised to supplement the PV system. HOGA was used for simulation and optimisation implementing a GA to determine the optimal combination of the available components with the objective being cost. Koutroulis et al. [24], Senjyu et al. [97], Kalantar and Mousavi [98] and Yang et al. [99, 100] all proposed methodologies for sizing a stand-alone RES using GA optimisation and all optimised for cost. Kornelakis and Koutroulis [101] implemented the same technique with the same objective but for a grid-connected PV system. The components of a CSP system was optimised by Cabello et al. [102]. Components to be sized include the solar collector fields, thermal energy storage and the power block which is a regenerative Rankine cycle. The objective was cost. Bilal et al. [23] proposed multi-objective sizing using Pareto ranking. Objectives were cost and loss of power supply probability (LPSP). Another regularly used heuristic optimisation technique is PSO. Kaviani [103] implemented PSO for sizing a stand-alone RES. PSO is also implemented by Kornelakis and Marinakis [104], Avril et al. [105] and Boonbumroong et al. [106] for optimising RESs connected to an existing grid. In all works the objective was cost. Boonbumroong et al. [106] simulated the system using TRNSYS simulation software [107]. For optimisation the GenOpt optimisation software [62] was used. PSO was used to determine the optimal system configuration with the objective being cost.

Various other optimisation algorithms and combinations have also been attempted. Kalogirou [108] used TRNSYS to simulated a CSP plant and optimised using artificial neural networks (ANN) and GA. The data from TRNSYS is used to train the ANN and get an understanding of the relationship between the collector area and storage size. The GA optimisation is then used to find the optimal component sizes for the lowest cost. Lagorse et al. [109] performs optimisation in two stages. The GA obtains the approximate optimal combination of components with the objective being cost. Once the GA starts to converge the simplex algorithm determines the local optimum. The simplex algorithm used requires a precise starting points which is obtained from the results of the GA. Results are obtained faster with the hybrid optimisation methodology compared to GA only. GA optimisation is also implemented by Masoum et al. [110] for optimising component sizes and location from a list of possible sites for a stand alone RES. The objective is again cost. Pelet et al. [111] and Bernal-Agustín et al. [112] implements Queuing multi-objective optimiser on a grid connected RES and SPEA for a stand-alone RES respectively. Objectives for both are cost and CO_2 emissions. Mellit et al. [113] reviews the AI techniques implemented for the sizing of different PV system configurations: stand-alone, grid-connected, H_2 based and hybrid WT/PV systems. AI techniques evaluated include ANN, fuzzy logic (FL), GA, wavelet transform and a number of hybrid techniques: ANN-GA and GA-FL. The same author in [114] proposed an ANN-GA model for the sizing of a stand-alone RES. The method develops a sizing curve from which the optimal number of PV panels and battery size can be determined with the objective being cost. Zangeneh et al. [115] proposed a mechanism to site and size RE sources. A modified version of NSGA is implemented (NSGA-II). Objectives cost and maximising the grant function as a pollution not emanated. Katsigiannis et al. [116] also implements NSGA-II for small-scale stand-alone system optimisation. NSGA-II optimisation

is applied with the objectives being cost and CO_2 emissions. del Real et al. [117] presents mixed integer quadratic programming optimisation for sizing a stand-alone RES. The objective is again cost. Belfkira et al. [118, 119] in two different papers present the sizing optimisation of a stand-alone RES using the dividing rectangles (DIRECT) algorithm with the objective being cost. The DIRECT algorithm is first introduced by Jones et al. [120]. DIRECT optimisation is a modification of the deterministic Lipschitzian optimisation algorithm.

3.2.5 Control

Dufo-López and Bernal-Augustín [121] presents a strategy implementing GA optimisation of a hybrid RES. The strategy optimizes the control of the hybrid system with the objective of minimizing system lifetime cost. Kongnam and Nuchprayoon [122] implements PSO with the objective of maximising the energy yield. Niknam et al. [123] presents a multi-objective fuzzy self adaptive hybrid PSO algorithm. The objectives are minimising the total electrical energy losses, minimising the total electrical energy cost and minimising CO_2 emissions. The energy losses evaluated are those that arise from the distribution network.

3.2.6 Combined placement and sizing

Not uncommon was the combination of purposes such as sizing and placement. Both Celli et al. [124] and Niknam et al. [125] implements MOO for the placement and sizing of RE sources as part of an existing grid.and ϵ-constrained MOGA and modified honey bee mating optimisation (MHBMO) methods are applied respectively to achieve similar objectives. Objectives are cost, CO_2 emissions and energy losses. In both works the losses considered are not due to the RES components but as a result of I^2R losses from the placement of the components in the electrical grid.

3.2.7 Combined sizing and control

More relevant is the combined sizing and control optimisation. Seeling-Hochmuth [6, 7] developed a new method for the sizing and control of a stand-alone hybrid RES. GA optimisation is employed with the objective being to minimise the combination of life cycle cost per kWh and penalty cost per kWh for unmet load and also includes the fuel cost of the diesel-generator. Although it might seem to be multiple objectives these are all cost related objectives combined into a single cost minimising objective. The algorithm is divided into a main and sub-algorithm dealing with sizing and control optimisation respectively. The proposed method incorporates operating strategy and sizing optimisation due to their interdependency. Similarly SPEA as a main algorithm and GA as a secondary algorithm is implemented by Dufo-López and Bernal-Augustín [8] and Bernal-Agustín and Dufo-López [9] for the multi-objective sizing and control optimisation of a stand-alone hybrid RES. The objectives are cost, CO_2 emissions and unmet load. Bernal-Agustín and Dufo-López [126] also present a single objective GA optimisation for sizing and control with the objective only focussed on cost. Similarly Hakimi and Moghaddas-

Tafreshi [127] implements PSO with the objective again only focussing on cost. Saif et al. [128] proposes multi-objective linear programming (MOLP) with the same purpose of sizing and control optimisation and the same objectives of cost and CO_2 emissions.

3.2.8 Interdependent sizing and control optimisation

In Section 3.2 it is shown that there are many different applications for optimisation algorithms of a hybrid RES ranging from various levels of mechanical design, electrical network layout, component geographic layout, weather forecasting, sizing and control. For optimising the performance of a hybrid RES especially the sizing and control optimisation have been identified as very important. Seeling-Hochmuth [6, 7] highlights the importance and also the interdependence of sizing and control optimisation and argues that in order to achieve the advantages possible with a hybrid RES, interdependent sizing and control optimisation is a necessity. Similarly Dufo-López and Bernal-Augustín [96] emphasise the necessity and implements interdependent sizing and control. The first approach to interdependent sizing and control optimisation is to group all sizing and control decision variables together and optimise sizing and control decision variables simultaneously as a single decision variable vector. This approach results in a very large search spaces increasing the optimisation time and reduces accuracy as a result of a reduction in the effectiveness of the optimisation operators. The more common approach from literature, when implementing interdependent sizing and control optimisation, is to split the control and sizing into a sizing decision variable vector and a control decision variable vector and have them optimised in cascade. Control optimisation is done first for a single objective and is then followed by the sizing optimisation which evaluates all objectives. This approach was first implemented by Dufo-López and Bernal-Augustín [96] and has since been repeated in literature [8, 9, 121, 126]. For sizing the objectives evaluated are cost, CO_2 emissions and unmet load, while control is only evaluated for one objective, cost, with a different cost objective function used for sizing and control optimisation.

3.3 Conclusion

More than 40 % of the literature reviewed in the field of RE implement a GA and a large portion implement PSO. This finding supports the result from Fadaee and Radzi [5] that GA and PSO are the most promising and useful methods for hybrid RES optimisation. A comparison study by Angeline [39] between EA and PSO conclude that PSO often finds near optimum solutions faster than EAs, but that EAs achieves better fitness in almost all scenarios evaluated. A possible application for PSO would be on-line optimisation where speed takes preference over accuracy. For optimal design which is achieved off-line the EA is preferred. Approximately 25 % of the work reviewed evaluate multiple objectives. All of these have cost as one of the objectives, with 44 % of these having CO_2 as a second objective. The most commonly implemented MOEA is the SPEA. Coello et al. [38] refers to SPEA as the most efficient MOO method and in comparison tests with other MOO methods yields the best results. Bernal-Augustín et al. [112] implemented SPEA for the first time on a stand-alone RES consisting of wind and PV sources, battery storage and a back-up diesel-generator. The objectives were cost and CO_2 emissions

for the sizing and for the control only cost. In conclusion, with regards to performance, the GA and SPEA are the best performing optimisation methods for single objective optimisation and MOO respectively.

Chapter 4

Modelling

This chapter describes the component models of the small-scale stand-alone hybrid RE H_2 production system. The chapter provides a discussion on the models' requirements which is followed by detail descriptions of the individual component models. Individual component models are developed for the weather input data for profiles of the solar irradiance and wind speed, a PV module, a WT generator, a PEM electrolyser cell, a LAB cell and power conversion devices (PCDs). Next a description of the system power management controller is provided which is followed by a discussion on the battery power management controller. The chapter concludes with a conclusion of the modelling chapter.

4.1 Introduction

An illustration of the small-scale stand-alone RE H_2 system used for this study is shown in Fig. 4.1. System design, analysis and optimisation requires a mathematical model for each of the individual system components [129]. The evaluated system consists of RE sources selected for reasons discussed in Section 2 to be wind energy and direct solar energy using PV technology. For H_2 generation the PEM electrolyser is selected for reasons provided in Section 2.9.1. Due to the intermittent sources and certain characteristics of the PEM electrolyser an energy storage medium serving as a buffer is selected to be LABs for reasons discussed in Section 2.9. Additional components include the power conditioning equipment in the form of MPPT, DC to DC converters (DC/DC) and battery charge controllers (CC). Wind speed and solar irradiation resources are also to be modelled. Individual components are modelled as modular system components. These models are required to be generic for ease of implementation with the optimisation algorithm while maintaining certain required characteristics.

4.2 Model requirements

The goal of modelling the system is to simulate important component characteristics required to perform combined sizing and control optimisation. A set of models taking into account

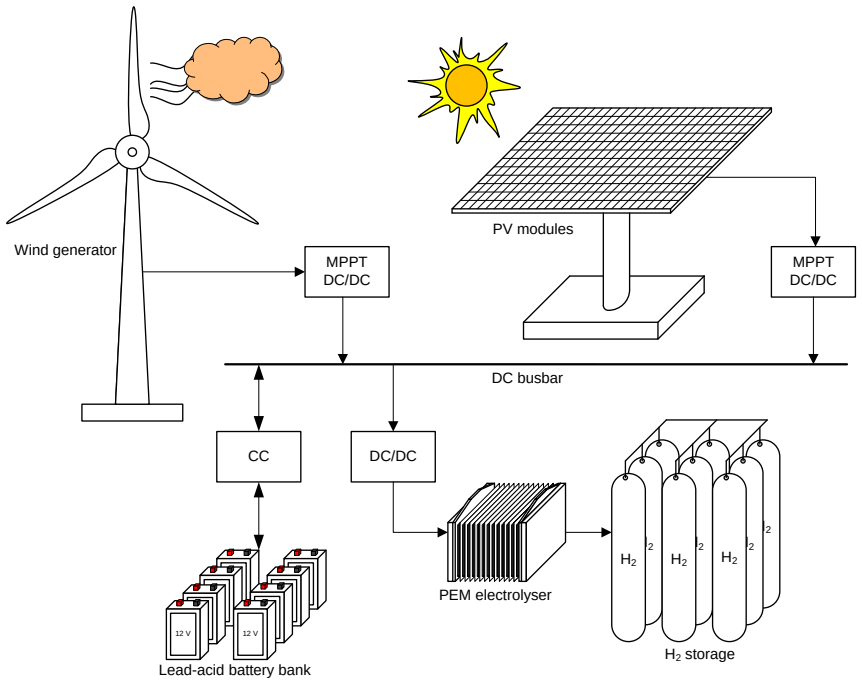

Figure 4.1: Schematic of a small-scale stand-alone hybrid RE hydrogen system.

certain dynamic and transient responses are required to achieve this. Necessary simplicity is required to ensure that each model is generic. For the optimisation to be discussed later in Chapter 6 efficiency and reliability are important and all characteristics that have an effect on efficiency and reliability should be included. Detail power flow simulation for the purpose of control system development to improve efficiency and reliability requires certain identified non-linear characteristics to be modelled sufficiently. From the literature reviewed in Chapter 3 both LABs and PEM electrolysers have non-linear characteristics as a function of voltage level, operating current and temperature. Reliability, in terms of degradation, is largely determined by intermittent operation.

LABs are designed and used for backup power and for starting engines. The first application experiences low cycles with a high depth of discharge (DOD) whereas the second application experiences a high number of cycles and a low DOD resulting in both having primarily single charge and discharge cycles. In intermittent RE applications the batteries experiences a high DOD and incremental charge and discharge cycles resulting in a high number of cycles. LABs have a limited number of cycles at specific DODs. Fig. 4.2 shows a graph of a typical LAB's cycle life vs. DOD at a $C/20$ *discharge rate*[1] [9]. Number of cycles increases exponentially with lower DOD. LAB efficiencies are affected by the cell operating temperature. Capacity increases with an increase in temperature [130]. Although battery temperature is not a controlled parameter, battery temperature has a direct influence on the battery efficiency and reliability and as a result the thermal effects need to be accounted for. Internal resistance changes as a function of state of charge (SOC). Internal resistance increases at high SOC for a charge cycle and at low

[1] $C/20$ refers to the current required to discharge a battery of capacity C [Ah] in 20 hours. $C/10$ is the current required to discharge the battery in 10 hours

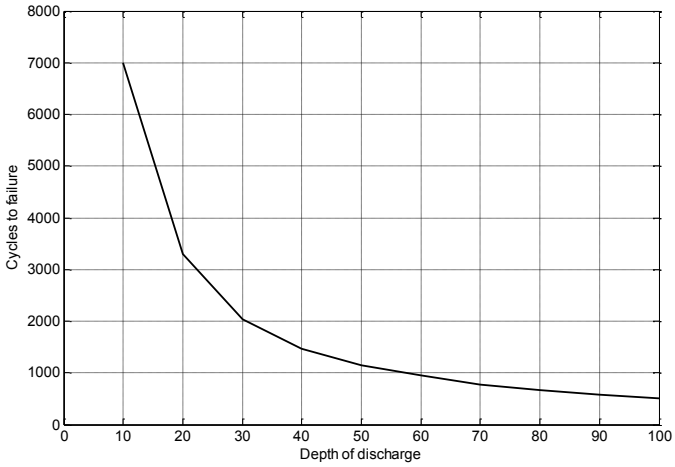

Figure 4.2: Lead-acid battery cycle life vs. DOD.

SOC for a discharge cycle. Internal resistance also changes as a results of the magnitude of the charge and discharge currents [131]. Batteries designed for intermittent RESs does not yet exist and as a result current batteries operate at a reduced efficiency [29]. To improve efficiency and reliability the power management strategy between the PEM electrolyser and LAB bank must be managed intelligently for improving efficiency and reliability. A method proposed to improve both efficiency and reliability is to operate two banks independently. A split battery bank will allow one battery bank to charge only and the second one to discharge only. Once the charging bank is full the assignments are switched. In this methodology each battery bank is charged to an desired level before discharged again, thus avoiding the incremental charge-discharge cycles.

Barbir [34] addresses implementation issues of PEM electrolysers in intermittent RESs. At low loads the permeation of H_2 and O_2 through the membrane might be higher than each gas' production rate resulting in a possible hazardous condition when H_2 mixes with oxygen[2] (O^2). A minimum of 5% of the rated power is suggested by Garcia-Valverde et al. [56] to avoid this from happening. PEM electrolysers are most efficient at a specific operating temperature. With intermittent operation the temperature fluctuates resulting in the unit rarely operating at the optimal temperature. Proper power management will ensure that the lead-acid BB and the PEM electrolyser are operated at their efficient. A higher electrolyser cell voltage results in a higher H_2 production rate. Typical cell voltage is around 2 V per cell. A lower voltage can be selected if efficiency is more important than cost [34]. A further requirement for the PEM electrolyser is the performance degradation with time. Anderson et al. [132] shows that a PEM electrolyser voltage increases by 20-50 μV/h for the first few thousand hours and then levels of to less than 3 μV/h thereafter.

DC/DC voltage regulators are designed with efficiencies as high as 95%. These high efficiencies are however only achieved in a very narrow power range [34]. Converter efficiency is a function of the power level and input voltage. With RE sources the supply of power and

[2] H_2 lower and upper flammability levels are 4% and 75% respectively.

voltages are highly variable and will operate at 95% efficiency for limited time periods. The DC/DC converter model should show the non-linear relationship of efficiency as a function of power level and input voltage. In this work a converter refers to any power electronics device, i.e. inverter, rectifier, MPPT and CCs.

Both PV and WT energy conversion devices have non-linear current-voltage characteristics. The power management strategy for these two intermittent RE sources are to extract the maximum power continuously. The control of these units are limited to the MPPT that should ensure that these units operate at the optimal voltage levels and are independent of the system control strategy. They merely provide information to the control strategy in terms of available power. The optimal combination of PV module and WT is however one of the optimisation parameters. The dynamic characteristics of these components are necessary to ensure that the optimal combination is chosen by the sizing optimisation strategy. The mathematical models for the individual components are described in detail the next section taking into consideration the required characteristics.

4.3 System component models

Validated models are obtained from literature and selected in terms of characteristics and dynamics required. Validation and verification is done in Chapter 5 by comparison with the original validated model. Individual component models detail is given in the next couple of sections. The individual models and complete system are developed and implemented in the Simulink^{TM} environment.

4.3.1 Weather input data

Designing a RES is a difficult task as the Re sources, in this study solar radiation and wind, are stochastic. Solar has a large deterministic component since the position of the sun and also the energy from the sun reaching the earth's surface can be accurately modelled. Solar energy is however only available during daylight hours requiring storage to supply energy requirements during the night time. Due to other weather phenomenon (i.e. rain, cloud cover.), which can not be precisely predicted, the input is considered a random fluctuating source. Wind resources are more stochastic than solar with the only predictability of wind is that the wind will blow, but when and how strong is not predictable. This stochastic nature of these RE sources are the major issue faced by RES designers. Although solar and wind energy both show some form of daily and seasonal average values for different geographic sites, the values can vary significantly at different times which is why comparing site resources in terms of time series data is not done. Availability of time series data in the resolution required is a big problem as it is not always available. For this reason average data values are analysed and fit to a distribution function which is used to produce a time series input signal that is suitable for use in this application. A variety of distribution functions are available that allow an entire site's measured data to be described in a few parameters. Distribution functions allow sites, times and seasons to be compared [22].

Solar irradiance

Solar irradiance model implemented in (4.1) to (4.11) is from Duffie and Beckman [133] which is also used computer simulation tool Hybrid2 [134]. Much detail about the model is omitted and can be found in [133]. The first concept to clarify is that of extraterrestrial radiation. Extraterrestrial radiation is defined as the theoretical upper limit for solar radiation available at the earth's surface. The calculation of extraterrestrial radiation is given by [133]

$$G_{on} = G_{sc}\left(1 + 0.033\cos\left(\frac{360n}{365}\right)\right), \tag{4.1}$$

where G_{on} is the extraterrestrial radiation [W/m^2], G_{sc} is the *solar radiation constant*[3] estimated at 1367 W/m^2 [133] and n is the day of the year. Fig. 4.3 illustrates the solar system orientation with all the angles involved [133]. All angles and calculations are in units of degrees. The

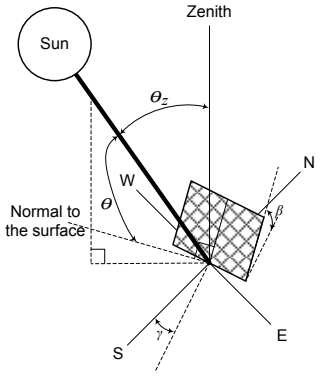

Figure 4.3: Solar radiation angles on a tilted surface in the Northern hemisphere.

angles shown in Fig. 4.3 are defined as:

- *Slope*, β - Angle between the plane of the surface and the horizontal. ($0 \leq \beta \leq 180$, although a β >90 implies a down facing surface).
- *Surface azimuth*, γ - Angle between the projection of the beam radiation on the horizontal plane and the normal to the surface with zero due south, east negative and west positive.
- *Angle of incidence*, θ - Angle between a line perpendicular to the surface and the beam radiation on the surface.
- *Zenith angle*, θ_z - Angle between the beam radiation and a line perpendicular to the earth's surface. For a horizontal surface this is also the angle of incidence, that is when $\beta = 0$.

Additional angles of importance not illustrated in Fig. 4.3 include:

[3]Energy from the sun received on a unit area perpendicular to radiation propagation at the mean distance between the sun and the earth [133].

- *Latitude*, ϕ - Angular location of the site, north (positive) or south (negative) of the equator, $-90 degree \leq \phi \leq 90 degree$.
- *Declination*, δ - Angular position of the sun with respect to the plane of the equator, at solar noon on each day (n), $-23.45 degree \leq \delta \leq 23.45 degree$
- *Hour angle*, ω - Angular displacement of the sun, east or west of the local meridian from the rotation of the earth on it's axis at $15 degree$ per hour (0.25 degree per minute). Morning negative and afternoon positive.

Solar time is calculated using

$$t_{sol} = t_{std} + 4\left(L_{stdm} - L_{loc}\right) + E, \tag{4.2}$$

where t_{sol} is the calculated solar time [minute], t_{std} is the standard time of the local time zone [minute], L_{stdm} is the standard meridian for the local time zone [^{o} west] and L_{loc} is the longitude of the site [^{o} west]. E corrects for difference between the mean and true solar times and is given by

$$E = 2.292\left(0.0075 + 0.1868\cos B - 3.2077\sin B - 1.4615\cos 2B - 4.089\sin 2B\right), \tag{4.3}$$

where B is given by

$$B = (n-1)\frac{360}{365}. \tag{4.4}$$

The sun's angular displacement per minute is calculated from

$$\omega = (t_{sol} - 720)\,0.25. \tag{4.5}$$

The sun's declination for each day of the year, n, is calculated from.

$$\delta = 23.45\sin\left(360\frac{284+n}{365}\right) \tag{4.6}$$

The angles given are related to the angle of incidence by the relationship given in

$$\begin{aligned}\cos\theta = {} & \sin\delta\sin\phi\cos\beta - \sin\delta\cos\phi\sin\beta\cos\gamma \\ & + \cos\delta\cos\phi\cos\beta\cos\omega + \cos\delta\sin\phi\sin\beta\cos\gamma\cos\omega \\ & + \cos\delta\sin\beta\sin\gamma\sin\omega\end{aligned} \tag{4.7}$$

For a fixed angle system in the Northern hemisphere, γ is equal to 0 degree from south and in the Southern hemisphere 180 degree (-180 degree) from south. β is dependent on the latitude and energy profile requirements. Using $\gamma = \pm 180^o$ for the Southern hemisphere reduces (4.7) to

$$\cos\theta = \cos(\phi+\beta)\cos\delta\cos\omega + \sin(\phi+\beta)\sin\delta. \tag{4.8}$$

Using $\gamma = \pm 0^o$ for the Northern hemisphere reduces (4.7) to

$$\cos\theta = \cos(\phi+\beta)\cos\delta\cos\omega + \sin(\phi+\beta)\sin\delta. \tag{4.9}$$

The zenith angle is determined from (4.8) or (4.9) by setting $\beta = 0$ degree. The relationship of θ_z with the angles of interest is given by

$$\cos\theta_z = \cos\phi\cos\delta\cos\omega + \sin\phi\sin\delta. \tag{4.10}$$

Including the zenith angle to (4.1) gives

$$G_o = G_{sc}\left(1 + 0.033\cos\left(\frac{360n}{365}\right)\right)\cos\theta_z, \tag{4.11}$$

where G_o is the solar radiation incident on a horizontal surface outside the atmosphere.

Radiation on a tilted surface ($\beta > 0$) is determined by the HDKR model named after it's developers: Hay, Davies, Klucher and Reindl and is described in detail in Duffie and Beckman [133] and also implemented in the computer simulation tool Hybrid 2 [134]. Only equations and sufficeint information to understand them is provided here. For detail about the model refer to [133]. Total radiation on a tilted surface is given by

$$G_T = (G_b + G_d A_i)\, R_b = G_d\,(1 - A_i)\left(\frac{1+\cos\beta}{2}\right) + G\rho_g\left(\frac{1-\cos\beta}{2}\right), \tag{4.12}$$

where G_T is the total radiation on a tilted surface [W/m^2] with slop β, G_b is the beam radiation [w/m^2], G_d is the diffuse radiation, A_i is the anisotropy index, R_b is the ratio of beam radiation on a tilted surface to that on a horizontal surface and ρ_g is the ground reflectance coefficient. A_i is determined by [133]

$$A_i = \frac{G_b}{G_0}, \tag{4.13}$$

and R_b is determined using

$$R_b = \frac{\cos\theta}{\cos\theta_z}. \tag{4.14}$$

Thevenard and Haddad [135] provides a summary given in Table 4.1 of estimates for ground reflectance coefficients (ρ_g) obtained from different sources for various ground surfaces in the absence of snow.

Table 4.1: Average ground reflectivity estimates.

Ground cover	**Reflectivity, ρ_g**
Water (large angels of incidence)	0.07
Coniferous forest	0.07
Bituminous and gravel roof	0.13
Dry bare ground	0.2
Weathered concrete	0.22
Green grass	0.26
Dry grassland	0.2-0.3
Desert sand	0.4
Light building surfaces	0.6

As implemented in this work, the clearness index k_T is defined as the ratio of measured data (G) to G_o from 4.11. Measured and calculated data provide a time series of clearness indices that are analysed and fitted to a fractional time distribution function which provides parameters easily incorporated into a model. For the clearness index Bendt et al. [136] proposes equations

for the clearness index distributions as functions of the average monthly clearness index ($\bar{K}_T$), and have good correlation to the measured values obtained from Liu and Jordan [137]. The fractional time distribution monthly clearness indices from [136] are given by

$$f\left(K_T\right) = \frac{\exp\left(\gamma K_{T,min}\right) - \exp\left(\gamma K_T\right)}{\exp\left(\gamma K_{T,min}\right) - \exp\left(\gamma K_{T,max}\right)}, \tag{4.15}$$

where γ is calculated from

$$\gamma = -1.498 + \frac{1.184\xi - 27.182\exp\left(-1.5\xi\right)}{K_{T,max} - K_{T,min}}, \tag{4.16}$$

and ξ is calculated from

$$\xi = \frac{K_{T,max} - K_{T,min}}{K_{T,max} - \bar{K}_T}. \tag{4.17}$$

Bendt et al. [136] proposes a value for $K_{T,min} = 0.05$ while $K_{T,max}$ is determined by [138]

$$K_{T,max} = 0.6313 + 0.267\bar{K}_T - 11.9\left(\bar{K}_T - 0.75\right)^8. \tag{4.18}$$

Although these equations are provided to give monthly clearness index, the hourly clearness index (k_T) can be replaced and the equations will approximate the distribution of hourly clearness index [133]. Each site thus only requires a value for the monthly clearness index, $\bar{K}_T$, to approximate horizontal solar radiation. A value for k_T is determined from the distribution and diffuse radiation component G_d and G. Diffuse radiation is derived from

$$\frac{G_d}{G} = \left\{ \begin{array}{ll} 1 - 0.09k_T & \text{for } k_T \leq 0.22 \\ 0.9511 - 0.1604k_T + 4.388k_T^2 - 16.638k_T^3 + 12.336k_T^4 & \text{for } 0.22 < k_T \leq 0.8 \\ 0.165 & \text{for } k_T > 0.8 \end{array} \right\} \tag{4.19}$$

as given by Erbs et al. [139]. Beam radiation (G_b) is calculated using [134]

$$G_b = G - G_d. \tag{4.20}$$

Wind

Similar to the solar radiation model wind data is presented as a probability distribution function. For the distribution of wind velocities the most widely accepted distribution function for wind speed distributions is the Weibull distribution function which fits daily wind distributions quite well and is utilised by the majority of available research works [74, 76, 122]. The Weibull function is given by

$$f\left(v_w\right) = \frac{k}{c}\left(\frac{v_w}{c}\right)^{(k-1)} e^{-\left(\frac{v_w}{c}\right)^k}, \tag{4.21}$$

where k is the shape factor and c is the scale factor [m/s]. k is approximated (for $1 \leq k \leq 10$) by [134].

$$k = \left(\frac{\sigma}{\bar{v}_w}\right)^{-1.086}, \tag{4.22}$$

where σ is the long term standard deviation and $\bar{v}_w$ is the long term mean for the wind velocity. c is approximated by [134].

$$c = \frac{\bar{v}_w}{\Gamma\left(1+\frac{1}{k}\right)}, \tag{4.23}$$

where $\Gamma(\cdot)$ is the *gamma function*[4]. From average monthly data, shape and scale factors given in 4.22 and 4.23 respectively, are determined. These values are used to generate daily time series data distributions for wind speeds (v_w) from the Weibull 4.21 coefficients. The *event based random number generator* function in Simulink™ is used to generate daily times series distributions from these coefficients. In this manner daily wind distributions can be generated from monthly average wind speed values. Additionally sites can be compared using the Weibull distribution 4.21.

4.3.2 Photovoltaic modules

The model PV model used is from Duffie and Beckman [133] with some refinement done by Ulleberg [140], Wang [141] and Kou et al. [142]. The model is set-up for a specific PV module. PV systems consist of multiple PV modules in series and parallel. To be used as a general model, the number of PV modules in series and parallel are varied to change the PV peak rated power. For generalisation of the model the PV modules in series and parallel are simply changed to vary the PV system input power. Only sufficient detail is provided. For more detail refer to [133]. The relationship between the PV module output voltage (V_{PV}) and current (I_{PV}) is given by

$$I_{PV} = I_L - I_D = I_L - I_o\left[\exp(\frac{V_{PV}+I_{PV}R_s}{\alpha})-1\right], \tag{4.24}$$

where I_L is the light current [A], I_o is the diode reverse saturation current [A], V_{PV} is the operating voltage [V], I_{PV} is the operating current [A], R_s is the series resistance [ohm] and α is the thermal voltage timing compilation factor [V]. Writing (4.24) for V_{PV} in terms of I_{PV} gives

$$V_{PV} = \alpha \ln\left[\frac{I_L - I_{PV}}{I_o}+1\right] - I_{PV}R_s. \tag{4.25}$$

The power output of the PV module is given by

$$P_{PV} = V_{PV}I_{PV}. \tag{4.26}$$

The four parameters I_L, I_o, R_s and α are determined from manufacturer provided operating points at *standard conditions*[5]. These are the open-circuit voltage ($V_{oc,std}$), short-circuit current ($I_{sc,std}$), maximum power point ($V_{mp,std}$, $I_{mp,std}$), the open-circuit voltage temperature coefficient (μ_{Voc}) and the short-circuit current temperature coefficient (μ_{Isc}). Fig. 4.4 illustrates these operating points on typical V-I and power curves of a typical PV module [133].

The light current (I_L), is given by [143]

$$I_L = \frac{S}{S_{std}}\left[I_{L,std} + \mu_{Isc}\left(T_c - T_{c,std}\right)\right], \tag{4.27}$$

[4]The gamma function is defined by $\Gamma(n) = (n-1)!$ if n is a positive integer.
[5]Standard conditions: $S_{std} = 1000W/m^2$ and $T_{std} = 25degreeC$

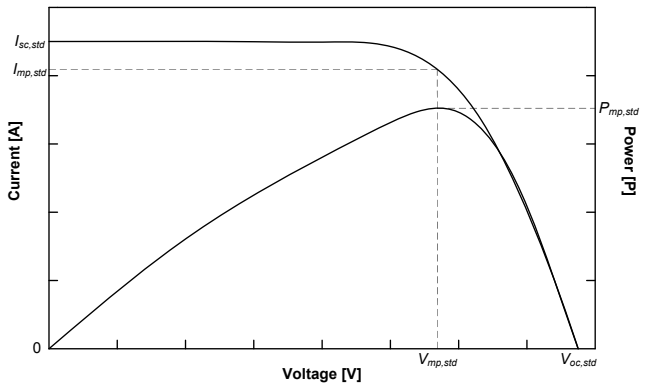

Figure 4.4: PV module V-I characteristic and power curve.

where S is the solar irradiance [W/m^2] and is equal to G_T given in 4.12, S_{std} is the solar irradiance at standard conditions [1000 W/m^2], $I_{L,std}$ is the light current at standard conditions [A], μ_{Isc} is the short-circuit current temperature coefficient [A/^{o}C], T_c is the cell temperature [^{o}C] and $T_{c,std}$ is the temperature at standard conditions [25 ^{o}C].

Diode reverse saturation current (I_o) is given by [143]

$$I_o = I_{o,std}\left(\frac{T_c + 273}{T_{c,std} + 273}\right)^3 \exp\left[\frac{\epsilon N_s}{\alpha_{std}}\left(1 - \frac{T_{c,std} + 723}{T_c + 273}\right)\right], \tag{4.28}$$

where $I_{o,std}$ is the diode reverse saturation current at standard conditions [A], ϵ is the band gap energy of the material (1.12 eV for silicon materials [133]), N_s is the number of cells in series of a PV module multiplied by the number of modules in series of a PV array and α_{std} is the thermal voltage timing compilation factor at standard conditions [V]. At open-circuit conditions the diode reverse saturation current at standard conditions is given by

$$I_{o,std} = I_{L,std} \exp\left(-\frac{V_{oc,std}}{\alpha_{std}}\right). \tag{4.29}$$

The thermal voltage timing compilation factor (α) is given by [143]

$$\alpha = \alpha_{std}\frac{T_c + 273}{T_{c,std} + 273}. \tag{4.30}$$

Differentiating $V_{oc,std}$ with respect to T in (4.29) and using (4.28), (4.30) and the manufacturer provided short circuit current temperature coefficient (mu_{Isc}) gives

$$\alpha_{std} = \frac{\mu_{Voc}\left(T_{c,std} + 273\right) - V_{oc,std} + \epsilon N_s}{\frac{\mu_{Isc}(T_{c,std}+273)}{I_{L,std}} - 3}. \tag{4.31}$$

The series resistance (R_s) through substitution is derived from (4.25) [133] and is given by

$$R_{s,std} = \frac{\alpha_{std}\ln\left(1 - \frac{I_{mp,std}}{I_{L,std}}\right) - V_{mp,std} + V_{oc,std}}{I_{mp,std}} \tag{4.32}$$

These four parameters I_L, I_o, R_s and α are used to determine the module current-voltage characteristic in (4.25) at different conditions. The power supplied by the PV modules is determined by 4.26.

Thermal model

PV module cell temperature is a function of ambient temperature, solar irradiance and output power. The thermal model used is fro Ulleberg [140]. The model requires little information about the design of the PV model and is therefore a good approximation for a generic PV model. Losses to the surroundings include convection, radiation and conduction through the framework. All these losses are combined in a single loss coefficient. The lumped thermal model is given by [140, 141]

$$C_{PV}\frac{\mathrm{d}T_c}{\mathrm{d}t} = k_{in,PV}S - \frac{V_{PV}I_{PV}}{A_{PV}} - k_{loss}\left(T_c - T_a\right), \tag{4.33}$$

where C_{PV} is the PV modules heat capacity per unit area [J/^{o}C$\cdot$ m^2], $k_{in,PV}$ is the PV cell transmittance-adsorption product, k_{loss} is the overall heat loss coefficient [W/^{o}C$\cdot$ m^2], T_a is the ambient temperature [^{o}C] and A_{PV} is the PV module effective area [m^2].

Maximum power point tracking

A short-circuit current based MPPT (CMPPT) method from Wang [141] is used. This method relies on a strong linear relationship between I_{sc} and I_{mp}. In the model I_{sc} and I_L are made equal and it is assumed true for all other conditions. Fig. 4.5 gives the relationship between I_L and I_{mp} for 200 W/m^2 to 1000 W/m^2 different cell temperatures The linear relationship between I_L

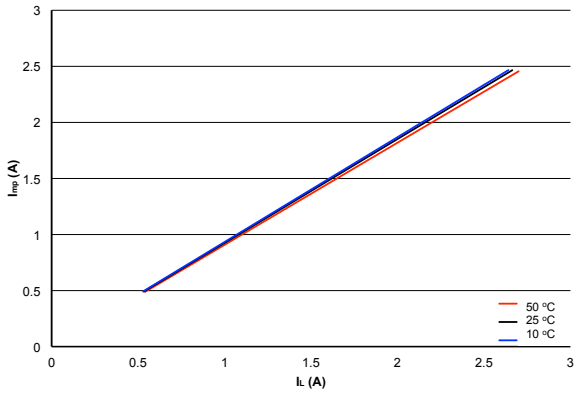

Figure 4.5: PV module I_L vs. I_{mp} linear relationship.

and I_{mp} is given by

$$I_{mp} = k_{CMPPT} \times I_{sc}, \tag{4.34}$$

where k_{CMPPT} is the slope of the linear function. Fig. 4.5 shows a small difference of slopes for the different cell temperature values. Fig. 4.6 plots these differences in slope against temperature. A linear fit for k_{CMPPT} is included. k_{CMPPT} is therefore a function of temperature given

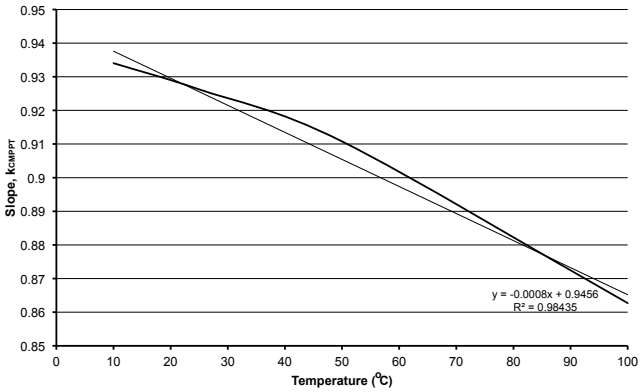

Figure 4.6: PV module I_{mp}/I_L slope vs. cell temperature.

by

$$k_{CMPPT} = -0.0008T_c + 0.9456. \tag{4.35}$$

Substitution of (4.34) into (4.35) gives the reference signal used to control the PV module current (I_{PV}).

4.3.3 Wind turbine generator

WT generators convert kinetic energy from the wind to usable electric energy. Designing individual components for a WT generator requires major component modelling such as the wind model, the turbine model, the shaft and gearbox model, the generator model and the control system mode. This study is mostly only concerned with the power flow from the WT and does not require these complicated detail mechanical models of a WT generator. WT generators are less affected by environmental conditions and as a result a very simple generic model can be used. The power produced by the WT generator is dependent on the wind's kinetic energy given by [144]

$$E_w = \frac{1}{2} m_w v_w^2, \tag{4.36}$$

where E_w is the kinetic energy of the moving air masses [J], m_w is the air mass [kg] and v_w is the wind velocity [m/s]. The air mass flowing through a particular surface is calculated using

$$m_w = A_{turbine} \rho_w v_w, \tag{4.37}$$

where $A_{turbine}$ is the swept area of the turbine [m^2] and ρ_w is the density of air [kg/m^3]. The power in the wind is given by

$$P_w = \frac{1}{2} A_{turbine} \rho_w v_w^3, \tag{4.38}$$

where P_w is the maximum power available in the wind [W]. It is however not possible to convert all the power available in the wind to usable power. Actual power that can be extracted from the wind and converted to mechanical energy is given by

$$P_{WT} = \frac{1}{2} A_{turbine} \rho_w v_w \left(v_u^2 - v_d^2 \right), \tag{4.39}$$

where P_{WT} is the power extracted from the wind by the rotor blades [W], v_u is the upstream wind velocity [m/s] and v_d^2 is the downstream wind velocity [m/s]. P_{WT} is ultimately given by

$$P_{WT} = \frac{1}{2} C_p A_{turbine} \rho_w v_u^3, \tag{4.40}$$

where C_p is the fraction of upstream wind power captured by the rotor blades. C_p is called the Betz limit and has a maximum possible value of $C_p = 0.593$ [144]. In practice the best of WT designs give maximum C_p values between 0.35 and 0.45. All commercially available WTs are tested and characterised with the power curves available providing measured output power of the WT generator as a function of the wind speed.

Most WTs are designed to have a maximum power output at around 15 m/s. Sites with higher average wind speeds are rare while sites with weaker wind speeds are not considered economically viable. At wind speeds higher than the manufacturer rated wind speed the excess energy is dumped to avoid turbine damage. Methods to achieve this include blade pitch control, stall control and for small WTs yaw orientation control [145]. Yaw orientation control is a simple method for small-scale units that changes the direction of the wind entering the rotor by yawing the rotor out of the wind to limit the power. For orientation control self aligning free yaw control is implemented for small stand-alone rural systems [145].

For the WT model, the normalised power vs wind speed function of an existing Hummer H4.8-3 kW [146] WT is used. Multiplying the rated power with the normalised function provides the power vs. wind speed functions for other small-scale WTs within acceptable tolerances. The normalised power curve from the Hummer H4.8-3 kW WT is given in Fig. 4.7. The normalised

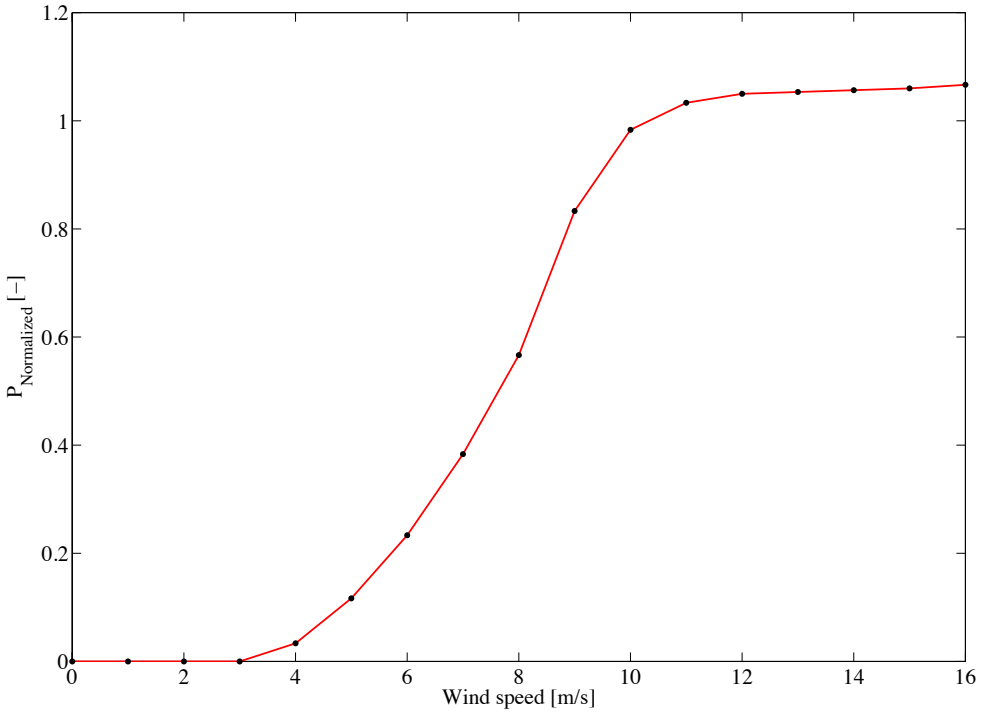

Figure 4.7: Normalised turbine power as a function of wind speed.

function is implemented in a lookup table with wind speed as the input and normalised power as an output. This output is multiplied with the WT power rating to obtain the output power from the WT. The characteristics of the WT is assumed to be included in the power vs. wind speed function.

4.3.4 Proton exchange membrane electrolyser

The PEM electrolyser dynamic model implemented is from Görgün [59]. This model considers temperature but does not include a dynamic model for temperature. The dynamic temperature model by Lebbal and Lecoeuche [147] is incorporated. Sufficient detail is given on the model. For detailed discussions refer to [59] and [147].

Voltage model

The electrolyser voltage is given by [59]

$$V_{ely} = V_{rev} + \eta_a - \eta_c + \eta_{ion} + \eta_{ohm} + \eta_{con}, \tag{4.41}$$

where V_{ely} is the applied electrolyser voltage, V_{rev} is the reversible potential or open circuit voltage, η_a and η_c are the activation over-potentials at the anode and cathode respectively representing tshe electrochemical kinetic behaviour, η_{ion} is the ionic over-potential due to the resistance of proton transfer through the membrane, η_{ohm} is the ohmic losses from the resistance of the electrodes, η_{con} is the concentration over-potential resulting from the gas and water concentration and propagation near the electrodes. These potentials are illustrated in Fig. 4.8 [56]. The concentration over-potential (η_{con}) only contribute losses at high current densities outside

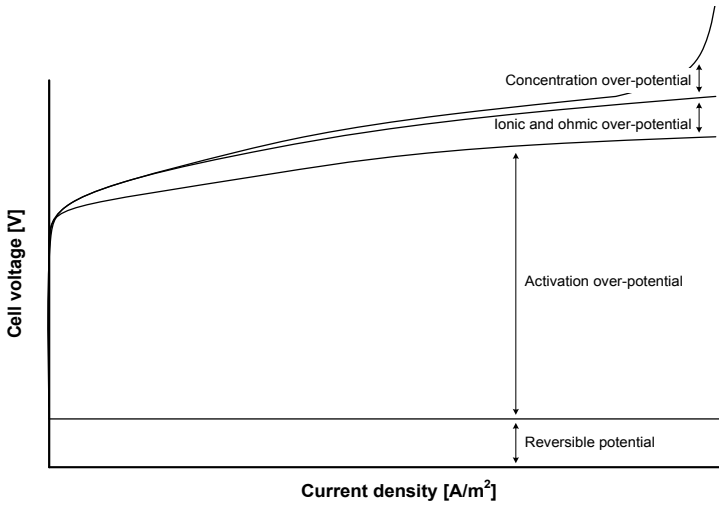

Figure 4.8: Simplified cross-section of a PEM electrolyser.

normal operation and is ignored [59]. Over-potentials caused by ohmic losses (η_{ohm}) is from

electrode support material, electrode materials, contact resistances and end plates. η_{ohm} is considered negligible by Görgün [59] and is therefore also ignored.

The reversible potential (V_{rev}) is given by the Nerst equation given by [59].

$$V_{rev} = E_0 + \frac{RT_{el}}{4F}\left[\ln\left(\frac{p_{H_2}^2 p_{O_2}}{a_{H_20}}\right)\right], \tag{4.42}$$

where E_0 is the standard reversible potential [V], R is the universal gas constant [8.3144 J/mol·K], F is Faraday's constant [96487 C/mol], T_{el} is the electrolyser cell temperature [K], p_{H_2} and p_{O_2} are the partial pressures of H_2 and O_2 respectively [atm] and a_{H_2O} is the water activity. A value if a_{H_2O}=1 is used for liquid H_2O. The standard reversible voltage is given empirically by

$$E_0 = 1.229 - 0.9 \times 10^{-3}\left(T_{el} - 298\right). \tag{4.43}$$

The final reversible voltage is given by

$$V_{rev} = 1.229 - 0.9 \times 10^{-3}\left(T_{el} - 298\right) + \frac{RT_{el}}{4F}\left[\ln\left(\frac{p_{H_2}^2 p_{O_2}}{a_{H_20}}\right)\right]. \tag{4.44}$$

The electrode activation over-potentials (η_a and η_c) is given by the Butler-Volmer equation which relates electrolyser current density to the activation over-potential at each electrode and is given by

$$J = J_{0,i}\left[\exp\left(\frac{\alpha v_e F \eta_i}{RT_{el}}\right) - \exp\left(\frac{(1-\alpha)\, v_e F \eta_i}{RT_e l}\right)\right], i = a, c, \tag{4.45}$$

where J is the electrolyser current density [A/m^2], $J_{0,i}$ is the exchange current density [A/m^2], α is the charge transfer coefficient, v_e is the stoichiometric coefficient of electrons, η_i is the activation over-potential with the subscripts a and c representing the anode and cathode respectively. For water electrolysis, α and v_e are selected to be $\alpha = 0.5$ and $v_e = 2$ for the anode and $\alpha = 0.5$ and $v_e = -2$ for the cathode [56]. The electrode activation over-potential for the anode and cathode is of the forms given by [56]

$$\eta_a = \frac{RT_{el}}{F}\text{sinh}^{-1}\left(\frac{J}{2J_{0,a}}\right), \text{and} \tag{4.46}$$

$$\eta_c = -\frac{RT_{el}}{F}\text{sinh}^{-1}\left(\frac{J}{2J_{0,c}}\right). \tag{4.47}$$

The anode and cathode exchange current densities are given by [56]

$$J_{0,a} = \gamma_M \text{exp}\left[-\frac{E_{A,a}}{R}\left(\frac{1}{T_{el}} - \frac{1}{T_{el,ref}}\right)\right] J_{0,a,ref}, \text{and} \tag{4.48}$$

$$J_{0,c} = \gamma_M \text{exp}\left[-\frac{E_{A,c}}{R}\left(\frac{1}{T_{el}} - \frac{1}{T_{el,ref}}\right)\right] J_{0,c,ref}, \tag{4.49}$$

where γ_M is the roughness factor ,$J_{0,a,ref}$ and $J_{0,c,ref}$ are the exchange current densities at the anode and cathode respectively at the reference temperature $T_{el,ref}$, and $E_{A,a}$ and $E_{A,c}$ are the activation energies for the anode and cathode respectively. Values for $J_{0,a,ref}$ and $J_{0,c,ref}$ at $T_{el,ref}$ = 353 K (80 ^{o}C) is providede in Table 4.2 [148]. Values for $E_{A,a}$ and $E_{A,c}$ are given to

Table 4.2: Model parameters for Pt based Nafion® anode and cathode electrodes.

Parameter	Symbol	Value	Unit
Anode exchange current density for Pt	$J_{0,a,ref}$	10^{-8}	A/m^2
Anode exchange current density for Pt-Ir	$J_{0,a,ref}$	10^{-3}	A/m^2
Cathode exchange current density for Pt	$J_{0,c,ref}$	10	A/m^2

be $76kJ/mol$ and $18kJ/mol$ respectively by Ni et al. [148]. A value for γ_M = 150 is given as good estimate for both electrodes [149]. The final electrode activation over-potentials are calculated by substituting (4.48) and (4.49) into (4.46) and (4.47) respectively.

The ionic over-potential (η_{ion}) across the membrane is as a result of the resistance of the membrane given by

$$\eta_{ion} = J\frac{L_{mem}}{\sigma_{mem}}, \tag{4.50}$$

where L_{mem} is the thickness of the membrane [m] and σ_{mem} is the ionic conductivity [S/m]. σ_{mem} is a function of the membrane humidification and temperature given by

$$\sigma_{mem} = (0.00514\lambda_{mem} - 0.00326)\exp\left(1268\left(\frac{1}{303} - \frac{1}{T_{el}}\right)\right), \tag{4.51}$$

where λ_{mem} is the water content of the membrane and given by

$$\lambda_{mem}(x) = \lambda_c + (\lambda_a - \lambda_c)\frac{x}{L_{mem}}, \tag{4.52}$$

where x is the location in the membrane measured from the anode [m], λ_a and λ_c are the water contents at the anode-membrane and cathode-membrane interfaces respectively. Values for λ_a and λ_c are given as 14 and 10 respectively in [148]. Assuming a completely hydrated membrane ($\lambda_{mem} = 14$)[6] these values give

$$\sigma_{mem} = \sigma_{mem,ref}\exp\left[1268\left(\frac{1}{T_{el,ref}} - \frac{1}{T_{el}}\right)\right], \tag{4.53}$$

where $\sigma_{mem,ref}$ is the ionic conductivity [s/m] at the reference temperature $T_{el,ref}$. A value of $\sigma_{mem,ref} = 0.14$ S/m is provided in [56] at $T_{el,ref} = 353$ k (80 ^{o}C) for a Nafion® 117 membrane. The final ionic over-potential is calculated from substituting (4.53) into (4.50) along with values for membrane thickness and current density.

Thermal model

The dynamic thermal model from Lebbal and Lecoeuche [147] is discussed here. Electrolyser $V - I$ relationship is affected by it's cell temperature. Four heat sources are present in the electrolyser; the chemical reaction (entropy), chemical component thermodynamics (water and gasses), ambient temperature (T_a) and the effect of current circulation (Joule effect). The Joule

[6] λ_{mem} = 7 dry enough; = 14 good hydration; =22 bathed [147].

effect is assumed to be negligible by [147]. The thermal model is based on the principle of heat energy conservation and can be expressed as a continuous dynamic equation given by

$$C_p \frac{\mathrm{d}\left(T_c - T_a\right)}{\mathrm{d}t} = \left(V_{el} - V_{th}\right) I_{el} - h\left(T_c - T_a\right), \tag{4.54}$$

where C_p is the electrolyser overall thermal capacity [J/K], T_c is the electrolyser temperature [K], T_a is the ambient temperature [K], V_{el} is the electrolyser operating voltage [V], V_{th} is the thermo-neutral cell voltage, I_{el} is the electrolyser operating current and h is the electrolyser overall thermal admittance [W/K]. It can further be noted that $\left(V_{el} - V_{th}\right) I_{el}$ is the chemical reaction generated heat transfer rate as a result of entropy energy and $\left(T_c - T_a\right)$ is the temperature difference resulting in the heat transfer rate caused by the ambient temperature and fluids movement.

4.3.5 Lead-acid battery storage

The LAB model implemented dis CIEMAT model. This is a general LAB model used for PV system simulation. Additionally a cycle-counting algorithm in [134] is implemented to incorporate the performance model with a lifetime model. The generic property of the CIEMAT model makes it appropriate for the optimisation exercises where the rating of the battery changes with every run of the simulation. Detail of the CIEMAT model as given by Copetti [150] and Gergaud et al. [151].

For each single cell the discharge voltage equation is given by

$$V_d = \left(2.085 - 0.12\left(1 - SOC\right)\right) - \frac{|I|}{C_{10}}\left(\frac{4}{1 + |I|^{1.3}} + \frac{0.27}{SOC^{1.5}} + 0.02\right)\left(1 - 0.007\Delta T\right), \tag{4.55}$$

and for charging up to the point where gassing starts the battery voltage is given by

$$V_c = \left(2 + 0.16SOC\right) - \frac{I}{C_{10}}\left(\frac{6}{1 + I^{0.86}} + \frac{0.48}{\left(1 - SOC\right)^{1.2}} + 0.036\right)\left(1 - 0.025\Delta T\right), \tag{4.56}$$

where SOC is the battery SOC which indicates how much electric charge is available in a cell at a given time, C_{10} is the 10 hour rated battery capacity [Ah], I is the battery current [A] and ΔT is the temperature variation [^{o}C] between the cell temperature and a reference temperature [25 ^{o}C]. The first term in both (4.55) and (4.56) represent the voltage as a function of SOC (electrolyte concentration) and the second terms represent the variation of voltage due to the battery internal resistance. SOC is calculated by determining the ratio between the charge available (either during charge and discharge) and the rated battery capacity and is given by

$$SOC = \frac{\eta_B}{C}\int_{t_0}^{t} I\left(t\right)\mathrm{d}t + SOC_0, \tag{4.57}$$

where SOC and $I\left(t\right)$ are the battery SOC and current [A] respectively at time t, SOC_0 is the SOC at the time t_0, η_B is the conversion efficiency and C is the battery capacity normalized with respect to the C_{10} discharge current, I_{10}. For $I\left(t\right) < 0$ the battery is discharging and for

$I(t) > 0$ the battery is charging. Battery discharge efficiency is assumed to be 100 % [150]. During charging however the battery charging efficiency (η_B) as a function of SOC and current rate is given by

$$\eta_B = 1 - \exp\left(\frac{20.73}{\frac{I}{I_{10}} + 0.55}(SOC - 1)\right). \tag{4.58}$$

Charging efficiency drops to zero as the battery approaches full charge. Available battery capacity is given by

$$C = C_{10}\frac{1.67}{1 + 0.67\left(\frac{I}{I_{10}}\right)^{0.9}}(1 - 0.005\Delta T). \tag{4.59}$$

The overcharge equation given by

$$V_{oc} = V_g + (V_{ec} - V_g)\left(1 - \exp\left(\frac{t - t_g}{\tau_g}\right)\right), \tag{4.60}$$

where V_g and V_{ec} are the beginning of gassing voltage and the end of charge voltage respectively and given by

$$V_g = \left(2.24 + 1.97\ln\left(1 + \frac{I}{C_{10}}\right)\right)(1 - 0.002\Delta T), \text{and} \tag{4.61}$$

$$V_{ec} = \left(2.45 + 2.011\ln\left(1 + \frac{I}{C_{10}}\right)\right)(1 - 0.002\Delta T). \tag{4.62}$$

In 4.60 τ_g is the time constant of the gassing phenomenon and given by

$$\tau_g = \frac{1.73}{1 + 852\left(\frac{I}{C_{10}}\right)^{1.67}}. \tag{4.63}$$

During the charge process the voltage is represented by (4.56) up to the point in time, t_g, where $V_c = V_g$. At this point the voltage is represented by (4.60) until a constant final voltage given by (4.62) is reached.

Battery life is modelled by implementing an adoption of Miner's rule which involves a combination of conventional battery lifetime information and a cycle counting algorithm that determines the number of cycles from DOD. A cycle counting algorithm is employed to cater for over-lapping cycles. Manwell et al. [134] implements a rain-flow cycle counting method. Rain-flow cycle counting is common in metal fatigue estimates. Bindner et al. [152] and Manwell et al. [134] use an empirical relationship that relates battery DOD to possible number of cycles. This data is provided by battery manufacturers as standard. The implemented model uses manufacturer data in a lookup table. The fractional life used up in a given cycle is calculated to be $1/C_F$. After sufficient cycles have passed the fractions multiplied by the number of cycles, N, add up to one indicating the end of battery life. End of battery life is defined to be when the battery has reached 80 % of the nominal capacity [152]. Fractional damage is given by

$$D = \sum N_i \frac{1}{C_{F,i}}, \tag{4.64}$$

where D is the fractional damage, N_i refers to the i^{th} cycle and $C_{F,i}$ is the fractional depth of the i^{th} cycle. The number (N_i) of equal values for $C_{F,i}$ are grouped together and the combined

contribution to the battery lifetime is calculated. A change is made to the calculation done in (4.64) to determine a new value q_{max} in order to keep track of the available battery capacity at any time during the simulation. For each cycle determined by the rain-flow cycle counting algorithm, a new capacity is calculated assuming that each fraction of a cycle contributes to the degradation of the battery from it's nominal capacity. The model is given by

$$q_{new} = q_{prev} - \frac{0.2 \times q_{nom}}{C_F}, \tag{4.65}$$

where q_{new} is the new battery capacity calculated, q_{prev} is the previous battery capacity calculated [Ah], q_{nom} is the manufacturer rated battery capacity [Ah] and C_F is the current fractional discharge measured [Ah] to determine q_{new}. When q_{new} reaches 80 % of the battery nominal capacity the battery has reached it's end of life.

The rain-flow cycle counting algorithm is based on reviewed work by Downing and Socie [153]. Each cycle's contribution to the reduction in lifetime is calculated immediately. An important assumption with the current method is that the battery SOC always starts at 100 %. The algorithm saves extremes (maximum and minimum DOD values) and looks for completed charge and discharge cycles and calculates each cycles individual DOD. As each cycle is completed the lookup table containing the battery life vs. % DOD along with (4.65) is used to calculate the cumulative wear on the battery. The remaining battery capacity determines the degradation of the battery in terms of capacity lost over the time period of the simulation. A flow diagram of the cycle counting algorithm employed is shown given Fig. 4.9.

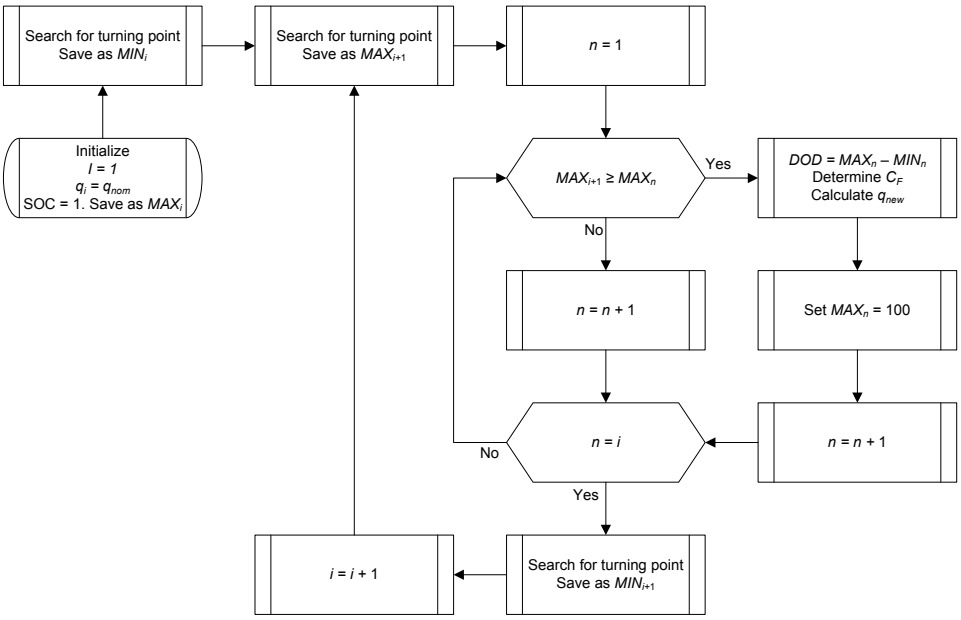

Figure 4.9: Flow diagram for rain-flow cycle counting algorithm.

4.3.6 Power conversion devices

A PCD is a device designed to convert power from one form and/or amplitude to another. Devices commonly referred to are AC/DC converters (rectifiers), DC/AC converters (inverters) and DC/DC converters. In RESs both AC and DC power are encountered since PV modules and battery banks are DC power while most wind generators and traditional loads are AC power. For RE H_2 production systems the electrolyser component is included and operates from DC. Both AC bus and DC bus configurations are encountered. Power conversion device's efficiency is primarily dependent on the current. Laukamp [154] provides a generic three-parameter model relating the input power to the output power given by

$$\frac{P_{in}}{P_{nom}} = \frac{P_0}{P_{nom}} + \left(1 + \frac{V_s}{V_{out}}\right)\frac{P_{out}}{P_{nom}} + \frac{R_i}{V_{out}^2}P_{nom}\left(\frac{P_{out}}{P_{nom}}\right)^2, \tag{4.66}$$

where P_{in} is the input power [W], P_0 is the idling power [W], V_s is the set point voltage [V], V_{out} is the output voltage [V], P_{out} is the output power [W] and R_i is the internal resistance. (4.66) is implemented when P_{out} is the input. However when P_{in} is the input (4.66) is used to analytically derive

$$\frac{P_{out}}{P_{nom}} = \frac{-\left(1 + \frac{V_s}{V_{out}}\right) + \sqrt{\left(1 + \frac{V_s}{V_{out}}\right)^2 - 4\left(\frac{R_i}{V_{out}^2}\right)(P_0 - P_{in})}}{2\left(\frac{R_i}{V_{out}^2}\right)P_{nom}}. \tag{4.67}$$

This model is based on empirical efficiency functions and is numerically robust and generic. The exact model is also implemented in Ulleberg [140] and also as the power conditioning unit in the transient simulation program TRNSYS [107] using the HYDROGEMS REHS toolbox [155]. The parameters P_0, V_s and R_i are obtained from the curve fitting of available converter data sheets.

4.4 Power management controller

The purpose of the power management controller is to make decision on power distribution between the different components based on certain pre-defined criteria which result in several operating modes (OM) for the controller. There are seven possible OM illustrated in Fig. 4.10. An additional eighth mode is the off mode (**OM0**). The main function of the power controller is to decide on producing H_2, charging or discharging batteries and/or dumping excess power. Ideally no power should ever be dumped. It is however a possibility and is therefore included in the logic of the controller. Each mode performs certain actions based on predefined conditions. In **OM0** no power is available from the RE source and the electrolyser is off. No power distribution takes place. For **OM1** RE source power level is between electrolyse minimum and maximum allowable power level in which case the RE source power is used to supply electrolyser alone. For **OM2** RE source power level is below the electrolyser minimum allowable power level and the SOC is below the maximum allowable SOC level. For these conditions the RE source power is used to charge batteries alone. In **OM3** no power is available from the RE source and the SOC is above the minimum allowable SOC level while the electrolyser is on.

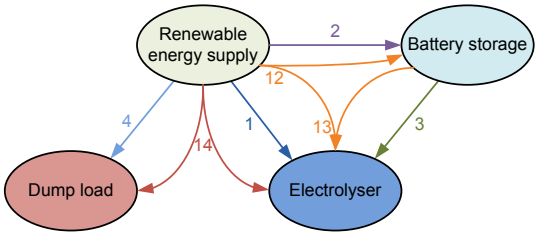

Figure 4.10: Power controller operating modes.

Battery energy is then used to supply the electrolyser. In **OM4** RE source power level is below the electrolyser minimum allowable power level and the SOC is equal to the maximum allowable SOC level. For these conditions all power from the RE source needs to be dumped. For **OM12** RE source power level is more than the electrolyser maximum allowable power level and the SOC is below the maximum allowable SOC level in which case the RE source power is used to supply the electrolyser and charge batteries. In **OM13** RE source power level is below the electrolyser maximum allowable power level and the SOC is above the minimum allowable SOC level. For these conditions a combination of RE source power and battery energy is used to supply the electrolyser. For **OM14** RE source power level is more than the electrolyser allowable maximum power level and the SOC is equal to the maximum allowable SOC level. RE source power is used to supply the electrolyser with the remainder of the power dumped. A detail logical block flow diagram for the described power controller showing all variables and conditions is provided in Fig. 4.11. The logic flow of the controller is discussed in detail:

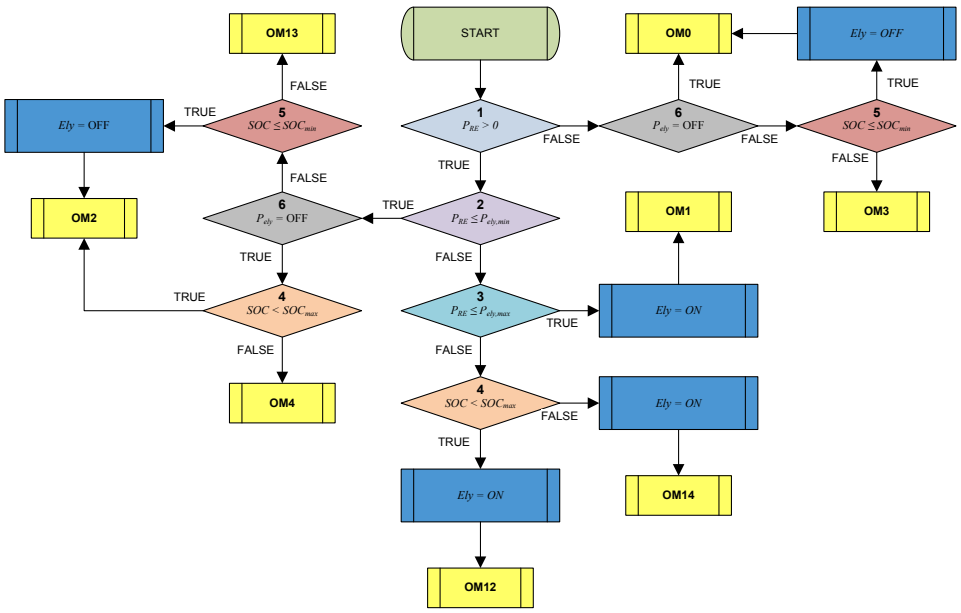

Figure 4.11: Logic block flow diagram for the power controller.

If $P_{RE} \not> 0$ and the electrolyser is off, **OM0** is selected. If the electrolyser is already on and $SOC \le SOC_{min}$ the electrolyser turns off and **OM0** is selected. If $SOC \not\le SOC_{min}$ **OM3** is selected. If $P_{RE} > 0$ but $P_{RE} \le P_{ely,min}$ the controller must decide on charging or discharging the battery, or dumping the load. If the electrolyser is off and $SOC \not< SOC_{max}$ **OM4** is selected

and if $SOC < SOC_{max}$ **OM2** is selected. If the electrolyser is on and $SOC \nleq SOC_{max}$ **OM13** is selected and if $SOC \leq SOC_{max}$ the electrolyser is turned off and **OM2** is selected. If $P_{RE} > 0$ and $P_{RE} \nleq P_{ely,min}$ the controller will turn on the electrolyser and must decide on dumping or charging batteries with any excess power. If $P_{RE} \leq P_{ely,max}$ the electrolyser is turned on and **OM1** is selected. If $P_{RE} \nleq P_{ely,max}$ and $SOC < SOC_{max}$ the electrolyser is turned on and **OM12** is selected. If $P_{RE} \nleq P_{ely,max}$ and $SOC \nless SOC_{max}$ the electrolyser will still be turned on and **OM14** is selected. Table 4.3 provides a list of the power management controller input variables and conditions numbered 1 to 6 as they are given in Fig. 4.11. Outputs variables are also provided. From the input variables, output variables, conditions, actions and the power controller logic

Table 4.3: Power controller inputs, conditions and, outputs.

Value	Type
Power from the RE source (P_{RE})	Input
Batteries SOC (SOC)	Input
Minimum allowable SOC level (SOC_{min})	Input
Maximum allowable SOC level (SOC_{max})	Input
Minimum allowable electrolyser power level ($P_{ely,min}$)	Input
Maximum allowable electrolyser power level ($P_{ely,max}$)	Input
Battery discharge constant for **OM3** (k_3)	Input
Battery/electrolyser constant for **OM12** (k_{12})	Input
$P_{RE} > 0$	Condition
$P_{RE} \leq P_{ely,min}$	Condition
$P_{RE} \leq P_{ely,max}$	Condition
$SOC < SOC_{max}$	Condition
$SOC < SOC_{min}$	Condition
$P_{ely} = OFF$	Condition
Power to the electrolyser (P_{ely})	Output
Battery charging ($P_{bat,c}$)	Output
Battery discharging ($P_{bat,d}$)	Output
Power dump (P_{dump})	Output

given in Fig. 4.11, the power controller is implemented using the truth table block available in the Simulink^{TM} programming environment. The implemented logic is given in Table 4.4.

4.5 Battery split bank controller

The battery bank controller ensures that one set of batteries is charged and the other set of batteries is discharged. This role switches when one set of batteries become either fully charged or discharged. The power controller discussed in Section 4.4 uses the average SOC between the two battery banks as SOC input. Average SOC is given by

$$SOC = \frac{SOC_1 + SOC_2}{2}, \tag{4.68}$$

where SOC_1 and SOC_2 is the SOC for battery banks 1 (BB1) and 2 (BB2) respectively. The battery bank controller's purpose is to manage the charge and discharge between the two battery banks based on certain pre-defined criteria. There are 4 possible OMs. This includes a charging and discharging mode for each of the two battery banks. An additional fifth mode is the off mode (**BM0**). The main function of the battery controller is to eliminate as far as possible incremental

Table 4.4: Power controller logic condition and action table

Mode	Conditions: 1. $P_{RE} > 0$	2. $P_{RE} <= P_{ely,min}$	3. $P_{RE} <= P_{ely,max}$	4. $SOC < SOC_{max}$	5. $SOC <= SOC_{min}$	6. $Ely_{OFF} >= 1$	Actions
OM0	F	-	-	-	-	T	$P_{ely} = 0$; $P_{bat,c} = 0$;
	F	-	-	-	T	F	$P_{bat,d} = 0$; $P_{dump} = 0$;
OM1	T	F	T	-	T	-	$P_{ely} = P_{RE}$; $P_{bat,c} = 0$;
							$P_{bat,d} = 0$; $P_{dump} = 0$;
OM2	T	T	-	T	-	T	$P_{ely} = 0$; $P_{bat,c} = -P_{RE}$;
	T	T	-	-	T	F	$P_{bat,d} = 0$; $P_{dump} = 0$;
OM3	F	-	-	-	F	F	$P_{ely} = k_3 \times P_{ely,max}$; $P_{bat,c} = 0$;
							$P_{dump} = 0$; $P_{bat,d} = k_3 \times P_{ely,max}$;
OM4	T	T	T	F	-	T	$P_{ely} = 0$; $P_{bat,c} = 0$;
							$P_{bat,d} = 0$; $P_{dump} = P_{RE}$;
OM12	T	F	F	T	-	-	$P_{ely} = k_{12} \times P_{ely,max}$; $P_{bat,d} = 0$; $P_{dump} = 0$;
							$P_{bat,c} = -\left(P_{RE} - \left(k_{12} \times P_{ely,max}\right)\right)$;
OM13	T	T	-	-	F	F	$P_{ely} = P_{ely,max}$; $P_{bat,c} = 0$;
	T	F	T	-	F	-	$P_{bat,d} = P_{ely,max} - P_{RE}$; $P_{dump} = 0$;
OM14	T	F	F	F	-	-	$P_{ely} = P_{ely,max}$; $P_{bat,c} = 0$;
							$P_{bat,d} = 0$; $P_{dump} = P_{RE} - P_{ely,max}$;

charge and discharge cycles which reduce battery life and efficiency. Each mode performs certain actions based on predefined conditions. In **BM0** no power is supplied to or required from the batteries by the power controller. Neither one of BB1 or BB2 are charged or discharged. In **BCM1** power is supplied to the batteries and BB1 is charged. In **BCM2** power is supplied to the batteries and BB2 is charged. In **BDM1** power is required from the batteries and BB1 is discharged. In **BDM2** power is required from the batteries and BB2 is discharged. The logical block flow diagram of the battery controller is shown in Fig. 4.12. One of the battery banks

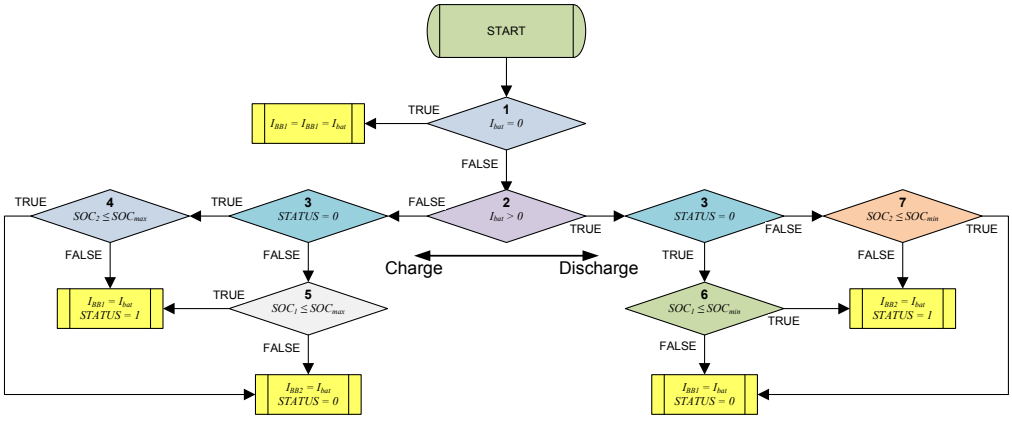

Figure 4.12: Logic block flow diagram for the split bank battery controller.

will always be in charge while the other is in discharge controlled by the $STATUS$ bit. For $STATUS = 1$ $BB1$ is charging and $BB2$ is discharging and for $STATUS = 0$ $BB2$ is charging and $BB1$ is discharging.

The logic flow of the controller is discussed in detail: When I_{bat} is positive ($I_{bat} > 0$) the battery is discharging and when I_{bat} is negative ($I_{bat} < 0$) the battery is charging. If $I_{bat} = 0$, no power flow takes place. For $I_{bat} < 0$ and $STATUS = 0$ BB2 should be charging. If however $SOC_2 = SOC_{max}$ the $STATUS$ will change to $STATUS = 1$ and BB1 will be charging. Similarly for $I_{bat} < 0$ and $STATUS = 1$ BB1 should be charging. If however $SOC_1 = SOC_{max}$ the $STATUS$ will change to $STATUS = 0$ and BB2 will be charging. For $I_{bat} > 0$ and $STATUS = 0$ BB1 should be discharging. If however $SOC_2 \leq SOC_{min}$ the $STATUS$ will change to $STATUS = 1$ and BB2 will be discharging. Similarly For $I_{bat} > 0$ and $STATUS = 1$ BB2 should be discharging. If however $SOC_2 \leq SOC_{min}$ the $STATUS$ will change to $STATUS = 0$ and BB1 will be discharging. Table 4.5 provides a list of the battery split bank controller input variables, conditions numbered 1 to 7 as they are given in Fig. 4.12 and outputs variables. From the

Table 4.5: Battery controller inputs, conditions and, outputs.

Value	**Type**
Current from the battery (I_{bat})	Input
Battery bank SOC (SOC_1 and SOC_2)	Input
Minimum allowable SOC level (SOC_{min})	Input
Maximum allowable SOC level (SOC_{max})	Input
$I_{bat} = 0$	Condition
$I_{bat} > 0$	Condition
$STATUS = 0$	Condition
$SOC_2 < SOC_{max}$	Condition
$SOC_1 < SOC_{max}$	Condition
$SOC_1 \leq SOC_{min}$	Condition
$SOC_2 \leq SOC_{min}$	Condition
Battery bank 1 charging and discharging current (I_{BB1})	Output
Battery bank 2 charging and discharging current (I_{BB2})	Output

input variables, output variables, conditions, actions and the battery controller logic given in Fig. 4.12, the battery controller is implemented using the truth table block available in the Simulink^{TM} programming environment. The implemented logic is given in Table 4.6.

Table 4.6: Battery controller logic condition and action table

Mode	**Conditions** 1. $I_{bat} == 0$	2. $I_{bat} > 0$	3. $STATUS == 0$	4. $SOC_2 < SOC_{max}$	5. $SOC < SOC_{max}$	6. $SOC_1 <= SOC_{min}$	7. $SOC_2 <= SOC_{min}$	**Actions**
BM0	T	-	-	-	-	-	-	$I_{BB1} = 0$; $I_{BB2} = 0$; $STATUS = STATUS$
BCM1	F	F	F	-	T	-	-	$I_{BB1} = I_{bat}$; $I_{BB2} = 0$;
	F	F	T	F	-	-	-	$STATUS = 1$
BCM2	F	F	T	T	-	-	-	$I_{BB1} = 0$; $I_{BB2} = I_{bat}$;
	F	F	F	-	F	-	-	$STATUS = 0$
BDM1	F	T	T	-	-	F	-	$I_{BB1} = I_{bat}$; $I_{BB2} = 0$;
	F	T	F	-	-	-	T	$STATUS = 0$
BDM2	F	T	F	-	-	-	F	$I_{BB1} = 0$; $I_{BB2} = I_{bat}$;
	F	T	T	-	-	T	-	$STATUS = 1$

4.6 Conclusion

In conclusion, individual component models are developed for the weather input data for profiles of the solar irradiance and wind speed, a PV module, a WT generator, a PEM electrolyser cell, a LAB cell and power conversion devices (PCDs). Additionally a novel power management controller and a split battery bank controller was developed for this work.

Chapter 5

Testing and verification of models

This chapter describes the testing and verification of the key system component models developed in Chapter 4. These models are to be used in the simulation and optimisation in Chapter 6 of a stand-alone RE H_2 energy system. The following models are evaluated: PV module, Wt generator, PEM electrolyser, LAB, power conditioning equipment and power controllers. The models are validated through comparison with experimental data. The complete system model and power controllers are validated by ensuring that there is no resultant energy and power flows between components.

5.1 Photovoltaic

A block diagram of the complete PV module model is given in Fig. 5.1. The model provided is

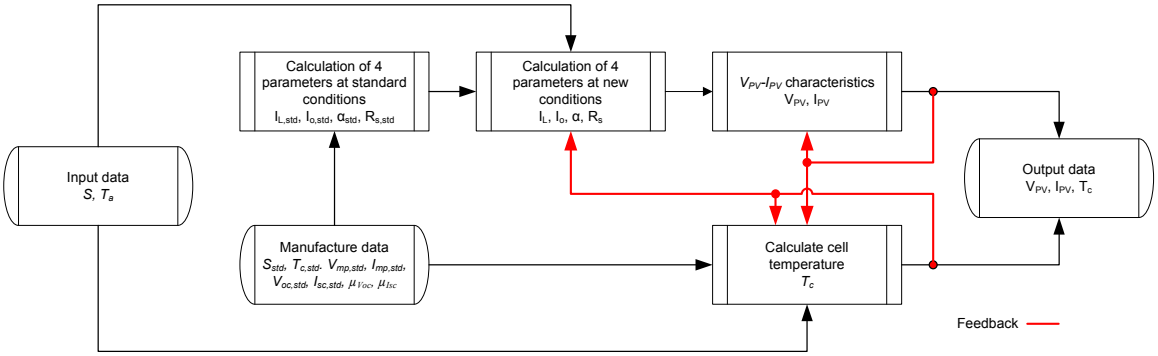

Figure 5.1: Flow diagram of the PV module model.

for a single 180 W PV module. For increased power modules are mounted in series and parallel. Each PV module will produce equal current (I_{PV}) and voltage (V_{PV}) and result in equal cell temperature T_c at all times. The series and parallel PV modules in an array is calculated using

$$V_{PV,A} = V_{PV} \times N_{m,s}, and \tag{5.1}$$

$$I_{PV,A} = I_{PV} \times N_{m,p}, \tag{5.2}$$

where $V_{PV,A}$ is the total PV array voltage [V], $I_{PV,A}$ is the total PV array current [A], $N_{m,s}$ is the number of PV modules in series and $N_{m,p}$ is the number of PV modules in parallel. Table 5.1 gives the PV parameters that are used to model the PV module [140]. Measured (from [140])

Table 5.1: PV parameters at standard conditions, S_{std} and T_{std}.

PV parameter	**Symbol**	**Value**	**Unit**
Open-circuit voltage	$V_{oc,std}$	87.72	V
Short-circuit current	$I_{sc,std}$	2.664	A
MPP voltage	$V_{mp,std}$	70.731	V
MPP current	$I_{mp,std}$	2.448	A
V_{oc} temperature coefficient	μ_{Voc}	-0.3318	V/degree C
I_{sc} temperature coefficient	μ_{Isc}	0.00148	A/degree C
Number of cells	N_s	153	-
PV area	A_{PV}	1.5	m^2
Solar radiation, STD	S_{std}	1000	W/m_2
Temperature, STD	$T_{c,std}$	25	degree C
Transmittance adsorption product	$k_{in,PV}$	1.247	W/degree C· m^2
Heat loss coefficient	k_{loss}	30	W/degree C· m^2
Heat capacity per unit area	C_{PV}	50000	J/degree C· m^2

and simulated I_{PV}-V_{PV} and P_{PV}-V_{PV} characteristics for solar radiation of 1000 W/m^2 at 25 ^oC and 50 ^oC and for 800 W/m^2 at 25 ^oC are given in Fig. 5.2. Fig 5.3 gives the temperature

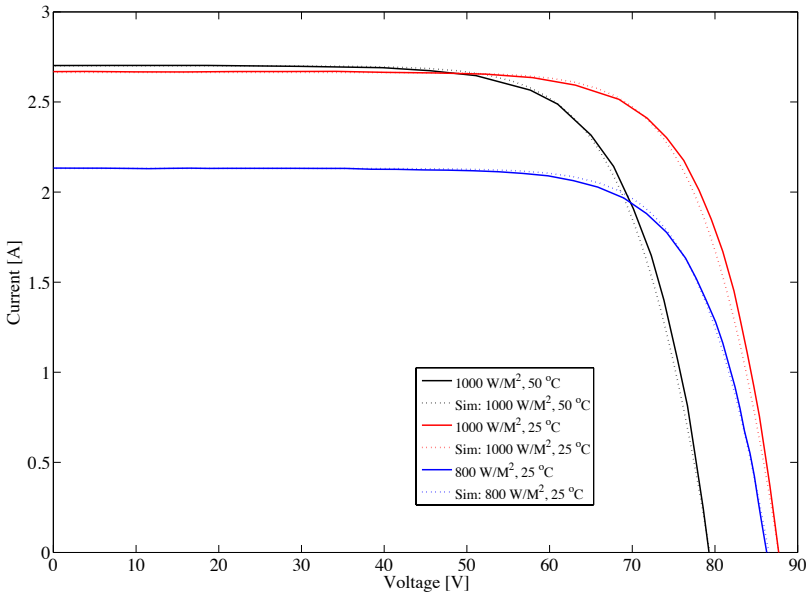

Figure 5.2: Simulated vs verified PV modules I-V characteristics.

response for the simulated and measured data from [140] for a single day. Both $I_{PV} - V_{PV}$ and

the thermal response provides acceptable fits with measured data.

As the solar radiation increases, V_{oc}, I_{sc} and P_{mp} also increase. Simulated I_{PV}-V_{PV} and P_{PV}-V_{PV} characteristic curves for various cell temperatures at standard solar radiation ($S_{std} = 1000$ W/m$_2$) are given in Fig. 5.3. As the cell temperature decreases, V_{oc} and P_{mp} increases, but I_{sc} very slightly increases. From Fig. 5.2 and Fig. 5.3 it is shown that changes in cell temperature has a larger effect on V_{mp} while changes in the solar radiation has a larger effect on I_{mp}. The V-I

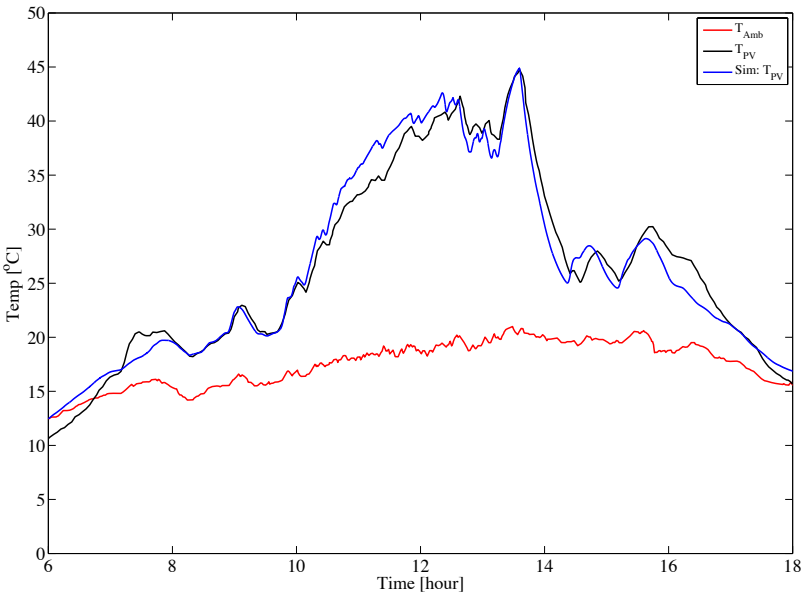

Figure 5.3: Temperature of PV using dynamic model.

characteristic model used is verified with experimental results in the works of both Ulleberg [140] and Wang [141] with the results shown in Fig. 5.2 and Fig. 5.3.

5.2 Wind turbine

A block diagram of the WT model is given in Fig. 5.4. WT generators are less affected by envi-

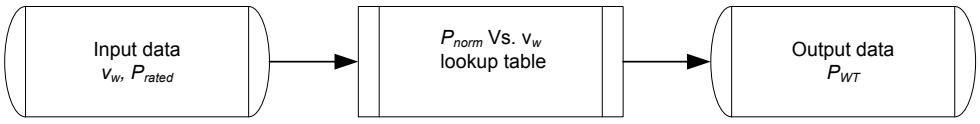

Figure 5.4: Flow diagram of the WT model.

ronmental conditions other than wind speed. An uncomplicated generic modelling approach is used. The power curve of a Hummer H4.8-3 kW [146] WT is used as reference. The power curve data is normalised to provide the optimisation with a general power curve for which a rated power value can simply be selected. It is assumed that small power rated WTs up to the

20 kW range exhibit similar power curves. Fig. 5.5 gives the normalised power curves for WTs from the same manufacturer ranging from 1 kW up to 20 kW all exhibiting the same characteristics. An average error between the 3 kW reference curve and the others is 4.4 %. All the WTs exhibit the same 3 m/s cut-in wind speed and 3-25 m/s working wind speed range.

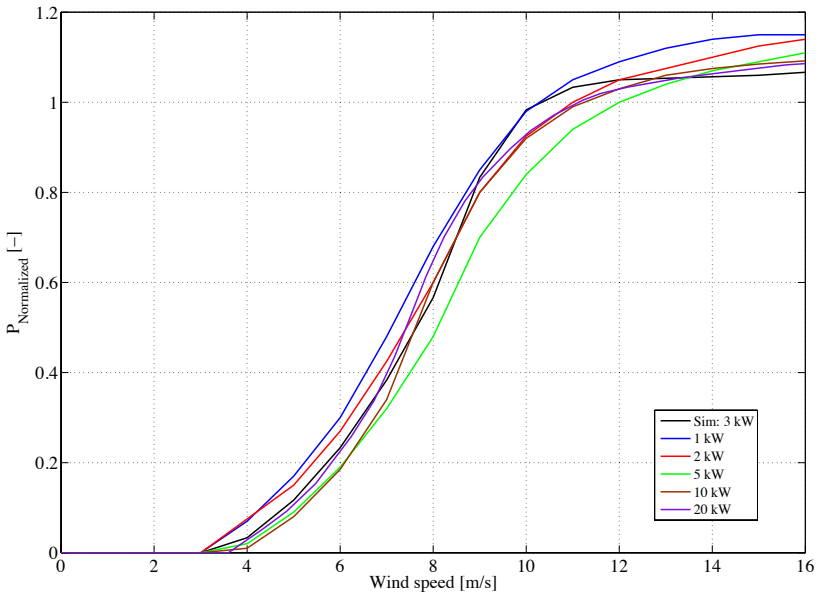

Figure 5.5: Wind turbine power curves.

5.3 Proton exchange membrane electrolyser

A block diagram of the complete PEM electrolyser model is given in Fig. 5.6. Electrolyser efficiency consist of two components. The voltage efficiency is given by [56]

$$\eta_V = \frac{V_{th}}{V_{el}}, \tag{5.3}$$

where η_V is the voltage efficiency, V_{th} is the thermo-neutral cell voltage and V_{el} is the electrolyser cell operating voltage. For V_{th} the higher heating value (HHV) of 1.48 V is used. The Faraday efficiency is given by [156]

$$\eta_F = \frac{F_{H_2}}{\frac{N_s I_{el}}{2F}}, \tag{5.4}$$

where η_F is the Faraday efficiency. The Faraday efficiency is in general assumed to be more than 99% [59]. Total electrolyser efficiency is given by [156]

$$\eta_{el} = \frac{1.48}{V_{el}} \frac{F_{H_2}}{\frac{N_s I_{el}}{2F}}. \tag{5.5}$$

The model provided is for a single cell PEM electrolyser cell with the number of cells (N_s) used appropriately to convert to a multiple cell electrolyser. To increase the power output of the

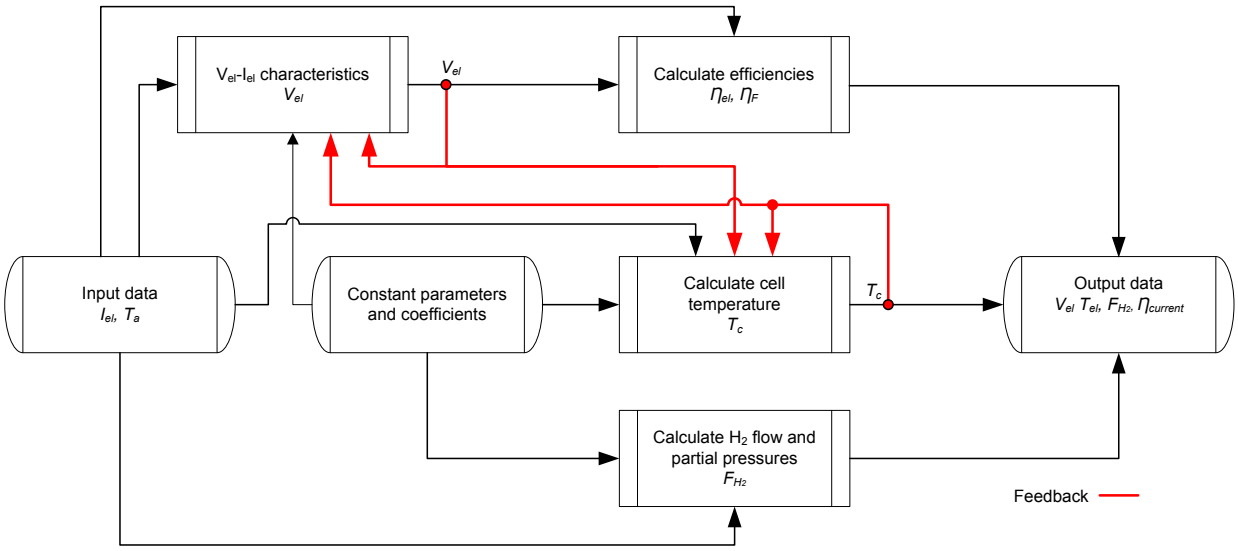

Figure 5.6: Flow diagram of the PEM electrolyser model.

electrolyser the cell active area A_{mem} can be increased thus increasing the operating current (I_{el}), or by increasing the number of cells thus increasing the electrolyser operating voltage (V_{el}). Table 5.2 gives the PEM electrolytic cell parameters and coefficients used in the model [59, 147]. Voltage model parameters are obtained from [148] and Choi et al. [149]. Thermal model

Table 5.2: PEM electrolyser model parameters.

Parameter	Symbol	Value	Unit
Membrane thickness Nafion® N-117 [157]	$_{mem}$	178×10^{-6}	m
Universal gas constant	R	8.3145	J/mol·K
Faraday's constant	F	96487(26.801)	C/mol(Ah/mol)
Water activity	a_{H_2O}	1	-
Roughness factor	γ_M	150	-
Anode activation energy	$E_{A,a}$	76000	J/mol
Cathode activation energy	$E_{A,c}$	18000	J/mol
Anode exchange current density at $T_{el,ref}$	$J_{0,a,ref}$	Table 4.2	A/m_2
Cathode exchange current density at $T_{el,ref}$	$J_{0,c,ref}$	Table 4.2	A/m_2
Reference temperature	$T_{el,ref}$	353 (80)	K (degree C)
Ionic conductivity at $T_{el,ref}$	$\sigma_{mem,ref}$	0.14	S/m
Electrolyser overall thermal capacity	C_p	68544	J/K
Thermo-neutral cell voltage	V_{th}	1.48	V
Electrolyser overall thermal admittance	h	10.71	W/K

parameters are obtained from Lebbal and Lecoeuche [147]. In Fig Fig. 5.7 the simulated and measured data from [158] is presented. The simulated model accurately represents the voltage characteristics of the PEM electrolyser. Fig. 5.8 provides the simulated temperature response against that of measured data from [147]. Both the cell voltage and temperature models show

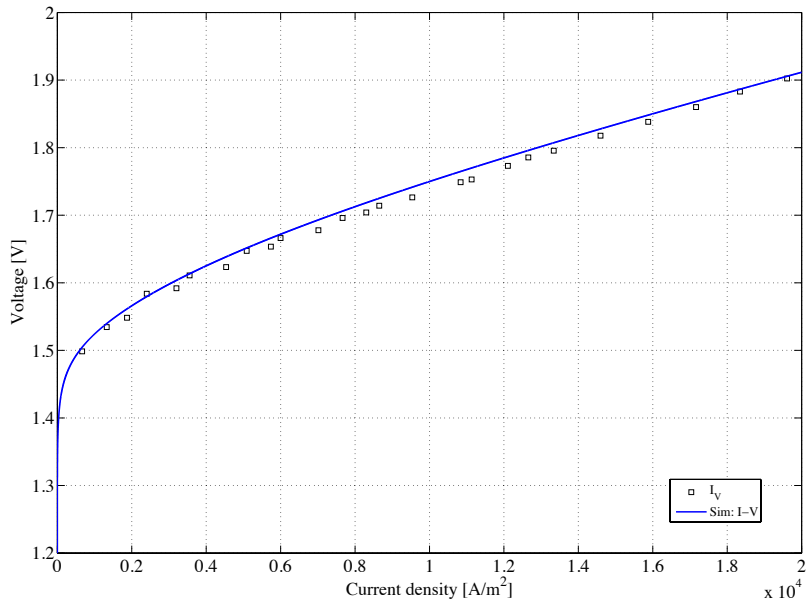

Figure 5.7: Electrolyser J-V characteristics at $T_c = 353$ K (80 degree C).

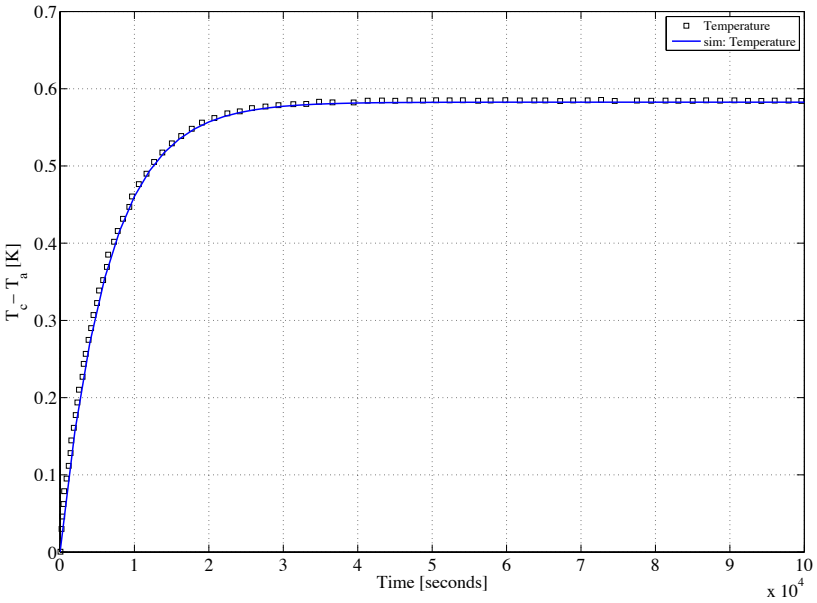

Figure 5.8: Electrolyser temperature response at $V_{el} = 1.74$ V and $I_{el} = 24$ A.

good fits with measured data.

5.4 Lead-acid battery

A block diagram of the complete battery model is given in Fig. 5.9. To increase the battery bank

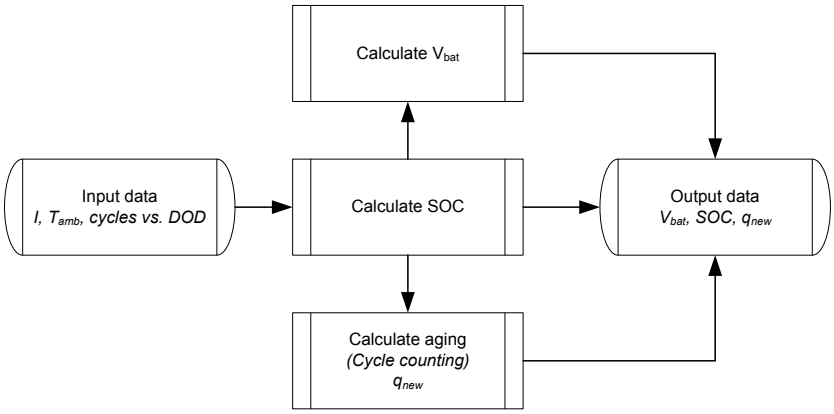

Figure 5.9: Lead-acid battery model flow diagram.

operating voltage (V_{BB}) batteries are placed in series and to increase the total required capacity [Ah], batteries are placed in parallel. Battery voltages and currents are calculated by

$$I_{bat} = \frac{I_{\text{from/to bus}}}{N_{b,p}}, and \tag{5.6}$$

$$V_{bat} = V_{cell} \times N_{b,s} \times N_{cells}, \tag{5.7}$$

where $I_{\text{from/to bus}}$ is the current supplied to or from the battery bank, $N_{b,p}$ is the number of batteries in parallel, V_{cell} is cell voltage calculated by the model, $N_{b,s}$ is the number of batteries in series and N_{cells} is the number of single cells in series. Experimental data from [159] is provided in Fig. 5.10 and Fig. 5.11 along with the simulated data for battery discharge and charge voltages over time for several battery charge and discharge rates. All but the C5 discharge rate

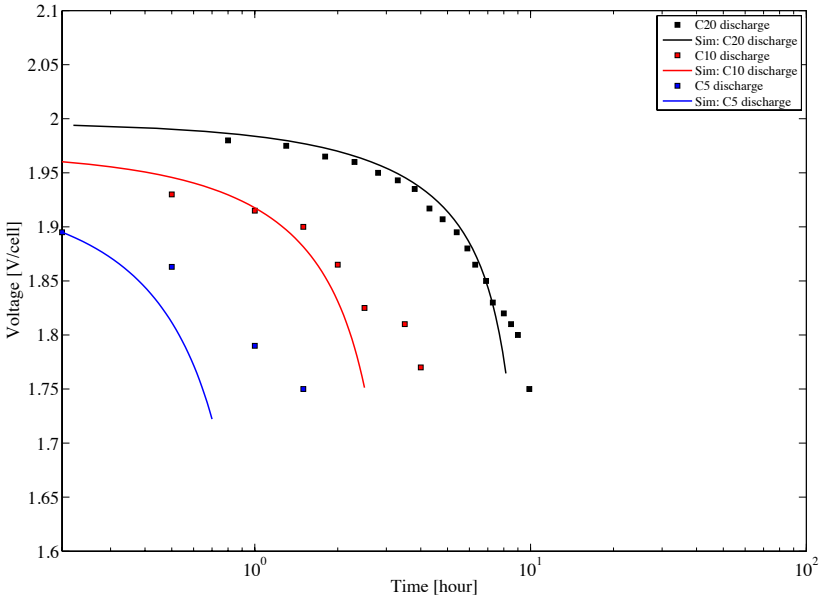

Figure 5.10: Model fits for battery discharging.

provide acceptable fits. For this work the results are acceptable for implementation.

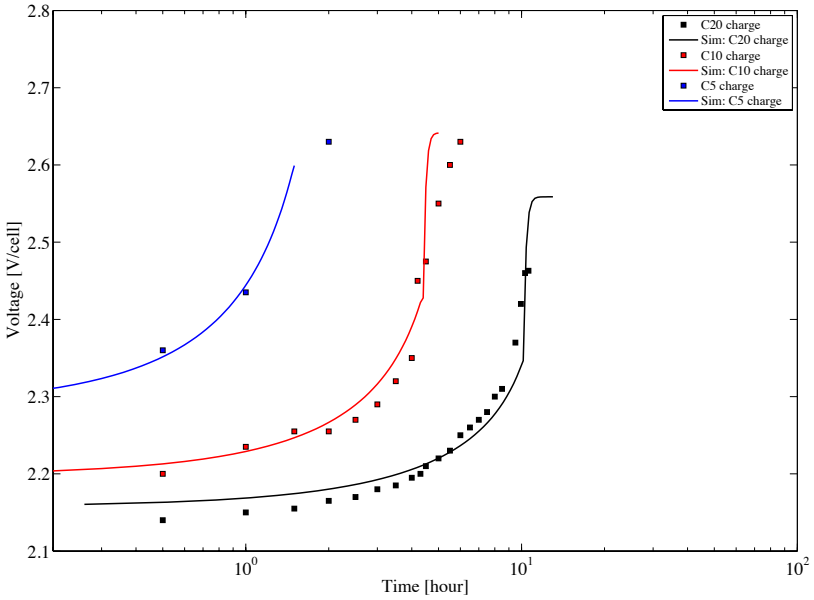

Figure 5.11: Model fits for battery charging.

5.5 Power conversion device

A block diagram of the complete PCD model is given in Fig. 5.12. The efficiency of the PCD is

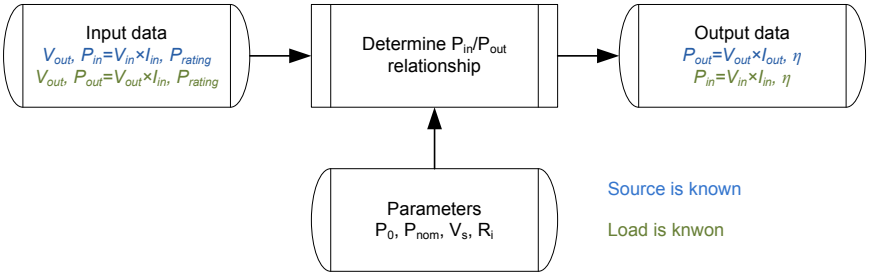

Figure 5.12: Flow diagram of the power conversion device model.

given by

$$\eta = \frac{P_{out}}{P_{in}}. \tag{5.8}$$

Normalised values of P_{in} and P_{out} are multiplied by P_{rating} of the PCDs. P_{rating} is determined by the accompanying component power rating. Normalisation is required to make the model generic and easy to implement for optimisation. Several sets of parameters are provided in the thesis of Ulleberg [140]. The same model is also implemented as part of the HYDROGEMS [155] REHS toolbox and uses the parameters given in Table 5.3. The HYDROGEMS [155] models have been tested and verified against various RE H_2 system demonstration plants around the world. Fig. 5.13 provide efficiency vs. P_{out}/P_{nom} relationships for simulated and measured data from [140].

Table 5.3: Power converter parameters.

Component	Parameter	Symbol	Value	Unit
PV & WT	Idling power	P_0	0.02489	kW
	Set point voltage	V_s	18.72	V
	Internal resistance	R_i	0.131689	ohm
	Nominal power	P_{nom}	10	kW
Electrolyser & BB	Idling power	P_0	0.151736	kW
	Set point voltage	V_s	2.06	V
	Internal resistance	R_i	0.005324	ohm
	Nominal power	P_{nom}	26	kW

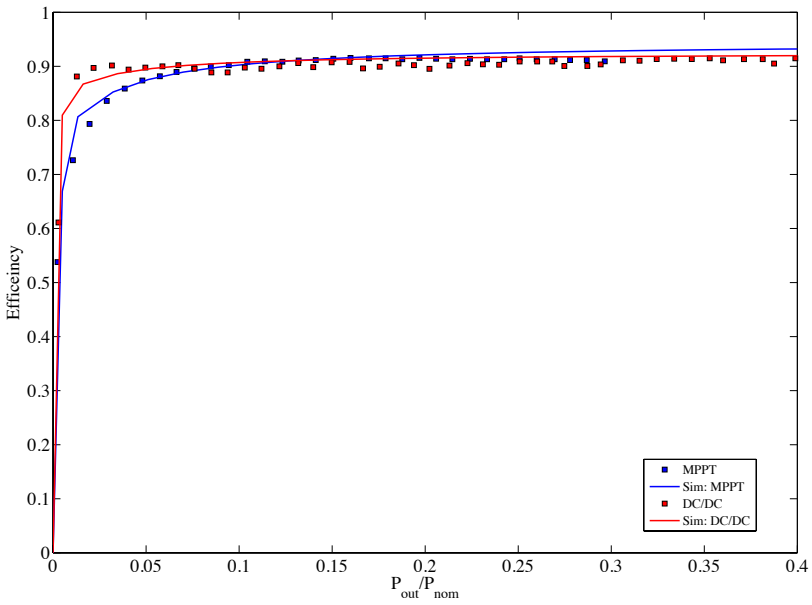

Figure 5.13: Efficiency curves for three different power conversion devices.

5.6 Integrated system model

In this section the component models described in Section 4.3 and the power controller and battery split bank controller given in Section 4.4 and Section 4.5 respectively are combined in a single integrated system model. Fig. 5.14 illustrates the flow diagram of the integrated system model. Each of the blocks in Fig. 5.14 represent an individual component. The individual components are connected together on the principle of power flow to and from each individual component model. All components are dependent on use as input and output voltage and current values from upstream and downstream components. Battery and electrolyser voltages are fed back to their individual power conversion devices as is indicated in Fig. 5.14 since these voltage levels are variable and need to be known to the upstream model to calculate output current values. Similar to what is done in Ulleberg [140] and Wang [141] components are veri-

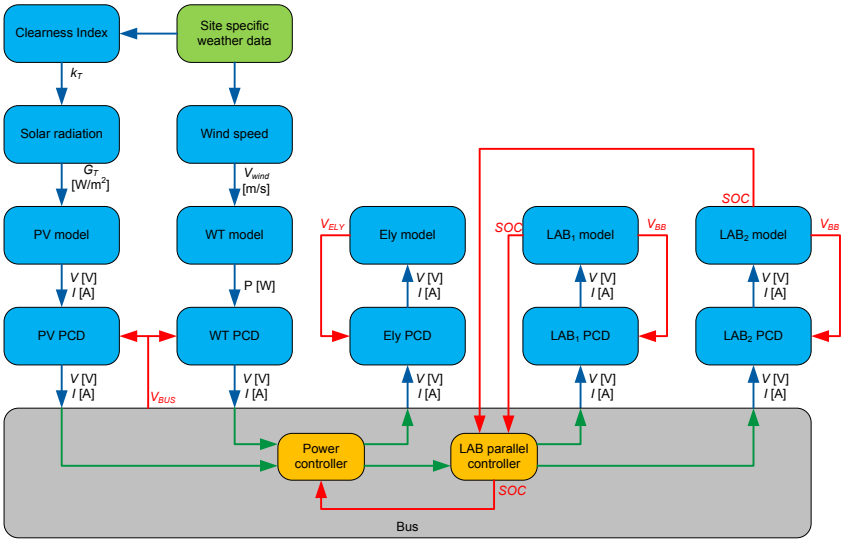

Figure 5.14: Integrated system model flow diagram.

fied and validated individually. The controller is responsible to ensure that the power through the system is managed correctly and this is verified by the principle of conservation of energy. At any time the energy-in and energy-out of the bus should be equal. This should be true regardless of the actions taken by controllers. The equation used to validate the conservation of energy is given by

$$E_{WT} + E_{PV} + E_{BB1} + E_{BB2} - E_{ely} - E_{dump} = 0, \tag{5.9}$$

where E_{WT} is the energy supplied to the bus from the WT, E_{PV} is the energy supplied to the bus from the PV array, E_{BB1} is the energy supplied to the bus or the energy drawn from the bus by BB1, E_{BB2} is the energy supplied to the bus or the energy drawn from the bus by BB2, E_{ely} is the energy supplied from the bus to the electrolyser and E_{dump} is the energy that is required to be dumped. To verify correct power flow calculations at the bus a simulation is performed over a 96 hour period. Parameters used in the simulation is provided in Fig. 5.15. Results for the simulation is provided in Fig. 5.16. The PV, WT, BB1, BB2 and electrolyser power at the bus termination is given in the top graph, and power and energy balance, based on the application of (5.9) in the bottom graph. Fig. 5.16 show results for PV and WT inputs. It is seen that the power balance remains exactly balanced (zero) and the error in energy remains negligibly small. Fig. 5.17 provides the power and energy balance an entire year. The power remains zero through the entire simulation and that the error in energy again is very small.

5.7 Conclusion

In conclusion, the major contributing characteristics of each individual components has been verified. Additionally the energy flow between the components in the combined system model is done. The interaction between the models and the power and energy management by the system controllers gives small errors.

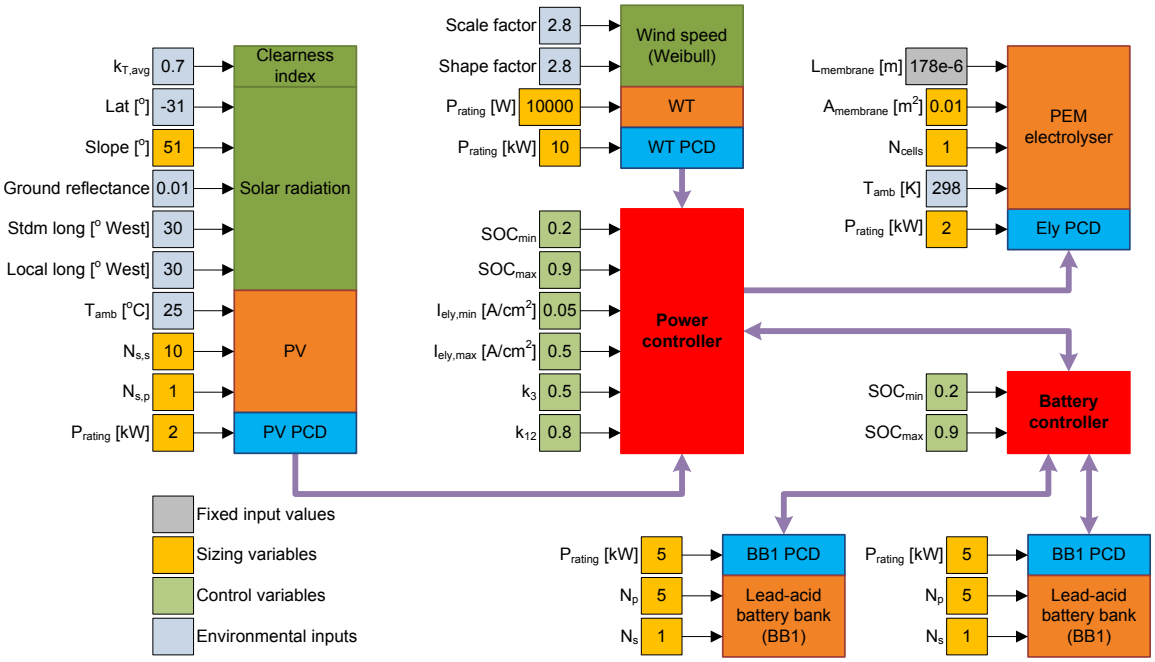

Figure 5.15: Simulation model input parameters.

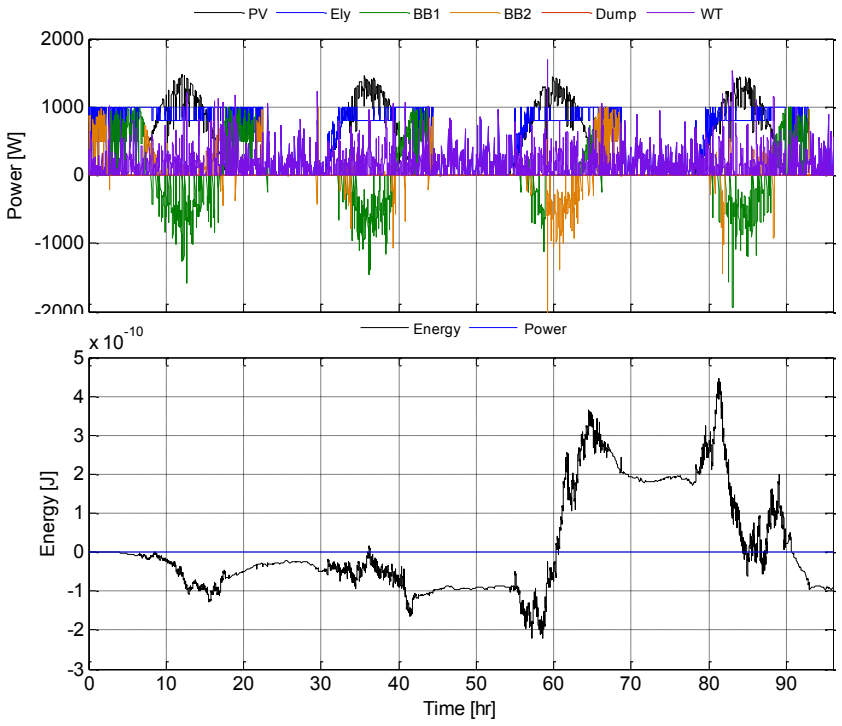

Figure 5.16: 96 hour simulation runs for system verification.

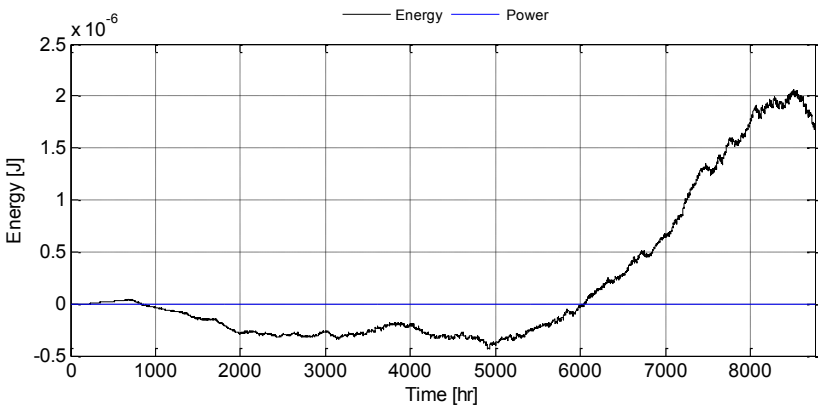

Figure 5.17: 8760 hour simulation run for system verification.

Chapter 6

Sizing and control optimisation

This chapter provides information about the optimisation strategy developed and implemented in this work. The chapter first provides a quick introduction to optimisation and fitness assignment using the Pareto optimality. Next a high level overview of the optimisation strategy is provided which is followed by a detailed discussion of the optimisation strategy developed. This is followed by information about the decision variables implemented and constraints. Finally detail about the determination of the objectives is provided in the final section.

6.1 Introduction

The general functions required for an optimisation exercise is given in Fig. 6.1 [6]. The First

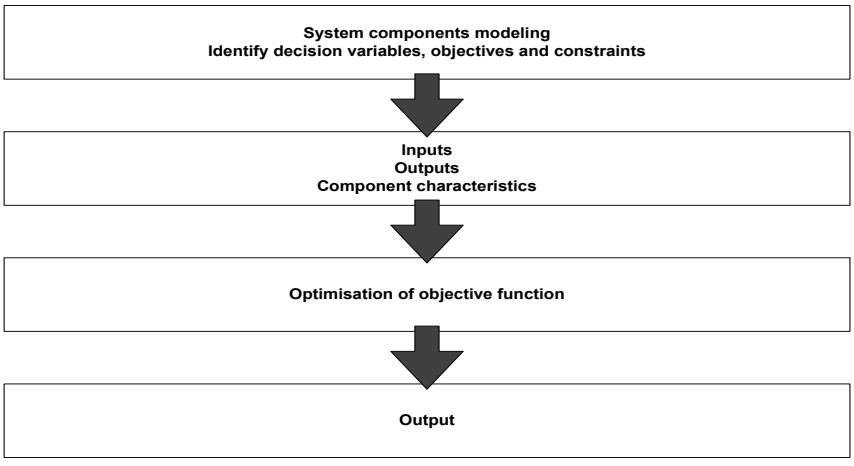

Figure 6.1: General optimisation structure.

function is the development of a general system model and the identification of the decision

variables, objectives and constraints for the system under discussion. A second function is to determine the component characteristics and the input and output data for specific systems to be used in a general system model. The third function is the selection and development of the optimisation strategy and the development of the objective functions. The last function is to construct an output that can be either in the form of text or graphic files.

This structure is followed in this work. In Chapter 4 components models are presented with inputs and outputs that are considered for optimisation. In chapter 5 the models are verified and a system model constructed. Chapter 6 continues to provide the constraints and decision variables which are part of the modesl in Chapter 4. Chapter 6 then continues to provide the optimisation strategy and provides detail about the objective functions. In Chapter 7 the output being the results from optimisation is presented and analysed.

6.1.1 Fitness assignment

When optimising a problem consisting of multiple conflicting objective functions the aim is to investigate a set of non-dominated solutions each satisfying the objectives at an acceptable level There are two possible practices for solving MOO problems. The first is by combining objective functions into a single objective function by assigning weights to each. The drawback of this practice is that it is difficult to determine weighted values because of the conflicting nature and non-commensurative objective values. The second is to implement Pareto optimum solution sets introduced by Vilfredo Pareto in 1897. A Pareto optimum consists of several non-dominated solutions referred to as the Pareto optimum set. Fig. 6.2 illustrates the concept of a Pareto optimum set in a population of 15 solutions for the two objectives, f_1 and f_2. Although

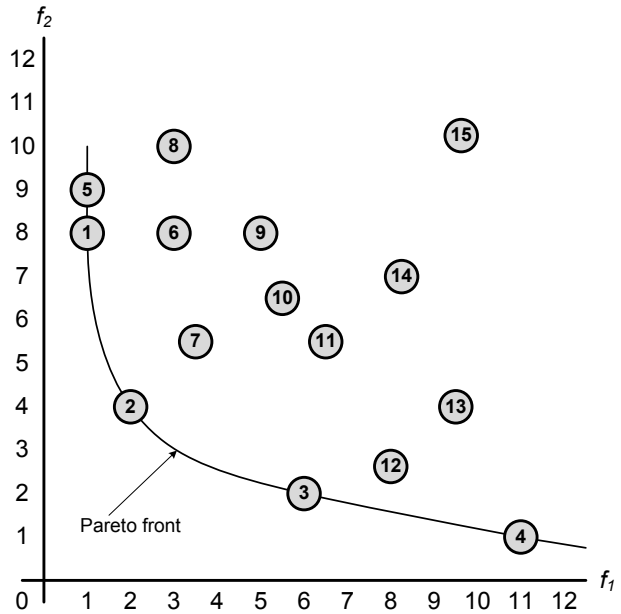

Figure 6.2: Illustration of Pareto optimum.

different ranking approaches exist the one by Goldberg [160] is considered. With this approach a solution set is assigned a fitness value equal to the number of solution sets that it is dominated by. All solution sets that are assigned a value of zero are not dominated by any other solution set and is included in the Pareto optimum solution set. A solution is part of the Pareto optimum set if it is non-dominated, meaning that for a viable solution $\bar{x}_\alpha$ there exists no other viable solution $\bar{x}_\beta$ such that $f_k(\bar{x}_\beta) \leq f_k(\bar{x}_\alpha)$ for $k = 1 : K$ (K being the number of objective functions) and $f_h(\bar{x}_\beta) < f_h(\bar{x}_\alpha)$ for at least one objective function h ($h = 1 : K$, & $h \neq k$), that would result in $\bar{x}_\alpha$ being dominated by $\bar{x}_\beta$ if the objective functions are to be minimised where $\bar{x}_\alpha$ and $\bar{x}_\beta$ are solution sets. The concept of Pareto optimality is integral in solving multiple objective problems [38].

6.2 High level optimisation

The sizing and control optimisation strategy implemented in the current work is a novel approach derived from the work done by Bernal-Augustín and Dufo-López [126]. Bernal-Augustín and Dufo-López [126] uses dissimilar objective functions for determining cost between the sizing and control optimisation. In the current work the same objective functions are evaluated for both sizing and control. Performing MOO for both sizing and control simultaneously is not possible due to the conflicting nature of the objectives. In the current work an strategy is developed where sizing and control are performed in cascade and evaluated for the same multiple objective functions. Objective functions are discussed in detail in Section 6.6. The optimisation strategy is developed and coded in the Matlab® environment.

The methodology applied determines the optimal control configuration for a single objective function within the sizing optimisation and then determines the optimal sizing configuration for all objective functions. This procedure is repeated with all objective functions for the control optimisation consecutively. Fig. 6.3 shows a high level block diagram of the optimisation strategy used. The optimisation algorithm starts by assigning the first objective function for control optimisation ($k = 1$) and then generates the initial set of *sizing solution vectors*[1] with values selected within a user specified set. Control optimisation is performed for the objective function k using a single objective GA (SOGA). The GA implemented is the standard Matlab® GA function which is configured for this application.

N_c iterations are performed for objective k. An optimum set of *control solution vectors*[2] are obtained for each sizing solution vector. Sizing optimisation is performed next for all objectives (1 to K) simultaneously using SPEA. The SPEA2 algorithm is developed in the "C" programming environment by the Hamburg University of Technology Institute of control systems. For this work the algorithm is altered for inclusion of integer decision variables and implemented in the Matlab® environment.

Based on the Pareto ranking method all non-dominated *solution vectors*[3] are considered to generate the next generation of sizing solution vectors by implementing the optimisation opera-

[1] Sizing solution vectors consists of all randomly initialised sizing decision variables.
[2] Control solution vectors consists of the optimised set of control decision variables.
[3] Solution vectors consists of the combined optimised sizing and control decision variables.

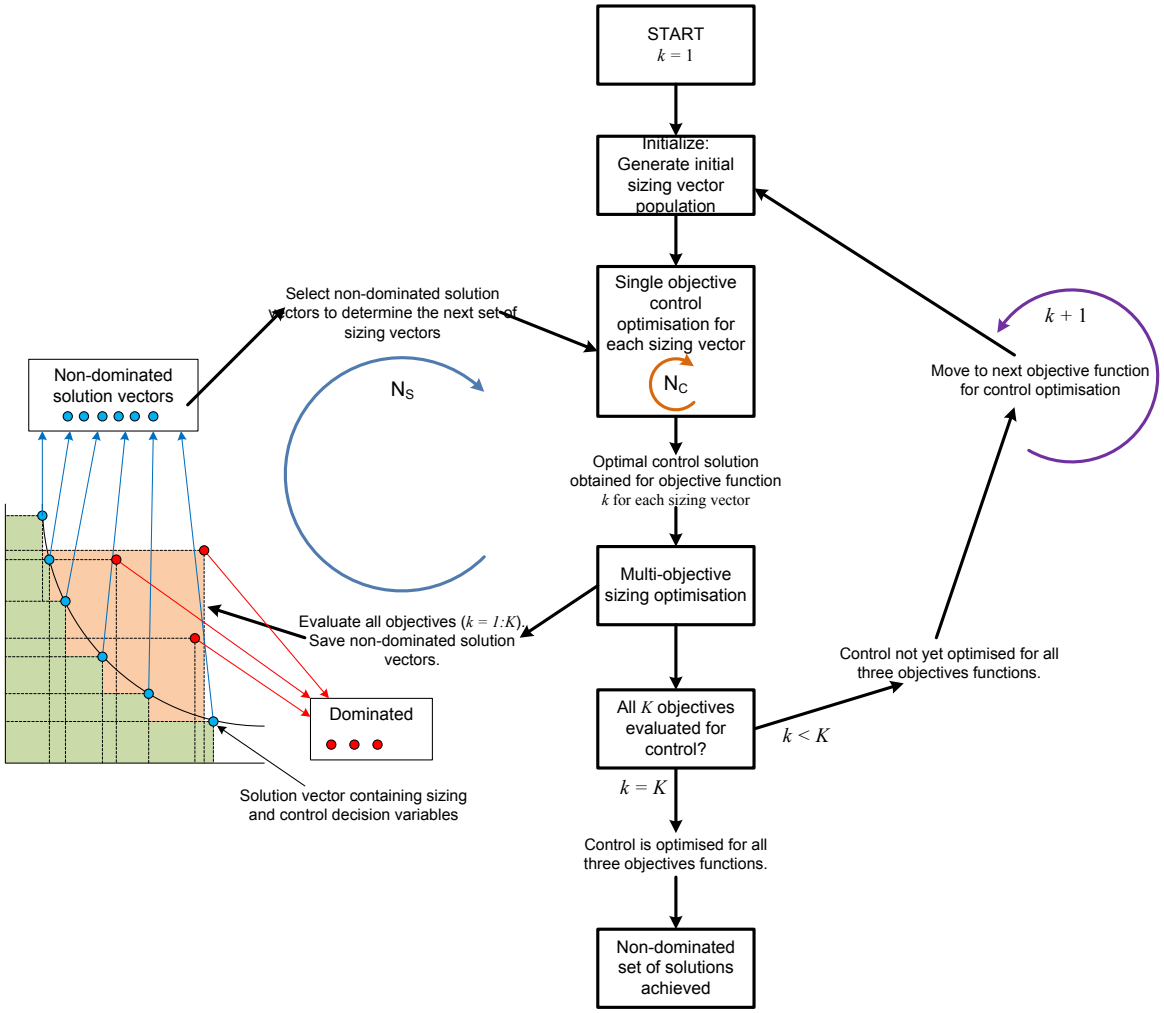

Figure 6.3: High level optimisation strategy flow diagram.

tors; selection, cross-over and mutation. N_s iterations are performed for the MOO before the next objective is optimised for control ($k = k + 1$). The entire procedure is repeated until all objectives are optimised for control ($k = K$). The result is a set of $K \times N_s$ non-dominated solution vectors.

6.3 Detail of the optimisation strategy

A detail flow diagram of the optimisation strategy is given in Fig. 6.4. A description of each of the steps is provided next:

1. Set objective function to first objective, $k = 1$ (f_1).
2. Generate initial random set of sizing population vectors.
3. Optimise control for objective function f_k using a GA. The GA is performed for N_c itera-

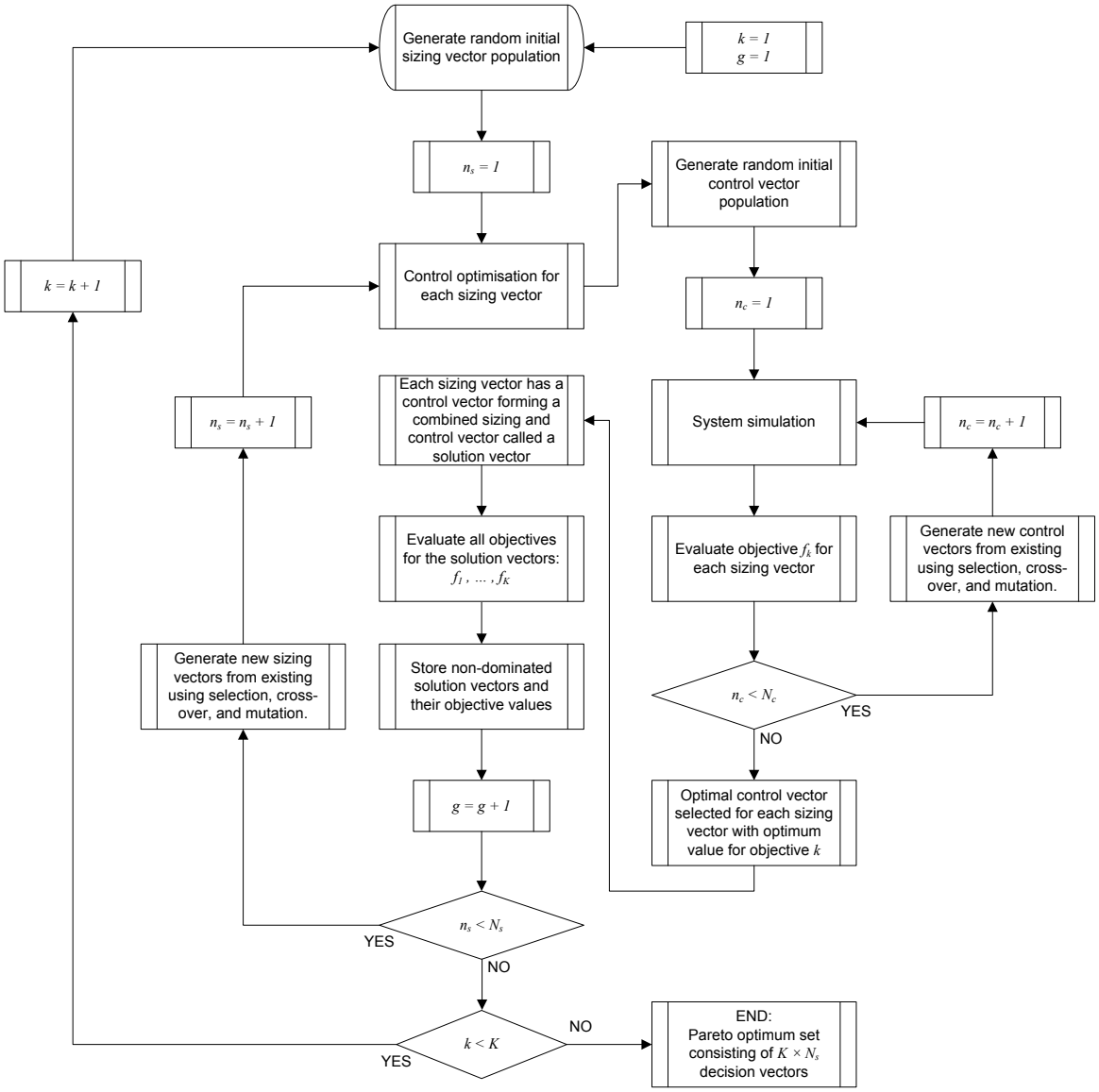

Figure 6.4: Detail optimisation strategy flowchart.

tions.

(a) Generate random initial set of control population vectors.

(b) Perform simulation runs using the solution vectors.

(c) Calculate the fitness of the objective function f_k.

(d) Implement the GA operators: selection, crossover and mutation.

(e) Repeat GA for N_s iterations.

(f) Select the solution vector with the optimum fitness value for each sizing solution vector for the objective function, f_k.

4. Calculate the fitness of the remaining objectives functions ($f_1, \ldots, f_K$).

5. Determine non-dominance of the current solution vector ($\bar{x}_g$) on the.

6. Store non-dominated objective function values and solution vector ($\bar{x}_g$) corresponding to the non-dominated objective function values.
7. Implement the SPEA operators: selection, crossover and mutation.
8. Repeat 3. to 7. for N_s iterations.
9. Select the next objective function for control optimisation, $k = k + 1$.
10. Repeat 2. to 9. K times to optimise all objective functions for control.
11. At the end of the optimisation exercise the Pareto solution set contains a maximum of $N_s \times K$ solution vectors for evaluation of both sizing and control.

There are K objectives and N_s iterations for the sizing optimisation SPEA. The SPEA evaluates all K objectives simultaneously and ranks them using Pareto ranking. The GA optimises each of the K objectives individually for every iteration of the SPEA. There is thus a control optimisation solution vector ($\bar{x}_c$) for every sizing optimisation solution vector ($\bar{x}_s$) resulting in a maximum of $g = N_s \times K$ solution vectors ($\bar{x}_g$) in the optimum Pareto solution set. The symbols used here and through the rest of the thesis are defined as:

- s subscript indicates sizing parameters.
- c subscript indicates control parameters.
- k is the identifier of the objective function, for $k = 1, K$, with K being the total number of objective functions.
- f_k is the objective function k.
- n_c is the iteration identifier of the GA, with N_c being the maximum number of iterations of the SOGA.
- n_s is the iteration identifier of the MOEA, with N_s being the maximum number of iterations of the MOEA.
- g is the iteration identifier for the combined optimisation, where $g = 1 : N_s \times K$.
- $\bar{x}_g$ is the solution vector for the decision variables and is the result of the concatenation of the sizing ($\bar{x}_s$) and control ($\bar{x}_c$) decision variable vectors and is given by (6.1).

$$\bar{x}_g = \begin{bmatrix} \bar{x}_c & \bar{x}_s \end{bmatrix} \tag{6.1}$$

6.4 Pareto ranking algorithm

The Pareto fitness assignment approach applied is a derivation of the Goldberg [160] approach. This approach assigns fitness values to all the solution sets obtained during the optimisation exercise. The value assigned is equal to the number of solution sets that it is dominated by.

For the current work a simplified version of the Goldberg [160] approach is derived which only evaluates solutions that lie on the Pareto front. The Pareto front is illustrated in Fig. 6.2. Therefore a value zero is assigned to a non-dominated solution set but all other solution sets are ignored. Fig. 6.5 gives a block diagram of the algorithm implemented.

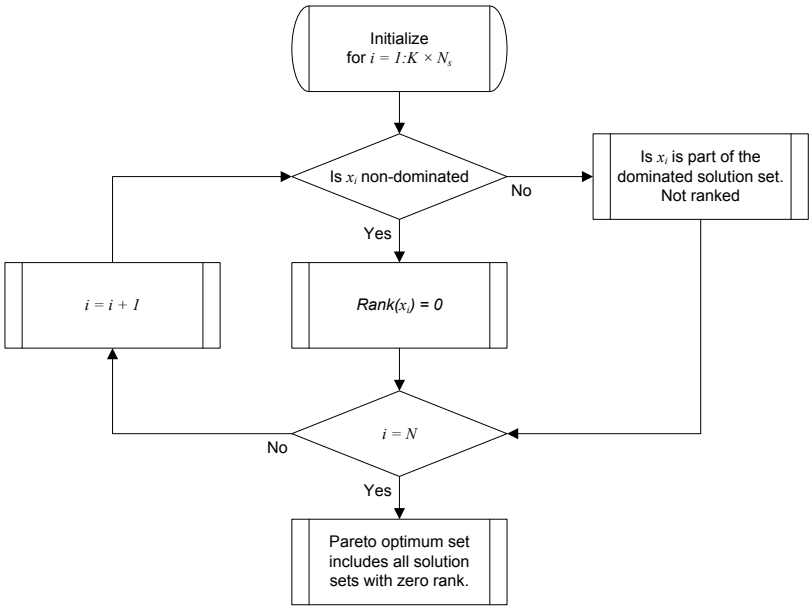

Figure 6.5: Pareto ranking algorithm.

6.5 Decision variables and constraints

Decision variables are the system variables to be determined by the optimisation exercise from a predetermined set of possible values. Constraints confine the decision variable search space to exclude unrealistic or undesirable values and in doing so improves optimisation time. Derived from the models discussed in Chapter 4 the sizing decision variables are summarised in Table 6.1 including lower and upper limits. Constraints are selected from the classification of the system and also technology limitations that exist. This type of small-scale stand alone system is classified as a medium size system having a power demand of up to 10 kW [140]. This requires 56 PV modules in total. To cater for low sky clearness and efficiencies the maximum of 20 is selected as the upper limit for PV modules in series and parallel each. For the WT an upper limit of 30 kW is selected. Electrolyser cell area upper limit is selected as 2500 cm^2 [161]. The lower limit is selected as 25 cm^2 which is not the smallest possible but for practical systems is a suitable value [161]. The number of cells are limited by the PCD model parameters implemented. The number of cells should be between 12 and 24 to limit the total voltage of the electrolyser to roughly between 24 V and 48 V. Similarly the number of 2 V single cell batteries in series are maintained between 12 and 24 to keep the voltage to around 24 V and 48 V. The rating of the battery is maintained between 120 Ah and 200 Ah as per the data sheets of valve regulated tubular batteries from HBL Power Systems Ltd. [162]. The number of batteries in

Table 6.1: Sizing decision variables.

Decision variable	Identifier	Symbol	Lower limit	Upper limit	Unit
Photovoltaic					
PV slope	x_1	β	0	90	$\angle degree$
PV panels in parallel	x_2	$N_{PV,p}$	0	10	-
PV panels in series	x_3	$N_{PV,s}$	1	10	-
Wind turbine					
WT power rating	x_4	P_{WT}	0	30	kW
PEM electrolyser					
Cell area	x_5	A_{ely}	25	150	cm^2
Number of cells	x_6	N_{ely}	12	24	-
Lead-acid batteries					
Battery bank rating	x_7	C_{10}	120	200	Ah
LAB in series	x_8	$N_{B,s}$	12	24	-
LAB in parallel	x_9	$N_{B,p}$	10	20	-

parallel are to be between 10 and 20 to ensure the search space caters for enough capacity.

From the models provided in Chapter 4 the control decision variables identified are given in Table 6.2. Table 6.2 also provides the upper and lower constraints for each of the control decision variables. For battery SOC limits 30-70 % is considered as the optimal zone for efficiency

Table 6.2: Control decision variables.

Decision variable	Identifier	Symbol	Lower limit	Upper limit	Unit
Battery minimum SOC	x_{10}	SOC_{min}	30	50	%
Battery maximum SOC	x_{11}	SOC_{max}	70	100	%
Electrolyser minimum setting	x_{12}	$I_{ely,min}$	0.05	0.5	A/cm^2
Electrolyser maximum setting	x_{13}	$I_{ely,max}$	1	2	A/cm^2
Operating mode OM3 variable	x_{14}	k_3	0	1	-
Operating mode OM12 variable	x_{15}	k_{12}	0	1	-

[151]. 30 % is selected as the SOC_{min} lower limit and 50 % as the SOC_{min} upper limit. 70 % is selected for the SOC_{max} lower limit and 100 % for the SOC_{max} upper limit. According to Carmo et al. [161] a PEM electrolyser can easily operate at current densities of 2 A/cm^2 and is therefore selected as the maximum upper limit. The minimum lower limit is selected as 0.05 A/cm^2. The control decision variables k_3 and k_{12} are fractions of the electrolyser maximum control decision variable and is given a upper limit of 1 (100 %) and lower limit of 0 (0 %).

6.6 Objective functions

In Section 3.2 it is noted that the majority of literature available mainly optimises for cost with a very small percentage also considering other objectives such as LPSP, LOLP, UL and CO_2 emissions. This study looks at three objectives simultaneously and evaluates the impact of each objective on the other. The three objectives identified are cost, efficiency and reliability. These three objectives are considered interdependent. The PEM electrolyser and LAB are negatively affected in terms of efficiency and lifetime when operated with intermittent sources. Improving the control of these two components to have them operate more efficiently and increase their lifetime will reduce their operation and maintenance costs. Detail of the calculation of the three objectives is provided in the next couple of sections.

6.6.1 Efficiency

Efficiency of a system over a time is defined as the ratio of work performed by the system to the input energy delivered to the system and is given by

$$\eta = \frac{E_{out}}{E_{in}}. \tag{6.2}$$

By improving system efficiency less input energy is required to perform the same amount of work or the same input energy is able to perform more work. This implies that improved system efficiency can reduce the system sizing and as a result also cost. For the current system efficiency is measured as the energy-out (E_{out}) over energy-in (E_{in}). Components that deliver power (E_{in}) to the system are the RE sources. Components that perform work (E_{out}) is the electrolyser. System efficiency is given by

$$\eta_{System} = \frac{\int \left(P_{Ely} \times \eta_{Ely}\right) \mathrm{dt}}{\int \left(P_{PV} + P_{WT}\right) \mathrm{dt}}, \tag{6.3}$$

where $P_{Ely} \times \eta_{Ely}$ is the power supplied to the electrolyser multiplied with the electrolyser efficiency which incorporates the H_2 production efficiency. P_{PV} and P_{WT} are the power supplied by the PV and WT respectively.

The objective function fitness value is the inverse of efficiency. The lowest fitness value will therefore produce the maximum efficiency. The objective function to be minimised for efficiency is given by

$$f_1(\bar{x}) = \frac{1}{\eta_{System}}. \tag{6.4}$$

6.6.2 Cost

The cost objective function to be minimised is the total life-cycle cost (TLCC) of the system per kilogram of H_2 produced. Equations used to determine the TLCC is described in detail in [163]. TLCC discounts all costs throughout the life of the system to an equivalent total present value

(PV) and includes all initial costs and future costs for the entire lifetime of the system. The life of the system is selected as 25 years as is commonly encountered in literature for similar systems [91]. The currency used is South African Rand (ZAR). For each component individually the TLCC is given by

$$C_{comp} = C_I + C_{O\&M} + C_R, \tag{6.5}$$

where C_I is the investment costs of the system [ZAR], $C_{O\&M}$ is the O&M costs [ZAR] and C_R is the replacement costs [ZAR]. Initial investment costs, O&M costs and the life expectancy for each component are given in Table 6.3 [164]. Cost information is obtained quotes and compared to information from a summary of RE power generation costs by the International Renewable Energy Agency (IRENA) [165].

Table 6.3: Component economic specifications.

Component	**Investment cost [ZAR]**	**O&M cost in first year [% of cost]**	**Life time [years]**
PV panels	3 600 module^{-1}	1	25
WT generator	21 700 kW^{-1}	1	25
PEM electrolyser	10 000 kW^{-1}	2	10
LAB	2 150 kWh^{-1}	1	4
Power conversion device	6 500 kW^{-1}	1	10

Investment cost per component ($C_{I_{comp}}$) is the initial purchase cost of the component and calculated by

$$C_{I_{comp}} = C_{comp} \times P_{comp}, and \tag{6.6}$$

$$C_{I_{comp}} = C_{comp} \times N_{comp}, \tag{6.7}$$

where C_{comp} is the components cost [ZAR/kW or ZAR/unit], P_{comp} is the power rating of the component and N_{comp} is the number of modules of a component. O&M costs include fuel cost, maintenance and repairs costs and recurring costs. For the current system fuel costs are zero. Present value total life-cycle O&M costs per component is calculated by

$$C_{O\&M_{comp}} = C_{O\&M_0} \times C_{I_{comp}} \times \frac{(1+d)^Y - 1}{d\,(1+d)^Y}, \tag{6.8}$$

where $C_{O\&M_0}$ is the O&M cost as a percentage of the investment cost in the first year of the system life, d is the discount rate [%] and Y is the lifetime of the system in years. Average nominal discount rate supplied by the South African Reserve Bank [166] is 9.65 %. Replacement costs is dependent on the number of components to be replaced over the lifetime of the system. Present value total life-cycle replacement costs are calculated by

$$C_{R_{comp}} = C_{comp} \times \frac{1}{(1+d)_r^Y}, \tag{6.9}$$

where Y_r in this case is the year in which the component needs to be replaced. LAB and PEM electrolysers are given a lifetime of 4 and 10 years respectively, however, it is evident from literature that these two components' lifetimes are dependent on the operating conditions (cycles,

DOD, current, etc.) that they are subjected to. For this reason the electrolyser and LAB include components that measure degradation (provided in 4.3.4 and 4.3.5 respectively) that give indication of the lifetime expectancy of the component. The number of times in the 25 year lifetime of the system the component will require to be replaced is determined. The system TLCC is given by

$$C_{total} = \sum_{i}^{p} C_{comp}, \tag{6.10}$$

with $i = 1, \ldots, p$, where p is the number of components. The objective function to be minimised for TLCC per kg of H_2 produced is given by

$$f_2(\bar{x}) = \frac{C_{total}}{m_{H_2} \times Y}, \tag{6.11}$$

where m_{H_2} is the mass of H_2 produced annually [kg] and Y is the system design life.

6.6.3 Reliability

In system engineering reliability is defined as the probability that a system or system component will accomplish its designated task satisfactorily over a certain time period when subjected to specified operating conditions [167]. The LAB and PEM electrolyser have been identified as the two components that have degradation mechanisms reducing the component's lifetime and thus reliability. These two components' reliability according to the definition provided and according to the principles of system engineering described in Blanchard and Fabrycky [167] is not well defined in literature. To define these parameters requires an in-depth study with years of data and experience.

The current work focusses on the sizing and control optimisation of a system taking into consideration certain degradation mechanisms and is therefore not concerned with the probability that the system or a component will continue to perform it's work, but rather requires a relative indication of the contribution of degradation of a certain rated component which is subjected to an intermittent operating profile. A relative value refers to a value that is used merely to compare and select the best of several different system configurations determined by the optimisation algorithm. This requires a different definition of reliability which incorporates intermittent operation and component ratings to end up with a relative indication of the component's reliability. *Reliability in this case refers to the quantification of certain identified degradation mechanisms for each component when it is subjected to an intermittent operating profile.*

From literature it is shown that the LAB's life expectancy is measured in number of cycles and dependent on the DOD that it is subjected to. In Section 4.3.5 the rain-flow cycle counting algorithm used to ultimately determine the battery capacity lost is described in detail. The overall reliability of the batteries is an exponential function of the average capacity lost between the two components and is given by

$$R_{BB} = \exp\left(\frac{-q_{BB1_{lost}} - q_{BB2_{lost}}}{2}\right), \tag{6.12}$$

where $q_{BB1_{lost}}$ and $q_{BB2_{lost}}$ are the percentage of capacity lost during the year. The maximum battery capacity that can be lost is 20 % after which the battery is considered dead.

For the electrolyser there is also a performance degradation over time. This degradation has been quantified in literature as a voltage increase over time [161]. Clarke et al. [31] evaluated the direct coupling of an electrolyser with a PV system and discovered that the electrolyser degradation was much more than expected. This is attributed to the highly fluctuating power input which adversely affects lifetime. Testing to date has not yet been performed to determine the extent to which lifetime degradation is directly contributed to the variability of the power input. Ulleberg [140] uses the number of starts and average run time as comparison between different simulation runs consisting of different operating strategies. The average run-time per ON cycle can be used as a method of comparing the reliability between several sizing and control configurations. The electrolyser reliability is an exponential function of the difference between the maximum possible average cycle time for the current site and the actual measured average cycle time and is given by

$$R_{ely} = \exp\left(-T_{ely,avg_{max}} + T_{ely,avg}\right), \tag{6.13}$$

where $T_{ely,avg_{max}}$ is the maximum possible average time per ON cycle that can be achieved at the specified geographic site and $T_{ely,avg}$ is the actual average operating time per ON cycle measured. The objective function to be minimised for the total relative reliability for this system is given by

$$f_3(\bar{x}) = \left(R_{ely} \times R_{BB}\right)^{-1}. \tag{6.14}$$

6.7 Conclusion

In conclusion, an new optimisation strategy is developed for this work. The new optimisation strategy uses both GA and SPEA combined into one SPEAGA. Further information about the decision variables implemented and constraints used were discussed. Objective functions are provided and discussed in detail.

Chapter 7

Results and discussion

This chapter gives the results obtained, analyses of the results and a summary of insights. The optimisation strategy described in Section 6 determines values for the independent variables and eliminates all dominated solutions resulting in solution sets that lie on the Pareto front. The first section gives information of the three different geographic sites and further gives an explanation of the analysis procedure implemented. Next, results from the optimisation exercise are provided. The process followed to perform the analysis is also described in detail. Next, a comparison is provided between the novel SPEAGA developed for this study and a standard SPEA algorithm. This is followed by the implementation of the GFS and membership function (MF) reduction used in the analysis to gain information from the Pareto sets. Finally the results are interpreted and insights gained are summarised.

7.1 Results analysis procedure

In this section the Pareto optimal sets determined for three different sites are discussed and analysed. Two different optimisation strategies are used to generate Pareto optimal sets. The first is the novel optimisation strategy (SPEAGA) and the second is a standard SPEA algorithm [168]. The analysis procedure followed for each site is provided in Fig. 7.1. The three sites represent three different combinations of wind and solar power resource potentials. Sites are identified based on wind and solar power classifications provided in Table 7.1 and Table 7.2 respectively with Table 7.3 providing the classification of the three sites studied for this study. Site A has excellent solar and poor wind resources. Site B has good solar and fair to almost good wind resources. Site C has marginal solar and outstanding wind resources.

7.2 Simulation and optimisation results

This section provides results obtained from the implementation of the simulation and optimisation exercises. Results from each of the geographic sites are provided as Pareto optimal sets. The Pareto surface plot giving all non-dominated solution sets for site A is provided in Fig.

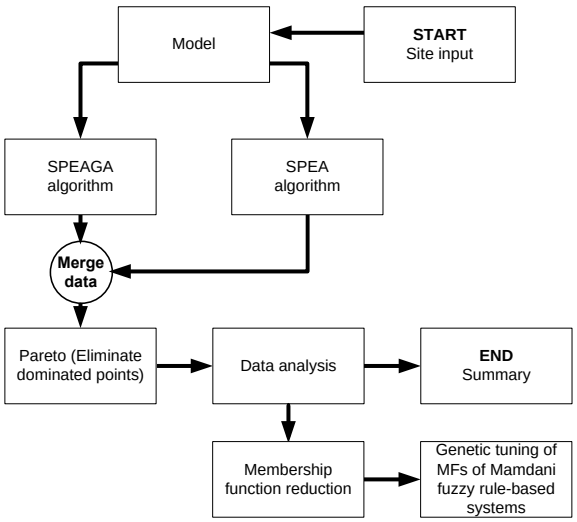

Figure 7.1: Results analysis procedure.

Table 7.1: Wind power classification.

Wind power class	Resource potential	Wind power density @ 10 m [W/m^2]	Wind speed @ 10 m [m/s]
1	Poor	0-100	0-3.2
2	Marginal	100-150	3.2-4.8
3	Fair	150-200	4.8-5.6
4	Good	200-250	5.6-6
5	Excellent	250-300	6-6.4
6	Outstanding	300-400	6.4-7
7	Superb	> 400	> 7

Table 7.2: Solar power classification.

Solar power class	Resource potential	Solar power density [kWh/m^2/day]
1	Poor	1.0-1.9
2	Marginal	2.0-2.9
3	Fair	3.0-3.9
4	Good	4.0-4.9
5	Excellent	5.0-5.9
6	Outstanding	6.0-6.9

Table 7.3: Sites classification.

	Site A			Site B			Site C		
Resource	Value	Class	Resource potential	Value	Class	Resource potential	Value	Class	Resource Potential
Wind [m/s]	1.7	1	Poor	5.5	3	Fair	6.5	6	Outstanding
Solar [kWh/m^2/day]	5.6	5	Excellent	4.84	4	Good	2.6	2	Marginal

7.2. The figure gives the 3D Pareto surface generated from the data of the Pareto optimal set as determined by the optimisation exercise for site A. The actual solution sets are the red squares in that can be seen in Fig. 7.2. The surface area is an extrapolation from the solution sets. Extrapolation of the 3D scattered data is performed using the *griddata* function in Matlab®. The colours of the 3D Pareto surface give an indication of the density of solution sets over the Pareto front and are directly related to the number of solution sets inside a closed ball defined in 7.1. Dark red areas are densely populated while blue areas are sparsely populated. The density of solution vectors on the Pareto front is used to evaluate the ability of the optimisation ap-

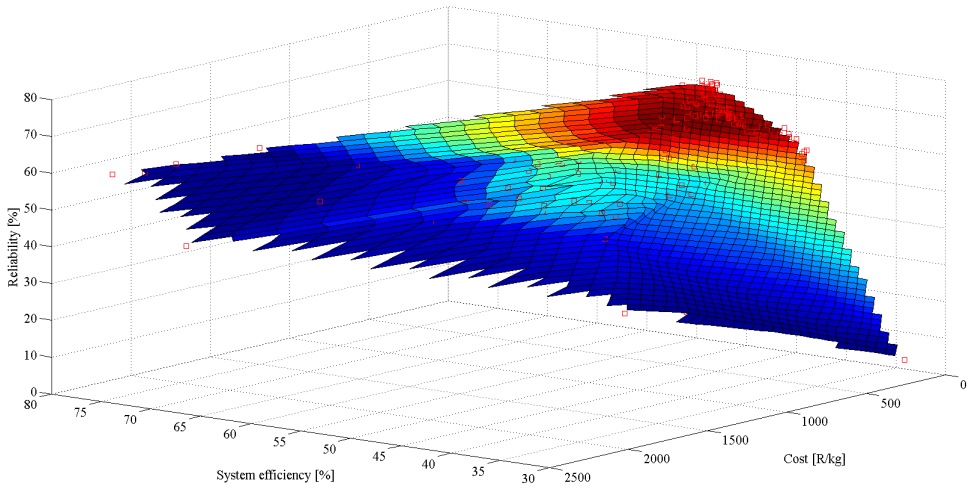

Figure 7.2: 3D Pareto surface for Site A.

proach to adequately search the entire search space. For each solution vector (F_1,...,F_b) on the Pareto front the average normalized distance to all other solution vectors is determined with the minimum of these averages selected as a closed ball defined by

$$\tilde{B}(F_{b_0}, r) = \{F_b \epsilon \mathbb{R} | d(F_b, F_{b_0}) \leq r\}, \tag{7.1}$$

for b solution vectors, with F_{b_0} the centre of the closed ball, and d the distance function which associates a distance $d(F_b,F_{b_0})=|F_b - F_{b_0}|$ for every pair of solution vectors. For each solution vector (F_{b_0}) the number of solution vectors with $d \leq r$ is counted providing a measure of solution vector density on the Pareto front.

The 3D Pareto surface is difficult to analyse due to the three dimensional visualization and the non-commensurative objectives. Fig. 7.3 gives the objective values for the solution sets for Site A in two dimensions using linked multiple two-dimensional scatter plots which are easier to analyse. Additionally, box plots for each objective are provided and gives a good overview of the distribution of objective values. An explanation of a box plot is provided in Fig. 7.4. Looking at the box plots of efficiency and cost in Fig. 7.3 a large number of outliers is observed. Further a group of detached solution sets are present in the *efficiency-cost* and *efficiency-reliability* scatter plots. These points have a *very low* efficiency and although they are part of the Pareto set are not considered desired solution sets. *Very low* reliability objective values are present which are also not desired. These undesired solution sets are eliminated resulting in a modified solution set [169]. The resulting 3D Pareto surface of the modified data are given in Fig. 7.5 and multiple scatter plots of the modified data are given in Fig. 7.6. Box plots in Fig. 7.6 show no outliers and have an improved distribution of objective values. Certain trends also become clearly visible from Fig. 7.6. A proportional linear relationship exists between efficiency and cost objectives implying that *high* cost results in *high* efficiency while *low* cost results in *low* efficiency. There are some less evident trends between efficiency and reliability and between cost and reliability.

The same methodology for site A is followed for site B and site C. The 3D Pareto surface plot with the already modified solution sets for site B is provided in Fig. 7.7 and multiple scatter

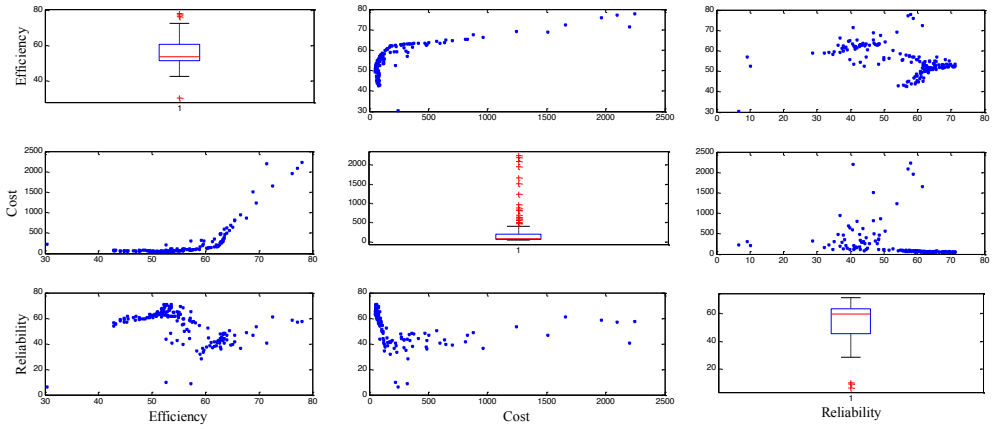

Figure 7.3: Multiple scatter plots for site A.

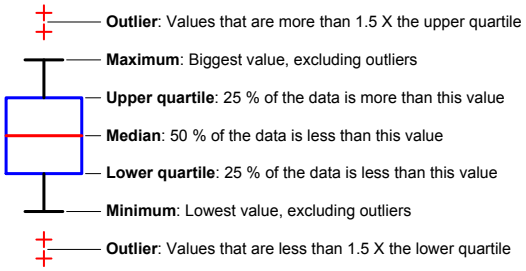

Figure 7.4: Box plots explained.

plots of the modified data are given in Fig. 7.8. The relationship between the three objectives show the same trends as observed for Site A in Fig. 7.6. A proportional linear relationship is observed between efficiency and cost implying that *high* cost results in *high* efficiency while *low* cost results in *low* efficiency. Again there are some less evident trends between efficiency and reliability and between cost and reliability. The 3D Pareto surface plot with the already modified solution sets for site C are provided in Fig. 7.9 and multiple scatter plots of the modified data are given in Fig. 7.10. The relationship between the three objectives again show similar trends as observed for Site A and B in Fig. 7.6 and Fig. 7.8 respectively. A proportional linear relationship is observed between efficiency and cost implying that *high* cost results in *high* efficiency while *low* cost results in *low* efficiency. Scatter plots of variables plotted against objectives are provided in Appendix A.

7.3 SPEAGA and SPEA compared

Two optimisation algorithms are implemented to generate Pareto solution sets. The first is the novel optimisation strategy developed in this work and discussed in detail in Chapter 6 and the second is the SPEA2 algorithm developed by the Hamburg University of Technology Institute of Control Systems [168]. The algorithm is developed in the C code, and implemented

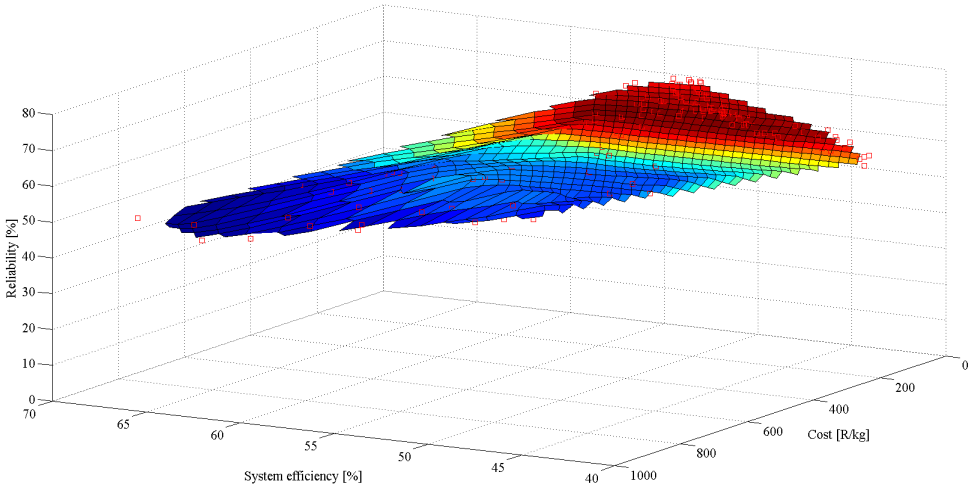

Figure 7.5: Site A modified 3D Pareto surface.

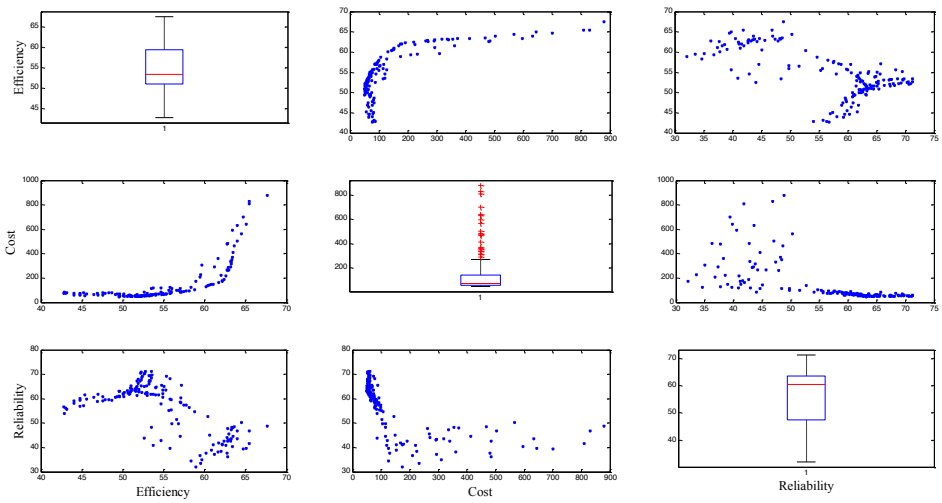

Figure 7.6: Site A modified multiple scatter plots.

in the Matlab® environment. The source code is altered for this application to include the use of integer values. Results of the two different strategies are compared for site A, B and C in Fig. 7.11, Fig. 7.12 and Fig. 7.13 respectively. SPEAGA show higher (improved) objective values for the two objectives efficiency and reliability for site A and site B while the cost objective values appear to be unaffected. Site C results show only a couple of solutions that have improved reliability but not as significant as sites A and B. For site C efficiency SPEAGA does not show improvement over SPEA. SPEAGA produce narrower results in a distribution of solutions. This shows that although improved single values are not achievable, the entire solution set has improved. The major difference between the SPEA and the SPEAGA is that the SPEAGA focusses on the control variables for each objective whereas the SPEA considers all variables for all objectives simultaneously. The fact that system efficiency and reliability show improved objective values when using the SPEAGA strategy implies that these two objectives are more dependent on the control variable settings. Having interdependent optimisation of sizing and

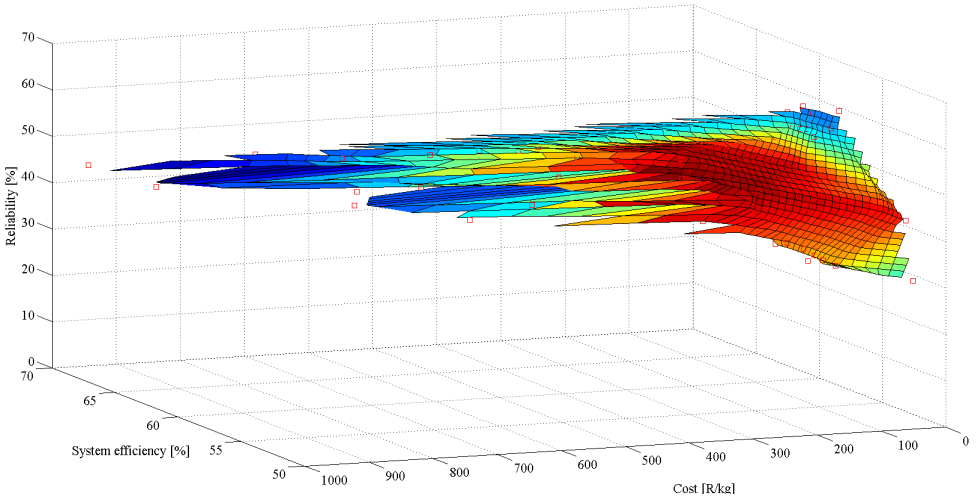

Figure 7.7: Site B modified 3D Pareto surface.

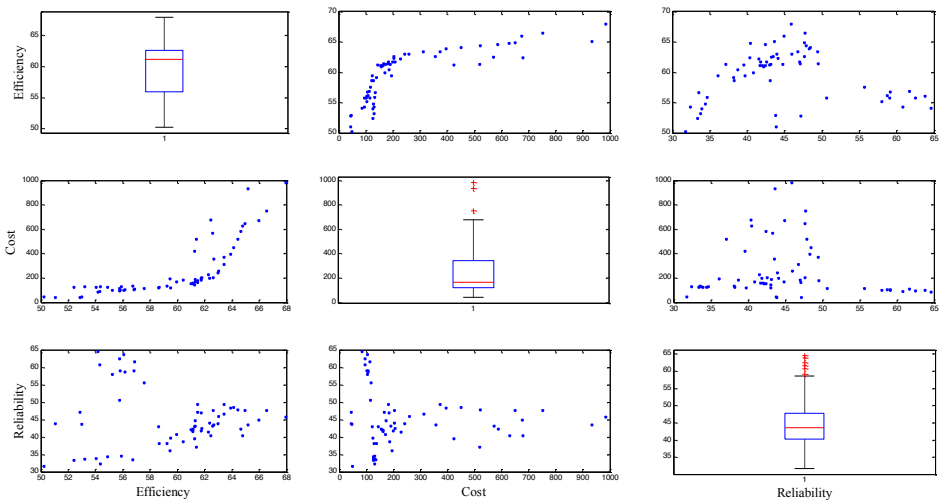

Figure 7.8: Site B modified multiple scatter plots.

control variables improves the efficiency and reliability objectives while not affecting the cost objective.

7.4 Genetic fuzzy rule-based system and MF reduction

This section provides the discussion and results of the genetic fuzzy rule-based system with membership function reduction. Firstly, detail on the method and implementation of the developed fuzzy rule-based system is provided. This is followed by a rule-base development for each site together with a corresponding interpretation and generalisation/insights.

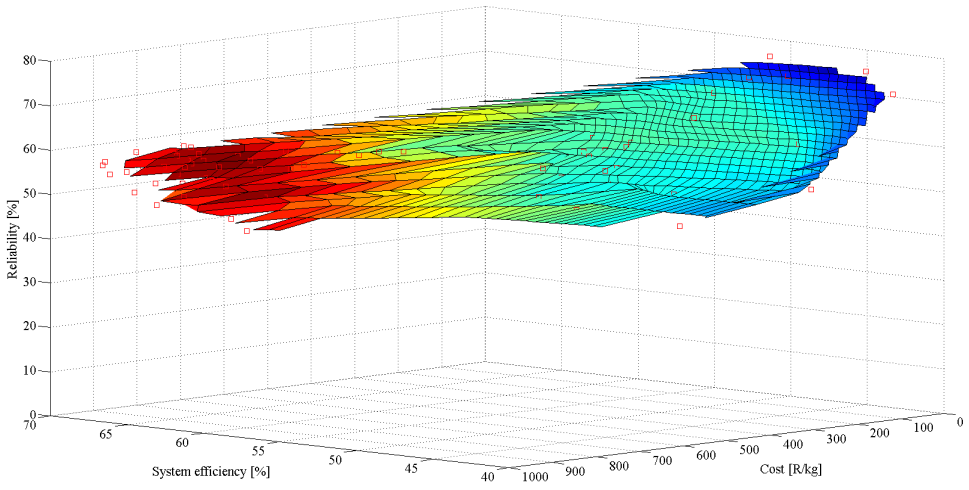

Figure 7.9: Site C modified 3D Pareto surface.

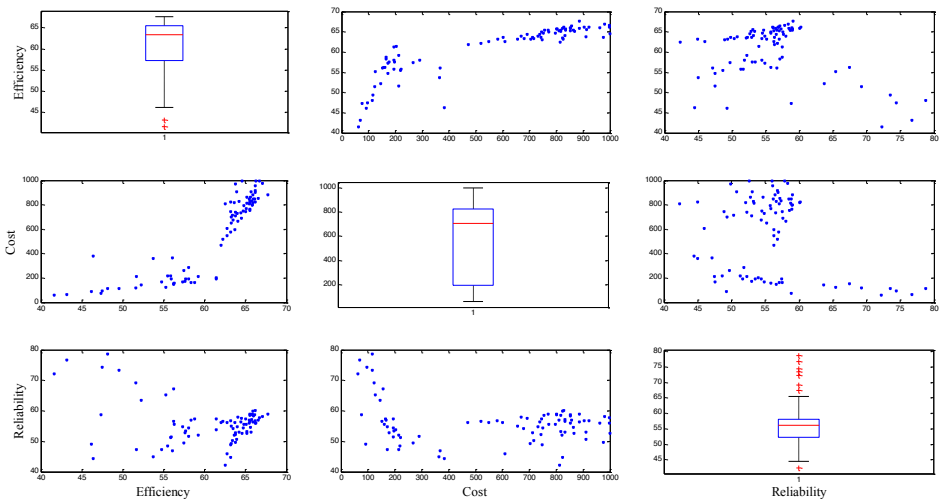

Figure 7.10: Site C modified multiple scatter plots.

7.4.1 Rule extraction procedure

Hybrid renewable H_2 systems are complex non-linear systems with multiple variables which make developing a model for predicting outputs a difficult task. One very successful modelling tool capable of coping with complex and poorly defined systems is rule-based fuzzy logic (FL) system. The application of FL to rule-based systems consider ”IF-THEN” statements called fuzzy rules. Using linguistic variables with linguistic values enhances the knowledge representation. Values for the linguistic variables are defined by context-dependent fuzzy sets whose meanings are specified by gradual membership functions. This chapter presents the hybrid procedure that implements a GA to train a FL rule-based system. Further the implementation of a rule reduction methodology to reduce the number of membership functions in each rule is given. A layout of the procedure is given in Fig. 7.14. Input data to the GFS is the Pareto optimal sets generated by the optimisation exercise. The k-means clustering function is

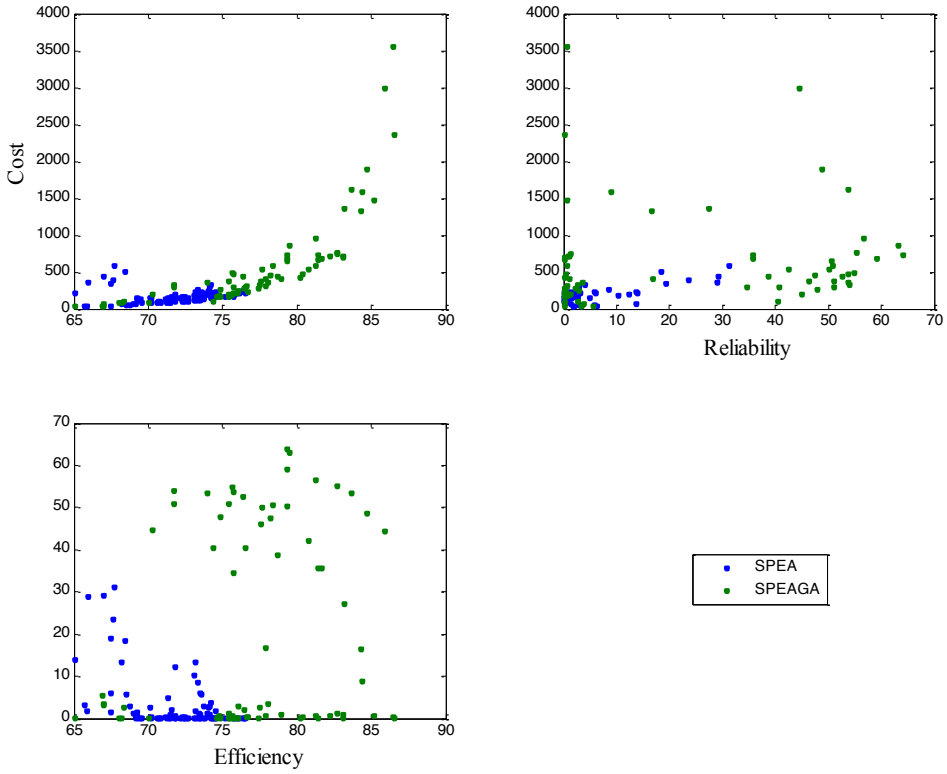

Figure 7.11: SPEA vs. SPEAGA for Site A.

implemented to determine the centres of MFs for the fuzzy rule-based system. A GA in implemented to train fuzzy rule-based system by determining values for the shape factor of the fuzzy rule-based system. Both the k-mean clustering and GA functions implemented are the standard functions available in the Matlab® environment. In order to reduce the complexity of the derived rule-base the MFs are removed using specified criteria.

For engineering applications where input and output data sets are real values, a FL rule-based system incorporating a fuzzifier and defuzzifier is most commonly used. The FL rule-base comprises IF-THEN rules that are mapped from fuzzy sets in the input universe of discourse $U \subset \mathbb{R}^n$ to fuzzy sets in the output universe of discourse $V \subset \mathbb{R}$.

The fuzzifier maps crisp points x in $U \in \mathbb{R}$ to fuzzy sets in U and the defuzzifier maps fuzzy sets in V to crisp points y in $V \in \mathbb{R}$. The fuzzy rule-base consists of fuzzy IF-THEN rules. A fuzzy inference engine uses these rules to map fuzzy sets in the input space U to fuzzy sets in the output space V using fuzzy logic principles. The form of the fuzzy rule-base is given by

$$R^{(\ell)} : \text{IF } x_1 \text{ is } F_1^\ell \text{ and } \ldots \text{ and } x_n \text{ is } F_n^\ell, \text{ THEN } y \text{ is } G^\ell, \tag{7.2}$$

where F_i^ℓ and G^ℓ are fuzzy sets in $U_i \subset \mathbb{R}$ and $V \subset \mathbb{R}$ respectively and $\underline{x} = (x_1, \ldots, x_n)^T \in U_1 \times \cdots \times U_n$ and $y \in V$ are linguistic variables. $\ell = 1, 2, \ldots, M$ with M being the number of rules (clusters). The $\underline{x}$ and y are the input and output to the fuzzy logic system. Each rule given by (7.2) defines a fuzzy set $F_i^\ell \times \cdots \times F_n^\ell \to G^\ell$ in $U \times V$. The FL rule-based system is given by

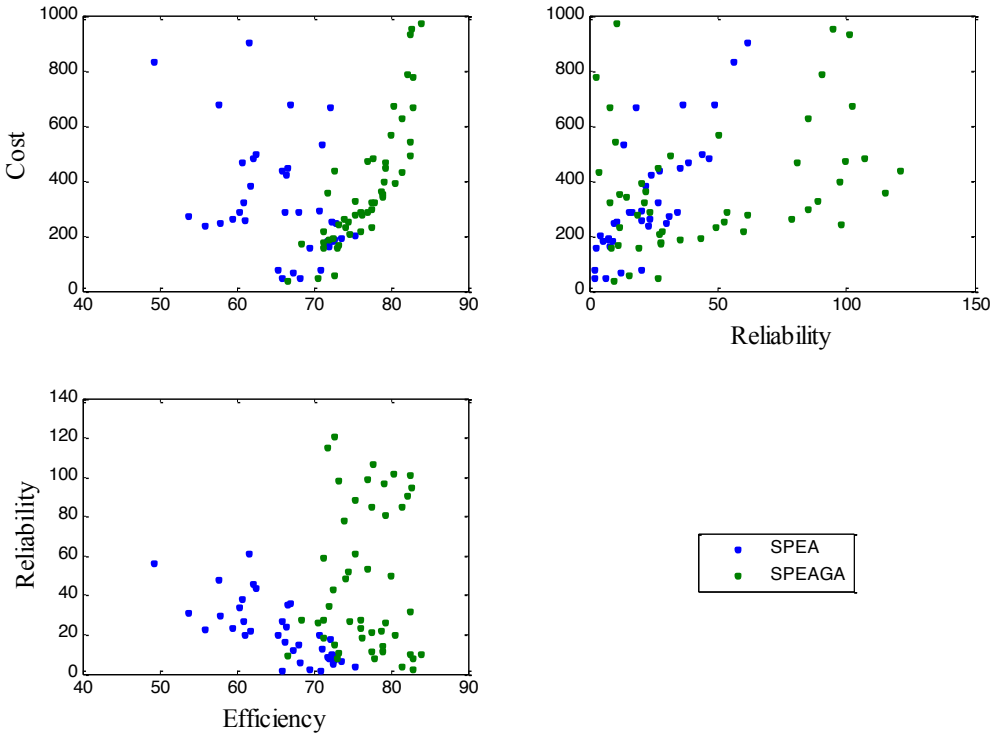

Figure 7.12: SPEA vs. SPEAGA for Site B.

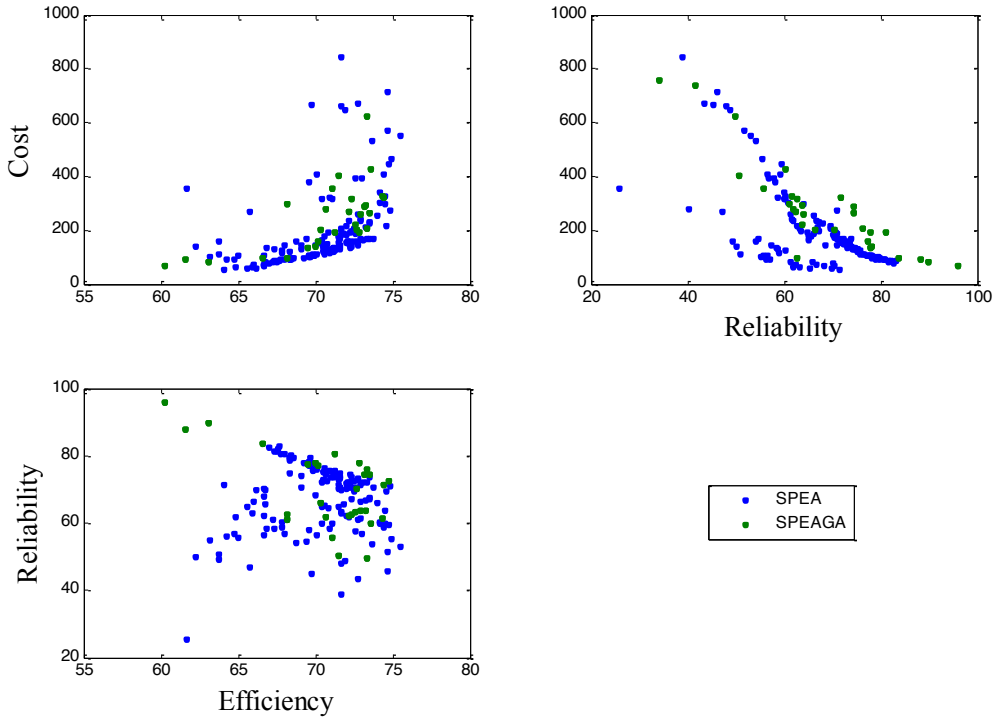

Figure 7.13: SPEA vs. SPEAGA for Site C.

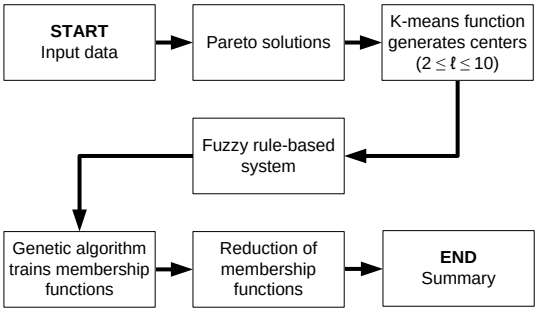

Figure 7.14: Genetic fuzzy rule extraction procedure.

[170]

$$f(\bar{x}) = \frac{\sum_{\ell=1}^{M} \tilde{y}^{\ell} \left[\prod_{i=1}^{n} exp\left(- \left(\frac{x_i - \tilde{x}_i^{\ell}}{\sigma_i^{\ell}} \right)^2 \right) \right]}{\sum_{\ell=1}^{M} \left[\prod_{i=1}^{n} exp\left(- \left(\frac{x_i - \tilde{x}_i^{\ell}}{\sigma_i^{\ell}} \right)^2 \right) \right]}, \tag{7.3}$$

where $\bar{x}$ is an input vector set, $\tilde{y}^{\ell}$ is the centre value of cluster ℓ of the output variable, $\tilde{x}_i^{\ell}$ is the centre value of cluster ℓ for input variable i and σ_i^{ℓ} is the Gaussian function shape factor. The FL rule-based system given in (7.3) implements a centre average defuzzifier, inference engine with product inference rule, singleton fuzzifier and Gaussian membership function (MF). One drawback of FL rule-based systems is the lack of learning ability. Two possible methods to determine rules include asking human experts or implementing training algorithms based on measured data [170].

In this thesis an GA is used to adjust certain adjustable parameters of a FL rule-based system. Such a genetically trained fuzzy-system is known as a GFS. The GA is a well known global search algorithm capable of exploring large complex search spaces. Adjustable parameters of the fuzzy system include, fuzzy membership function parameters, fuzzy rules and number of rules [171]. For this work a GA is implemented to determine the shape parameter (σ) of a Gaussian MF. The algorithm developed for training the FL rule-based system is given in Fig. 7.15. This process is followed for each objective function. Input data used for the training of the genetic fuzzy rule-based system is obtained from the Pareto optimal set results. 70 % of the input data set is used to train the FL rule-based system while the remaining 30 % of the input data set is reserved to test the resulting FL rule-based system. The number of clusters are determined by executing the GA optimisation of the fuzzy system for different cluster values consecutively starting at two. The final number of clusters selected is determined from the root mean squared error (RMSE). The RMSE is the objective function of the GA training the fuzzy system [171]. As the number of clusters increases the RMSE value converges. The optimal cluster is selected based on the RMSE value. The total number of MFs is the product of the number of clusters and the number of input variables. In order to reduce the number of MFs of each rule, MFs are eliminated one by one. Only the MFs resulting in a difference in RMSE value less than 10 % are eliminated. The RMSE is determined by

$$RMSE = \sqrt{\frac{\sum_{j=1}^{N} \left(f\left(\bar{x}_j\right) - \hat{y}_j \right)^2}{N}}, \tag{7.4}$$

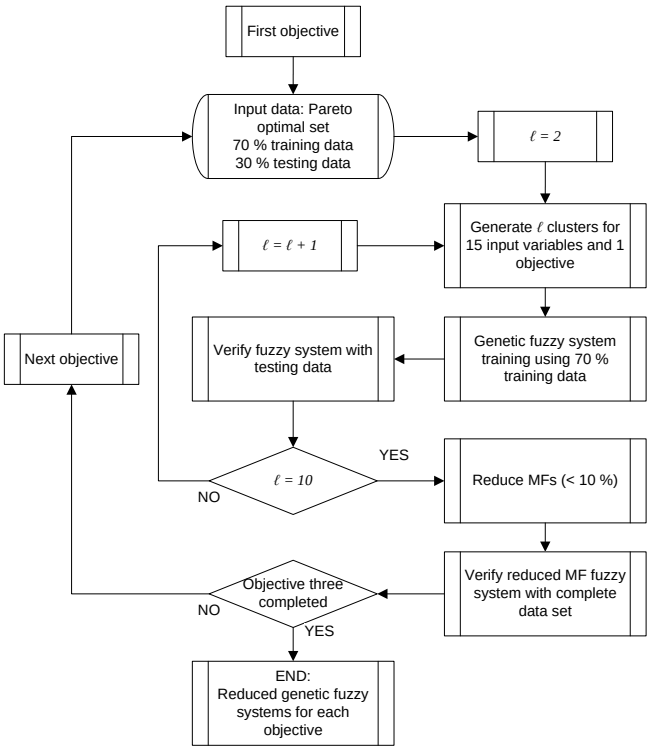

Figure 7.15: Detailed genetic fuzzy system process.

where $f\left(\bar{x}_j\right)$ is the predicted output. $\bar{x}_j$ is the input variable set reserved for testing, $\hat{y}_j$ is the corresponding output variable. N is the number of input output pairs in the test set.

For reference purposes detail of the 15 independent variables and three objectives with their fuzzy linguistic classification are provided in Table 7.4. The table lists each input variable and objective, gives the reference used in figures and tables for simplicity, provides a symbol, the range used in the optimisation exercise and values of the linguistic variables. Each input variable and objective is divided into five linguistic variables: *low*, *very low*, *mid*, *high* and *very high*. These linguistic variables are used in the fuzzy rule-base. Results for each of the sites are provided in the next three sections followed by a comparison of the results from the three sites.

7.4.2 Site A

The first task is to determine the optimal number of clusters for each objective to ensure the least number of rules is used while sufficient accuracy is maintained. The number of clusters is also the number of rules that will be used in the rule base. Once the number of rules is fixed the reduction of the MFs is done and the resulting rule bases provided. Through interpretation of the rule bases, much sought after insights in terms of sizing and controlling small-scale hybrid RESs are derived.

Optimal clusters

Fig. 7.16 illustrates RMSE values achieved using (7.4) for different numbers of clusters for each of the three objectives. The number of clusters also imply the number of rules in a rule base. From Fig. 7.16 the least number of rules providing an acceptable RMSE value for each objective needs to be determined. The objectives are non-commensurable and as a result the RMSE values differ. The optimal number of rules used for each objective are determined as the cluster for which the RMSE value converges to an acceptable RMSE value which still fits the data sufficiently accurate. For the efficiency objective the optimal number of rules is determined to be seven. For cost the optimal number of rules is determined to be nine and for reliability the optimal number of rules is determined to be nine.

Membership function reduction

The MF reduction process involves removing MFs one by one from each rule while monitoring the RMSE value. Removing MFs reduces the complexity of the fuzzy system and makes interpretation of the fuzzy rule base much simpler. Only MFs that result in a RMSE value difference of less than 10 % are eliminated. Fig. 7.17 provides fits of the GFS before and after MF reduction for the three objectives against the measured data.

Table 7.4: Independent variable and objective definition and linguistic classification.

Variabels	Reference	Symbol	Unit	Range	*Very low*	*Low*	*Mid*	*High*	*Very high*
Sizing variables									
PV slope	Var 1	β	$\angle^o$	0-90	< 18	18-36	36-54	54-72	> 72
PV panels in series	Var 2	$N_{PV,s}$	-	0-10	< 2	2-4	4-6	6-8	> 8
PV panels in parallel	Var 3	$N_{PV,p}$	-	1-10	< 2.8	2.8-4.6	4.6-6.4	6.4-8.2	> 8.2
WT power rating	Var 4	P_{WT}	kW	0-30	< 6	6-12	12-18	18-24	> 24
Electrolyser cell area	Var 5	A_{ely}	cm^2	25-150	< 50	50-75	75-100	100-125	> 125
Electrolyser number of cells	Var 6	N_{ely}	-	12-24	< 14.4	14.4-16.8	16.8-19.2	19.2-21.6	> 21.6
LAB Ah rating	Var 7	C_{10}	Ah	120-200	< 136	136-152	152-168	168.184	> 184
LAB in series	Var 8	$N_{B,s}$	-	12-24	< 14.4	14.4-16.8	16.8-19.2	19.2-21.6	> 21.6
LAB in parallel	Var 9	$N_{B,p}$	-	10-20	< 12	12-14	14-16	16-18	> 18
Control variables									
Minimum battery SOC	Var 10	SOC_{min}	%	30-50	< 34	34-38	38-42	42-46	> 46
Maximum battery SOC	Var 11	SOC_{max}	%	70-100	< 76	76-82	82-88	88-94	> 94
Minimum electrolyser current density	Var 12	$I_{ely,min}$	A/dm^2	5-50	< 14	14-23	23-32	32-41	> 41
Maximum electrolyser current density	Var 13	$I_{ely,max}$	A/dm^2	100-200	< 120	120-140	140-160	160-180	> 180
OM3 (Energy distribution parameter)	Var 14	k_3	%	0-100	< 20	20-40	40-60	60-80	> 80
OM12 (Energy distribution parameter)	Var 15	k_{12}	%	0-100	< 20	20-40	40-60	60-80	> 80
Optimisation objectives									
Efficiency	Obj X	Eff	%	0-100	< 20	20-40	40-60	60-80	> 80
Cost	Obj Y	Cost	R/kg	0-1000	< 200	200-400	400-600	600-800	> 800
Reliability	Obj Z	Rel	%	0-100	< 20	20-40	40-60	60-80	> 80

The reduced MF rules are graphically illustrated in Fig. 7.18, Fig. 7.19 and Fig. 7.20 for efficiency, cost and reliability respectively. MFs that have been eliminated show light grey variable information and no MF plot. MFs that are included show blue variable information and red graphs showing the Gaussian MF plot. The first 15 columns give the 15 independent variables and the last (16^{th}) column gives the specific objective information.

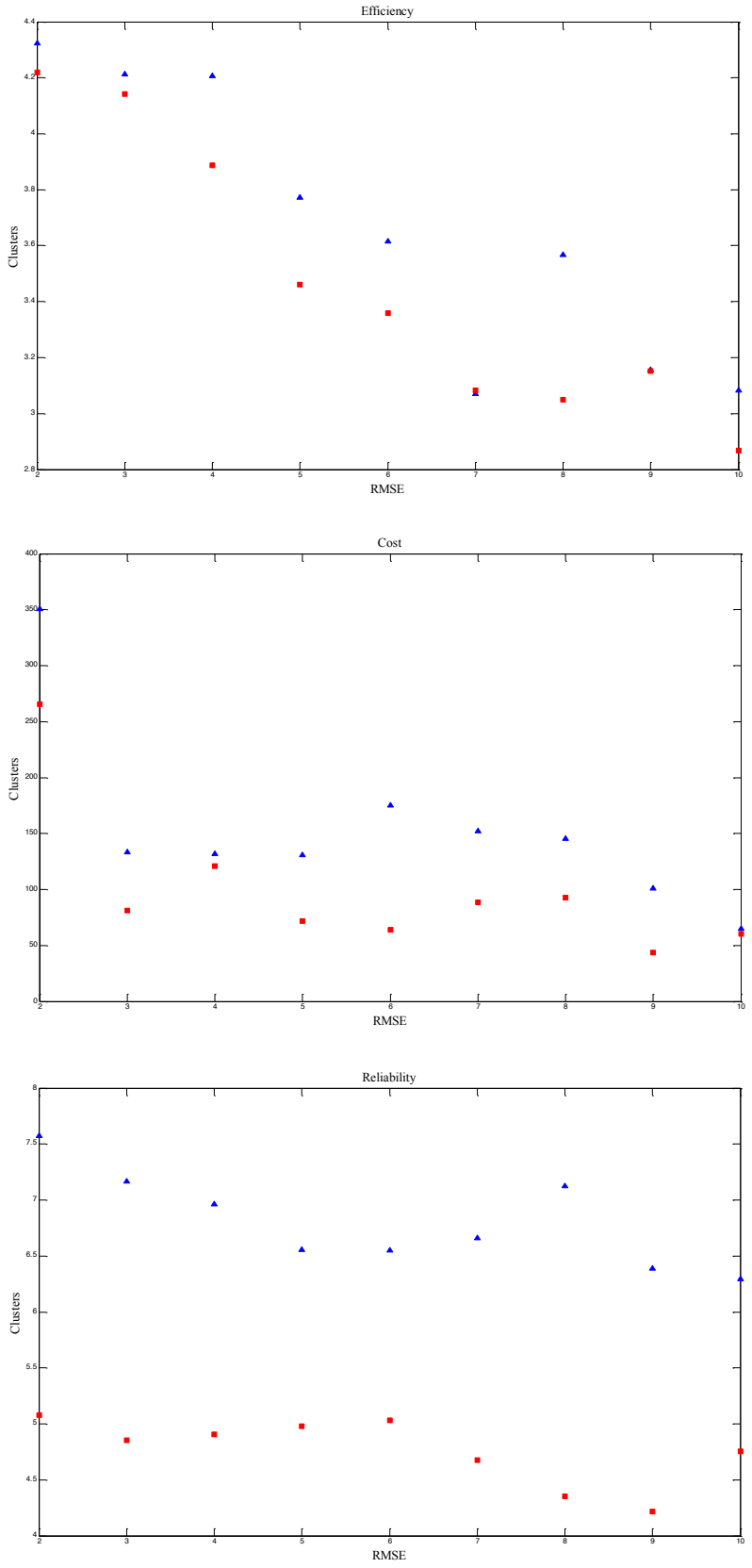

Figure 7.16: Site A RMSE values vs. clusters (Red square - Training data, Blue triangle - Testing data).

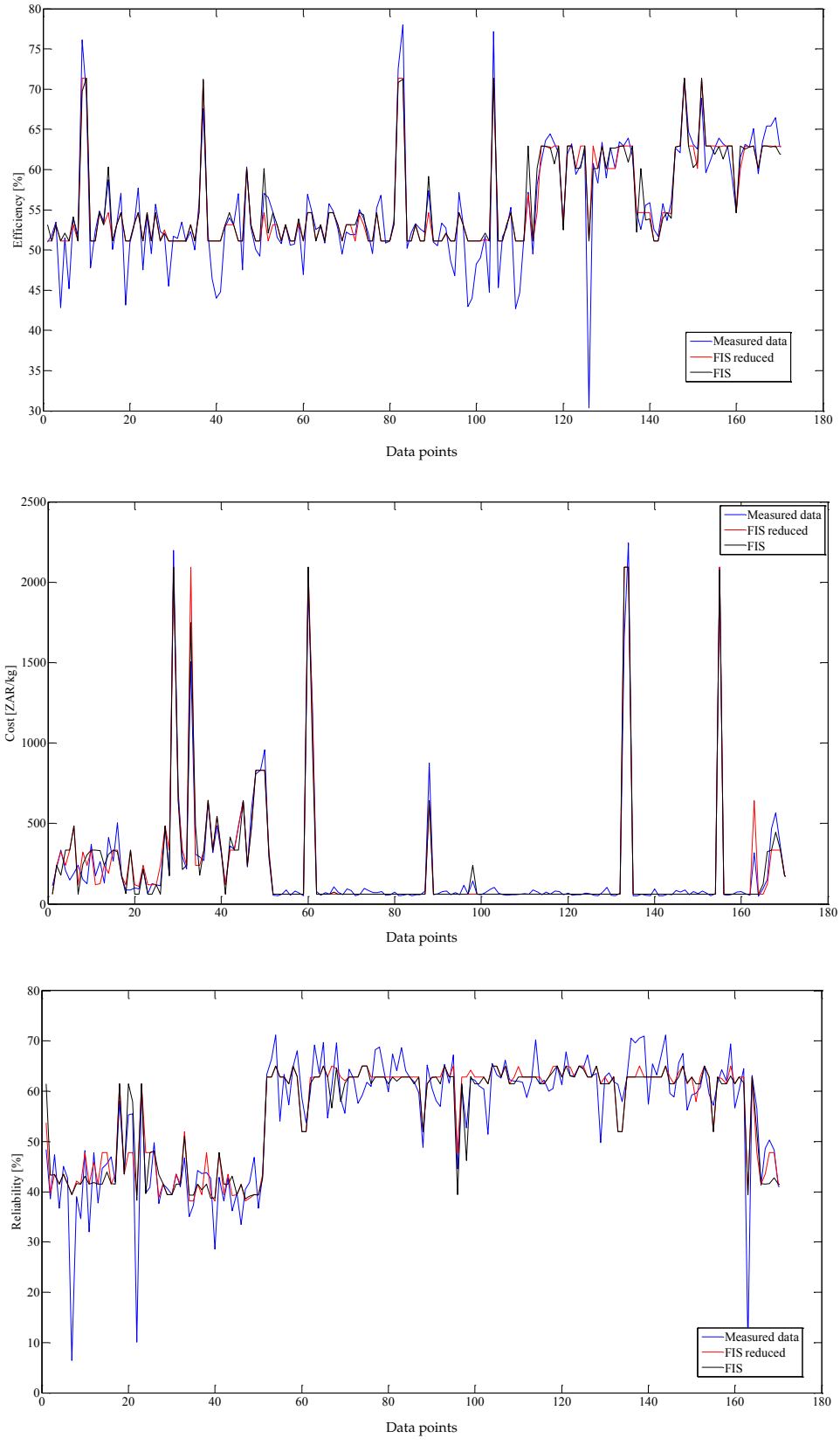

Figure 7.17: Site A original, reduced and measured data.

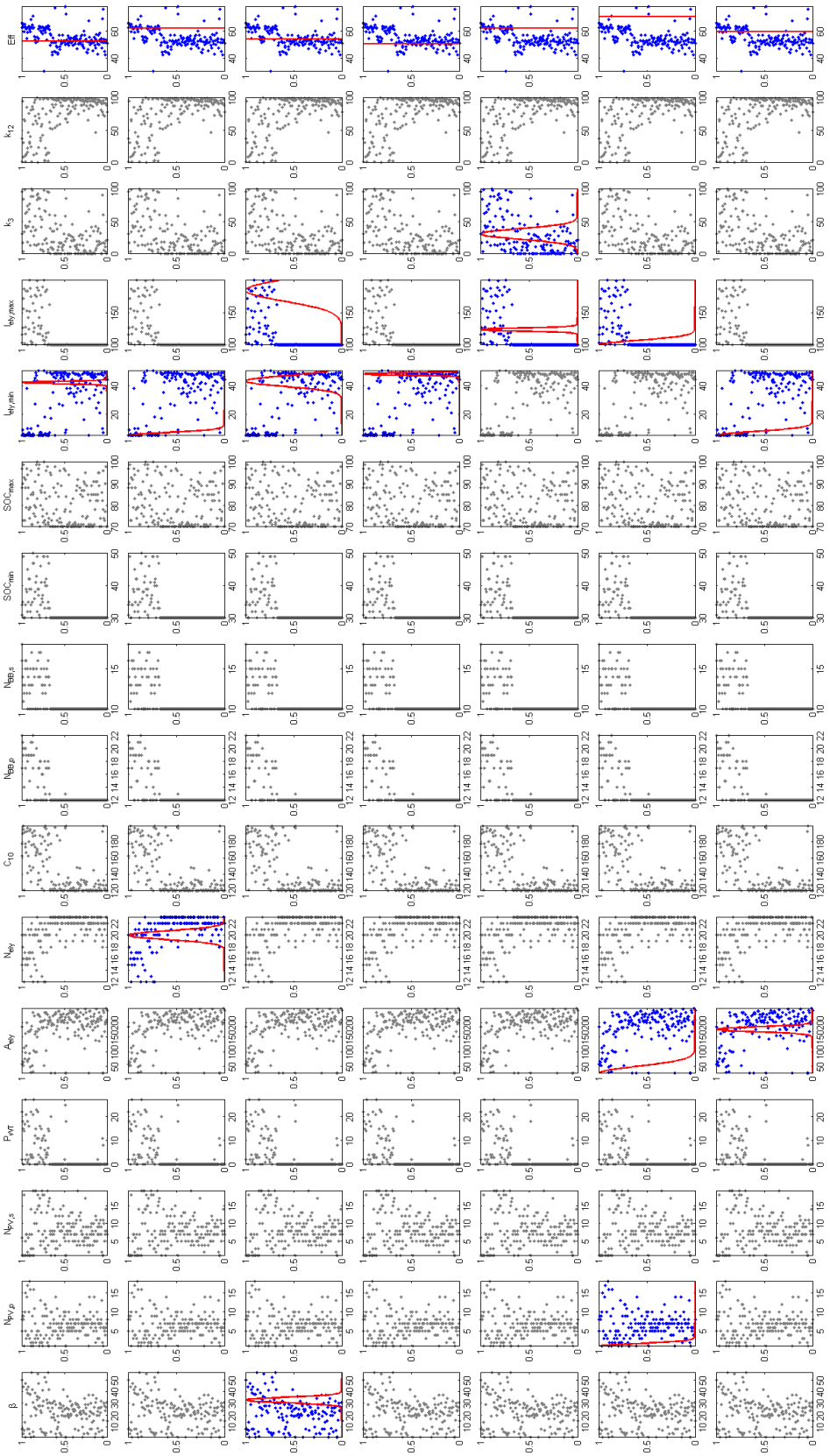

Figure 7.18: Reduced fuzzy rules for site A efficiency objective.

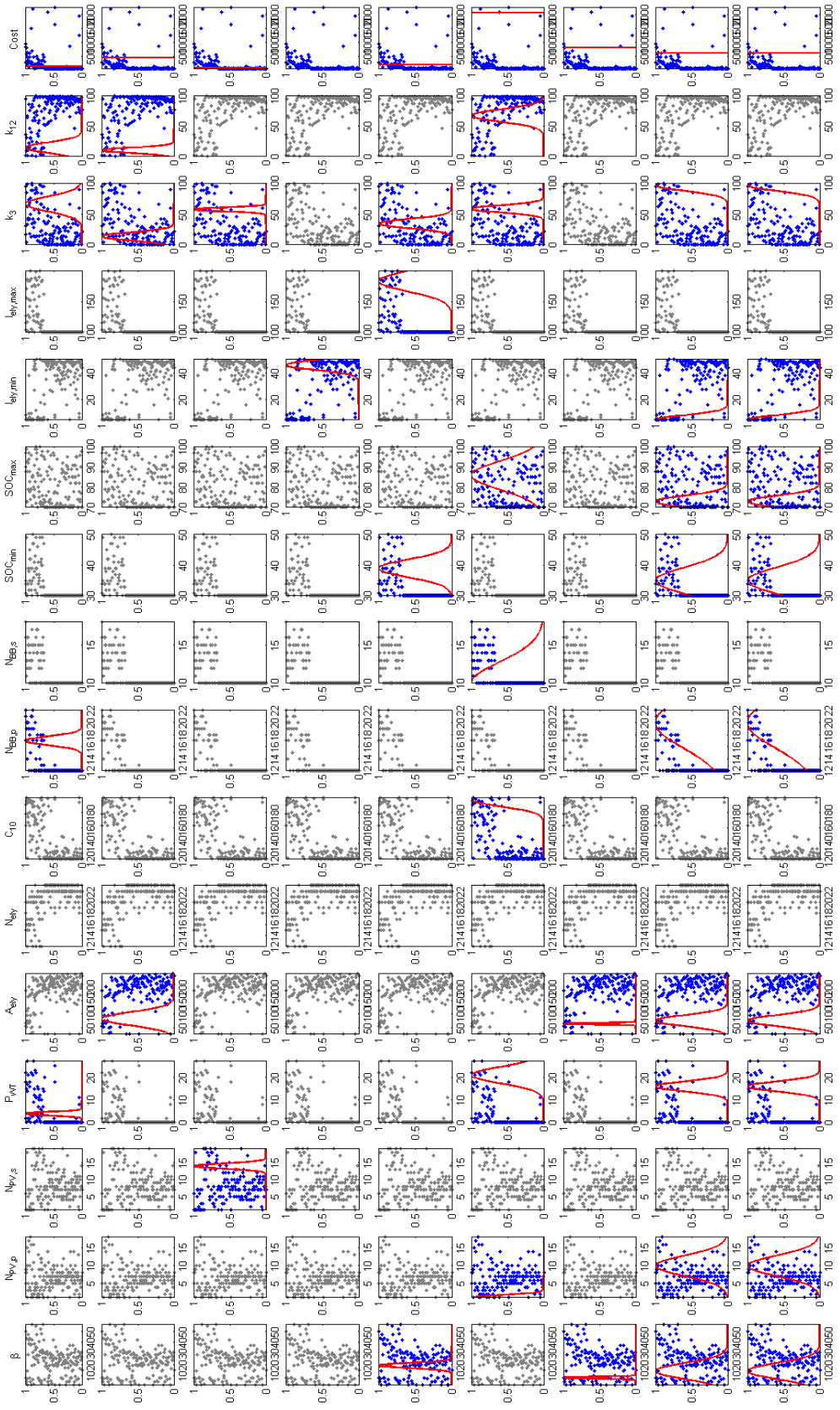

Figure 7.19: Reduced fuzzy rules for site A cost objective.

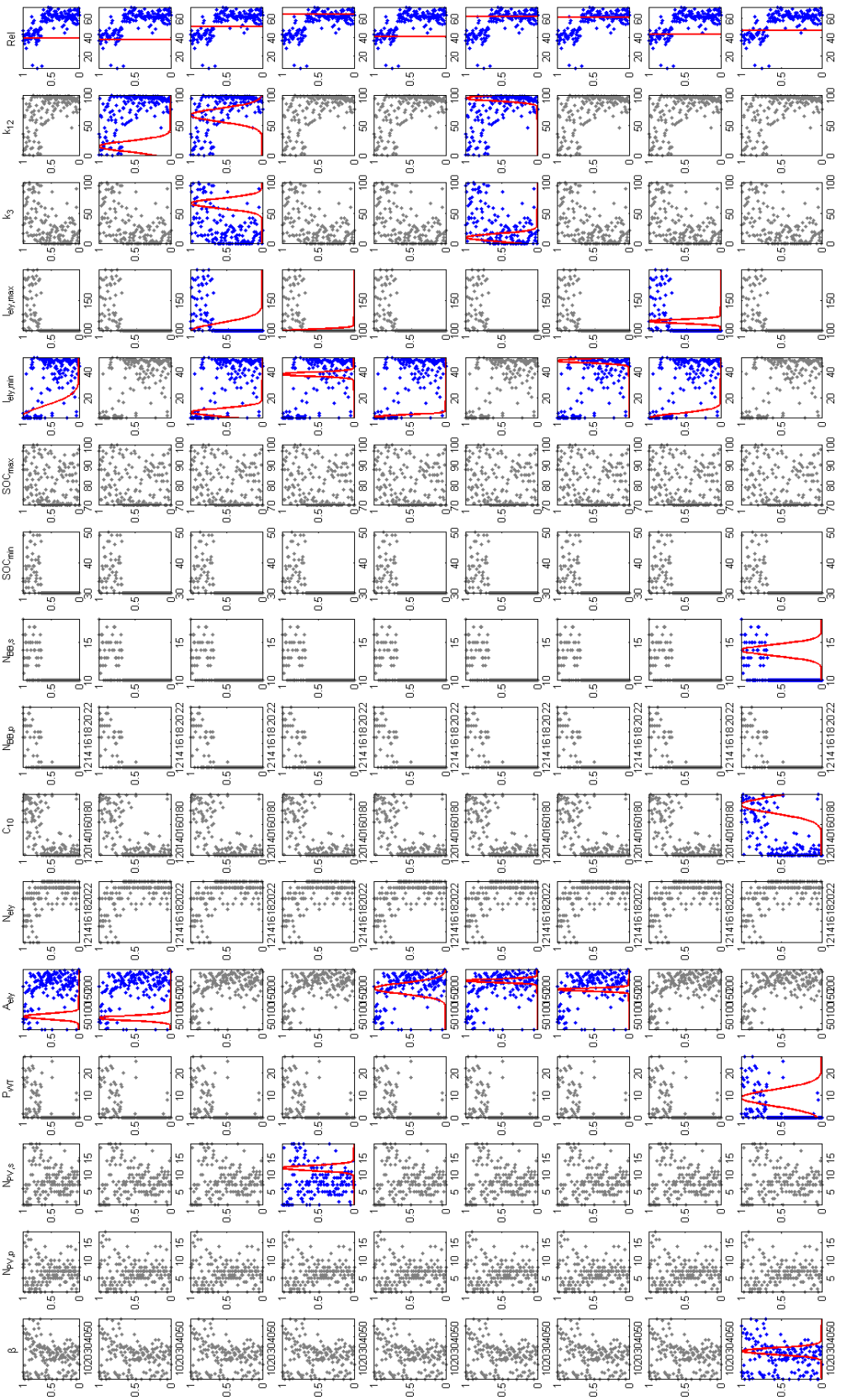

Figure 7.20: Reduced fuzzy rules for site A reliability objective.

Rule base

Detailed results and statistics of the reduced MF rule base for all three objectives are provided in Table 7.5. Names and linguistic classification for independent variables and the three objectives are provided earlier in Table 7.4. Fuzzy rules are in the form given by (7.2). The product-operation rule implemented in (7.3) follows from the fuzzy conjunction implication. The $\wedge$ symbol is used for the logical conjunction (and) (7.2). Table 7.5 gives efficiency, cost and reliability objective statistical information and rule base. For each of the three objectives the following information is provided: number of rules; RMSE value before MF reduction; RMSE value after MF reduction; % of total MFs eliminated; % of sizing variable MFs eliminated; % of control variable MFs eliminated; RMSE increase as a result of eliminating all sizing variable MFs; and RMSE increase as a result of eliminating all control variable MFs. For each of the rules columns with the following information is provided: the rule number; the rank of the rule; and the RMSE increase as a result of removing the entire rule from the rule base. Rules are ranked starting from 1 being the rule resulting in the highest RMSE increase when eliminated. A rank = 1 implies that the rule base has the highest dependency on that specific rule and that this rule is considered to be the most important rule in the rule base.

Table 7.5: Site A reduced MF rules and statistics.

Efficiency			
Number of rules = 7, Original RMSE = 3.0744, Reduced MF RMSE = 3.1718			
Total MF reduction = 87 %, Sizing MF reduction = 92 %, Control MF reduction = 79 %			
RMSE error removing sizing variables = 410 %, RMSE error removing control variables = 210 %			
Rule	Rank	Error	Linguistic rule
1	6	185 %	IF $I_{ely,min}$ is VH THEN Eff is M
2	2	259 %	IF N_{ely} is H $\wedge$ $I_{ely,min}$ is VL THEN Eff is H
3	7	177 %	If β is L $\wedge$ $I_{ely,min}$ is VH $\wedge$ $I_{ely,max}$ is VH THEN Eff is M
4	5	207 %	IF $I_{ely,min}$ is VH THEN Eff is M
5	3	256 %	IF $I_{ely,max}$ is L $\wedge$ k_3 is L THEN Eff is H
6	1	440 %	IF $N_{PV,s}$ is VL $\wedge$ A_{ely} is VL $\wedge$ $I_{ely,max}$ is VL THEN Eff is H
7	4	213 %	IF A_{ely} is VH $\wedge$ $I_{ely,min}$ is VL THEN Eff is H
Cost			
Number of rules = 9, Original RMSE = 87.8474, Reduced MF RMSE = 80.5778			
Total MF reduction = 73 %, Sizing MF reduction = 78 %, Control MF reduction = 67 %			
RMSE error removing sizing variables = 671 %, RMSE error removing control variables = 436 %			
Rule	Rank	Error	Linguistic rule
1	7	454 %	IF P_{WT} is M $\wedge$ $N_{B,s}$ is M $\wedge$ k_3 is H $\wedge$ k_{12} is VL THEN Cost is VL
2	5	471 %	IF A_{ely} is M $\wedge$ k_3 is VL $\wedge$ k_{12} is VL THEN Cost is M
3	6	471 %	IF $N_{PV,p}$ is VH $\wedge$ k_3 is M THEN Cost is VL
4	4	495 %	IF $I_{ely,min}$ is VH THEN Cost is VL
5	8	441 %	IF β is L $\wedge$ SOC_{min} is M $\wedge$ $I_{ely,max}$ is VH $\wedge$ k_3 is L THEN Cost is L
6	1	1794 %	IF $N_{PV,s}$ is VL $\wedge$ P_{WT} is VH $\wedge$ C_{10} is VH $\wedge$ $N_{B,p}$ is VL $\wedge$ SOC_{max} is M $\wedge$ k_3 is M $\wedge$ k_{12} is H THEN Cost is VH
7	2	673 %	IF β is VL $\wedge$ A_{ely} is L THEN Cost is VH
8	3	547 %	IF β is VL $\wedge$ $N_{PV,s}$ is VH $\wedge$ P_{WT} is VH $\wedge$ A_{ely} is M $\wedge$ $N_{B,s}$ is H $\wedge$ SOC_{min} is L $\wedge$ SOC_{max} is VL $\wedge$ $I_{ely,min}$ is VL $\wedge$ k_3 is VH THEN Cost is H
9	9	438 %	IF A_{ely} is VH $\wedge$ $N_{B,p}$ is M $\wedge$ k_3 is H $\wedge$ k_{12} is L THEN Cost is L
Reliability			
Number of rules = 9, Original RMSE = 5.8234, Reduced MF RMSE = 5.8740			
Total MF reduction = 77 %, Sizing MF reduction = 84 %, Control MF reduction = 67 %			
RMSE error removing sizing variables = 185 %, RMSE error removing control variables = 230 %			
Rule	Rank	Error	Linguistic rule
1	2	321 %	IF A_{ely} is M $\wedge$ $I_{ely,min}$ is VL THEN Rel is L
2	1	336 %	IF A_{ely} is L $\wedge$ k_{12} is VL THEN Rel is L
3	9	201 %	IF $I_{ely,min}$ is VL $\wedge$ $I_{ely,max}$ is VL $\wedge$ k_3 is H $\wedge$ k_{12} is H THEN Rel is M
4	6	228 %	IF $N_{PV,p}$ is VH $\wedge$ $I_{ely,min}$ is H $\wedge$ $I_{ely,max}$ is VL THEN Rel is H
5	3	295 %	IF A_{ely} is VH $\wedge$ $I_{ely,min}$ is VL THEN Rel is M
6	7	211 %	IF A_{ely} is VH $\wedge$ k_3 is VL $\wedge$ k_{12} is VH THEN Rel is H
7	8	202 %	IF A_{ely} is VH $\wedge$ $I_{ely,min}$ is VH THEN Rel is H
8	4	274 %	IF $I_{ely,min}$ is VL $\wedge$ $I_{ely,max}$ is VL THEN Rel is M
9	5	230 %	IF β is L $\wedge$ P_{WT} is VH $\wedge$ C_{10} is VH $\wedge$ $N_{B,p}$ is M THEN Rel is M

Rule base interpretation

Interpretation of each rule in the rule base is provided in Table 7.6, Table 7.8 and Table 7.10 for efficiency, cost and reliability respectively. It is important to know that these rules are derived as part of a fuzzy rule-base system and the rules derived are interdependent and cannot be viewed as a single rule on its own. For this reason each rule is interpreted and an effort is made to make a connection to the other rules. This is however not a simple task since interpretation is done manually. As a result it is not always possible to find the link across the rules by looking at the data and where possible that link is stated. Another important note is that the term cost used in this work refers to TLCC/kg H_2 and should be interpreted as such whenever cost is mentioned. Where capital cost is intended it is clearly stated.

Table 7.6: Site A interpretation of efficiency objective rule base.

General: 87 % of the MFs are eliminated with the RMSE remaining within the specified 10 % error. 92 % of sizing MFs are eliminated and 79 % of control MFs are eliminated. This observation indicates that system efficiency is more dependent on control variables. The same conclusion is made in Section 7.3.
Rule 1: IF $I_{ely,min}$ is VH THEN Eff is M Rule 1 consists of a single control variable. The rule states that for a *very high* $I_{ely,min}$ result in a *medium* system efficiency. Electrolyser efficiencies are higher at lower current densities. With the minimum current setting very high, the electrolyser operates at a lower efficiency resulting in medium system efficiency.
Rule 2: IF N_{ely} is H $\wedge$ $I_{ely,min}$ is VL THEN Eff is H Rule 2 consists of one sizing variable and one control variable, both directly related to the electrolyser. The rule states that for a *high* number of electrolyser cells and a *very low* minimum electrolyser current setting the efficiency is *high*. As stated in rule 1 electrolyser efficiencies are higher at lower current densities and thus the *very low* value will result in high electrolyser efficiency. Having a *high* number of cells increases the hydrogen production rate but maintains the *very low* and minimum electrolyser current setting, which result in an overall *high* system efficiency.
Rule 3: If β is L $\wedge$ $I_{ely,min}$ is VH $\wedge$ $I_{ely,max}$ is VH THEN Eff is M Rule 3 consists of one sizing variable and two control variables. The rule states that for a *low* PV slope, a *very high* minimum electrolyser current setting and a *very high* maximum electrolyser setting result in a *medium* system efficiency. Again the fact that electrolyser efficiencies are higher at lower current densities is important for this rule. In this rules the *very high* values for the electrolyser current settings result in the electrolyser efficiency being low. The *low* slope would result in high production at low electrolyser efficiencies during summer for this site and low to now production during winter for this site, all resulting in a *medium* system efficiency.

Table 7.7: Site A interpretation of efficiency objective rule base - Continued.

Rule 4: IF $I_{ely,min}$ is VH THEN Eff is M After the membership function reduction exercise rule 4 result in exactly the same rule as rule and the same explanation is valid.
Rule 5: IF $I_{ely,max}$ is L $\wedge$ k_3 is L THEN Eff is H Rule 5 consists of two control variables, both related to the electrolyser operation. The rule states that for a *low* maximum electrolyser current setting and a *low* k_3 variable result in a *high* system efficiency. The control variable k_3 determines the % of power from the battery bank to the electrolyser. With k_3 *low* little power from the battery is used for electrolysis. Both these values result in *high* system efficiency .
Rule 6: IF $N_{PV,s}$ is VL $\wedge$ A_{ely} is VL $\wedge$ $I_{ely,max}$ is VL THEN Eff is H Rule 6 consists of two sizing variables and one control variables. The rule states that for a *very low* number of PV panels in series, a *very low* electrolyser cell area and a *very low* maximum electrolyser current setting result in a *high* system efficiency. *Very low* number of PV panels in series implies low power. The corresponding *very low* cell area implies low power requirement for the electrolyser, with the *very low* maximum setting again resulting in a high electrolyser efficiency which result in a *high* system efficiency.
Rule 7: IF A_{ely} is VH $\wedge$ $I_{ely,min}$ is VL THEN Eff is H Rule 7 consists of a single sizing variables and a single control variables. Both are directly related to the electrolyser. The rule states that for a *very high* electrolyser cell area and a *very low* minimum electrolyser current setting result in *high* efficiency. Contrary to the previous rule 6 the cell area in this rule is *very high* implying high power requirement, however in this rule the *very low* minimum electrolyser current setting result in the *high* electrolyser efficiency and thus high system efficiency.

Table 7.8: Site A interpretation of cost objective rule base.

General: 73 % of the MFs are eliminated with the RMSE remaining within the specified 10 % error. 78 % of sizing MFs are eliminated and 67 % of control MFs are eliminated. This indicates that cost is more dependent on control variables since less control variables are eliminated.
Rule 1: IF P_{WT} is M $\wedge$ $N_{B,s}$ is M $\wedge$ k_3 is H $\wedge$ k_{12} is VL THEN Cost is VL Rule 1 contains two sizing variables and the two power management control variables k_3 and k_{12}. The rule states that for a *medium* WT rated power, a *medium* number of batteries in series, a *high* k_3 and a *very low* k_{12} result in *very low* cost. This being a primarily solar site, the *medium* WT rated power implies that low cost is achieved by not having a large wind turbine. Additionally a *medium* number of batteries in series implies also that a large battery bank is not desired for *very low* cost. A *high* k_3 result in a high supply of energy from the batteries, and a *very low* k_{12} result in majority of energy being sent to the battery banks. This allows component sizes to be small resulting in *very low* cost.
Rule 2: IF A_{ely} is M $\wedge$ k_3 is VL $\wedge$ k_{12} is VL THEN Cost is M Rule 2 contains one sizing and again the power management control variables k_3 and k_{12}. The rule states that for a *medium* electrolyser cell area, a *very low* k_3 and a *very low* k_{12} result in medium cost. The electrolyser being a high cost component, a *medium* cell area would result in *medium* cost while a *very low* k_3 and very low k_{12} little power is sent directly to the electrolyser from the batteries and the renewable sources resulting in *medium* cost.
Rule 3: IF $N_{PV,p}$ is VH $\wedge$ k_3 is M THEN Cost is VL Rule 3 contains one sizing and one power management control variable k_3. The rule states that for a *very high* number of PV panels in parallel and a medium k_3 result in *very low* cost. A *very high* number of PV paanels in paralle implies high input power from the RE source. The *medium* k_3 result in an medium power supply from the batteries to the electrolyser during no RE osurce availability. This allows the electrolyser to produce hydrogen for longer times due to high PV input power and also during no and low PV input power via k_3. This would result in *very low* cost.
Rule 4: IF $I_{ely,min}$ is VH THEN Cost is VL Rule 4 consists only one control variables. The rule states that for a *very high* minimum electrolyser current setting result in very low cost. This setting allows the electroluyser to produce hydrogen at a higher production rate resulting in very low cost.
Rule 5: IF β is L $\wedge$ SOC_{min} is M $\wedge$ $I_{ely,max}$ is VH $\wedge$ k_3 is L THEN Cost is L Rule 5 consists of sizing variable and three control variables. The rule states that for a *low* PV slope, a *medium* minimum battery SOC setting, a *very high* maximum electrolyser current setting and a *low* k_3 result in low cost. With a low β the total energy in a year for site A is high resulting in more hydrogen production which result in *low* cost. A *medium* minimum SOC setting for the battery wallows for relatively lo discharge of the batteries resulting in more energy for hydrogen production. Also, the *very high* maximum electrolyser current setting result in high production rates resulting in *low* cost.

Table 7.9: Site A interpretation of cost objective rule base - Continued.

Rule 6: IF $N_{PV,s}$ is VL $\wedge$ P_{WT} is VH $\wedge$ C_{10} is VH $\wedge$ $N_{B,p}$ is VL $\wedge$ SOC_{max} is M $\wedge$ k_3 is M $\wedge$ k_{12} is H THEN Cost is VH Rule 6 consists of four sizing variables and three control variables. The rule states that for a *very low* number of PV panels in series, a *very high* wind turbine power rating, a *very high* battery Ah rating, a *very low* number of batteries in parallel, a *medium* maximum battery SOC setting, a medium k_3 and a high k_{12} setting result in *very high* cost. For site A having a *very high* rated wind turbine would result in high cost since the wind is poor at this site. Additionally a *very high* battery Ah rating with *very high* number of batteries in parallel but *very low* maximum SOC setting would result in a large and expensive battery bank with only the only the lower part of the battery in *very high* costs. A *very low* number of PV panels in series implies low power input resulting in even higher cost due to the further inefficient use of the large battery bank. With a *medium* k_3 energy from the battery will be used for the electrolyser but the low power input from the sources result in low available energy. Further the high k_{12} result in low energy supplied to the batteries for charging. All this would result in *very high* system cost.
Rule 7: β is VL $\wedge$ A_{ely} is L THEN Cost is VH Rule 7 consists of two sizing variables. The rule states that for a *very low* slope and a *low* electrolyser cell area would result in *very high* cost. The *very low* slope would result in the maximum energy production in a year for this site, however not a very constant production rate. However with a *low* cell area, the hydrogen production rate is low resulting in *low* cost.
Rule 7 consists of one sizing variable and four control variables. The PV panel slope value is *medium* which is in the range of the optimal PV panel slope for site A. Battery minimum SOC and minimum electrolyser current are both *very high* resulting in *high* start-up currents for the electrolyser and *high* minimum SOC for the batteries. The power supplied to the electrolyser from the battery in unavailable RE times is a *very high* fraction of the maximum electrolyser current and the fraction of power to the electrolyser during a surplus of RE sources is *very low* (k_{12}). The operating ranges and conditions of the electrolyser and batteries result in *very high* cost.
Rule 8: IF β is VL $\wedge$ $N_{PV,s}$ is VH $\wedge$ P_{WT} is VH $\wedge$ A_{ely} is M $\wedge$ $N_{B,s}$ is H $\wedge$ SOC_{min} is L $\wedge$ SOC_{max} is VL $\wedge$ $I_{ely,min}$ is VL $\wedge$ k_3 is VH THEN Cost is H Rule 8 consists of five sizing variables and four control variables. The rule states that for a *very low* PV slope, a *very high* number of PV panels in series, a *very high* rated wind turbine, a *medium* electrolyser cell area, a *high* number of batteries in series, a *low* minimum battery SOC, a *very low* maximum battery SOC, a *very low* electrolyser minimum current setting and a *very high* k_3 result in a *high* cost. This rule accounts for most of the components having *very high* sizing components except for the electrolyser which is medium. This result in inefficient energy use, resulting in *high* cost. Further again a *very high* rated wind turbine is not optimal for the poor wind resource of site A and reulsts in additional *high* cost.The control variables values selected for this rule also result in inefficient use of the battery capacity and energy management between the source, battery and electrolyser. All this would result in *high* cost.
Rule 9: IF A_{ely} is VH $\wedge$ $N_{B,p}$ is M $\wedge$ k_3 is H $\wedge$ k_{12} is L THEN Cost is L Rule 9 consists of two sizing variables and again the two power management control variables k_3 and k_{12}. The rule states that for a *very high* electrolyser cell area, a *medium* number of batteries in parallel, a *high* k_3 and a *low* k_{12} result in *low* cost. In rule 9 the *very high* cell area allows for high production rates, and corresponding *high* k_3 allows for long production times during low and no RE source availability. A *low* k_{12} allows for charging of the *medium* number of Batteries in parallel. All result in *low* cost.

Table 7.10: Site A interpretation of reliability objective rule base.

General: General: 77 % of the MFs are eliminated with the RMSE remaining within the specified 10 % error. 84 % of sizing MFs are eliminated and 67 % of control MFs are eliminated. This indicates that reliability is more dependent on control variables since less control variables are eliminated. For site A the linguistic classification provided in Table 7.4 for reliability result in a *medium* value to be the highest possibility for reliability. Reliability is defined in Section 6.6 and is relative for each site.
Rule 1: IF A_{ely} is M $\wedge$ $I_{ely,min}$ is VL THEN Rel is L Rule 1 consists of one sizing variables and one control variable, both directly related to the electrolyser. The rule states that for a *medium* electrolyser cell area and a *very low* minimum electrolyser current setting result in a *low* reliability. A *medium* cell area and *very low* minimum electrolyser current setting will result in the electrolyser turning on at very low power values resulting in multiple ON/OFF cycles due to low power inputs during low RE source input times, such as early mornings and late nights for the PV specifically. Due to the manner of including degradation in the model this will result in *low* electrolyser and thus system reliability. This will be true for cell areas of medium and lower.
Rule 2: IF A_{ely} is L $\wedge$ k_{12} is VL THEN Rel is L Rule 2 consists of one sizing variable and on power management control variable, both related to the electrolyser control. The rule stated that a *low* electrolyser cell area and a very low k_{12} result in low reliability. Rule 2 is similar to rule 1 in that the *low* cell area would result in a relative *low* minimum current setting. The *very low* k_{12} would result additionally in the electrolyser receiving very little power from the RE sources, instead of charging the batteries. This will result in *low* electrolyser reliability and thus also system reliability.
Rule 3: IF $I_{ely,min}$ is VL $\wedge$ $I_{ely,max}$ is VL $\wedge$ k_3 is H $\wedge$ k_{12} is H THEN Rel is M Rule 3 consists of four control variables all related to the electrolyser control. The rule states that for a *very low* minimum electrolyser current setting, a *very low* maximum electrolyser current setting, a *high* k_3 and a *high* k_{12} result in a *medium* reliability. Similar than rules 1 and 2 rule 3 has a *very low* ON setting for the electrolyser and also a *very low* maximum value. The low ON setting again result in Multiple ON/OFF cycles. A *high* k_3 and *high* k_{12} result in high values of power during no, low and excess RE which result in a *medium* reliability rather than low again.
Rule 4: IF $N_{PV,p}$ is VH $\wedge$ $I_{ely,min}$ is H $\wedge$ $I_{ely,max}$ is VL THEN Rel is H Rule 4 consists of one sizing variables and two control variables. The rule states that for a *very high* number of PV panels in parallel, a *high* minimum electrolyser current setting and a *very low* maximum electrolyser current setting result in *high* reliability. The *very high* number of PV panels in parallel implies high input power from the RE source. The *high* minimum and *very low* maximum electrolyser current settings result in a high ON value and narrow band of power supply, ensuring that the electrolyser will run for long periods at a time, resulting in the *high* reliability.
Rule 5: IF A_{ely} is VH $\wedge$ $I_{ely,min}$ is VL THEN Rel is M Rule 5 consists of one sizing and one control variable, both directly related to the electrolyser. The rule states that for a *very high* electrolyser cell area and a *very low* minimum electrolyser current setting result in a *medium* reliability. The *very low* minimum current setting would result in *low* reliability however the *very high* cell area increases the minimum current setting resulting in the medium reliability.

Table 7.11: Site A interpretation of reliability objective rule base - Continued.

Rule 6: IF A_{ely} is VH $\wedge$ k_3 is VL $\wedge$ k_{12} is VH THEN Rel is H Rule 6 consists of one sizing variable and the two power management control variables k_3 and k_{12}. The rule states that for a *very high* electrolyser cell area, a *very low* k_3 and a very low k_{12} result in a high reliability. Rule 6 is with the exception of the addition of k_3 the inverse of rule 2 with the opposite reasoning being valid. The exclusion of k_3 in rule 2 is possible since the value of k_3 would not make a difference to the negative (*low*) outcome of rule 2, however in rule 6 the positive (*high*) outcome can be effected for a another value of k_3. The *very high* cell area implies at least a high minimum electrolyser current while the *very high* k_{12} ensures that the electrolyser receives power from the RE sources rather than storing in the batteries. A *very low* k_3 would prevent the electrolyser from getting power during low and no RE sources, but will not result in ON/OFF cycles affecting the reliability.
Rule 7: IF A_{ely} is VH $\wedge$ $I_{ely,min}$ is VH THEN Rel is H Rule 7 consists of a singe sizing variable and a single control variables both directly related to the electrolyser. Rule 7 is the opposite of rule 1 with the opposite reasoning applying. A *very high* cell area and *very high* minimum electrolyser current setting will result in a high ON value resulting in fewer ON/OFF cycles resulting in a *high* reliability.
Rule 8: IF $I_{ely,min}$ is VL $\wedge$ $I_{ely,max}$ is VL THEN Rel is M Rule 8 consists of two control variables both directly related to the electrolyser. The rule states that for a *very low* minimum electrolyser current and a *very low* maximum electrolyser current result in a *medium* reliability. Rule 8 are similar to rules 3 and 4. The *very low* minimum and maximum electrolyser current settings can cause unnecessary ON/OFF cycles. The *very low* maximum current will compensate that the unit can operate at low power from the batteries and RE sources, thus a *medium* instead of *low* reliability is possible.
Rule 9: IF β is L $\wedge$ P_{WT} is VH $\wedge$ C_{10} is VH $\wedge$ $N_{B,p}$ is M THEN Rel is M Rule 9 consists of four sizing variables. Rule 9 is the only rule where these four are used. The rule states that for a *low* PV slope, a *very high* rated wind turbine, a *very high* battery Ah rating and a *medium* number of batteries in parallel result in *medium* reliability. Rule 9 is the only rule that accounts for the reliability of th batteries. The *low* slope result in high power during the summer months of site A and low power during the winter months. The *very high* wind turbine rating can result in poor wind resources supplying intermittent power to the batteries. A *very high* battery Ah rating and medium number of batteries in parallel implies a high overall batteries rating. Due to the intermittent wind source the batteries result in a medium reliability, even with a high possible PV source potential. This rule simply states the effect of intermittent operation on the batteries.

Insights from rule base

For the efficiency objective the following insights are derived using information provided in Fig. 7.18, Table 7.5 and interpretations made in Table 7.6:

- Total MFs have been reduced by 87 %. Sizing MFs have been reduced by 92 %. Control MFs have been reduced by 79 %. Fewer control variables are eliminated indicating a stronger dependency on control variables for the system efficiency. This observation is consistent with the findings in Section 7.3.
- The two most important variables are $I_{ely,min}$ and $I_{ely,max}$ since they feature respectively in five and three of the seven fuzzy rules, once together. $I_{ely,min}$ after reduction appears twice resulting in exactly the same fuzzy rule (Rules 1 and 4). Only two fuzzy rules contain variables that are not related to the sizing or control of the electrolyser.
- Between the seven rules the current density of the electrolyser shows to be of importance. The rules consistently imply that a lower current density result n higher system efficiency. This is due to the electrolyser efficiency itself which is higher at lower current densities.
- Majority of the remaining MFs are from variables related to the electrolyser. Not one single MF variable specific to the batteries is remaining. System efficiency is therefore primarily dependent on the electrolyser operating variables and has no indicated dependence on the RE source inputs or the sizing of the batteries.
- Rule 6 is the highest ranking rule (HRR). The rule emphasises the finding that is seen throughout, that the electrolyser parameters are important for efficeincy, and more specifically that having low current results in better efficiencies.
- Findings show that system efficiency has very little dependence on sizing variables. Variables for controlling the electrolyser are important. Desired system efficiency is achieved when the electrolyser on current value is *low* and the range of operation is narrow.
- The efficiency objective for site A is primarily determined on the control parameters and less on sizing parameters.
- A main finding for site B is that the system tends to be more efficient at low current densities. This is true for the electrolyser itself.

For the cost objective the following insights are derived using information provided in Fig. 7.19, Table 7.5 and interpretations made in Table 7.8:

- Total MFs have been reduced by 73 %. Sizing MFs have been reduced by 78 % and control MFs have been reduced by 67 % resulting in fewer control MFs eliminated than sizing MFs. This finding indicates a stronger dependency on control variables for the cost objective.
- Although system capital cost would be primarily dependent on sizing, cost in terms of \$/kg is shown to be dependent on control variables, but primarily on the power distribution control variables k_3 and k_{12} which manages the power flow between the batteries,

electrolyser and RE sources. Cost is not shown to be much dependent on the electrolyser and battery direct control variables.

- The HRR is rule 6. Rule 6 caters for problems where cost results in a *very high* value. Rule 6 highlights that sizing variables are not always responsible for *high* cost and that poor control variable selection including power management control variables result in *very high* cost.
- From the rules-base the three main components that drive cost are identified as the component sizing variables and also management of power between the electrolyser, batteries and RE sources. The control variables do however also have effect on the cost.
- Rules 1, 6 and 8 include the WT power sizing variable. All three rules state that a *low* to *medium* value results in *low* to *very low* cost while a *very high* value results in *high* to *very high* cost. This rule implies that having a small to no wind component is more economic. This is as expected, since site A is a poor wind site.
- The cost objective for site B is primarily determined by the power management control parameters and somewhat on the rest of the control parameters for all components also somewhat and the sizing of all components.
- A main finding for site B is that the cost is low when less power is used by the electrolyser and instead stored in batteries. This would allow for a smaller electrolyser which operates over longer periods. This finding would be true for the small scale system considered in this work, since small electrolysers in the range of a couple of kW are expensive per kW. If large scale is considered the cost objective would result in a completely different finding.

For the reliability objective the following insights are derived using information provided in Fig. 7.20, Table 7.5 and interpretations made in Table 7.10:

- Total MFs have been reduced by 77 %. Sizing MFs have bee reduced by 84 % and control MFs have been and reduced by 67 %. There is a strong dependency on control for reliability and is consistent with what is discussed in Section 7.3. Analysis shows the minimum electrolyser current and cell area are present in the majority of the rules for the reliability rule base. Control, mostly of the electrolyser, therefore does show a strong dependency for reliability.
- The HRR of this rule-base is rule 2. Rule 2 includes only two variables being the electrolyser area and the power management control parameter k_{12} which determines the split of energy between the batteries and the electrolyser. These two variables are shown to be important for the reliability objective and this HRR therefore emphasises its importance. This is a key finding since the electrolyser and the batteries have been identified as components that have degradation resulting in low reliability, and also that the management of energy specifically related to these two components are important to improve reliability.
- The majority of MFs remaining are variables related to the electrolyser sizing and control. Battery variables which are expected to also be important for reliability is limited to

one MF. Second most dependent variables are related to the power management control variables. This is expected as these to variables have a large impact on the control of the electrolyser ON-OFF cycles.

- The reliability for site A is primarily determined by the electrolyser cell area and the minimum and maximum electrolyser current settings.

- A main finding for site B is that a very high electrolyser cell area result in a high system reliability. Further adding to this is that a low maximum and high minimum electrolyser current settings result in a narrow operating range. This result in the electrolyser ON/OFF cycles to be limited.

Electrolyser sizing, control and power management between sources, electrolyser and batteries are shown to be the most important design variables. All three objectives show dependence on either the sizing or control of the electrolyser with the majority of rules having both important. Second most dependent variables are those of the battery with the power management variables between the electrolyser and batteries of importance for the cost objective. For reliability these battery variables are not important however the electrolyser sizing and control variables are important. The minimum electrolyser current is the one control variable that is present in the majority of rules of the reliability rule-base and indicates a strong dependency of reliability on control also.

Minimum electrolyser current features most frequent in rules for efficiency and reliability rule-bases. Second most frequent is the electrolyser cell area and number of cells. The combination of these three variables determine the H_2 production rate. The power management control variables k_3 and k_{12} are the variables featuring most for the cost rule base. For efficiency sizing variables are not much present except ofr some of the electrolyser sizing variables. The cost objective value is *low* to *very low* if the wind source is itself selected to be *low* to *very low* and vice versa.

7.4.3 Site B

The analysis procedure implemented in Section 7.4.2 is followed. No explanations of tables and figures are given unless they are unique to site B.

Optimal clusters

Fig. 7.21 gives RMSE values calculated using (7.4) for different number of rules (clusters) for each of the three objectives individually.

For efficiency the optimal number of rules is selected to be seven. For cost the optimal number of rules is selected to be six and for reliability the optimal number of rules is selected to be seven.

Membership function reduction

Fig. 7.22 give the fits of the GFS before and after MF reduction for the three objectives against the measured data.

The corresponding reduced MF rules are graphically illustrated in Appendix B, Fig. B.1, Fig. B.2 and Fig. B.3 for efficiency, cost and reliability respectively.

Rule base

Table 7.12 gives detailed results and statistics of the reduced MF rules for all three objectives.

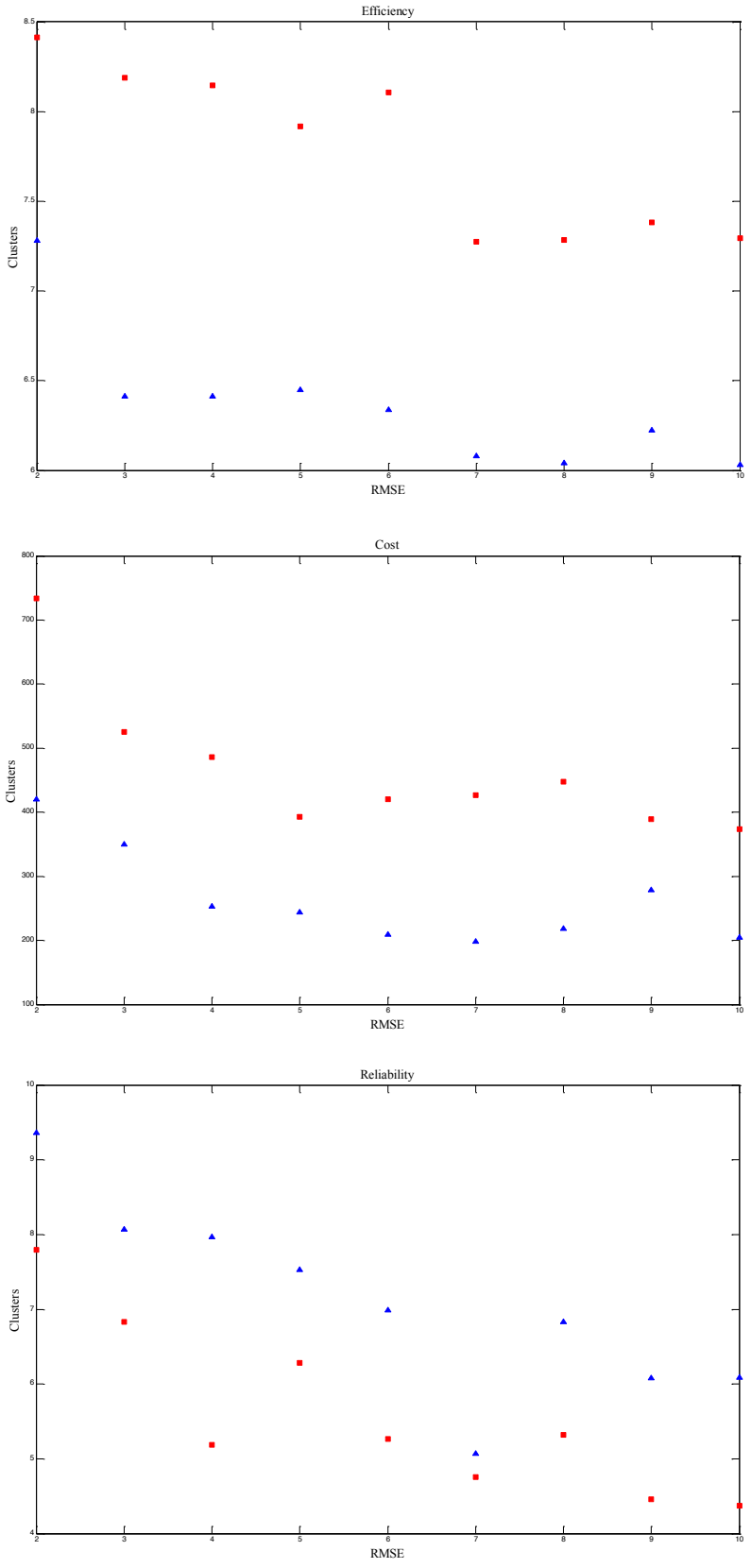

Figure 7.21: Site B RMSE values vs. clusters (Red square - Training data, Blue triangle - Testing data).

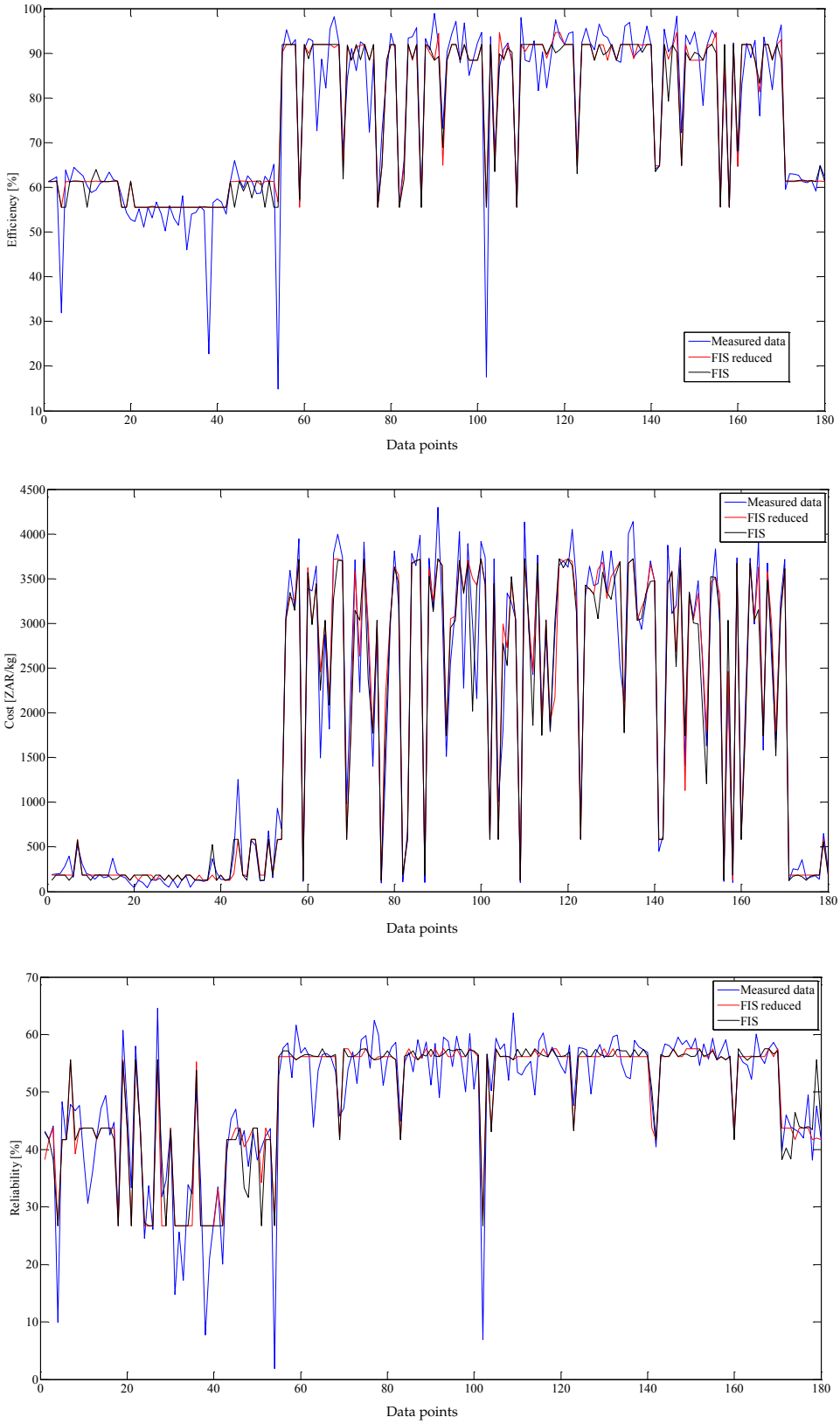

Figure 7.22: Site B original, reduced and measured data.

Table 7.12: Site B reduced MF rules and statistics.

Efficiency			
Number of rules = 7, Original RMSE = 6.4611, Reduced MF RMSE = 6.6965			
Total MF reduction = 77 %, Sizing MF reduction = 79 %, Control MF reduction = 74 %			
RMSE error removing sizing variables = 240 %, RMSE error removing control variables = 137 %			
Rule	Rank	Error	Linguistic rule
1	7	274 %	IF β is L $\wedge$ P_{WT} is VL $\wedge$ N_{ely} is H $\wedge$ $N_{B,s}$ is VL $\wedge$ SOC_{max} is M $\wedge$ $I_{ely,max}$ is VL $\wedge$ k_3 is L THEN Eff is H
2	3	320 %	IF $N_{PV,s}$ is VL $\wedge$ A_{ely} is VL $\wedge$ N_{ely} is M $\wedge$ k_{12} is VL THEN Eff is VH
3	1	347 %	IF $N_{PV,s}$ is VH THEN Eff is M
4	4	298 %	IF A_{ely} is H $\wedge$ C_{10} is H $\wedge$ $I_{ely,max}$ is H $\wedge$ k_3 is M THEN Eff is H
5	5	297 %	IF β is L $\wedge$ k_3 is VL THEN Eff is H
6	6	291 %	IF $N_{PV,p}$ is VL $\wedge$ SOC_{max} is VL $\wedge$ k_3 is VH THEN Eff is VH
7	2	345 %	IF C_{10} is VH $\wedge$ k_3 is VH $\wedge$ k_{12} is VL THEN Eff is VH
Cost			
Number of rules = 6, Original RMSE = 289.546, Reduced MF RMSE = 315.383			
Total MF reduction = 67 %, Sizing MF reduction = 69 %, Control MF reduction = 64 %			
RMSE error removing sizing variables = 441 %, RMSE error removing control variables = 170 %			
Rule	Rank	Error	Linguistic rule
1	6	407 %	IF β is VL $\wedge$ $N_{PV,p}$ is VL $\wedge$ P_{WT} is L $\wedge$ N_{ely} is H $\wedge$ k_3 is VL $\wedge$ k_{12} is VL THEN Cost is VH
2	1	728 %	IF $N_{PV,s}$ is VL $\wedge$ P_{WT} is VL $\wedge$ A_{ely} is VL $\wedge$ $I_{ely,min}$ is VL $\wedge$ k_3 is VL $\wedge$ k_{12} is VL THEN Cost is VH
3	2	578 %	IF $N_{PV,s}$ is VL $\wedge$ A_{ely} is VL $\wedge$ N_{ely} is H $\wedge$ $N_{B,s}$ is H $\wedge$ $I_{ely,min}$ is VL $\wedge$ k_3 is VL THEN Cost is VH
4	5	481 %	IF β is L $\wedge$ A_{ely} is L $\wedge$ $N_{B,s}$ is VL $\wedge$ SOC_{max} is M $\wedge$ $I_{ely,min}$ is VL $\wedge$ k_3 is M $\wedge$ k_{12} is L THEN Cost is M
5	3	561 %	IF A_{ely} is VH $\wedge$ k_{12} is H THEN Cost is VL
6	4	550 %	IF P_{WT} is L $\wedge$ A_{ely} is VH $\wedge$ k_{12} is M THEN Cost is VL
Reliability			
Number of rules = 7, Original RMSE = 4.9756, Reduced MF RMSE = 5.7980			
Total MF reduction = 71 %, Sizing MF reduction = 71 %, Control MF reduction = 71 %			
RMSE error removing sizing variables = 250 %, RMSE error removing control variables = 224 %			
Rule	Rank	Error	Linguistic rule
1	1	404 %	IF $N_{PV,s}$ is VH $\wedge$ A_{ely} is VH $\wedge$ C_{10} is VH $\wedge$ SOC_{max} is H $\wedge$ $I_{ely,min}$ is H $\wedge$ k_{12} is L THEN Rel is L
2	5	257 %	IF P_{WT} is L $\wedge$ N_{ely} is VH $\wedge$ C_{10} is L $\wedge$ $I_{ely,min}$ is H THEN Rel is M
3	7	221 %	IF $N_{PV,p}$ is VH $\wedge$ A_{ely} is VH $\wedge$ N_{ely} is H $\wedge$ C_{10} is M $\wedge$ SOC_{min} is L $\wedge$ $I_{ely,min}$ is VL $\wedge$ k_{12} is M THEN Rel is M
4	6	232 %	IF $I_{ely,min}$ is VL $\wedge$ k_3 is M $\wedge$ k_{12} is M THEN Rel is M
5	3	262 %	IF P_{WT} is VL $\wedge$ A_{ely} is VL $\wedge$ $N_{B,s}$ is H $\wedge$ $I_{ely,min}$ is VL THEN Rel is M
6	4	261 %	IF $N_{PV,p}$ is VH $\wedge$ A_{ely} is VH $\wedge$ $I_{ely,min}$ is VL THEN Rel is L
7	2	275 %	IF $N_{PV,p}$ is VL $\wedge$ P_{WT} is VL $\wedge$ $N_{B,s}$ is VH THEN Rel is M

Rule base interpretation

Interpretation of the results in Table 7.12 is provided in Appendix B, Table B.1, Table B.3 and Table B.5 for efficiency, cost and reliability respectively.

Insights from rule base

For the efficiency objective the following insights are derived using information provided in Fig. B.1, Table 7.12 and interpretations made in Table B.1:

- Total MFs have been reduced by 77 %. Sizing MFs have been reduced by 79 %. Control MFs have been reduced by 74 %. Slightly fewer control variables are eliminated which indicate a stronger dependency on control variables for the system efficiency. This observation is consistent with the findings in Section 7.3.
- Majority of the remaining MFs are from variables related to the system sizing parameters and also the power management control variables k_3 and k_{12}. k_3 determines the fraction of maximum electrolyser current from the batteries when no RE input power is available and k_{12} determines the ratio of electrolyser current to battery current for specific SOC and RE input power conditions. Efficiency for site B is therefore greatly dependent on the power distribution between the electrolyser and battery when no RE input power is available.
- Contrary to site A, site B has become more dependent on the system component sizing.
- The HRR for this rule-base is rule 3, which is also the rule with only one MF remaining. Rule 3 is the only rule that caters for efficiency being *medium*. Rule 3 is the only rule that caters for a medium efficiency. All other rules result in either high or very high values.
- Findings show that system efficiency for site B has a high dependence on the sizing variables and the power management control variables. The remaining control variables have an almost negligible contribution.
- A main finding for site B is that a *low* to *medium* value for k_3 result in *high* efficiency. A *low* value for k_3 limits the amount of power to the electrolyser resulting in the electrolyser operating at a low power. It has been previously emphasised that an electrolyser is most efficient at lower current desensitises.

For the cost objective the following insights are derived using information provided in Fig. B.2, Table 7.12 and interpretations made in Table B.3:

- Total MFs have been reduced by 67 %. Sizing MFs have been reduced by 69 %. Control MFs have been reduced by 64 % resulting in slightly fewer control MFs eliminated than sizing MFs. This finding indicates a slightly stronger dependency on control variables for the cost objective.

- Majority of the remaining MFs are from variables related to the electrolyser sizing and control parameters, and the power management control parameters. Cost shows to be very dependent on the electrolyser sizing variables and also the electrolyser input power through $I_{ely,min}$, k_3 and k_{12}. Power management and control thus has a notable effect on the system cost.
- The HRR of this rule-base is rule 2. Rule 2 consists of six variables with all of them in the *very low* range resulting in a *very high* cost. Having the sizing variables *very low* would result in *very low* capital cost. This is however not the best configuration for overall system efficiency.
- Rules 5 and 6 are almost exactly the same with the exception of the addition of P_{WT} in rule 6. The two variables A_{ely} and k_{12} are shown to be important and result in *very low* cost when selected to be *very high* and *medium-high* respectively.
- The cost objective is shown to be primarily dependent on the electrolyser sizing variables. A large electrolyser shows to result in *low* cost, however a small rated electrolyser is also shown to have at least *medium* cost if power management control variables are optimally selected.

For the reliability objective the following insights are derived using information provided in Table 7.12, Fig. B.3 and interpretations made in Table B.5:

- Total MFs have been reduced by 71 %. Sizing MFs have bee reduced by 71 % while control MFs have been and reduced by 71 %. This is an indication that there is an equally strong dependency for reliability on both sizing and control variables.
- The HRR of this rule-base is rule 1. Rules 1 consists of six variables all in the *high* to *very high* range except for k_{12} in the *low* range resulting in a *low* reliability.
- Majority of MFs remaining are variables related to the electrolyser sizing and control. Battery variables nd RE source sizing variables are present in few of the rules.
- I_ely, min is present in six out of the 7 rules and is therefore considered important. A value in the *very low* to *low* range can result in *medium* reliability, however the selection of other variables do influence the outcome.

Electrolyser sizing and control are shown to be the most important design parameters. All three objectives show dependence on either the sizing or control of the electrolyser with the majority of cases both being important. Second most dependent parameters are those of the power management control variables. With site B the wind resource is increased and as a result the parameters related to batteries and RE source inputs are increased in all three rule bases.

7.4.4 Site C

The same analysis procedure described in Section 7.4.2 is followed.

Optimal clusters

Fig. 7.23 gives RMSE values calculated using (7.4) for different number of rules (clusters) for each of the three objectives individually. For efficiency the optimal number of rules is selected to be ten. For cost the optimal number of rules is selected to be five and for reliability the optimal number of rules is selected to be ten.

Membership function reduction

Fig. 7.24 give the fits of the GFS before and after MF reduction for the three objectives against the measured data. The corresponding reduced MF rules are graphically illustrated in Appendix C, Fig. C.1, Fig. C.2 and Fig. C.3 for efficiency, cost and reliability respectively.

Rule base

Detailed results and statistics of the reduced MF rules for all three objectives are given in Table 7.13.

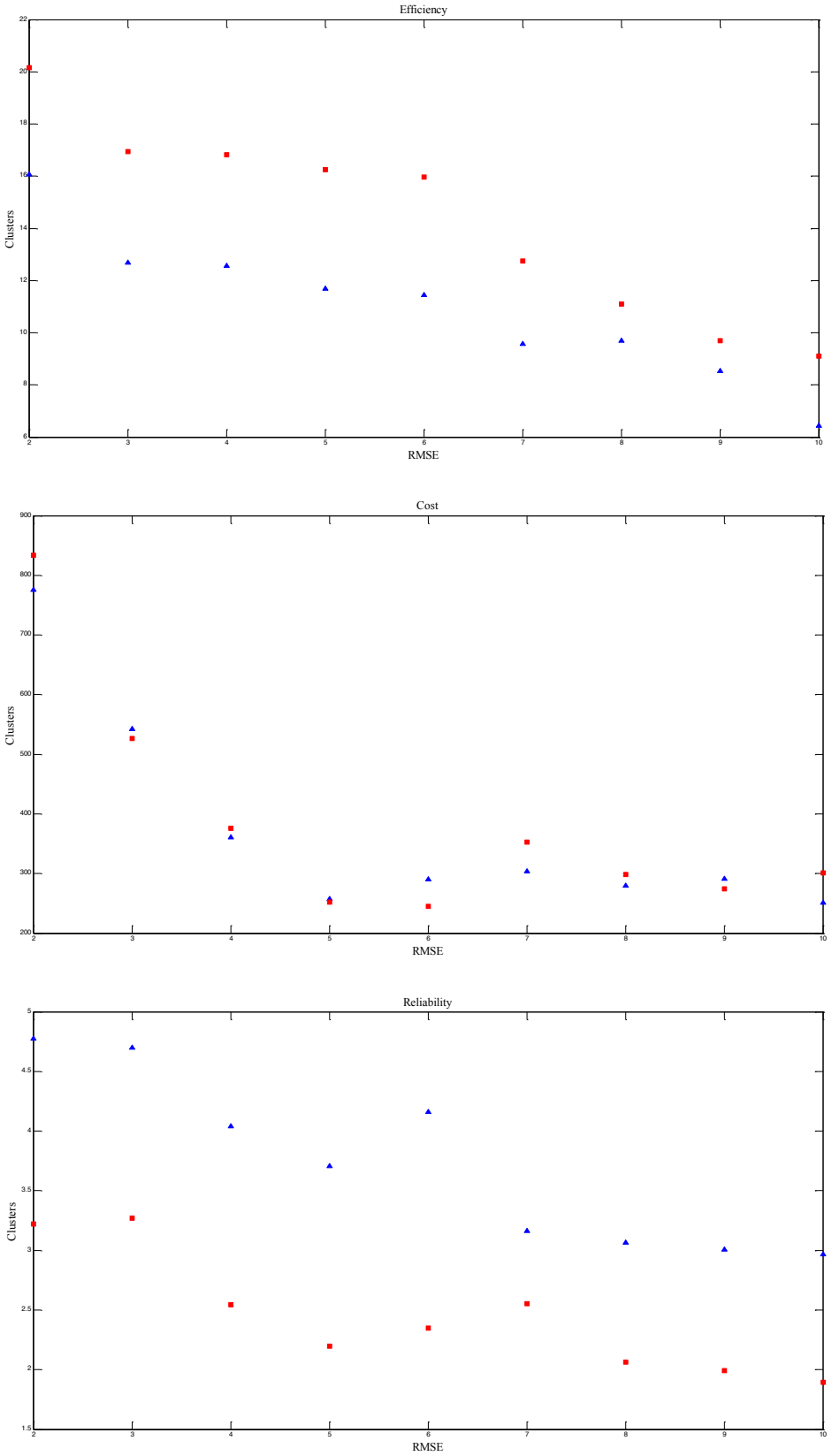

Figure 7.23: Site C RMSE values vs. clusters (Red square - Training data, Blue triangle - Testing data).

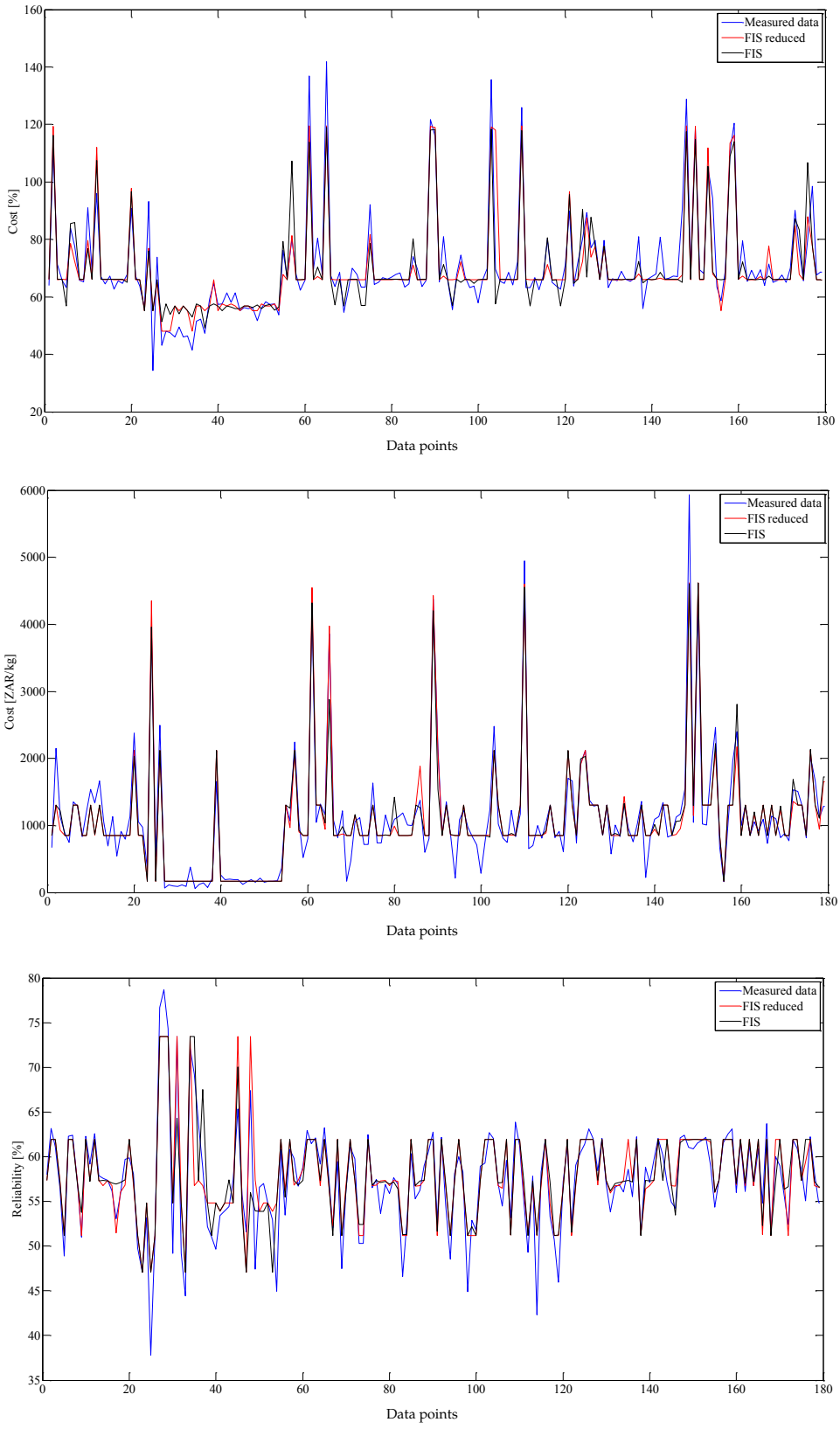

Figure 7.24: Site C original, reduced and measured data.

Table 7.13: Site C reduced MF rules and statistics.

Efficiency			
Number of rules = 10, Original RMSE = 7.3421, Reduced MF RMSE = 7.3333			
Total MF reduction = 85 %, Sizing MF reduction = 86 %, Control MF reduction = 83 %			
RMSE error removing sizing variables = 263 %, RMSE error removing control variables = 388 %			
Rule	Rank	Error	Linguistic rule
1	8	226 %	IF β is VL $\wedge$ $N_{PV,s}$ is H $\wedge$ $N_{B,s}$ is VL $\wedge$ k_3 is L $\wedge$ k_{12} is VL THEN Eff is H
2	6	275 %	IF $N_{PV,p}$ is H THEN Eff is M
3	4	352 %	IF $I_{ely,min}$ is VH THEN Eff is M
4	5	281 %	IF $N_{PV,s}$ is VH THEN Eff is M
5	10	214 %	IF $N_{B,p}$ is L $\wedge$ k_3 is L $\wedge$ k_{12} is L THEN Eff is H
6	2	552 %	IF β is VL $\wedge$ $N_{PV,s}$ is VL $\wedge$ P_{WT} is VL $\wedge$ N_{ely} is L $\wedge$ k_3 is M $\wedge$ k_{12} is VL THEN Eff is VH
7	1	643 %	IF $I_{ely,min}$ is H THEN Eff is VL
8	9	225 %	IF $N_{PV,s}$ is H $\wedge$ P_{WT} is VL THEN Eff is H
9	3	293 %	IF A_{ely} is H THEN Eff is M
10	7	230 %	IF $I_{ely,max}$ is VL $\wedge$ k_{12} is L THEN Eff is H
Cost			
Number of rules = 5, Original RMSE = 256.053, Reduced MF RMSE = 264.135			
Total MF reduction = 51 %, Sizing MF reduction = 63 %, Control MF reduction = 42 %			
RMSE error removing sizing variables = 462 %, RMSE error removing control variables = 237 %			
Rule	Rank	Error	Linguistic rule
1	2	494 %	IF β is VL $\wedge$ $N_{PV,s}$ is VL $\wedge$ $N_{PV,p}$ is VL $\wedge$ P_{WT} is VL $\wedge$ A_{ely} is VL $\wedge$ N_{ely} is H $\wedge$ $N_{B,s}$ is VL $\wedge$ SOC_{min} is VL $\wedge$ k_{12} is VL THEN Cost is VH
2	3	447 %	IF β is H $\wedge$ P_{WT} is L $\wedge$ A_{ely} is VH $\wedge$ N_{ely} is H $\wedge$ $N_{B,p}$ is L $\wedge$ SOC_{min} is M $\wedge$ $I_{ely,max}$ is M $\wedge$ k_3 is M THEN Cost is VL
3	5	313 %	IF β is L $\wedge$ $N_{PV,s}$ is H $\wedge$ $N_{PV,p}$ is VL $\wedge$ P_{WT} is VL $\wedge$ N_{ely} is VH $\wedge$ $N_{B,p}$ is VL $\wedge$ k_{12} is L THEN Cost is VH
4	1	1341 %	IF β is VL $\wedge$ $N_{PV,s}$ is VL $\wedge$ C_{10} is VH $\wedge$ $I_{ely,max}$ is VL $\wedge$ k_3 is L $\wedge$ k_{12} is VL THEN Cost is VH
5	4	317 %	IF $N_{PV,s}$ is VL $\wedge$ N_{ely} is VH $\wedge$ C_{10} is VH $\wedge$ $N_{B,s}$ is VL $\wedge$ $N_{B,p}$ is VL $\wedge$ SOC_{max} is M $\wedge$ k_{12} is L THEN Cost is VH
Reliability			
Number of rules = 10, Original RMSE = 2.6873, Reduced MF RMSE = 2.7946			
Total MF reduction = 83 %, Sizing MF reduction = 80 %, Control MF reduction = 86 %			
RMSE error removing sizing variables = 202 %, RMSE error removing control variables = 217 %			
Rule	Rank	Error	Linguistic rule
1	6	189 %	IF SOC_{min} is H $\wedge$ $I_{ely,min}$ is VL THEN Rel is M
2	5	197 %	IF $I_{ely,max}$ is VH $\wedge$ k_{12} is H THEN Rel is M
3	3	239 %	IF $N_{PV,s}$ is VL $\wedge$ P_{WT} is VL THEN Rel is H
4	1	510 %	IF SOC_{min} is M $\wedge$ $I_{ely,min}$ is VH THEN Rel is H
5	2	321 %	IF P_{WT} is M $\wedge$ $I_{ely,min}$ is VL $\wedge$ $I_{ely,max}$ is VH $\wedge$ k_{12} is VH THEN Rel is M
6	10	183 %	IF β is VL $\wedge$ $N_{PV,s}$ is H $\wedge$ P_{WT} is VL THEN Rel is M
7	9	184 %	IF β is L $\wedge$ $N_{PV,s}$ is H THEN Rel is M
8	4	235 %	IF β is VL $\wedge$ $N_{PV,s}$ is H $\wedge$ k_{12} is VL THEN Rel is M
9	7	185 %	IF SOC_{max} is H $\wedge$ k_{12} is L THEN Rel is M
10	7	185 %	IF $N_{PV,s}$ is H $\wedge$ P_{WT} is VL $\wedge$ $N_{B,p}$ is VL THEN Rel is M

Rule base interpretation

Discussions on the results given in Table 7.13 is provided in Appendix C, Table C.1, Table C.3 and Table C.5 for efficiency, cost and reliability respectively.

Insights from rule base

For the efficiency objective the following insights are derived using information provided in Fig. C.1, Table 7.13 and interpretations made in Table C.1:

- Total MFs have been reduced by 85 %. Sizing MFs have been reduced by 86 % while control MFs have been reduced by 83 %. System efficiency is equally dependent on both sizing and control variables.
- Majority of the remaining MFs are from variables RE source sizing variables and power management control variables.
- The HRR for this rule-base is rule 7. Rule 7 is the only rule that provides variables that result in the efficiency being *very low*. All other rules cater for combinations where efficiency is *medium* to *very high*.
- Almost all the rules are based on the fact that the electrolyser has higher efficiency at lower current densities. All variables of each rule are chosen to ensure that the electrolyser is operated at a low current density. This would also ensure a high efficiency for the system.
- Rules 2, 3, 4, 7 and 9 all consist of a single variable with all of them having the result medium. *Medium* is the lowest value given for this sight and is therefore considered the *low* value.
- Almost all the rules with efficiency *high* have the power management variable k_{12} either *low* or *very low*.

For the cost objective the following insights are derived using information provided in Fig. C.2, Table 7.13 and interpretations made in Table C.3:

- Total MFs have been reduced by 51 %. Sizing MFs have been reduced by 63 %. Control MFs have been reduced by 42 % resulting in fewer control MFs eliminated than sizing MFs. This finding indicates a stronger dependency on control variables for the cost objective.
- Majority of the remaining MFs are from variables related to system sizing. The second most MFs are related to the power management control variables. Cost shows to be very dependent on the ration between electrolyser and RE source inputs. This finding is expected since the electrolyser is the more expensive part of the system and is consistent with literature.

- The HRR of this rule-base is rule 4. Rule 1 is one of four rules that end with *very high* cost. Rule 4 includes a *high* battery component which is oversized for the control settings provided. Thus the costs are considerably higher.
- A low RE source input results in *high* system costs while a *high* RE source input with corresponding *high* electrolyser rating result in low system cost. This is opposite from the efficiency objective which prefers *high* rating for the electrolyser component and low RE input. This is consistent with literature since cost and efficiency are conflicting objectives.
- Rule 2 is the only rule that includes a *high* β value. A *high* value is the optimal slope angle for site C. This shows that for a site with marginal RE input resources, an optimal PV module angle is essential.

For the reliability objective the following insights are derived using information provided in Table 7.13, Fig. C.3 and interpretations made in Table C.5:

- Total MFs have been reduced by 83 %. Sizing MFs have bee reduced by 80 % while control MFs have been and reduced by 86 %. This is an indication that there is a dependency for reliability on both sizing and control.
- The HRR of this rule-base is rule 4. Rule 5 is the only rule that caters for a *low* reliability.
- The majority of remaining variables are from the RE source sizing variables.
- Electrolyser and battery sizing are both important when considering reliability. When components are to small they are over stressed and as a result will fail. Further the RE sources feeding these loads should be matched.
- The power management control variables are necessary to
- For site C a to small wind turbine power rating results in low reliability. A finding from this work is that the RE system components should be sized properly to ensure reliability

Electrolyser sizing and control is shown to be the most important design parameters, except for the reliability objective where the RE souece sizing is the important parameters along with the power management control variables. All three objectives show dependence on the power management control variables. For site C more reliance is placed on the sizing variables than the control variables, and even more so on the RE sources.

7.4.5 Sites compared

Table 7.14 provides percentage of MF reduced for each objective per site. Also provided is the total number of rules and the key variables from the HRR from each rule-base. The table gives insight into the dependency of each rule-base on sizing and control. Fig. 7.25 represents the data in Table 7.14 graphically which illustrates the dependency of sizing and control variables on the RE resource potentials. The x-axis gives the ratio of wind over solar resource potentials. A summary of the key findings from the analysis of all three sites are listed below:

Table 7.14: Summary of the results from MF reduction.

Efficiency	Number of rules	Total MF reduction	Sizing MF reduction	Control MF reduction
Site A	7	87 %	92 %	79 %
Site B	7	77 %	79 %	74 %
Site C	10	85 %	86 %	83 %
Cost				
Site A	9	73 %	78 %	67 %
Site B	6	67 %	69 %	64 %
Site C	5	51 %	42 %	63 %
Reliability				
Site A	9	77 %	84 %	67 %
Site B	7	71 %	71 %	71 %
Site C	10	83 %	80 %	86 %

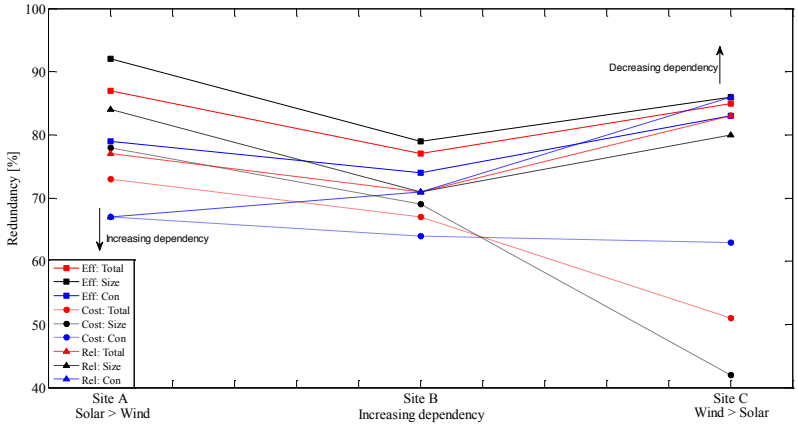

Figure 7.25: MF reduction for the three sites.

- System efficiency shows a prominent dependency on control variables for the first two sites which are predominantly solar. Site C efficiency is very much dependent on sizing variables as well as power management control variables. This supports the argument in Chapter 3 that a system's efficiency is dependent on system power management.
- From Fig. 7.25 the dependency of efficiency on control increases for a site with mixed resources and decreases as the solar and wind resource potentials reduce. At the same time the dependency of efficiency on sizing shows the same trend.
- The efficiency of sites with mixed solar and wind resources have an increased dependency on control variables and a on sizing variables.
- Power management between the electrolyser and batteries has a considerable effect on system efficiency.
- Electrolyser efficiency is responsible for a large part of the overall system efficiency. System efficiency is therefore also high when electrolyser operating current densities are low.
- System cost shows slightly greater dependency on sizing than control variables. This supports the argument in Chapter 3 that cost is dependent on system sizing but that

control also plays a role.

- From Fig. 7.25, the dependency of cost on both sizing and control are at the highest for site B and at the lowest for site C where wind resources are dominant.
- System cost is primarily dependent on the electrolyser sizing and control variables and secondly on the battery variables along with the controller's power distribution variables. Additionally, some PV module variables are also included. The sizing and power management between the electrolyser and batteries have the biggest effect on system cost.
  - System cost is shown to be higher when the electrolyser is operated over a wide power range.
  - System cost is shown to be higher when RE input source meets the electrolyser rating. This is opposite to the efficiency objective.
- System reliability shows dependency on control and sizing variables. Especially site three is more dependent on sizing variables. This partially supports the argument in Chapter 3 that reliability is dependent on power management.
- From Fig. 7.25 the dependency of reliability on sizing reduces for equal solar and wind resource potentials. The dependency of reliability on control follows the same trend.
- The reliability of sites with *high* solar and *low* wind resources have an increased dependency on sizing variables. As the wind resource increases over the solar resources the dependency on sizing decreases.
- System reliability is primarily dependent on the electrolyser sizing and control variables.
- Consulting Tables 7.5, 7.12 and 7.13 gives the following insights:
  - An important variable is $I_{ely,min}$. With $I_{ely,min}$ in the *medium* to *very high* range results in undesired objective values. With $I_{ely,min}$ either *very low* or *low*, the electrolyser operating range will be wide.
  - A low electrolyser operating current results in a more efficient system.
  - The average number of variables per rule are lower for a higher number rules/clusters. Having less variables in a rule makes interpretation much easier.
  - Site A is mainly dependent on control variables for efficiency whereas site C is more dependent on sizing variables for all three objectives.

7.5 Conclusion

The Pareto optimal sets for each of the sites show the conflicting nature of the three objectives. Results for all three sites show a proportional linear relationship between cost and efficiency. This relationship implies that *high* cost result in *high* efficiency and *low* cost result in a *low* efficiency. This finding is consistent with discussions in Chapter 3 in the sense that performance and cost are conflicting objectives and is shown to be true for all sites. From the comparison

of SPEA and SPEAGA it is shown that the SPEAGA improves on both efficiency and reliability for all three objectives. For site A and B, efficiency and reliability objective values are improved while for site C the distribution of values for efficiency and reliability are improved. The conflicting nature of performance and cost is always present and independent of available RE resources. Site A having a poor wind resource shows rules for cost that result in *low* cost when the WT power rating is *low*. This result is expected due to the poor wind resource and acts as a validation of the method. The minimum electrolyser current is highlighted as the most important variable for each of the three objectives for all sites. The electrolyser sizing variable is also shown to have significant importance for the three objectives. Sizing of and power management between the electrolyser and battery components are identified as the crucial aspect of small-scale hybrid RE H_2 systems.

Chapter 8

Conclusions and future perspectives

In this chapter the multi-objective combined sizing and control optimisation strategy is discussed in terms of its benefits and uniqueness . Additionally the GFS and MF reduction analysis technique is also discussed in terms of it's benefits and uniqueness. Finally, the shortcomings of both are discussed. Recommendations are also made for future work in the area of MOO.

8.1 Introduction

RE H_2 systems consist of complex non-linear components and RE sources that are intermittent and require energy storage to be reliable. Along with the stochastic nature of the RE sources and the large number of input variables and objectives, sizing of these systems is not an easy task. RE system simulation and optimisation computer-based software tools already exist however only a small number can perform both simulation and optimisation. The work of Bernal-Augustí and Dufo-Ló pez [3] highlighted the need for multi-objective system design and the need to consider other objectives. This study is unique in that it considers the objectives efficiency, cost and reliability as well as the combined sizing and control optimisation which is revealed by Seeling-Hochmuth [6] to be necessary.

The focus of this study was therefore the development of an optimisation strategy that considers multiple conflicting objectives and incorporates both sizing and control variables. Bernal-Agustín and Dufo-López [9] for the first time implemented a sizing and control optimisation strategy operating in cascade which included multiple objectives for sizing and only a single completely different objective for control. In this thesis an optimisation strategy is implemented using a single objective GA that optimises the six control variables during each of the sizing optimisation runs. Sizing optimisation is performed using a multi-objective SPEA. This strategy is referred to the SPEAGA. This strategy allows multiple objectives for interdependent sizing and control optimisation.

The optimisation strategy was implemented on three geographically different sites. Information revealed include a conflicting relationship between system efficiency and cost. An im-

proved cost results in a higher efficiency and visa versa. Further it was shown that the SPEAGA outperformed the SPEA. To analyse the non-linear Pareto data sets - consisting of 15 sizing variables and six control variables - a GFS with MF reduction approach was developed. The technique was successfully implemented which resulted in reduced fuzzy rule-bases for each of the three objectives. From the analysis performed, several insights were derived regarding the design and control of RE H_2 systems.

8.2 Unique contribution

The entire process from optimisation, through analysis to deriving insights is the contribution of this work. The process consists of three major parts, which are considered three separate main contributions.

Multi-objective combined sizing and control optimisation strategy: Previous work [6, 7, 9] implemented combined sizing and control optimisation with the objectives being efficiency, cost and reliability. Only sizing optimisation had multiple objective cost, CO_2, and unmet load while the control optimisation implemented a different cost objective than that of the sizing optimisation. The first contribution of this thesis is the development and successful implementation of a multi-objective combined sizing and control optimisation strategy. Three objectives are evaluated for both sizing and control optimisation. These objectives are efficiency, cost and reliability. To accomplish the reliability, a secondary unique contribution is the inclusion of a degradation model component for both the electrolyser and LABs.

Analysis technique implementing a genetic fuzzy rule-based system with membership function reduction: Results obtained from the optimisation exercise are objective values given as Pareto optimal sets for the three objectives. As a result, the second contribution from this thesis is the implementation of an analysis technique using GFSs and a membership function reduction approach. A GA is used to train the parameters of a fuzzy-logic system. The result of the GFS is a rule-base consisting of several rules and membership functions. To reduce the complexity of the rule-bases, MFs are reduced by eliminating MFs that result in RMSE smaller than a specified value. Objectives are considered not to show a large dependency on the eliminated MFs. The resulting rule-base has an reduced number of MFs. The reduced rule-bases are used to derive several insights and generalisations from the remaining MFs.

New insights: Following the analysis of the Pareto optimal sets, the reduced fuzzy rule-bases are used to derive insights regarding the design of these systems. Specific aspects of the rule-bases that show to be useful is the percentage reduction of total MFs, sizing MFs alone and control MFs alone. The MF reduction of sizing variable MFs and control variable MFs provide insight into the dependency of a type of site and objective on the sizing and control variables respectively. Further, the HRR from each rule-base is used to provide some important insights as well. Additionally, the rule-bases are studied to look for other insights in the rule-bases.

8.3 Future work

The optimisation strategy developed is not limited to the specific objectives and is also not limited to small-scale systems. Various other energy sources and storage technologies can be used with slight alterations of the simulation and interface between the simulation file and the optimisation program. Future work should include various other components as well as objectives.

To fully determine the capabilities of the optimisation strategy, the implementation on a practical system would be beneficial. The insights that are derived should be used to help in the design of such a system. With new information on degradation mechanisms of PEM electrolysers and LABs certain to be researched and published in the near future, the reliability study must be updated for improvement.

For future work the analysis technique can be refined. The GA used to train the fuzzy system can be improved on to include not only the sigma value, but to also include the MF reduction, as well as the capability to fine-tune the cluster's centre values as the optimisation is performed. The MF reduction should be investigated to develop an automatic reduction technique that is not user dependent. The current reduction is performed on a one by one basis which wastes time.

Deriving insights is an action performed by the human operator. This allows for oversights and due to the large amount of data, inability to discover certain trends or insights. Future work should include ongoing implementation of the process which will result in new insights from different data sets. In parallel, future work can investigate the possibilities of obtaining insights automatically.

8.4 Closure

Three main objectives have been achieved in this thesis. The three main objectives form part of a completely new process for optimisation and data analysis. The first objective to develop a multi-objective combined sizing and control optimisation strategy is achieved. The strategy is successfully used to determine optimised Pareto data sets for three different geographic sites. The strategy comprises of combination of existing optimisation methods and previous work to achieve a new method. The second objective of the thesis, to analyse Pareto optimal sets using a genetic fuzzy rule-based system and a membership function reduction approach, is achieved. The data obtained is also analysed in a new way. This leads to the third objective which is insights derived from the analysis. Several insights and recommendations are derived through the entire process. The originally identified objective to include control optimisation resulted in valuable insights from the work. Additionally, the added objectives, efficiency and reliability also resulted in valuable insights.

Bibliography

[1] J. Kaldellis, D. Zafirakis, and K. Kavadias, "Techno-economic comparison of energy storage systems for island autonomous electrical networks," *Renewable and Sustainable Energy Reviews*, vol. 13, no. 2, pp. 378 – 392, 2009.

[2] E. I. Baring-Gould, H. Wenzl, R. Kaiser, N. Wilmot, F. Mattera, S. Tselepis, F. Nieuwenhout, C. Rodrigues, A. Perujo, A. Ruddell, P. Lundsager, V. Svoboda, and J. Manwell, "Detalied evaluation of renewable energy power system operation." in *A summary of the European Union hybrid power system component benchmarking project.*, 2005.

[3] J. L. Bernal-Agustín and R. Dufo-López, "Simulation and optimization of stand-alone hybrid renewable energy systems," *Renewable and Sustainable Energy Reviews*, vol. 13, no. 8, pp. 2111 – 2118, 2009.

[4] R. Banõs, F. Manzano-Agugliaro, F. Montoya, C. Gil, A. Alcayde, and J. Gmez, "Optimization methods applied to renewable and sustainable energy: A review," *Renewable and Sustainable Energy Reviews*, vol. 15, no. 4, pp. 1753 – 1766, 2011.

[5] M. Fadaee and M. Radzi, "Multi-objective optimization of a stand-alone hybrid renewable energy system by using evolutionary algorithms: A review," *Renewable and Sustainable Energy Reviews*, vol. 16, no. 5, pp. 3364 – 3369, 2012.

[6] G. Seeling-Hochmuth, "Optimisation of hybrid energy systems sizing and operation control," Ph.D. dissertation, University of Kassel, 1998.

[7] G. C. Seeling-Hochmuth, "A combined optimisation concept for the design and operation strategy of hybrid-pv energy systems," *Solar Energy*, vol. 61, no. 2, pp. 77 – 87, 1997.

[8] R. Dufo-López and J. L. Bernal-Agustín, "Multi-objective design of pv-wind-diesel-hydrogen-battery systems," *Renewable Energy*, vol. 33, no. 12, pp. 2559 – 2572, 2008.

[9] J. L. Bernal-Agustín and R. Dufo-López, "Multi-objective design and control of hybrid systems minimizing costs and unmet load," *Electric Power Systems Research*, vol. 79, no. 1, pp. 170 – 180, 2009.

[10] B. Metz, O. Davidson, H. de Coninck, M. Loos, and L. Meyer, *Intergovernmental panel on climate change (IPCC) special report on carbon dioxide capture and storage*, G. S. W. G. I. Intergovernmental Panel on Climate Change, Ed. Cambridge University Press, New York, NY (United States), 2005.

[11] R. Press, K. Santhanam, M. Miri, A. Bailey, and G. Takacs, *Introduction to Hydrogen Technology*. Wiley, 2008.

[12] D. Mathis, *Hydrogen technology for energy*, ser. Energy technology review. Noyes Data Corp., 1976.

[13] F. Kreith and D. Goswami, *Handbook oF Energy Efficiency and Renewable Energy*, ser. Mechanical Engineering Series. Taylor & Francis, 2007.

[14] H. van Antwerpen, "Review of the technology options for hydrogen production in reducing co_2 emissions. section 2: Heat source system study." JHydrogen infrastructure: Hydrogen South Africa, Tech. Rep., 2010.

[15] U. E. information administration. [Online]. Available: http://www.eia.gov/oiaf/aeo/tablebrowser/

[16] T. P. Fluri, "The potential of concentrating solar power in south africa," *Energy Policy*, vol. 37, no. 12, pp. 5075 – 5080, 2009.

[17] G. Human, G. van Schoor, and K. Uren, "Sizing of renewable energy hydrogen systems," in *AFRICON, 2011*, sept. 2011, pp. 1 –6.

[18] K. Hagemann, "Mesoscale wind atlas of south africa," Ph.D. dissertation, Department of environmental and geographical science, University of Cape Town, November 2008.

[19] P. Moriarty and D. Honnery, "Intermittent renewable energy: The only future source of hydrogen?" *International Journal of Hydrogen Energy*, vol. 32, pp. 1616 – 1624, 2007.

[20] "Hydropower resource assessment of africa," in *Ministerial conference on water for agrucultural and energy in Africa: the challenges of climate change*, 2008.

[21] D. Banks and J. Schäffler, "The potential contribution of renewable energy in south africa," Sustainable energy and climate change project (SECCP), Tech. Rep., 2006.

[22] M. Kaltschmitt, W. Streicher, and A. Wiese, *Renewable energy technology, economics and environment*, M. Kaltschmitt, W. Streicher, and A. Wiese, Eds. Springer, 2007.

[23] B. O. Bilal, V. Sambou, P. Ndiaye, C. Kb, and M. Ndongo, "Optimal design of a hybrid solar-wind-battery system using the minimization of the annualized cost system and the minimization of the loss of power supply probability (lpsp)," *Renewable Energy*, vol. 35, no. 10, pp. 2388 – 2390, 2010.

[24] E. Koutroulis, D. Kolokotsa, A. Potirakis, and K. Kalaitzakis, "Methodology for optimal sizing of stand-alone photovoltaic/wind-generator systems using genetic algorithms," *Solar Energy*, vol. 80, no. 9, pp. 1072 – 1088, 2006.

[25] I. Hadjipaschalis, A. Poullikkas, and V. Efthimiou, "Overview of current and future energy storage technologies for electric power applications," *Renewable and Sustainable Energy Reviews*, vol. 13, no. 6-7, pp. 1513–1522, Sep. 2009.

[26] D. Nelson, M. Nehrir, and C. Wang, "Unit sizing and cost analysis of stand-alone hybrid wind/PV/FC power generation systems," *Renewable Energy*, vol. 31, pp. 1641 – 1656, 2006.

[27] M. Korps, "Distributed energy systems with wind power and energy storage," Ph.D. dissertation, Norweigian University of Science and Technology, 2004.

[28] C.-H. Li, X.-J. Zhu, G.-Y. Cao, S. Sui, and M.-R. Hu, "Dynamic modeling and sizing optimization of stand-alone photovoltaic power systems using hybrid energy storage technology," *Renewable Energy*, vol. 34, pp. 815 – 826, 2009.

[29] J. Stevens and G. Corey, "A study of lead-acid battery efficiency near top-of-charge and the impact on pv system design," in *Photovoltaic Specialists Conference, 1996., Conference Record of the Twenty Fifth IEEE*, May 1996, pp. 1485 –1488.

[30] S. Vosen and J. Keller, "Hybrid energy storage systems for stand-alone electric power systems: optimization of system performance and cost through control strategies," *International Journal of Hydrogen Energy*, vol. 24, no. 12, pp. 1139 – 1156, 1999.

[31] R. Clarke, S. Giddey, F. Ciacchi, S. Badwal, B. Paul, and J. Andrews, "Direct coupling of an electrolyser to a solar pv system for generating hydrogen," *International Journal of Hydrogen Energy*, vol. 34, no. 6, pp. 2531 – 2542, 2009.

[32] E. Troncoso and M. Newborough, "Electrolysers as a load management mechanism for power systems with wind power and zero-carbon thermal power plant," *Applied Energy*, vol. 87, no. 1, pp. 1 – 15, 2010.

[33] S. Badwal, S. Giddey, and F. Ciacchi, "Hydrogen and oxygen generation with polymer electrolyte membrane PEM-based electrolytic technology," *Ionics*, vol. 12, pp. 7–14, 2006.

[34] F. Barbir, "Pem electrolysis for production of hydrogen from renewable energy sources," *Solar Energy*, vol. 78, no. 5, pp. 661 – 669, 2005, solar Hydrogen.

[35] J. Nocedal and S. J. Wright, *Numerical Optimization*. Springer, Aug. 2000.

[36] G. Venter, *Review of Optimization Techniques*. John Wiley & Sons, Ltd, 2010.

[37] T. Weise, *Global optimization algorithms - Theory and spplication*, 2008.

[38] C. A. C. Coello, G. B. Lamont, and D. A. V. Veldhuizen, *Evolutionary Algorithms for Solving Multi-Objective Problems (Genetic and Evolutionary Computation)*. Springer-Verlag New York, Inc., 2006.

[39] P. J. Angeline, "Evolutionary optimization versus particle swarm optimization: Philosophy and performance differences," in *Proceedings of the 7th International Conference on Evolutionary Programming VII*. Springer-Verlag, 1998.

[40] A. Rangel-Merino, J. López-Bonilla, and R. L. y Miranda, "Optimiszation method based on genetic algorithms," *Apeiron*, vol. 12, no. 4, pp. 393–408, October 2005.

[41] A. Konak, D. W. Coit, and A. E. Smith, "Multi-objective optimization using genetic algorithms: A tutorial," *Reliability Engineering & System Safety*, vol. 91, no. 9, pp. 992 – 1007, 2006, ¡ce:title¿Special Issue - Genetic Algorithms and Reliability¡/ce:title¿ ¡xocs:full-name¿Special Issue - Genetic Algorithms and Reliability¡/xocs:full-name¿.

[42] E. Zitzler, M. Laumanns, and S. Bleuler, "A tutorial on evolutionary multiobjective optimization," in *In Metaheuristics for Multiobjective Optimisation*. Springer-Verlag, 2003, pp. 3–38.

[43] E. Zitzler and L. Thiele, "An evolutionary algorithm for multiobjective optimization: The strength pareto approach," Swiss Federal Institute of Technology, Tech. Rep., 1998.

[44] ——, "Multiobjective evolutionary algorithms: a comparative case study and the strength pareto approach," *Evolutionary Computation, IEEE Transactions on*, vol. 3, no. 4, pp. 257–271, Nov.

[45] G. T. Klise and J. S. Stein, "Models used to assess the performance of photovoltaic systems," Sandia National Laboratories, Livermore, California, 94550, Sandia report, December 2009.

[46] T. Morgan, R. Marshall, and B. Brinkworth, "A refined simulation program for the sizing and optimisation of autonomous hybrid energy systems," *Solar Energy*, vol. 59, no. 46, pp. 205 – 215, 1997, ¡ce:title¿Selected Proceeding of ISES 1995: Solar World Congress. Part IV¡/ce:title¿.

[47] P. Aronsson, P. Fritzson, C. Hger, G. Kurzbach, J. Mattsson, H. Olsson, A. Pop, M. Sjlund, and S. Vorkoetter, *Modelica® - A unified object-oriented language for physical systems modeling*, 3rd ed., Modelica ® association, February 2012. [Online]. Available: http://www.Modelica.org/

[48] R. Dufo-López and J. L. Bernal-Agustín, *HOGA User manual 1.95*, 1st ed., Department of Electrical Engineering, University of Saragossa (Spain), September 2010.

[49] T. Lambert, P. Gilman, and P. Lilienthal, *Micropower system modeling with HOMER®*, National Renewable Energy Laboratory, 2006.

[50] E. I. Baring-Gould, *HYBRID 2 - A hybrid system simulation model: User manual*, 1st ed., National Renewable Energy Laboratory, 1617 Cole Boulevard Golden, Colorado 80401-3393, June 2006.

[51] A. Costa, "Hysys hybrid power system balance analyser," in *Workshop on status and development of software tools for PV hybrid and mini-grid systems, organized by IEA PVPS*, 2008.

[52] *Getting started with insel 8*, 15th ed., Doppelintegral GmbH, Stuttgart, Germany, September 2009. [Online]. Available: www.insel.eu

[53] H. Binder, O. Gehrke, P. Lundsager, J. C. Hansen, and T. Cronin, "Ipsys - a tool for performance assessment and supervisory controller development of integrated power systems with deistributed renewable energy," in *Solar 2004: Life, the Universe and renewables*, 2004.

[54] M. of natural resources Canada 2001 2005, *Clean energy project analysis: RETScreen® engineering & cases textbook*. RETScreen® International, 2005.

[55] O. Ulleberg and R. Glockner, "Hydrogems - hydrogen energy models," in *14th World Hydrogen Energy Conference*, 2002.

[56] R. Garca-Valverde, C. Miguel, R. Martnez-Bjar, and A. Urbina, "Optimized photovoltaic generator-water electrolyser coupling through a controlled dc-dc converter," *International Journal of Hydrogen Energy*, vol. 33, no. 20, pp. 5352 – 5362, 2008.

[57] M. J. Khan and M. T. Iqbal, "Dynamic modeling and simulation of a small wind-fuel cell hybrid energy system," *Renewable Energy*, vol. 30, no. 3, pp. 421 – 439, 2005.

[58] H. Miland, "Operational experience and control strategies for a stand-alone power system based on renewable energy and hydrogen," Ph.D. dissertation, Norweigian University of Science and Technology, 2005.

[59] H. Görgün, "Dynamic modelling of a proton exchange membrane (pem) electrolyzer," *International Journal of Hydrogen Energy*, vol. 31, no. 1, pp. 29 – 38, 2006.

[60] M. Doumbia, K. Agbossou, and C.-L. Proulx, "Lab view modelling and simulation of a hydrogen based photovoltaic/wind energy system," jul. 2009, pp. 1 –6.

[61] M. Uzunoglu, O. Onar, and M. Alam, "Modeling, control and simulation of a pv/fc/uc based hybrid power generation system for stand-alone applications," *Renewable Energy*, vol. 34, no. 3, pp. 509 – 520, 2009.

[62] M. Wetter, *GenOpt® Generic Optimisation program user manual*, 3rd ed., Lawrence Berkeley National Laboratory, Berkeley, CA 94720, February 2009. [Online]. Available: http://SimulationResearch.lbl.gov

[63] S. Chakraborty, T. Senjyu, A. Y. Saber, A. Yona, and T. Funabashi, "Optimal thermal unit commitment integrated with renewable energy sources using advanced particle swarm optimization," *IEEJ Transactions on Electrical and Electronic Engineering*, vol. 4, no. 5, pp. 609–617, 2009.

[64] Y. Cai, G. Huang, Q. Tan, and Z. Yang, "Planning of community-scale renewable energy management systems in a mixed stochastic and fuzzy environment," *Renewable Energy*, vol. 34, no. 7, pp. 1833 – 1847, 2009.

[65] M. Dicorato, G. Forte, and M. Trovato, "Environmental-constrained energy planning using energy-efficiency and distributed-generation facilities," *Renewable Energy*, vol. 33, no. 6, pp. 1297 – 1313, 2008.

[66] A. Alarcon-Rodriguez, G. Ault, and S. Galloway, "Multi-objective planning of distributed energy resources: A review of the state-of-the-art," *Renewable and Sustainable Energy Reviews*, vol. 14, no. 5, pp. 1353 – 1366, 2010.

[67] A. Soroudi, M. Ehsan, and H. Zareipour, "A practical eco-environmental distribution network planning model including fuel cells and non-renewable distributed energy resources," *Renewable Energy*, vol. 36, no. 1, pp. 179 – 188, 2011.

[68] J. Matevosyan, M. Olsson, and L. Sder, "Hydropower planning coordinated with wind power in areas with congestion problems for trading on the spot and the regulating market," *Electric Power Systems Research*, vol. 79, no. 1, pp. 39 – 48, 2009.

[69] E. Castronuovo and J. Lopes, "On the optimization of the daily operation of a wind-hydro power plant," *Power Systems, IEEE Transactions on*, vol. 19, no. 3, pp. 1599 – 1606, aug. 2004.

[70] T.-Y. Lee and C.-L. Chen, "Wind-photovoltaic capacity coordination for a time-of-use rate industrial user," *Renewable Power Generation, IET*, vol. 3, no. 2, pp. 152 –167, june 2009.

[71] S. Grady, M. Hussaini, and M. Abdullah, "Placement of wind turbines using genetic algorithms," *Renewable Energy*, vol. 30, no. 2, pp. 259 – 270, 2005.

[72] B. P. Rauo and A. C. Bengin, "Optimization of wind farm layout," *FME Transactions*, vol. 38, pp. 107–114, 2010.

[73] A. Emami and P. Noghreh, "New approach on optimization in placement of wind turbines within wind farm by genetic algorithms," *Renewable Energy*, vol. 35, no. 7, pp. 1559 – 1564, 2010, ¡ce:title¿Special Section: IST National Conference 2009¡/ce:title¿.

[74] J. S. Gonzlez, A. G. G. Rodriguez, J. C. Mora, J. R. Santos, and M. B. Payan, "Optimization of wind farm turbines layout using an evolutive algorithm," *Renewable Energy*, vol. 35, no. 8, pp. 1671 – 1681, 2010.

[75] I. Mustakerov and D. Borissova, "Wind turbines type and number choice using combinatorial optimization," *Renewable Energy*, vol. 35, no. 9, pp. 1887 – 1894, 2010.

[76] A. Kusiak and Z. Song, "Design of wind farm layout for maximum wind energy capture," *Renewable Energy*, vol. 35, no. 3, pp. 685 – 694, 2010.

[77] M. Zhao, Z. Chen, and F. Blaabjerg, "Optimisation of electrical system for offshore wind farms via genetic algorithm," *Renewable Power Generation, IET*, vol. 3, no. 2, pp. 205 –216, june 2009.

[78] E. Benini and A. Toffolo, "Optimal design of horizontal-axis wind turbines using blade-element theory and evolutionary computation," *Journal of Solar Energy Engineering*, vol. 124, pp. 357–363, 2002.

[79] K. Y. Maalawi and H. M. Negm, "Optimal frequency design of wind turbine blades," *Journal of Wind Engineering and Industrial Aerodynamics*, vol. 90, no. 8, pp. 961 – 986, 2002.

[80] H. Li, Z. Chen, and H. Polinder, "Optimization of multibrid permanent-magnet wind generator systems," *Energy Conversion, IEEE Transactions on*, vol. 24, no. 1, pp. 82 –92, march 2009.

[81] S. Varun, "Thermal performance optimization of a flat plate solar air heater using genetic algorithm," *Applied Energy*, vol. 87, no. 5, pp. 1793 – 1799, 2010.

[82] M. Zagrouba, A. Sellami, M. Bouacha, and M. Ksouri, "Identification of pv solar cells and modules parameters using the genetic algorithms: Application to maximum power extraction," *Solar Energy*, vol. 84, no. 5, pp. 860 – 866, 2010.

[83] A. Kusiak, Z. Zhang, and M. Li, "Optimization of wind turbine performance with data-driven models," *Sustainable Energy, IEEE Transactions on*, vol. 1, no. 2, pp. 66 –76, july 2010.

[84] B. Borowy and Z. Salameh, "Methodology for optimally sizing the combination of a battery bank and pv array in a wind/pv hybrid system," *Energy Conversion, IEEE Transactions on*, vol. 11, no. 2, pp. 367 –375, jun. 1996.

[85] W. Kellogg, M. Nehrir, G. Venkataramanan, and V. Gerez, "Generation unit sizing and cost analysis for stand-alone wind, photovoltaic, and hybrid wind/pv systems," *Energy Conversion, IEEE Transactions on*, vol. 13, no. 1, pp. 70 –75, mar 1998.

[86] P. C. Ghosh, "Cost optimisation of a self-sufficient hydrogen based energy supply system," Ph.D. dissertation, Institut fr Werkstoffe und Verfahren der Energietechnik Institut 3:Energieverfahrenstechnik, Forschungszentrum Jlich, 2003.

[87] M. Badejani, M. Masoum, and M. Kalantar, "Optimal design and modeling of stand-alone hybrid pv-wind systems," in *Power Engineering Conference, 2007. AUPEC 2007. Australasian Universities*, dec. 2007, pp. 1 –6.

[88] R. S. Garcia and D. Weisser, "A wind-diesel system with hydrogen storage: Joint optimisation of design and dispatch," *Renewable Energy*, vol. 31, no. 14, pp. 2296 – 2320, 2006.

[89] S. Ashok, "Optimised model for community-based hybrid energy system," *Renewable Energy*, vol. 32, no. 7, pp. 1155 – 1164, 2007.

[90] H. Yang, L. Lu, and W. Zhou, "A novel optimization sizing model for hybrid solar-wind power generation system," *Solar Energy*, vol. 81, pp. 76–84, 2007.

[91] S. Diaf, G. Notton, M. Belhamel, M. Haddadi, and A. Louche, "Design and techno-economical optimization for hybrid pv/wind system under various meteorological conditions," *Applied Energy*, vol. 85, no. 10, pp. 968 – 987, 2008.

[92] G. Dalton, D. Lockington, and T. Baldock, "Feasibility analysis of stand-alone renewable energy supply options for a large hotel," *Renewable Energy*, vol. 33, no. 7, pp. 1475 – 1490, 2008.

[93] S. Shaahid and M. Elhadidy, "Technical and economic assessment of grid-independent hybrid photovoltaicdieselbattery power systems for commercial loads in desert environments," *Renewable and Sustainable Energy Reviews*, vol. 11, no. 8, pp. 1794 – 1810, 2007.

[94] J. Kenfack, F. P. Neirac, T. T. Tatietse, D. Mayer, M. Fogue, and A. Lejeune, "Microhydro-pv-hybrid system: Sizing a small hydro-pv-hybrid system for rural electrification in developing countries," *Renewable Energy*, vol. 34, no. 10, pp. 2259 – 2263, 2009.

[95] P. Balamurugan, S. Ashok, and T. L. Jose, "Optimal operation of biomass/wind/pv hybrid energy system for rural areas," *International Journal of Green Energy*, vol. 6, no. 1, pp. 104–116, 2009.

[96] R. Dufo-López and J. L. Bernal-Agustín, "Design and control strategies of pv-diesel systems using genetic algorithms," *Solar Energy*, vol. 79, no. 1, pp. 33 – 46, 2005.

[97] T. Senjyu, D. Hayashi, A. Yona, N. Urasaki, and T. Funabashi, "Optimal configuration of power generating systems in isolated island with renewable energy," *Renewable Energy*, vol. 32, no. 11, pp. 1917 – 1933, 2007.

[98] M. Kalantar and S. Mousavi, "Dynamic behavior of a stand-alone hybrid power generation system of wind turbine, microturbine, solar array and battery storage," *Applied Energy*, vol. 87, no. 10, pp. 3051 – 3064, 2010.

[99] H. Yang, W. Zhou, L. Lu, and Z. Fang, "Optimal sizing method for stand-alone hybrid solarwind system with lpsp technology by using genetic algorithm," *Solar Energy*, vol. 82, no. 4, pp. 354 – 367, 2008.

[100] H. Yang, Z. Wei, and L. Chengzhi, "Optimal design and techno-economic analysis of a hybrid solar-wind power generation system," *Applied Energy*, vol. 86, no. 2, pp. 163 – 169, 2009, iGEC III - Special Issue of the Third International Green Energy Conference (IGEC-III), June 18-20, 2007, Vsters, Sweden.

[101] A. Kornelakis and E. Koutroulis, "Methodology for the design optimisation and the economic analysis of grid-connected photovoltaic systems," *Renewable Power Generation, IET*, vol. 3, no. 4, pp. 476 –492, december 2009.

[102] J. Cabello, J. Cejudo, M. Luque, F. Ruiz, K. Deb, and R. Tewari, "Optimization of the size of a solar thermal electricity plant by means of genetic algorithms," *Renewable Energy*, vol. 36, no. 11, pp. 3146 – 3153, 2011.

[103] A. K. Kaviani, G. Riahy, and S. Kouhsari, "Optimal design of a reliable hydrogen-based stand-alone wind/pv generating system, considering component outages," *Renewable Energy*, vol. 34, no. 11, pp. 2380 – 2390, 2009.

[104] A. Kornelakis and Y. Marinakis, "Contribution for optimal sizing of grid-connected pv-systems using pso," *Renewable Energy*, vol. 35, no. 6, pp. 1333 – 1341, 2010.

[105] S. Avril, G. Arnaud, A. Florentin, and M. Vinard, "Multi-objective optimization of batteries and hydrogen storage technologies for remote photovoltaic systems," *Energy*, vol. 35, no. 12, pp. 5300 – 5308, 2010, ¡ce:title¿The 3rd International Conference on Sustainable Energy and Environmental Protection, SEEP 2009¡/ce:title¿.

[106] U. Boonbumroong, N. Pratinthong, S. Thepa, C. Jivacate, and W. Pridasawas, "Particle swarm optimization for ac-coupling stand alone hybrid power systems," *Solar Energy*, vol. 85, no. 3, pp. 560 – 569, 2011.

[107] S. Klein, W. Beckman, J. Mitchell, J. Duffie, N. Duffie, T. Freeman, J. Mitchell, J. Braun, B. Evans, J. Kummer, R. Urban, A. Fiksel, J. Thornton, N. Blair, P. Williams, D. Bradley, T. McDowell, M. Kummert, and D. Arias, *TRNSYS 16 Mathematical reference*, volume 5 ed., Solar Energy Laboratory, University of Wisconsin-Madison, 1500 Engineering Drive, 1303 Engineering Research Building Madison, WI 53706, U.S.A., 03 2007.

[108] S. A. Kalogirou, "Optimization of solar systems using artificial neural-networks and genetic algorithms," *Applied Energy*, vol. 77, no. 4, pp. 383 – 405, 2004.

[109] J. Lagorse, D. Paire, and A. Miraoui, "Sizing optimization of a stand-alone street lighting system powered by a hybrid system using fuel cell, pv and battery," *Renewable Energy*, vol. 34, no. 3, pp. 683 – 691, 2009.

[110] M. Masoum, S. Mousavi Badejani, and M. Kalantar, "Optimal placement of hybrid pv-wind systems using genetic algorithm," in *Innovative Smart Grid Technologies (ISGT), 2010*, jan. 2010, pp. 1 –5.

[111] X. Pelet, D. Favrat, and G. Leyland, "Multiobjective optimisation of integrated energy systems for remote communities considering economics and co2 emissions," *International Journal of Thermal Sciences*, vol. 44, no. 12, pp. 1180 – 1189, 2005, ¡ce:title¿A tribute to Bernard Spinner (1940-2004)¡/ce:title¿.

[112] J. L. Bernal-Agustín, R. Dufo-López, and D. M. Rivas-Ascaso, "Design of isolated hybrid systems minimizing costs and pollutant emissions," *Renewable Energy*, vol. 31, no. 14, pp. 2227 – 2244, 2006.

[113] A. Mellit, S. Kalogirou, L. Hontoria, and S. Shaari, "Artificial intelligence techniques for sizing photovoltaic systems: A review," *Renewable and Sustainable Energy Reviews*, vol. 13, no. 2, pp. 406 – 419, 2009.

[114] A. Mellit, S. A. Kalogirou, and M. Drif, "Application of neural networks and genetic algorithms for sizing of photovoltaic systems," *Renewable Energy*, vol. 35, no. 12, pp. 2881 – 2893, 2010.

[115] A. Zangeneh, S. Jadid, and A. Rahimi-Kian, "Promotion strategy of clean technologies in distributed generation expansion planning," *Renewable Energy*, vol. 34, no. 12, pp. 2765 – 2773, 2009.

[116] Y. Katsigiannis, P. Georgilakis, and E. Karapidakis, "Multiobjective genetic algorithm solution to the optimum economic and environmental performance problem of small autonomous hybrid power systems with renewables," *Renewable Power Generation, IET*, vol. 4, no. 5, pp. 404 –419, september 2010.

[117] A. J. del Real, A. Arce, and C. Bordons, "Optimization strategy for element sizing in hybrid power systems," *Journal of Power Sources*, vol. 193, no. 1, pp. 315 – 321, 2009, ¡ce:title¿Scientific Advances in Fuel Cell Systems¡/ce:title¿.

[118] R. Belfkira, P. Reghem, J. Raharijaona, G. Barakat, and C. Nichita, "Non-linear optimization based design methodology of wind/pv hybrid stand alone system," 2009.

[119] R. Belfkira, L. Zhang, and G. Barakat, "Optimal sizing study of hybrid wind/pv/diesel power generation unit," *Solar Energy*, vol. 85, no. 1, pp. 100 – 110, 2011.

[120] D. R. Jones, C. D. Perttunen, and B. E. Stuckman, "Lipschitzian optimization without the lipschitz constant," *J. Optim. Theory Appl.*, vol. 79, no. 1, pp. 157–181, Oct. 1993.

[121] R. Dufo-López, J. L. Bernal-Agustín, and J. Contreras, "Optimization of control strategies for stand-alone renewable energy systems with hydrogen storage," *Renewable Energy*, vol. 32, no. 7, pp. 1102 – 1126, 2007.

[122] C. Kongnam and S. Nuchprayoon, "A particle swarm optimization for wind energy control problem," *Renewable Energy*, vol. 35, no. 11, pp. 2431 – 2438, 2010.

[123] T. Niknam, H. Z. Meymand, and H. D. Mojarrad, "A practical multi-objective pso algorithm for optimal operation management of distribution network with regard to fuel cell power plants," *Renewable Energy*, vol. 36, no. 5, pp. 1529 – 1544, 2011.

[124] G. Celli, E. Ghiani, S. Mocci, and F. Pilo, "A multiobjective evolutionary algorithm for the sizing and siting of distributed generation," *Power Systems, IEEE Transactions on*, vol. 20, no. 2, pp. 750 – 757, may 2005.

[125] T. Niknam, S. I. Taheri, J. Aghaei, S. Tabatabaei, and M. Nayeripour, "A modified honey bee mating optimization algorithm for multiobjective placement of renewable energy resources," *Applied Energy*, vol. 88, no. 12, pp. 4817 – 4830, 2011.

[126] J. L. Bernal-Agustín and R. Dufo-López, "Efficient design of hybrid renewable energy systems using evolutionary algorithms," *Energy Conversion and Management*, vol. 50, no. 3, pp. 479 – 489, 2009.

[127] S. Hakimi and S. Moghaddas-Tafreshi, "Optimal sizing of a stand-alone hybrid power system via particle swarm optimization for kahnouj area in south-east of iran," *Renewable Energy*, vol. 34, no. 7, pp. 1855 – 1862, 2009.

[128] A. Saif, K. Elrab, H. Zeineldin, S. Kennedy, and J. Kirtley, "Multi-objective capacity planning of a pv-wind-diesel-battery hybrid power system," in *Energy Conference and Exhibition (EnergyCon), 2010 IEEE International*, dec. 2010, pp. 217 –222.

[129] D. Ipsakis, S. Voutetakis, P. Seferlis, F. Stergiopoulos, and C. Elmasides, "Power management strategies for a stand-alone power system using renewable energy sources and hydrogen storage," *International Journal of Hydrogen Energy*, vol. 34, no. 16, pp. 7081 – 7095, 2009, 4th Dubrovnik Conference, 4th Dubrovnik Conference.

[130] "Genesis selection guide, third edition," Hawker Energy Products Inc., Tech. Rep., 1998. [Online]. Available: www.hepi.com

[131] M. Drr, A. Cruden, S. Gair, and J. McDonald, "Dynamic model of a lead acid battery for use in a domestic fuel cell system," *Journal of Power Sources*, vol. 161, no. 2, pp. 1400 – 1411, 2006.

[132] E. Anderson, F. Mitlitsky, and T. Molter, "Recent advances in hydrogen generation using pem water electrolysis," Proton Energy Systems Inc., Tech. Rep., 2002.

[133] J. Duffie and W. Beckman, *Solar Engineering of Thermal Processes*, ser. A Wiley-Interscience Publication. John Wiley & Sons, 1991.

[134] J. F. Manwell, A. Rogers, G. Hayman, C. T. Avelar, J. G. McGowan, U. Abdulwahid, and K. Wu, *Hybrid2 - A hybrid system simulation model: Theory manual*, National Renewable Energy Laboratory, 2006.

[135] D. Thevenard and K. Haddad, "Ground reflectivity in the context of building energy simulation," *Energy and Buildings*, vol. 38, no. 8, pp. 972 – 980, 2006.

[136] P. Bendt, M. Collares-Pereira, and A. Rabl, "The frequency distribution of daily insolation values," *Solar Energy*, vol. 27, no. 1, pp. 1 – 5, 1981.

[137] B. Y. Liu and R. C. Jordan, "The interrelationship and characteristic distribution of direct, diffuse and total solar radiation," *Solar Energy*, vol. 4, no. 3, pp. 1 – 19, 1960.

[138] K. Hollands and R. Huget, "A probability density function for the clearness index, with applications," *Solar Energy*, vol. 30, no. 3, pp. 195 – 209, 1983.

[139] D. Erbs, S. Klein, and J. Duffie, "Estimation of the diffuse radiation fraction for hourly, daily and monthly-average global radiation," *Solar Energy*, vol. 28, no. 4, pp. 293 – 302, 1982.

[140] O. Ulleberg, "Stand-alone power systems for the future: Optimal design, operation & convtrol of solar-hydrogen energy systems," Ph.D. dissertation, Norweigian University of Science and Technology, Trondheim, 1998.

[141] C. Wang, "Modeling and control of hybrid wind/photovoltaic/fuel cell distributed generation systems," Ph.D. dissertation, Montana State University, 2006.

[142] Q. Kou, S. Klein, and W. Beckman, "A method for estimating the long-term performance of direct-coupled pv pumping systems," *Solar Energy*, vol. 64, no. 13, pp. 33 – 40, 1998.

[143] T. U. Townsend, "A method for estimating the long-term performance of direct-coupled photovoltaic systems," Master's thesis, University of Wisconsin - Madison, 1989.

[144] A. Manyonge, R. M. Ochieng, F. N. Onyango, and J. M. Shichikha, "Mathematical modelling of wind turbine in a wind energy conversion system: power coefficient analysis," *Applied Mathematical Sciences*, vol. 6, no. 91, pp. 4527–4536, 2012.

[145] J. F. Manwell, J. G. McGowanRogers, and A. L. Rogers, *Wind energy explained*. Wiley, 2002.

[146] http://www.hummerwindenergy.com/category/products/18.

[147] M. Lebbal and S. Lecoeuche, "Identification and monitoring of a pem electrolyser based on dynamical modelling," *International Journal of Hydrogen Energy*, vol. 34, no. 14, pp. 5992 – 5999, 2009.

[148] M. Ni, M. Leung, and D. Leung, "Electrochemistry modeling of proton exchange membrane (pem) water electrolysis for hydrogen production," in *World Hydrogen Energy Conference*, 2006.

[149] P. Choi, D. G. Bessarabov, and R. Datta, "A simple model for solid polymer electrolyte (spe) water electrolysis," *Solid State Ionics*, vol. 175, no. 1-4, pp. 535 – 539, 2004, fourteenth International Conference on Solid State Ionics.

[150] J. B. Copetti, E. Lorenzo, and F. Chenlo, "A general battery model for pv system simulation," *Progress in photovoltaics: Research and applications*, vol. 1, pp. 283–292, 1993.

[151] O. Gergaud, G. Robin, B. Multon, H. B. E. N. Ahmed, S. B. Branch, E. N. S. D. Cachan, K. Lann, and B. France, "Energy modeling of a lead-acid battery within hybrid wind photovoltaic systems," *Proc EPE*, pp. 1–10, 2003.

[152] H. Bindner, T. Cronin, P. Lundsager, J. F. Manwell, U. Abdulwahid, and I. Baring-Goould, "Lifetime modelling of lead acid batteries," Risø National Laboratory, Roskilde, Denmark, Tech. Rep. Risø-R-1515, 2005.

[153] S. D. Downing and D. Socie, "Simple rainflow counting algorithms," *International Journal of fatigue*, pp. 31–40, January 1982.

[154] H. Laukamp, "Inverter for photovoltaic systems. user-written trnsys source code," 1988.

[155] O. Ulleberg and R. Glöckner, *Hydrogems hydrogen energy models*, version 1.1 ed., Institute for energy technology, Norway.

[156] K. Sopian, M. Z. Ibrahim, W. R. W. Daud, M. Y. Othman, B. Yatim, and N. Amin, "Performance of a pv-wind hybrid system for hydrogen production," *Renewable Energy*, vol. 34, no. 8, pp. 1973 – 1978, 2009, 2007 World Renewable Energy Conference - Pacific Rim Region.

[157] DuPont™, "Nafion® pfsa membranes n-112, ne-1135, n-115, n-117, ne-1110," DuPont™, Tech. Rep., 2004.

[158] B. Han, S. M. S. III, J. Mo, and F.-Y. Zhang, "Electrochemical performance modeling of a proton exchange membrane electrolyzer cell for hydrogen energy," *International Journal of Hydrogen Energy*, vol. 40, no. 22, pp. 7006 – 7016, 2015. [Online]. Available: http://www.sciencedirect.com/science/article/pii/S036031991500837X

[159] N. Achaibou, M. Haddadi, and A. Malek, "Lead acid batteries simulation including experimental validation," *Journal of Power Sources*, vol. 185, no. 2, pp. 1484 – 1491, 2008.

[160] D. E. Goldberg, *Genetic Algorithms in Search, Optimization and Machine Learning*, 1st ed. Boston, MA, USA: Addison-Wesley Longman Publishing Co., Inc., 1989.

[161] M. Carmo, D. L. Fritz, J. Mergel, and D. Stolten, "A comprehensive review on {PEM} water electrolysis," *International Journal of Hydrogen Energy*, vol. 38, no. 12, pp. 4901 – 4934, 2013.

[162] *Tubular gel valve regulated lead-acid batteries technical manual*, HBL Power Systems Ltd., Road number 10, Banjara Hills, Hyderabad - 500 034, India.

[163] "Guidelines for life-cycle costing on state building projects," State of Wisconson, Department of Administration. Division of Facilities Development, Tech. Rep., 1993.

[164] S. Diaf, M. Belhamel, M. Haddadi, and A. Louche, "Technical and economic assessment of hybrid photovoltaic/wind system with battery storage in corsica island," *Energy Policy*, vol. 36, no. 2, pp. 743 – 754, 2008.

[165] M. Talyor, "Sumary for policy makers: renewable power generation costs," Internation Renewable Energy Agency, Tech. Rep., 2012.

[166] SARB. (2013) South African Reserve Bank. [Online]. Available: http://www.resbank.co.za/Pages/ default.aspx

[167] B. S. Blanchard and W. J. Fabrycky, *Systems engineering and analysis*, 4th ed., ser. International series in industrial and systems engineering, W. J. Fabrycky and J. H. Mize, Eds. Prentice Hall, 2006.

[168] A. Popov, *MOEA user manual*, Institute of Control Systems, Hamburg University of Technology, 2002.

[169] R. A. Johnson and D. W. Wichern, *Applied Multivariate Statistical Analysis (5th Edition)*, 5th ed. Prentice Hall, Dec. 2001. [Online]. Available: http://www.worldcat.org/isbn/0130925535

[170] L. Wang, *Adaptive Fuzzy Systems and Control: Design and Stability Analysis*, ser. Electrical engineering. PTR Prentice Hall, 1994. [Online]. Available: https://books.google.co.za/books?id=spIeAQAAIAAJ

[171] O. Cordón, *Genetic Fuzzy Systems: Evolutionary Tuning and Learning of Fuzzy Knowledge Bases*, ser. Advances in fuzzy systems - Applications and theory. World Scientific, 2001. [Online]. Available: https://books.google.co.za/books?id=BWmSV-38fKAC

Appendix A

Pareto solution set data

Site A: Scatter plots showing the nine sizing variables plotted against the objectives are given in Fig. A.1, Fig. A.2 and Fig. A.3 and scatter plots showing the six control variables plotted against the objectives are given in Fig. A.4, Fig. A.5 and Fig. A.6.

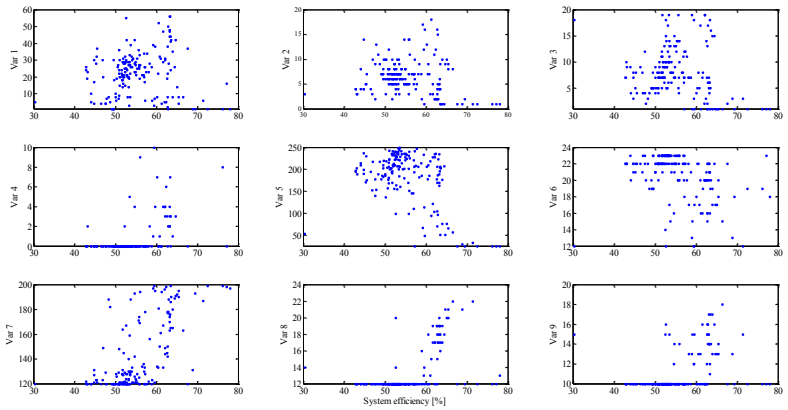

Figure A.1: Site A sizing independent variables vs. efficiency objective.

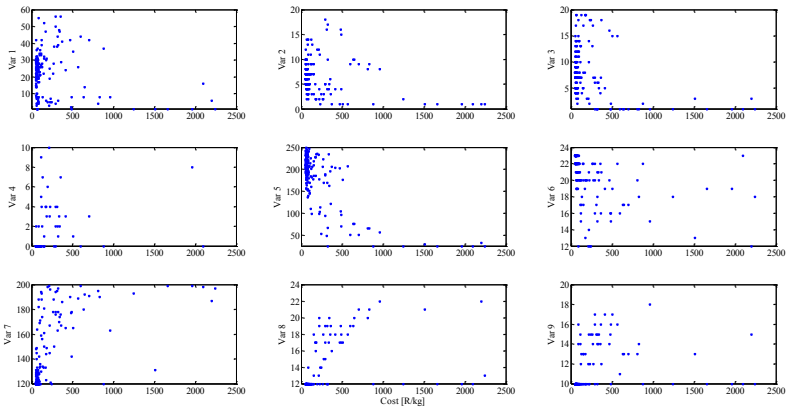

Figure A.2: Site A sizing independent variables vs. cost objective.

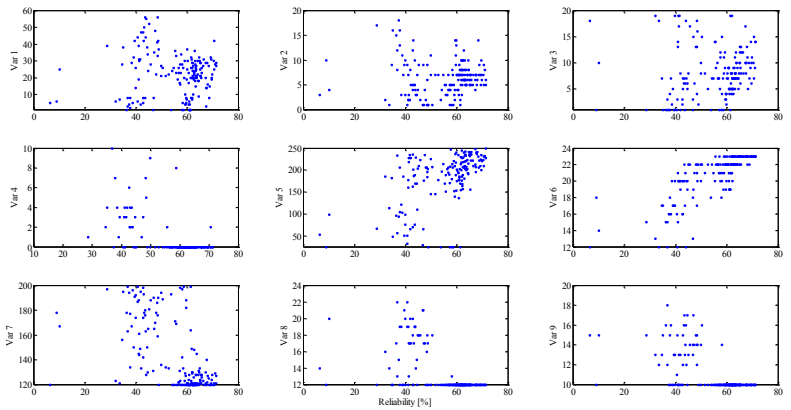

Figure A.3: Site A sizing independent variables vs. reliability objective.

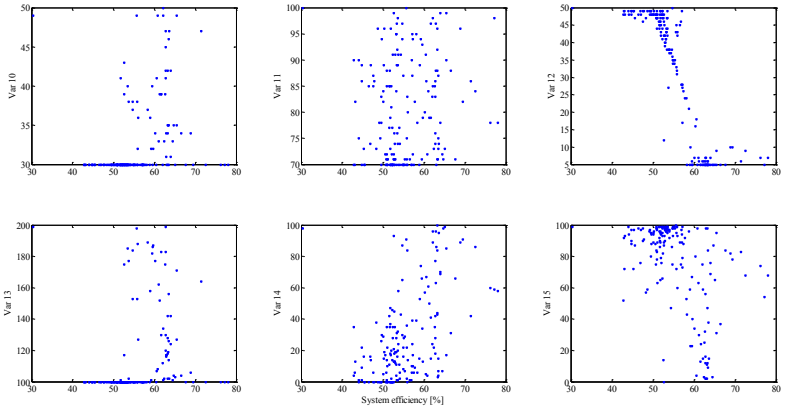

Figure A.4: Site A control independent variables vs. efficiency objective.

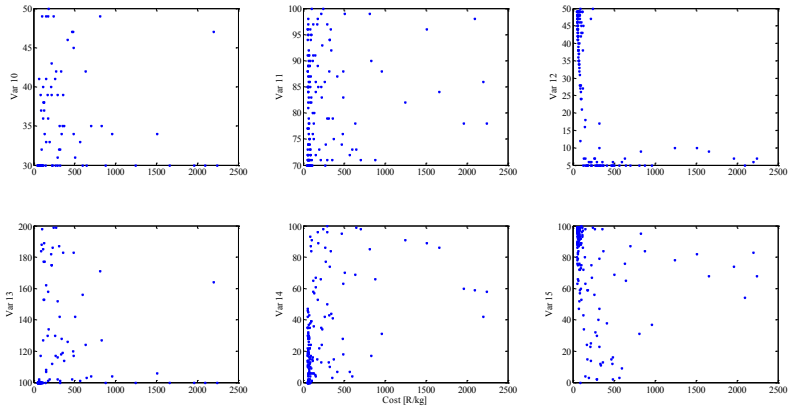

Figure A.5: Site A control independent variables vs. cost objective.

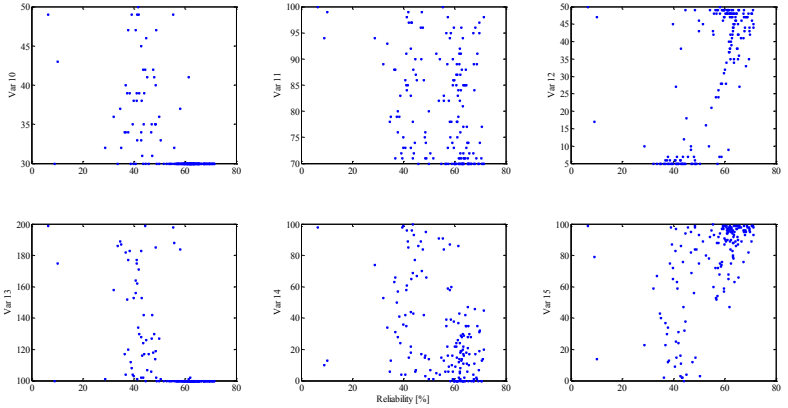

Figure A.6: Site A control independent variables vs. reliability objective.

Site B: Scatter plots showing the nine sizing variables are given in Fig. A.7, Fig. A.8 and Fig. A.9 and scatter plots showing the nine sizing variables are given in Fig. A.10, Fig. A.11 and Fig. A.12.

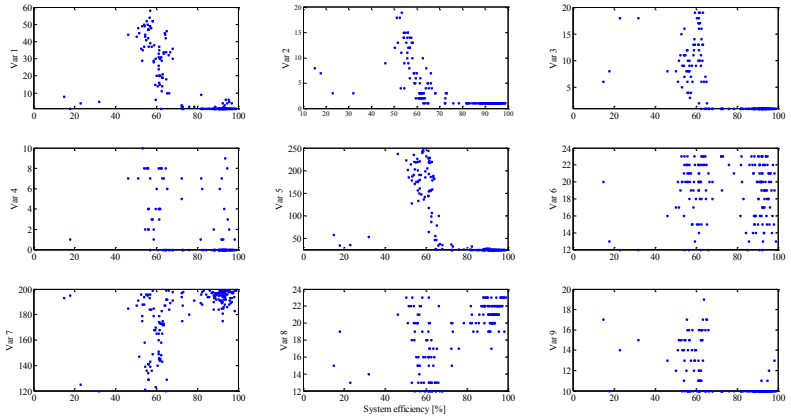

Figure A.7: Site B sizing independent variables vs. efficiency objective.

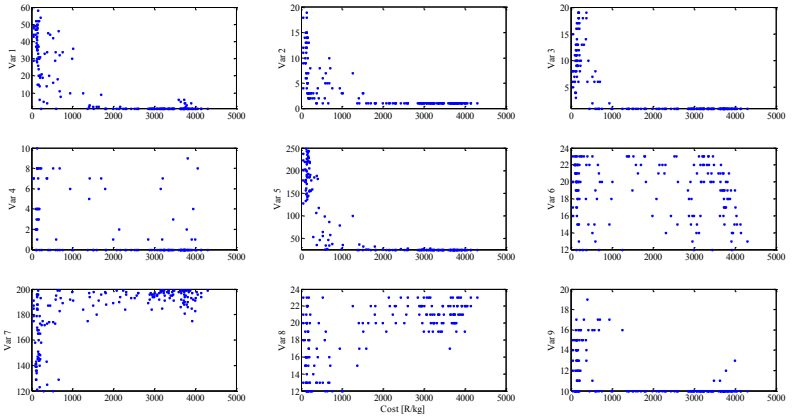

Figure A.8: Site B sizing independent variables vs. cost objective.

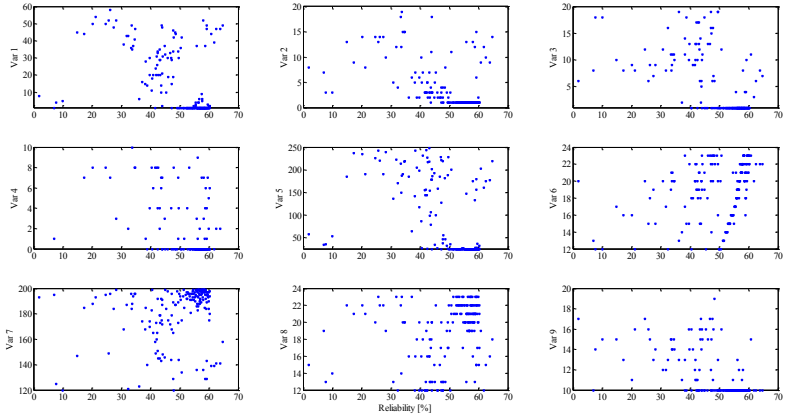

Figure A.9: Site B sizing independent variables vs. reliability objective.

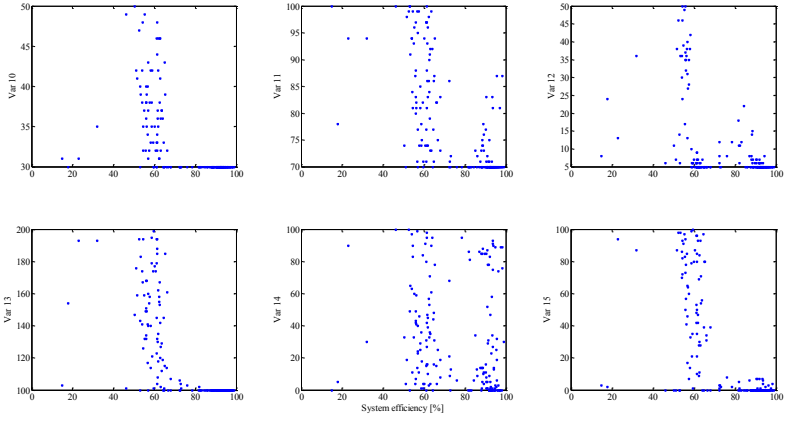

Figure A.10: Site B sizing independent variables vs. efficiency objective.

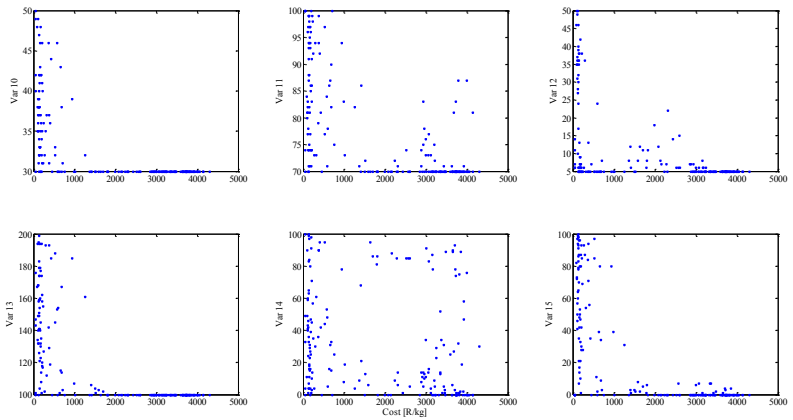

Figure A.11: Site B sizing independent variables vs. cost objective.

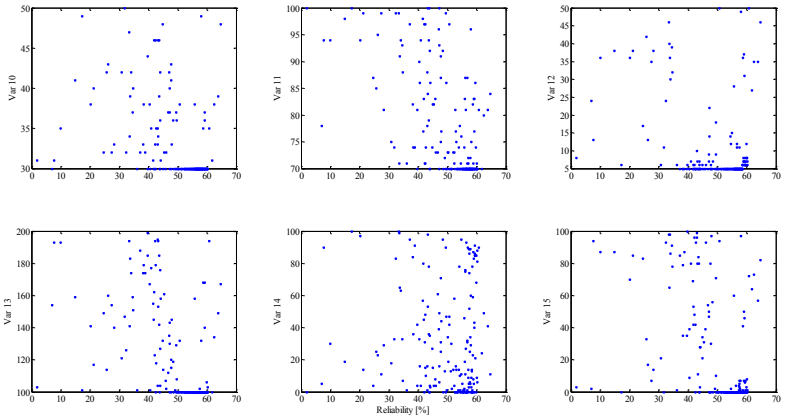

Figure A.12: Site B control independent variables vs. reliability objective.

Site C: Scatter plots showing the nine sizing variables are given in Fig. A.13, Fig. A.14 and Fig. A.15 and scatter plots showing the nine sizing variables are given in Fig. A.16, Fig. A.17 and Fig. A.18.

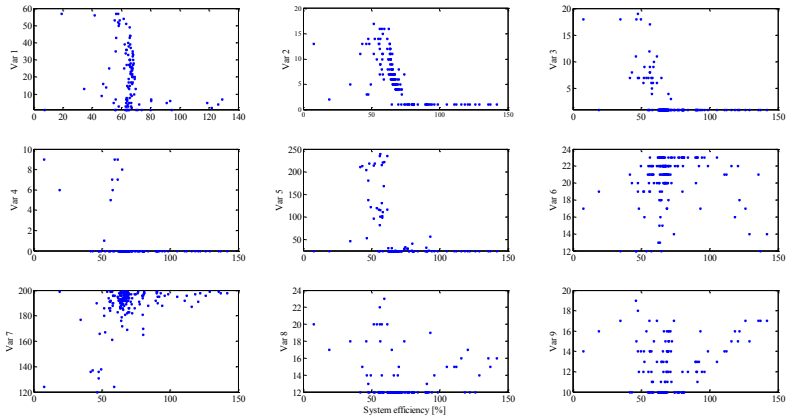

Figure A.13: Site C sizing independent variables vs. efficiency objective.

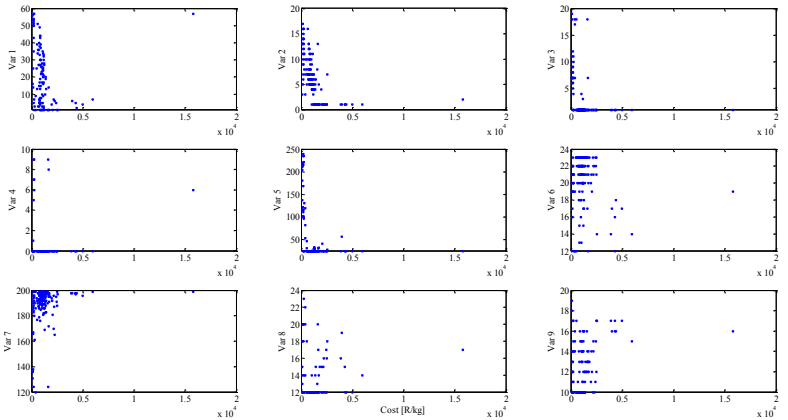

Figure A.14: Site C sizing independent variables vs. cost objective.

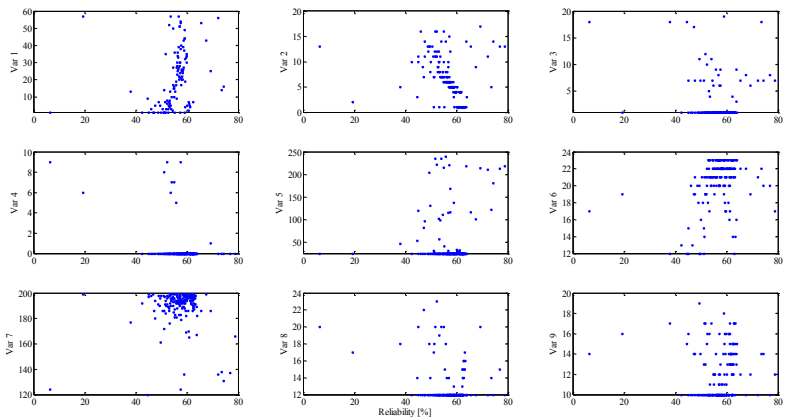

Figure A.15: Site C sizing independent variables vs. reliability objective.

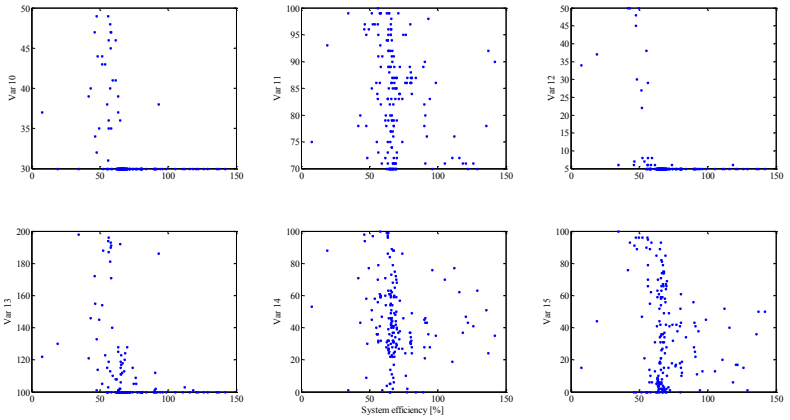

Figure A.16: Site C sizing independent variables vs. efficiency objective.

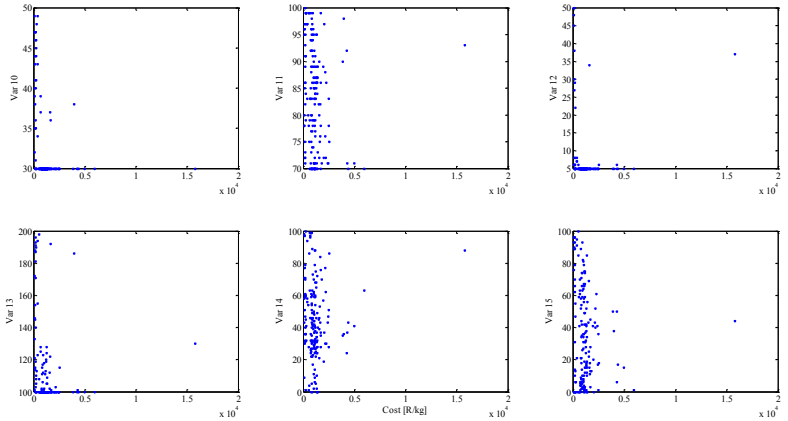

Figure A.17: Site C sizing independent variables vs. cost objective.

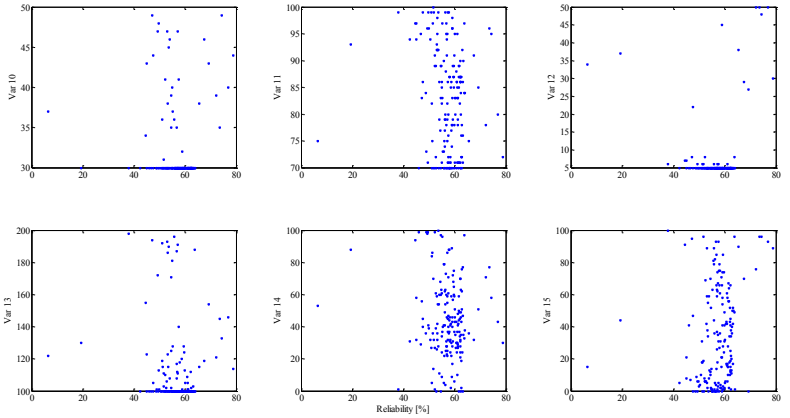

Figure A.18: Site C control independent variables vs. reliability objective.

Appendix B

Genetic fuzzy system figures and tables for site B

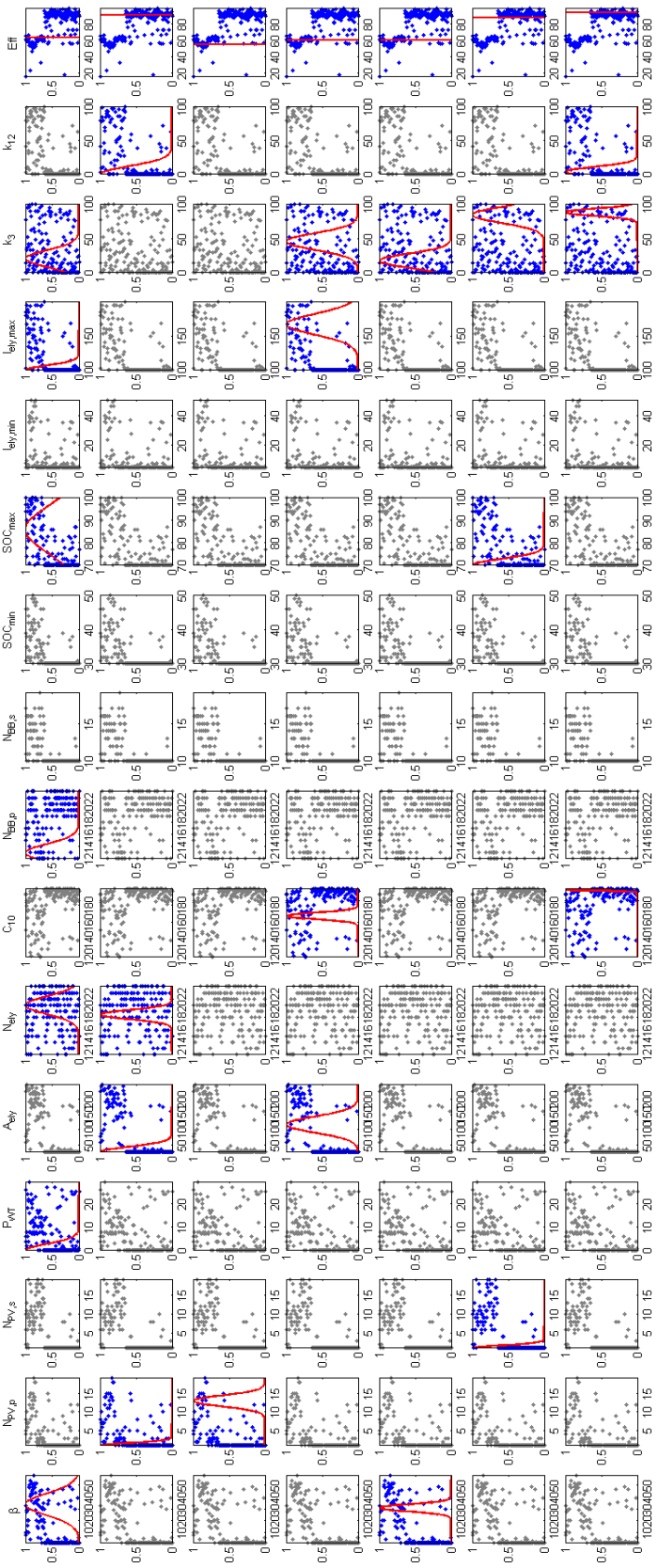

Figure B.1: Reduced fuzzy rules for site B efficiency objective.

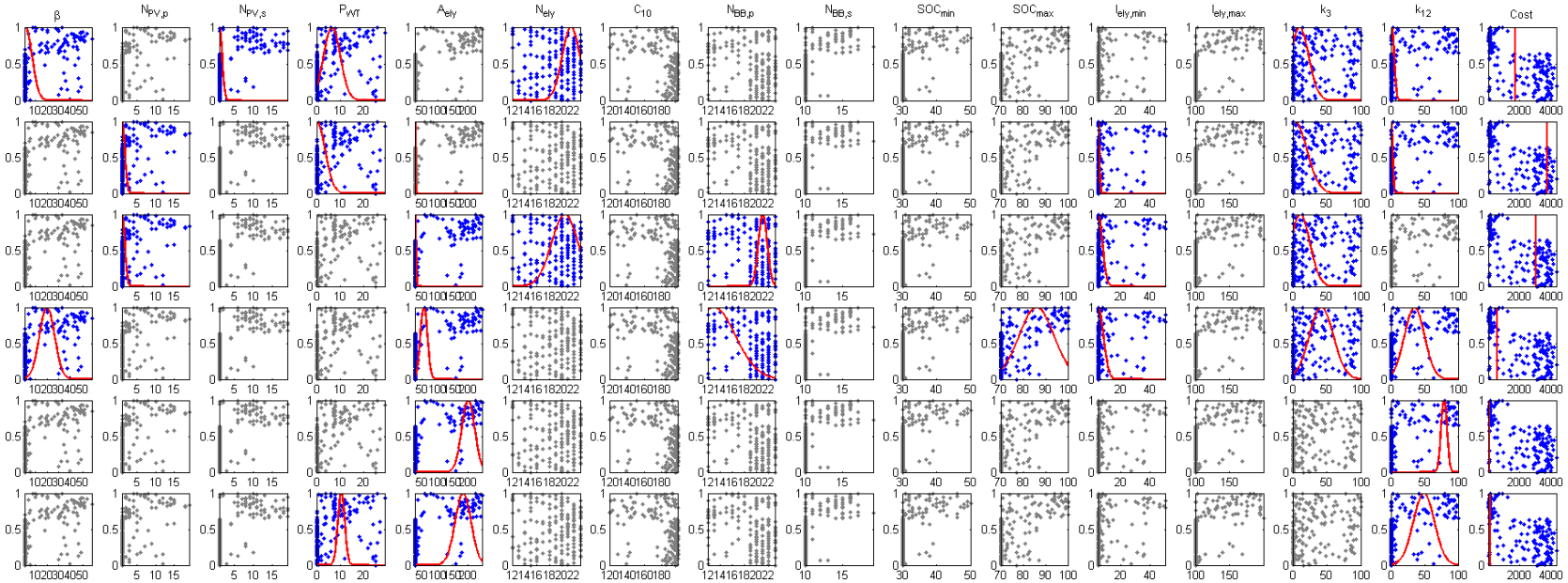

Figure B.2: Reduced fuzzy rules for site B cost objective.

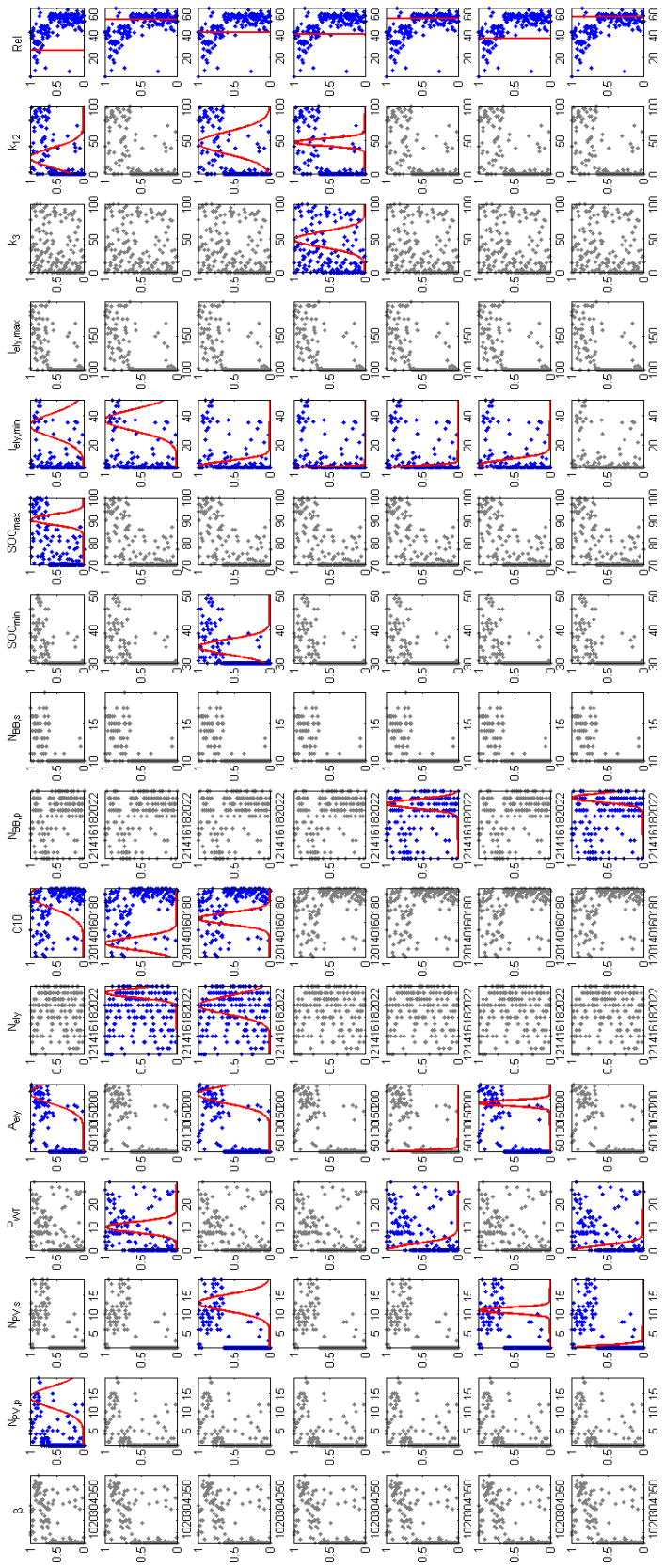

Figure B.3: Reduced fuzzy rules for site B reliability objective.

Table B.1: Site B description/findings/explanation of efficiency rules.

General: 77 % of the MFs are eliminated with the RMSE remaining within the specified 10 % error. 79 % of sizing MFs are eliminated while 74 % of control MFs are eliminated. This observation indicates that system efficiency is slightly more dependent on control variables since less control variables have been eliminated.
Rule 1: IF β is L $\wedge$ P_{WT} is VL $\wedge$ N_{ely} is H $\wedge$ $N_{B,s}$ is VL $\wedge$ SOC_{max} is M $\wedge$ $I_{ely,max}$ is VL $\wedge$ k_3 is L THEN Eff is H Rule 1 consists of four sizing variables and three control variables. The rule states that for a *low* PV slope, a *very low* wind turbine power rating, a *high* number of electrolyser cells, a *very low* number of batteries in series, a *medium* maximum battery SOC setting, a *very low* maximum electrolyser current setting and a low k_3 result in a *very high* efficiency. A *low* PV slope result in the maximum peak power from PV. This is not the optimal solution, but will provide the highest amount of energy in terms of kWh production. A *very low* wind turbine rating implies the energy supplied by wind power to be low or excluded. This site is classified as having fair wind resources and good solar resources given in 7.3 thus PV would take the preference. A *high* number of electrolyser cells and a *very low* maximum electrolyser current would result in a low current densities. Electrolyser efficiencies are higher at lower current densities. This will result in high system efficiency also. A *very low* number of batteries in series and a *low* k_2 implies that the battery component is small and that there is little power from the batteries to the electrolyser. Additionally the maximum battery SOC is selected to be *medium* which also would result that the batteries operate in the most efficient range of the batteries adding to the *high* system efficiency.
Rule 2: IF $N_{PV,s}$ is VL $\wedge$ A_{ely} is VL $\wedge$ N_{ely} is M $\wedge$ k_{12} is VL THEN Eff is VH Rule 2 consists of three sizing variables and a single power management control variable. The rule states that for a *very low* number of PV modules in series, a *very low* electrolyser cell area, a *medium* number of electrolyser cells and a *very low* k_{12} result in *very high* efficiency. A *very low* electrolyser cell area and a *medium* number of cells result in a small sized electrolyser. The rule shows that a *very high* system efficiency can result from a small electrolyser when operated with a very low number of PV cells is needed. Further a *very low* k_{12} implies that energy is used to charge the batteries rather than producing hydrogen resulting in low electrolyser power which is previously shown to have higher efficiencies.
Rule 3: IF $N_{PV,s}$ is VH THEN Eff is M Rule 3 consists of a single sizing variable. The rule states that for a *very high* number of PV modules in series the system efficiency is *medium*. The number of PV modules is directly related to maximum input power. This rule might be as a result of the range of possible component sizes and control parameters for the other components are to low for the PV range available. This rule basically then result in a *medium* efficiency if the PV resource is sized to large for efficient use of all energy obtained from the sun.

Table B.2: Site A interpretation of efficiency objective rule base - Continued.

Rule 4: IF A_{ely} is H $\wedge$ C_{10} is H $\wedge$ $I_{ely,max}$ is H $\wedge$ k_3 is M THEN Eff is H Rule 4 consists of two sizing variables and two control variables. The rules states that for a *high* electrolyser cell area, a *high* battery Ah rating, a *high* maximum electrolyser current setting and a *medium* k_3 result in a *high* system efficiency. A *high* electrolyser cell are and high maximum cell current would normally imply *high* efficiency, which is not the case always as some other components can bring down the efficiency as in this rule. A *high* battery Ah rating and medium k_3 result in roughly half the energy being stored in the battery which would result in the electrolyser operating current being a relatively low value. This would result in a *high* efficiency.
Rule 5: IF β is L $\wedge$ k_3 is VL THEN Eff is H Rule 5 consists of a single sizing parameter and a single control parameter. The rules states that a *low* PV module slope and a *very low* k_3 result in a *high* efficiency. A *low* PV slope result in a higher energy yield through the year for the PV modules and thus a the high system efficiency. A very low k_3 implies that the majority of the energy is diverted to the batteries which allow the electrolyser to operate at a lower point which also result in *high* system efficiency.
Rule 6: IF $N_{PV,p}$ is VL $\wedge$ SOC_{max} is VL $\wedge$ k_3 is VH THEN Eff is VH Rule 6 consists of a single sizing variable and two control variables. The rule states that for a *very low* number of PV modules in parallel, a *very low* maximum battery SOC and a *very high* k_3 result in a *very high* efficiency. A *very low* battery maximum SOC ensures that the batteries are operated in an efficient operating range. A *verh high* k_3 result in majority of power supplied to the electrolyser. A *very low* number of PV modules in parallel implies low power input. There is thus little power available, implying a small system and *low* electrolyser operating current resulting in high electrolyer efficiency which along with the battery efficiency result in a *very high* system efficiency.

Table B.3: Site B description/findings/explanation of cost rules.

General: 67 % of the MFs are eliminated with the RMSE remaining within the specified 10 % error. 69 % of sizing MFs are eliminated and 64 % of control MFs are eliminated. This indicates that cost is slightly more dependent on control variables since less control variables are eliminated.
Rule 1: IF β is VL $\wedge$ $N_{PV,p}$ is VL $\wedge$ P_{WT} is L $\wedge$ N_{ely} is H $\wedge$ k_3 is VL $\wedge$ k_{12} is VL THEN Cost is VH Rule 1 consists of four sizing variables and the two power management control variables. The rule states that for a *very low* PV module slope, a *very low* number of PV modules in parallel, a *Low* wind turbine power rating, a *high* number of electrolyser cells, a *very low* k_3 and a *very low* k_{12} result in *very high* cost. A *very low* slope for this site result in high yearly energy yield. More energy is thus available for hydrogen production reducing cost. A *very low* number of PV modules in parallel and *low* wind turbine rating result in low power from the RE sources. A *very low* k_3 and *very low* k_{12} result in low power to the electrolyser during low and no RE source availability. Having a *high* number of electrolyser cells imply a large electrolyser which is an expensive component. The electorlyser would be oversized compared to the rest of the components and power management control variable settings resulting in *very high* cost.
Rule 2: IF $N_{PV,s}$ is VL $\wedge$ P_{WT} is VL $\wedge$ A_{ely} is VL $\wedge$ $I_{ely,min}$ is VL $\wedge$ k_3 is VL $\wedge$ k_{12} is VL THEN Cost is VH Rule 2 consists of three sizing variables and three control variables. The rule states that for a *very low* number of PV modules in parallel, a *very low* wind turbine power rating, a *very low* electrolyser cell area, a *very low* minimum electrolyser current setting, a *very low* k_3 and a *very low* k_{12} result in *very high* cost. The *very low* number of electrolyser cells and wind turbine power rating implies low power input from the RE sources. A *very low* electrolyser cell area implies a low small rated electrolyser. With all the control variable settings *very low* the power to the electrolyser is low. This configuration will show a high efficiency however result in *very high* cost.
Rule 3: IF $N_{PV,s}$ is VL $\wedge$ A_{ely} is VL $\wedge$ N_{ely} is H $\wedge$ $N_{B,s}$ is H $\wedge$ $I_{ely,min}$ is VL $\wedge$ k_3 is VL THEN Cost is VH Rule three consists of four sizing variables and two control variables. The rule states that for a *very low* number of PV panels in series, a *very low* electrolyser cell area, a *high* number of electrolyser cells, a *high* number of batteries in series, a *very low* minimum electrolyser current setting and a *very low* k_3 result in *very high* cost. A *very low* number of PV modules in series would result in low capital cost but limited energy to produce hydrogen reducing the (TLCC) cost. A *high* number of batteries in series result in high capital cost. A *very low* k_3 result in limited power to the electrolyser which result in majority of power to the batteries. Having a *very low* electrolyser cell area and a *high* number of cells result in a medium electrolyser rating with a *very low* minimum electrolyser current result in low hydrogen production resulting in *very high* cost.

Table B.4: Site A interpretation of efficiency cost rule base - Continued.

Rule 4: IF β is L $\wedge$ A_{ely} is L $\wedge$ $N_{B,s}$ is VL $\wedge$ SOC_{max} is M $\wedge$ $I_{ely,min}$ is VL $\wedge$ k_3 is M $\wedge$ k_{12} is L THEN Cost is M Rule 4 consists of three sizing variables and four control variables. The rule states that for a *low* PV module slope, a *low* electrolyser cell area, a *very low* number of batteries in series, a *medium* maximum battery SOC setting, a *very low* minimum electrolyser current setting, a *medium* k_3 and a *low* k_{12} result in *medium* cost. A *low* PV slope for site B result in maximum yield of energy production but not the optimal energy profile through the year. A *low* electrolyser cell area implies a low power rated electrolyser and with the minimum electrolyser current *very low*, k_3 *medium* and k_{12} *low* little energy is used by the electrolyser which means the energy should be stored in the battery. With the battery maximum SOC *medium* a very large battery storage component would be required which has a high cost.
Rule 5: IF A_{ely} is VH $\wedge$ k_{12} is H THEN Cost is VL Rule 5 consists of one sizing variables and one control variable. The rule states that for a *very high* electrolyser cell area and a *high* k_{12} result in a *very low* cost. A *very high* electrolyser cell are implies a large rated electrolyser which has a high capital cost. Having k_{12} high result in high power to the electrolyser resulting in high hydrogen production. This will result in *very low* (TLCC) cost.
Rule 6: IF P_{WT} is L $\wedge$ A_{ely} is VH $\wedge$ k_{12} is M THEN Cost is VL Rule 6 consists of two sizing variables and one control variable. The rule states that for a *low* wind turbine power rating, a very high electrolyser cell area and a medium k_{12} result in very low cost. This is similar to rule 5 with the addition of the wind turbine power rating variable. With k_{12} being *medium* less power is transferred to the electrolyser. With the addition of a small wind turbine the energy from the wind turbine will be intermittent and therefore the *medium* setting. This result in again a *very low* cost.

Table B.5: Site B description/findings/explanation of reliability rules.

General: 71 % of the MFs are eliminated with the RMSE remaining within the specified 10 % error. 71 % of sizing MFs are eliminated and 71 % of control MFs are eliminated. This indicates that reliability is equally dependent on sizing variables and control variables.
Rule 1: IF $N_{PV,s}$ is VH $\wedge$ A_{ely} is VH $\wedge$ C_{10} is VH $\wedge$ SOC_{max} is H $\wedge$ $I_{ely,min}$ is H $\wedge$ k_{12} is L THEN Rel is L Rule 1 consists of three sizing variables and three sizing variables. The rule states that for a *very high* number of PV modules in series, a *very high* electrolyser cell area, a *very high* battery AH rating, a *high* maximum battery SOC value, a *high* minimum electrolyser current setting and a *low* k_{12} result in *low* reliability. With the sizing variables $N_{PV,s}$, A_{ely} and C_{10} *very high* the system components are sized big. A *high* maximum battery SOC value and a low k_{12} result in the battery receiving high power from the RE sources which are intermittent. Electrolyser minimum current setting is *high* implying that the electrolyser does not experience multiple ON/OFF cycles and should have good reliability. However, the cycles experienced by the battery result in the *low* system reliability.
Rule 2: IF P_{WT} is L $\wedge$ N_{ely} is VH $\wedge$ C_{10} is L $\wedge$ $I_{ely,min}$ is H THEN Rel is M Rule 2 consists of three sizing variables and one control variable. The rule states that for a *low* wind turbine power rating, a *very high* number of electrolyser cells, a *low* battery AH rating and a *high* minimum electrolyser current setting result in *medium* reliability. A *very high* number of electrolyser cells implies a large rated electrolyser with a *high* minimum electrolyser current setting. With the *low* wind turbine power rating and the *low* battery Ah rating, the battery will undergo many intermittent operations. Again the electrolyser will not undergo many ON/OFF cycles but with this configuration the batteries will be cycled and would result in *medium* reliability.
Rule 3: IF $N_{PV,p}$ is VH $\wedge$ A_{ely} is VH $\wedge$ N_{ely} is H $\wedge$ C_{10} is M $\wedge$ SOC_{min} is L $\wedge$ $I_{ely,min}$ is VL $\wedge$ k_{12} is M THEN Rel is M Rule 3 consists of four sizing variables and three control variables. The rule states that for a *very high* number of PV modules in parallel, a *very high* electrolyser cell area, a *high* number of electrolyser cells, a *medium* battery Ah capacity, a *low* minimum battery SOC setting, a *very low* minimum electrolyser current setting and a medium k_{12}. A *very high* number of PV modules in parallel would result in high PV power while the *very high* electrolyser cell area and *high* number of cells suggest a very large rated electrolyser. Having a *very low* minimum electrolyser current setting would result in low reliability for the electrolyser. A *medium* battery Ah rating and a *low* minimum SOC value results in more energy being supplied from the battery to the electrolyser preventing intermittent operation of the electrolyser and similarly a medium k_{12} would divert exces energy equally to the battery and electrolyser also preventing intermittent operation of the electrolyser. This results in *medium* reliability.

Table B.6: Site A interpretation of efficiency reliability rule base - Continued.

Rule 4: IF $I_{ely,min}$ is VL $\wedge$ k_3 is M $\wedge$ k_{12} is M THEN Rel is M Rule 4 consists of three control variables. The rule states that for a *very low* minimum electrolyser current, a *medium* k_3 and a medium k_{12} result in a *medium* reliability. With a *very low* minimum electrolyser current setting the electrolyser turns on at low power values and can cause multiple ON/OFF cycles and a low electrolyser reliability. The *medium* setting of k_3 ensures that the batteries supply power during intermittent operation preventing to many ON/OFF cycles from the battery. A *medium* k_{12} splits equally the power from the RE sources allowing battery charging and electrolyser operation resulting in a *medium* system reliability.
Rule 5: IF P_{WT} is VL $\wedge$ A_{ely} is VL $\wedge$ $N_{B,s}$ is H $\wedge$ $I_{ely,min}$ is VL THEN Rel is M Rule 5 consists of three sizing variables and one control variable. The rule states that for a *very low* wind turbine power rating, a *very low* electrolyser cell area, a *high* number of batteries in series and a *very low* minimum electrolyser current setting result in *medium* reliability. Having a *very low* wind turbine result in low power from the RE source. A *very low* electrolyser cell area result in low power electrolyser. A *very low* minimum electrolyser current setting can cause unnecessary ON/OFF durign intermittent RE source supply resulting in low electrolyser reliability. A *high* number of batteries in series result in high battery energy storage capacity and with the low power input operates only in a narrow operating range, resulting in high battery reliability. A resulting *medium* system reliability is observed.
Rule 6: IF $N_{PV,p}$ is VH $\wedge$ A_{ely} is VH $\wedge$ $I_{ely,min}$ is VL THEN Rel is L Rule 6 consists of one sizing variable and two control variables. The rule states that for a *very high* number of PV modules in parallel, a *very high* electrolyser cell area and a *very low* minimum electrolyser current setting result in *low* reliability. A *very high* number of PV modules in parallel implies a high RE source input power. A *very high* electrolyser cell area implies a high rated electrolyser. With a *very low* minimum electrolyser setting the electrolyser turns on at low power values and can cause multiple ON/OFF cycles and a low electrolyser reliability and results in a *low* system reliability.
Rule 7: IF $N_{PV,p}$ is VL $\wedge$ P_{WT} is VL $\wedge$ $N_{B,s}$ is VH THEN Rel is M Rule 7 consists of three sizing variables. The rule states that a *very low* number of PV modules in parallel, a *very low* power rated wind turbine and a *very high* number of batteries in series result in a medium reliability. A *very low* number of PV modules in parallel and *very low* wind turbine power rating implies low energy input from the RE sources. A *very high* number of batteries in parallel with the low power input would result in the batteries operating only in a narrow operating range. Depending on the electrolyser rating, a *medium* system reliability is observed.

Appendix C

Genetic fuzzy system figures and tables for site C

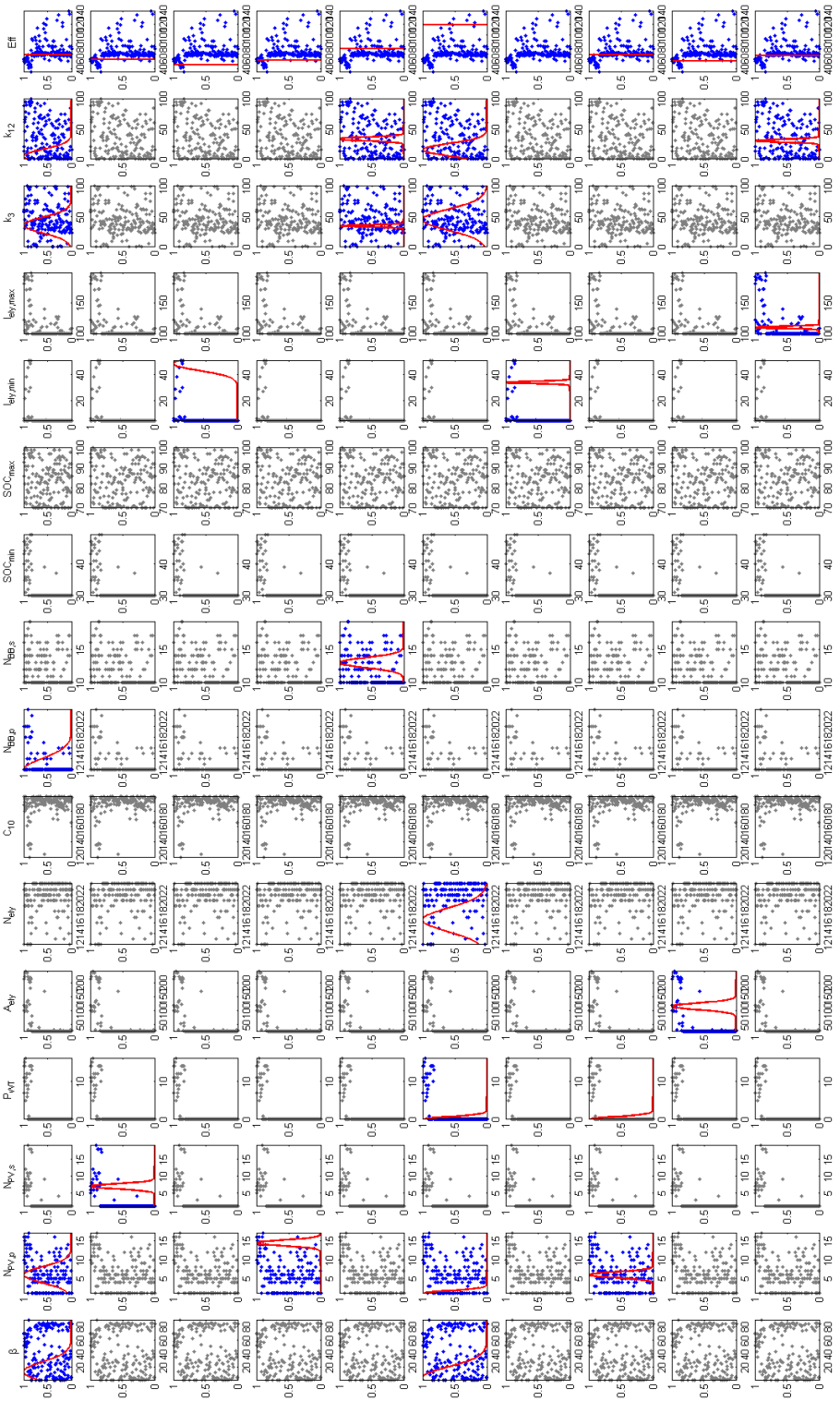

Figure C.1: Reduced fuzzy rules for site C efficiency objective.

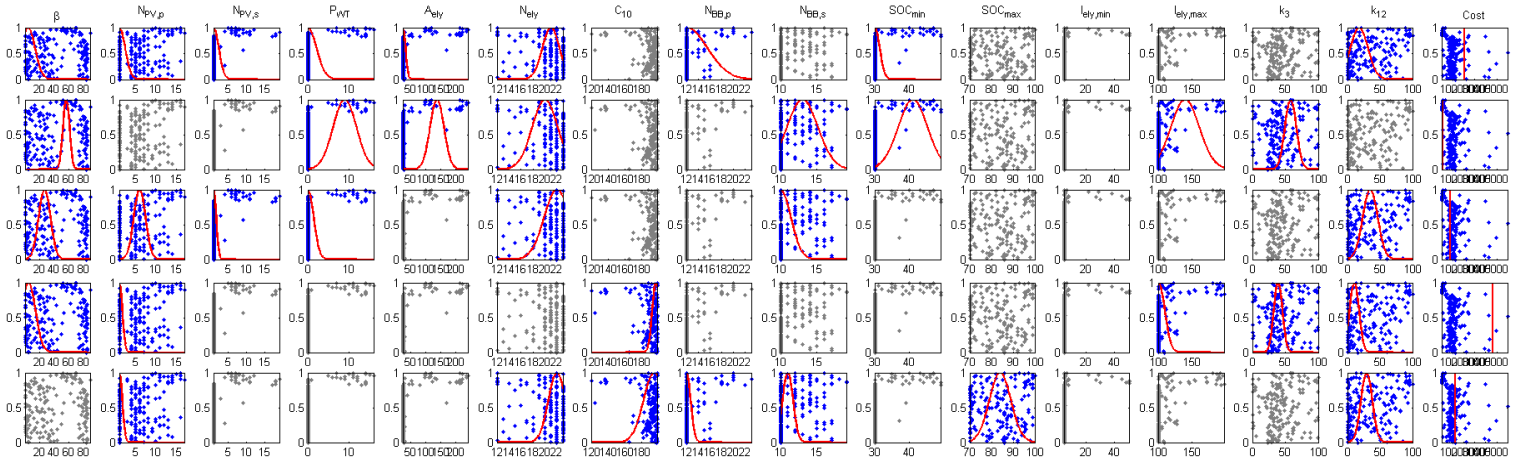

Figure C.2: Reduced fuzzy rules for site C cost objective.

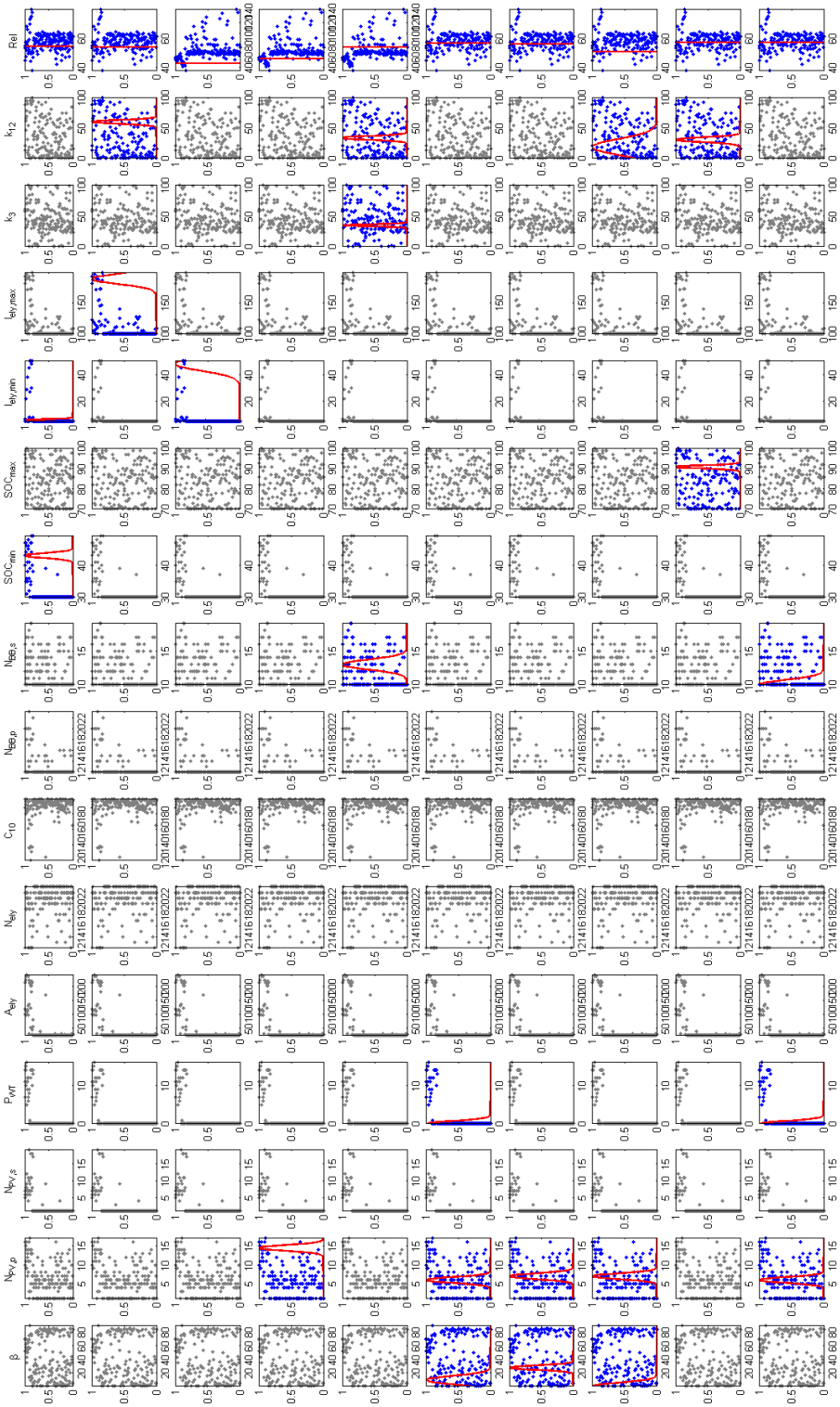

Figure C.3: Reduced fuzzy rules for site C reliability objective.

Table C.1: Site C description/findings/explanation of efficiency rules.

General: 83 % of the MFs are eliminated with the RMSE remaining within the specified 10 % error. 83 % of sizing MFs are eliminated while 81 % of control MFs are eliminated. This observation indicates an equal dependency between sizing and control variables.
Rule 1: IF β is VL $\wedge$ $N_{PV,s}$ is H $\wedge$ $N_{B,s}$ is VL $\wedge$ k_3 is L $\wedge$ k_{12} is VL THEN Eff is H Rule 1 consists of three sizing variables and the two power management control variables. The rule states that for a *very low* PV module slope, a *high* number of PV modules in parallel, *very low* number of batteries in series, a *low* k_3 and a very low k_{12} result in *high* efficiency. A *very low* PV module slope is not optimal for site C. Having a *high* number of PV modules in series with the *very low* result in low power from the RE source. Having a *very low* number of batteries in series, a *low* k_3 and *very low* k_{12} ensures that the electrolyser current density remain low. Again, a low electrolyser current density result in high electrolyser and thus system efficiency.
Rule 2: IF $N_{PV,p}$ is H THEN Eff is M Rule 2 consists of one sizing variable. The rule states that for a *high* number of PV modules in parallel result in medium efficiency.Site C is classified as a marginal solar resource site. The rule implies that with a high value for $N_{PV,p}$ efficiency can only be *medium*. Rule therefore identifies the marginal resource capability of the soalr resource.
Rule 3: IF $I_{ely,min}$ is VH THEN Eff is M Rule 3 consists of a single variable. The rule states that for a *very high* minimum electrolyser current setting result in medium efficiency. An electrolyser is most efficient at low current densities. The rule confirms this in that a *very high* minimum electrolyser current setting can only result in a medium efficiency.
Rule 4: IF $N_{PV,s}$ is VH THEN Eff is M Rule 4 consists of a single sizing variables. The rule states that a *very high* number of PV modules in series result in medium efficiency. Rule 4 is exactly the same with the same explanation and conclusion as rule 2.
Rule 5: IF $N_{B,p}$ is L $\wedge$ k_3 is L $\wedge$ k_{12} is L THEN Eff is H Rule 5 consists of one sizing variables and the two power management control variables. The rule stated that for a *low* number of batteries in parallel, a *low* k_3 and a low k_{12} result in *high* efficiency. With a *low* number of batteries in series and k_3 and k_{12} both *low* low power is available for the electrolyser. Again, operating at low current density, electrolyser efficiency and system efficiency is *high*.

Table C.2: Site A interpretation of efficiency objective rule base - Continued.

Rule 6: IF β is VL $\wedge$ $N_{PV,s}$ is VL $\wedge$ P_{WT} is VL $\wedge$ N_{ely} is L $\wedge$ k_3 is M $\wedge$ k_{12} is VL THEN Eff is VH Rule 6 consists of four sizing variables and the two power management control variables. The rule states that for a *very low* PV module slope, a *very low* number of PV modules in series, a *very low* wind turbine power rating, a *low* number of electrolyser cells, a *medium* k_3 and a *very low* k_{12} result in a *very high* efficiency. All the variables result in low power from the RE sources and low power flow to the electrolyser. Again, this result in *very high* electrolyser and system efficiency.
Rule 7: IF $I_{ely,min}$ is H THEN Eff is VL Rule 7 consists of a single control variable. The rule states that for a *high* minimum electrolyser current result in *very low* efficiency. As is previously stated, an electrolyser is more efficient at lower current densities. Rule 7 is exactly the same with the same explanation and conclusion as rule 3.
Rule 8: IF $N_{PV,s}$ is H $\wedge$ P_{WT} is VL THEN Eff is H Rule 8 consists of two sizing variables. The rule states that for a *high* number of PV modules in series and a *very low* wind turbine power rating results in *high* efficiency. Having a high number of PV modules in series and a *very low* implies low input power from the RE sources. Assuming the electrolyser is at least medium to large rated, the electrolyser and system will operate at a high efficiency.
Rule 9: IF A_{ely} is H THEN Eff is M Rule 9 consists of a single sizing variable. The rule states that for a *high* electrolyser cell area result in *medium* efficiency. Rule 9 appears to have insufficient information to derive any insight from the rule. A *high* electrolyser cell area will only result in *medium* efficiency of another control variables has specific values that would result in the electrolyser operating at medium efficiencies.
Rule 10: IF $I_{ely,max}$ is VL $\wedge$ k_{12} is L THEN Eff is H Rule 10 consists of two control variables. The rule states that for a *very low* maximum electrolyser current setting and a *low* k_{12} result in *high* efficiency. Again it is stated that an electrolyser operates more efficiently at lower current densities. For both a *very low* maximum electrolyser current and for a low k_{12} the electrolyser current density is limited resulting in high efficiency.

Table C.3: Site C description/findings/explanation of cost rules.

General: 51 % of the MFs are eliminated with the RMSE remaining within the specified 10 % error. 63 % of sizing MFs are eliminated while 42 % of control MFs are eliminated. This indicates that cost for site C is more dependent control than sizing variables sine less control variables are eliminated..
Rule 1: IF β is VL $\wedge$ $N_{PV,s}$ is VL $\wedge$ $N_{PV,p}$ is VL $\wedge$ P_{WT} is VL $\wedge$ A_{ely} is VL $\wedge$ N_{ely} is H $\wedge$ $N_{B,s}$ is VL $\wedge$ SOC_{min} is VL $\wedge$ k_{12} is VL THEN Cost is VH Rule 1 consists of 7 sizing variables and two control variables. The rule states that for a *very low* PV module slope, a *very low* number of PV modules in series, a *very low* number of PV modules in series, a *very low* wind turbine power rating, a *very low* electrolyser cell area, a *high*, a *very low* number of batteries in series, a *very low* minimum battery SOC setting and a *very low* k_{12} result in very high cost. All the above variables for this rule are *very low* except for the number of electrolyser cells that are *high*. This results in a very low RE source inputs, and a *very low* PV module slope is not optimal for this site. The electrolyser power rating is *medium* with a *very low* battery rating and *very low* minimum battery SOC. All this should result in low capital costs, but this sizing configuration is not optimal and the result is *very high* system (TLCC) cost.
Rule 2: IF β is H $\wedge$ P_{WT} is L $\wedge$ A_{ely} is VH $\wedge$ N_{ely} is H $\wedge$ $N_{B,p}$ is L $\wedge$ SOC_{min} is M $\wedge$ $I_{ely,max}$ is M $\wedge$ k_3 is M THEN Cost is VL Rule 2 consists of five sizing variables and three control variables. The rule states that for a *high* PV module slope, a *low* wind turbine power rating, a *very high* electrolyser cell area, a *high* number of electrolyser cells, a *low number of batteries in parallel, a medium minimum battery SOC setting, a medium maximum electrolyser current value and a medium* k_3 *result in very low cost.* A *high* PV module slope is optimal for this site. A *low* wind turbine power rating result in low power from the wind turbine but possible high power input from the PV modules. A *very high* electrolyser cell area and a *high* number of cells result in high electrolyser rating. A *low* number of batteries in parallel result in low battery energy storage with *medium* minimum battery SOC setting allowing only *medium* level of depth of discharge. This is an optimal configuration for the batteries to ensure they last. A *medium* maximum electrolyser current setting allows medium power to the electrolyser. With k_3 also medium, the electrolyser has a possible high PV module input for operation. This sizing configuration is optimal and result in *very low* cost. Rule 2 is the only rule that results in *very low* cost with all the others resulting in *very high* cost.
Rule 3: IF β is L $\wedge$ $N_{PV,s}$ is H $\wedge$ $N_{PV,p}$ is VL $\wedge$ P_{WT} is VL $\wedge$ N_{ely} is VH $\wedge$ $N_{B,p}$ is VL $\wedge$ k_{12} is L THEN Cost is VH Rule 3 consists of six sizing variables and one control variable. The rule states that a *low* PV module slope, a *high* number of PV modules in series, a *very low* number of PV modules in parallel, a *very low* wind turbine power rating, a *very high* number of electrolyser cells, a *very low* number of batteries in parallel and a *low* k_{12} result in *very high* cost. A *low* PV module slope is not optimal for site C. a high number of PV modules in series and a *very low* number of PV modules in parallel with a *very low* wind turbine power rating result in *low* RE source input. A *very high* number of electrolyser cells and *very low* number of batteries in parallel result in high electrolyser rating and small battery energy storage component. With k_{12} *low* majority energy is diverted in the batteries which has *low* capacity. This sizing configuration result in *very high* cost due to the mismatch between low power input and high electrolyser ratings. This configuration would be efficient.

Table C.4: Site A interpretation of cost objective rule base - Continued.

Rule 4: IF β is VL $\wedge$ $N_{PV,s}$ is VL $\wedge$ C_{10} is VH $\wedge$ $I_{ely,max}$ is VL $\wedge$ k_3 is L $\wedge$ k_{12} is VL THEN Cost is VH Rule 4 consists of three sizing variables and three control variables. The rule states that a *very low* PV module slope, a *very low* number of PV modules in series, a *very high* battery AH rating, a *very low* maximum electrolyser current setting, a *low* k_3 and a very low k_{12} result in a *very high* cost. A moduels slope is not optimal for site C. With the $N_{PV,s}$ very low and C_{10} very high there is a *very low* RE source input with *very high* battery storage capacity. With the maximum electrolyser current setting *very low*, k_3 low and k_{12} very low the cost will be *very high*. This is again a possibly efficient sizing configuration.
Rule 5: IF $N_{PV,s}$ is VL $\wedge$ N_{ely} is VH $\wedge$ C_{10} is VH $\wedge$ $N_{B,s}$ is VL $\wedge$ $N_{B,p}$ is VL $\wedge$ SOC_{max} is M $\wedge$ k_{12} is L THEN Cost is VH Rule 5 consists of five sizing variables and two control variables. The rule states that for a *very low* number of PV modules in series, a *very high* number of electrolyser cells, a *very high* battery Ah rating, a *very low* number of batteries in series, a *very low* number of batteries in series, a *medium* maximum battery SOC setting and a *low* k_{12} result in a *very high* cost. Rule 5 again consists of *low* to *very low* RE input sources with *very high* electrolyser rating and *high* battery energy storage. This configuration is again not economical since the *medium* maximum battery SOC setting results in only half the capacity being used, and a *low* k_{12} only allow low power to the electrolyser during excess RE input. This configuration again reaults in very high cost. Might also be an efficient system configuration.

Table C.5: Site C description/findings/explanation of reliability rules.

General: 83 % of the MFs are eliminated with the RMSE remaining within the specified 10 % error. 82 % of sizing MFs are eliminated while 83 % of control MFs are eliminated. This observation indicates an equal dependency between sizing and control variables.
Rule 1: IF SOC_{min} is H $\wedge$ $I_{ely,min}$ is VL THEN Rel is M Rule 1 consists of two control variables. The rule states that for a *high* minimum battery SOC and a *very low* minimum electrolyser current setting result in *medium* reliability. A *high* battery SOC results in more usable energy by the batteries and as a result have more energy from each cycle and *high* battery reliability. A *very low* minimum electrolyser current setting will result in low on current that might cause multiple ON/OFF cycles, reducing electrolyser reliability. The combination will result in medium reliability.
Rule 2: IF $I_{ely,max}$ is VH $\wedge$ k_{12} is H THEN Rel is M Rule 2 consists of two control variables. The rule states that a *very high* maximum electrolyser current setting and a high k_{12} result in medium reliability. Having electrolyser maximum current setting and k_{12} *very high* and *high* respectively, ensure that power is supplied to the electrolyser. This can result in multiple ON/OFF cycles reducing electrolyser reliability and thus system reliability.
Rule 3: IF $N_{PV,s}$ is VL $\wedge$ P_{WT} is VL THEN Rel is H Rule 3 consists of two sizing variables. The rule states that for a *very low* number of PV modules in series and a *very low* wind turbine power rating result in high reliability. Having both the number of PV modules in series and the wind turbine power rating variables *very low* implies little power is available for the electrolyser. The electrolyser will then operate less and thus have a better electrolyser.
Rule 4: IF SOC_{min} is M $\wedge$ $I_{ely,min}$ is VH THEN Rel is H Rule 4 consists of two control variables. The rule states that for a **medium** battery SOC setting and a *very high* minimum electrolyser current setting result in *highW* reliability. With the *medium* minimum battery SOC setting and *very high* minimum electrolyser current setting requires high current to ensure electrolyser operation. This will allow electrolyser to operate less and thus have *high* reliability.
Rule 5: IF P_{WT} is M $\wedge$ $I_{ely,min}$ is VL $\wedge$ $I_{ely,max}$ is VH $\wedge$ k_{12} is VH THEN Rel is M Rule 5 consists of one sizing variable and three control variables. The rule states that for a *medium* wind turbine power rating, a *very low* minimum electrolyser current settings, a *very high* maximum electrolyser current setting and a *very high* k_{12} result in *medium* reliability. A *very low* minimum electrolyser current setting and *very high* maximum electrolyser current setting result in a very large operating range for the electrolyser. A *medium* wind turbine power rating will result in intermittent operation of the electrolyser. A *very high* k_{12} will result in all excess power going to the electrolyser. Therefore, the electrolyser will be subjected to intermittent RE source and cause multiple ON/OFF cycles resulting in medium electrolyser and thus system reliability.

Table C.6: Site A interpretation of reliability objective rule base - Continued.

Rule 6: IF β is VL $\wedge$ $N_{PV,s}$ is H $\wedge$ P_{WT} is VL THEN Rel is M Rule 6 consists of three sizing variables and one control variable. The rule states that for a *very low* PV module slope, a *high* number of PV modules in series and a *very low* wind turbine power rating result in medium reliability. A *very low* PV module slope is not the optimal for site C. PV for site C is classified as marginal and wind as outstanding. In this rule the PV resource sizing is *high* and the wind resource is *low*. This is thus not the optimal configuration of RE sources, and will thus result in medium reliability.
Rule 7: IF β is L $\wedge$ $N_{PV,s}$ is H THEN Rel is M Rule 7 Consists of two sizing variables. The rule states that for a *low* PV module slope and a *high* number of PV modules in series result in *medium* reliability. Rule 7 is almost identical to rule 6 with the difference being the addition of the wind turbine power rating in rule 6. The same thinking as in rule 6 is used, that the PV resources is marginal, and the sizing and combination of RE sizing is not optimal for this site. By not including the wind turbine rule 7 emphasises that this site is not suited for wind.
Rule 8: IF β is VL $\wedge$ $N_{PV,s}$ is H $\wedge$ k_{12} is VL THEN Rel is M Rule 8 consists of two sizing variables and one control variable. The rule states that for a *very low* PV module slope, high number of PV modules in series and very low k_{12}. Rule 8 is similar to rules 6 and 7. Each of the rules 6, 7 and 8 include a different variables for different scenarios. The same rational as in rule 6 is used with the addition of a *very low* value for k_{12}. Having k_{12} *very low* result in multiple ON/OFF cycles.
Rule 9: IF SOC_{max} is H $\wedge$ k_{12} is L THEN Rel is M Rule 9 consists of two control variables. The rule states that a *high* maximum battery SOC and a *low* k_{12} result in *medium* reliability. With a *high* battery SOC the battery can operate in a wide range, implying that less charge/discharges will be experienced, however the *low* k_{12} result in the intermittent operation of the electrolyser from the RE sources causing low reliability with the result being medium system reliability.
Rule 10: IF $N_{PV,s}$ is H $\wedge$ P_{WT} is VL $\wedge$ $N_{B,p}$ is VL THEN Rel is M Rule 10 consists of three sizing variables. The rule states that for a *high* number of PV modules in series, a *very low* wind turbine power rating, a *very low* number of batteries in series result in *medium* reliability. Again the *low* wind turbine power rating and *high* number of PV modules in series are not optimal for site C. The *very low* number of batteries in series also implies low rated battery energy storage which will due to its size charge and discharge multiple time. The result is a medium reliability.

Appendix D

Simulation, optimisation and analysis files

This Appendix provides information regarding the supporting files for the thesis. Supporting files include Matlab® .mat files and m. files, Simulink™ .mdl files, and Microsoft Office Excel files.

The folders and files are given below:

Supporting files and documents: Main folder.
→ **Results:** Contains results files and analysis files.
→ → **Site #:** Contains site specific results for site #. Fig. D.1 gives the flow diagram showing the order and providing explanation of the files used.
→ → **Generate_x_y_z.m:** Matlab® m.file used to combine information from the output files from the SPEA and SPEAGA optimisation for several runs.
→ → **Process_x_y_z.m:** Matlab® m.file used to process and plot Pareto information from the output files from the SPEA and SPEAGA optimisation.
→ **Work:** Contains the main files used for simulation and optimisaion.
→ → **Input files:** Contains the input files required for each of the three sites.
→ → **Model SPEA:** Fig. D.2 gives the flow diagram showing the order and providing explanation of the files used.
→ → **Model SPEAGA:** Fig. D.3 gives the flow diagram showing the order and providing explanation of the files used.

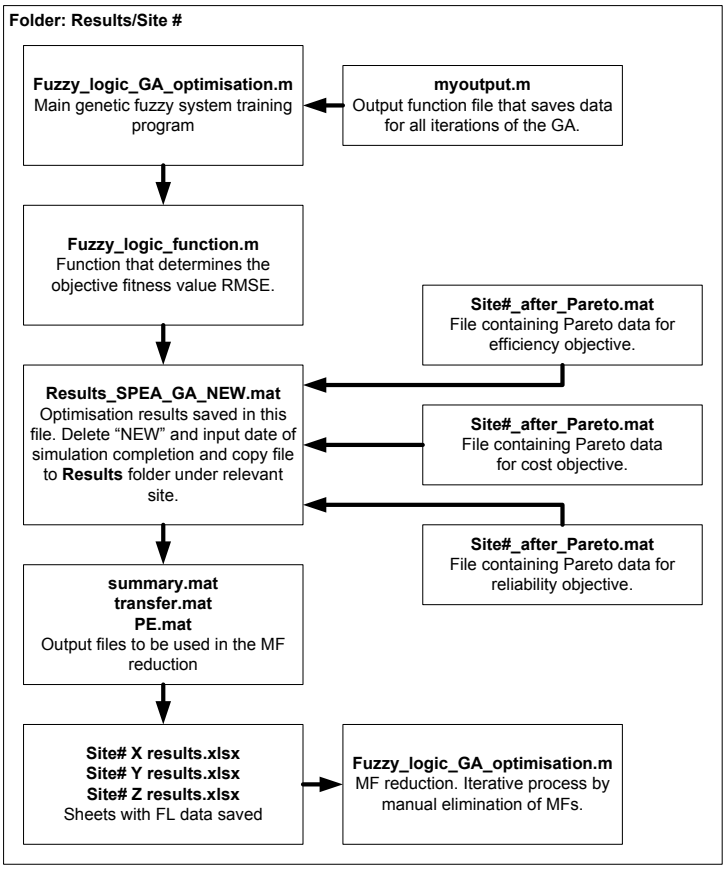

Figure D.1: Flow diagram of the genetic fuzzy system process.

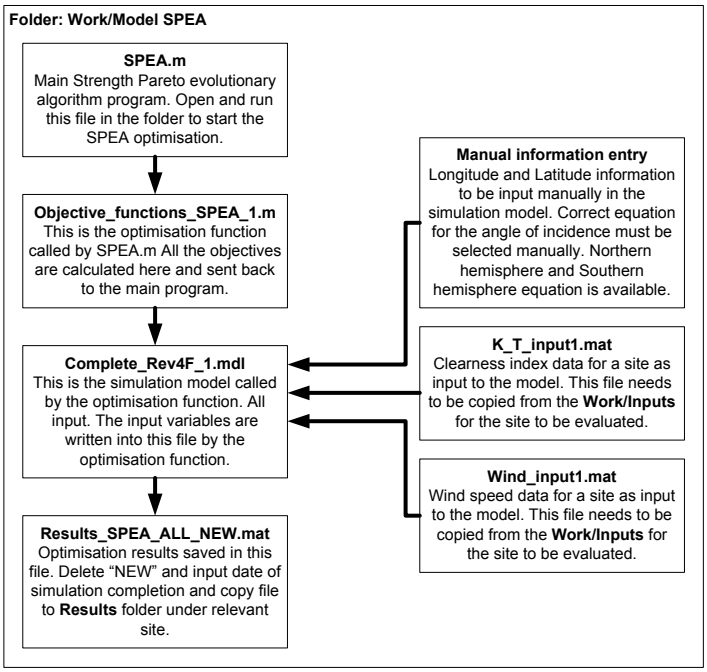

Figure D.2: Flow diagram of the SPEA process.

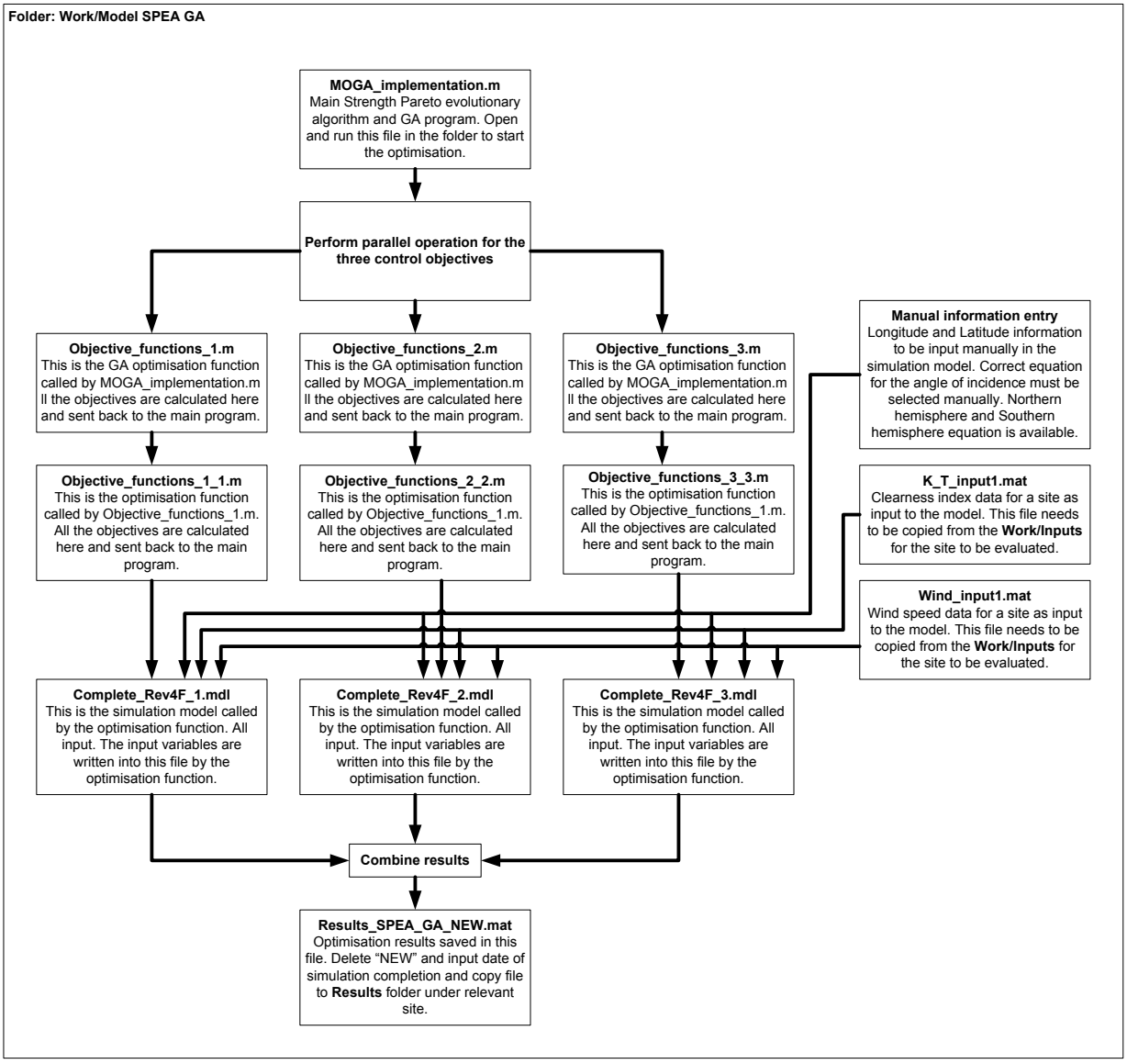

Figure D.3: Flow diagram of the SPEAGA process.